The role of Foxg1 in retinal axon divergence at the optic chiasm.

By Natasha Tian

Thesis submitted for the Degree of Doctor of Philosophy at the University of Edinburgh.

July 2007

This thesis is dedicated to two fiercely intelligent friends who were taken prematurely from this world and who provided me with inspiration and kindness during the short time I knew them.

Margaret Davidson, 1979 - 2006

Elizabeth Daplyn, 1978 - 2005

Disclaimer

I (Natasha Tian) composed this thesis and performed all of the experiments presented herein unless otherwise clearly indicated in the text. No part of this work has been, or is being submitted for any other degree or professional qualification.

Signed:

Date:

Acknowledgements

The paving that led to this completed PhD thesis was crazy but like a navigating axon I was provided with crucial guide-posts along the way. A big thank you goes to my excellent supervisors Prof David Price and the ever-optimistic Dr Thomas Pratt for their advice, patience, technical expertise and intellectual input. This thesis would not have been possible without you. Thanks also to my thesis committee chair, Prof Jamie Davies, for his helpful input. I am immensely grateful to Katie Gillies and Ian Simpson for first class technical support, Linda Wilson for confocal microscopy expertise and friendly chats, Grace and Viv for imparting their knowledge of histology and the whole of DBUG (past and present) for being so supportive, particularly Anna, Celestial, Dennis, Jeni, Louise, Mark B, Mike, Tammy, Tian and Vassiliki. Catherine, Chris, Dario, Mark H and Petrina: you helped me along my journey in many different ways. Thanks also to Duncan, Lee and Larraine for jovially looking after my mice and the Scots banter.

Outside the University of Edinburgh, I am extremely grateful to Carol Mason, Eloisa Herrera, Robert Hindges, Glen Jeffery and Lynda Erskine for interesting discussions and advice about my research. Thanks also to Steven Brown at Columbia University for providing me with 20µl of his precious Zic2 antibody.

Special mentions should go to Fozia and Louise for being fantastic and efficient co-founders of the postgraduate seminars and organizing spectacular lunch meetings. I appreciate Jan Barfoot's help in assigning me to various science communication activities that kept me sane and also Ian Johnston's support at 'The Scotsman' for providing me with a voice outside the lab and a greater appreciation of the 'big picture'.

Stress relief was provided by the 'Wellcome girls' in the form of Irish craic, impromptu parties and salsa/Irish dancing, the 'Habs girls' down South for keeping me firmly in the loop, to fellow 'Hildabeasts' Kate, Lisa, Liz and Helen for bags of support and visits, and John (piano) and Lola (cello) for creating 'interesting' major/minor music and providing much needed laughter. Special mentions go to Effie and Leah for listening and cheering me up through hard times, both inside and outside the lab, and also to Florin for providing me with many happy memories of my time in Edinburgh.

Finally, thanks to mum and dad for countless trips to Edinburgh and unwavering support. I know these past 4 years have not been easy and I appreciate you having walked alongside me all the way.

This thesis would not have been possible without generous funding from 'The Wellcome Trust', which not only provided financial support for experiments but also enabled me to keep the major coffee and tea houses, chocolatiers, vineyards and Italian eateries in business. I would also like to thank 'Brain' and 'BSDB' for providing me with travel grants to attend international conferences in stunning locations.

If —

by Rudyard Kipling

If you can keep your head when all about you
Are losing theirs and blaming it on you;
If you can trust yourself when all men doubt you,
But make allowance for their doubting too;
If you can wait and not be tired by waiting,
Or, being lied about, don't deal in lies,
Or, being hated, don't give way to hating,
And yet don't look too good, nor talk too wise;

If you can dream - and not make dreams your master;
If you can think - and not make thoughts your aim;
If you can meet with triumph and disaster
And treat those two impostors just the same;
If you can bear to hear the truth you've spoken
Twisted by knaves to make a trap for fools,
Or watch the things you gave your life to broken,
And stoop and build 'em up with wornout tools;

If you can make one heap of all your winnings
And risk it on one turn of pitch-and-toss,
And lose, and start again at your beginnings
And never breathe a word about your loss;
If you can force your heart and nerve and sinew
To serve your turn long after they are gone,
And so hold on when there is nothing in you
Except the Will which says to them: "Hold on";

If you can talk with crowds and keep your virtue,
Or walk with kings - nor lose the common touch;
If neither foes nor loving friends can hurt you;
If all men count with you, but none too much;
If you can fill the unforgiving minute
With sixty seconds' worth of distance run -
Yours is the Earth and everything that's in it,
And - which is more - you'll be a Man, my son!

Table of Contents

List of Figures

CHAPTER 1:

CHAPTER 3:

CHAPTER 4:

CHAPTER 5:

CHAPTER 6:

CHAPTER 7:

CHAPTER 8:

List of Tables

CHAPTER 1:

CHAPTER 3:

ABBREVIATIONS

A	Anterior
AP	Anteroposterior
β-gal	Beta-galactosidase
BMP	Bone morphogenetic protein
bp	Base pairs
BSA	Bovine serum albumin
ctl	Control
CMZ	Ciliary marginal zone
CNS	Central nervous system
Contra	Contralateral
D	Dorsal
DAB	3,3'-diaminobenzidine
ddH_20	Double-distilled water
DiI	Dioctadecyltetramethylindocarbocyanine perchlorate
DMSO	Dimethylsulphoxide
DN	Dorsonasal
DNA	Deoxyribonucleic Acid
DT	Dorsotemporal
dNTP	Deoxyribonucleotide triphosphates
DV	Dorsoventral
E	Embryonic age
ER	Extended retina
Foxg1	Forkhead box g1
Hy	Hypothalamus
Ipsi	Ipsilateral
L	Lens
n	Number of samples
N	Nasal
NT	Nasotemporal
Oc	Optic chiasm
OFL	Optic fibre layer
Os	Optic stalk
Ot	Optic tract
P	Posterior
PBS	Phosphate buffered saline
PCR	Polymerase chain reaction
PFA	Paraformaldehyde
qRT PCR	Quantitative RT PCR
R	Retina
RGC	Retinal ganglion cell

RNA	Ribonucleic acid
RPE	Retinal pigment epithelium
rpm	Rotations per minute
RT PCR	Reverse Transcriptase PCR
SEM	Standard error of the mean
T	Temporal
Tel	Telencephalon
V	Ventral
VN	Ventronasal
VT	Ventrotemporal
VTC	Ventrotemporal crescent

ABSTRACT

During murine development, retinal ganglion cell (RGC) axons are presented with multiple navigational choices as they exit the eyes and follow a complex path to targets in the thalamus and superior colliculus of the brain. The optic chiasm is a major choice point, positioned at the ventral midline of the hypothalamus, where the majority of retinal axons cross to the contralateral side of the brain whilst only 3% remain uncrossed and project ipsilaterally. Identifying the cellular and molecular processes involved in retinal axon divergence at the chiasm is an intense area of study and knockout mice have proved useful tools.

Foxg1 is a winged helix transcription factor that is expressed in the nasal retina, nasal optic stalk and anterior ventral hypothalamus, which are all structures that retinal axons encounter as they project out of the RGC layer towards the chiasm. The coincidence between the expression pattern of Foxg1 and the route followed by retinal axons led to the hypothesis that Foxg1 plays a role in guiding retinal axons at the optic chiasm. Previous experiments in this laboratory lent support to this idea by revealing an increase in the number of ipsilateral projections in *Foxg1*$^{-/-}$ mouse embryos from both nasal and temporal retina.

Since *Foxg1* is expressed in both the nasal retina and at the optic chiasm midline, the main hypotheses for this thesis are that *Foxg1* influences retinal axon divergence by transcriptionally regulating the expression of cell surface molecules on (1) growth cones from the nasal retina or (2) guidance molecules on chiasm cells.

In order to address these possibilities, the key aims of this thesis were (i) to investigate whether *Foxg1* is primarily required in the nasal retina or at the chiasm

for retinal axon divergence, (ii) to determine whether the *Foxg1* null retina and chiasm are patterned differently from those of wild types and (iii) to investigate the expression of candidate molecules in the retina or chiasm known to influence retinal axon navigation.

Foxg1$^{-/-}$ ↔ *Foxg1*$^{+/+}$ chimeric co-cultures of retinal explants and chiasm cells were used to investigate the relative roles of the retina and chiasm in midline crossing. Axonal outgrowth was significantly reduced in co-cultures containing dorsonasal retina or chiasm cells from *Foxg1* null embryos, suggesting that Foxg1 is normally required in both these tissues for nasal axons to cross the ventral midline.

The dorsoventral and nasotemporal patterning of the retina was investigated to assess whether the ventral or temporal regions, from which ipsilateral RGCs originate, were larger in *Foxg1* null mutants compared to age-matched wild types. Similar ephrin-B2 dorsal^{high} – ventral^{low} and EphB2 ventral^{high} – dorsal^{low} gradients were observed in both during the peak period of retinal axon divergence. Nasotemporal patterning was assessed using X-gal staining of *Foxg1*^{LacZ} reporter mice. In *Foxg1*$^{lacZ/+}$ embryos, transcriptional activation of *Foxg1* was most widespread in the dorsonasal retina and absent ventrotemporally. *Foxg1*$^{lacZ/lacZ}$ embryos showed increased *Foxg1* activation in temporal regions but reduced activation in the dorsonasal retina, suggestive (but not conclusive proof) of disrupted nasotemporal patterning.

A significant increase in the number of RGCs expressing the ipsilateral determinant Zic2 was observed in the nasal but not temporal retina of *Foxg1*$^{-/-}$ embryos, suggesting that Foxg1 normally represses Zic2 expression in these RGCs. It has been previously demonstrated that the quantity of retinal cells expressing Zic2 and EphB1, through which Zic2 is thought to mediate its effects, is correlated with the

size of the ipsilateral projection. Therefore, Zic2 provides an explanation for the extra ipsilateral projections from nasal but not temporal retina.

Finally, the expression patterns of molecules Nkx2.2, SSEA-1 and CD44 that are key markers of chiasm cells were examined using immunohistochemistry. The protein expression patterns were maintained in wild type and *Foxg1*$^{-/-}$ embryos at the time when the ipsilateral projection is forming. Midline expression of ephrin-B2 that repels ipsilateral axons was also unchanged.

In summary, the co-cultures revealed a requirement for *Foxg1* in the nasal retina and at the chiasm to allow axons from *Foxg1*-expressing RGCs to cross the ventral midline. In the absence of *Foxg1*, Zic2 expression increases in the nasal retina and may explain the rise in ipsilateral projections. These data are consistent with a model in which Foxg1 normally represses Zic2 expression in the nasal retina, hence repressing the ipsilateral pathway in contralateral RGC axons.

CHAPTER 1: Introduction.

1.1. An overview of axon guidance.

In the developing mammalian brain, billions of nerve axons navigate over long distances to form connections with their targets and thereby establish neuronal circuits. Pathfinding axons are tipped with highly motile structures called growth cones that are constructed from actin filaments originating from a central microtubule core, with finger-like extensions called filopodia (Suter and Forscher, 1998). As growth cones sample the external environment, receptors on their surface bind diffusible or tethered molecules that act as guidance cues, in the extracellular matrix or on cell surfaces. Receptor-ligand binding triggers intracellular signaling cascades that alter the cytoskeletal architecture by rearranging actin or tubulin. The addition of cytoskeletal components in response to attractive guidance cues is thought to drive the growth cone forward, whereas disassembly of the cytoskeleton in response to chemorepulsive cues produces growth cone retraction. Asymmetric signaling on one side of the growth cone leads to axon turning towards or away from a guidance cue (Song et al., 1998; Song and Poo, 1999). Despite this basic knowledge, the precise mechanisms that underlie growth cone guidance are still not fully understood.

Growth cones are guided by both contact-mediated and diffusible pathway and target-derived cues that mediate contact attraction, contact repulsion, chemoattraction and chemorepulsion (Tessier-Lavigne and Goodman, 1996). Axon navigation usually occurs via several intermediate targets *en route* to an axon's final destination, where growth cones sample guidance cues in the extracellular environment. It is remarkable how multiple axon populations from different regions of the brain manage to respond solely to appropriate cues and navigate accurately to their correct destinations. Targeting errors do occur but axons that are found in inappropriate locations are simply pruned by cell death postnatally (Provis and Penfold, 1988; Oppenheim, 1991).

1.2. Commissural axon tracts.

Commissural tracts connect the left and right hemispheres of the brain and coordinate activity between them. The commissural tracts include the large tracts of the corpus callosum and anterior commissure (connecting the two cerebral hemispheres) and the hippocampal commissure (connecting the hippocampi), but also smaller commissures, including the optic chiasm, which relays visual information from the eyes to left and right visual brain targets in the thalamus and superior colliculi via retinal axons. The formation of these tracts is accurately regulated (1) cell-autonomously by transcription factors that regulate the expression of receptors on growth cones and signalling cascades and (2) cell-non-autonomously by the extracellular environment, involving pioneering axons and pathway-derived guidance cues that exist as diffusible gradients or as cues anchored to midline glial structures or other intermediate targets (reviewed in (Lindwall et al., 2007).

1.2.1. Long-range guidance.

It is well established that long-range diffusible guidance cues guide axons towards and across the brain midline. These include the 'classic' guidance molecules Netrins and Slits and their receptors: Deleted in colorectal cancer (DCC) and Roundabout (Robo) and also morphogens, such as Sonic hedgehog (Shh), Fibroblast growth factors (FGFs) and Wingless-type (Wnt) proteins that play a dual role in patterning tissues as well as guiding axons (Salie et al., 2005; Charron et al., 2003; Butler and Dodd, 2003; Lyuksyutova et al., 2003; Yoshikawa et al., 2003; Yoshikawa and Thomas, 2004; Augsburger et al., 1999). Gradients of guidance cues serve either to attract or repel axons. For example, at the vertebrate spinal cord and the *Drosophila* ventral nerve cord the long-range, diffusible chemoattractant netrin is secreted by the floor plate and attracts axons to the midline (Serafini et al., 1996; Serafini et al., 1994; Mitchell et al., 1996). In contrast, the chemorepellent Slit prevents commissural axons from recrossing the midline and prevents ipsilateral axons from crossing at all via contact repulsion

following the binding of Slit to Robo receptors on these axons (Kidd et al., 1999; Kidd et al., 1998; Brose et al., 1999; Long et al., 2004; Kennedy et al., 1994; Placzek et al., 1990; Tessier-Lavigne et al., 1988). Although netrin expression has not been identified directly at the optic chiasm, netrin-1-mediated attraction at the optic nerve head is thought to facilitate the exit of retinal axons from the eye to the optic stalk (Deiner et al., 1997).

1.2.2. Short-range guidance.

Not all axons are guided from a distance. Short-range guidance molecules, such as Ephrins and Eph receptors are expressed by cells and axons at the optic chiasm midline of the developing mouse forebrain (Marcus et al., 2000; Williams et al., 2003). Ephrins and Ephs mediate cell-cell contact repulsion, which play important roles in retinotectal mapping and are able to signal bidirectionally (Drescher et al., 1997; Braisted et al., 1997; Hindges et al., 2002; Mann et al., 2002; Klein, 2004; Kullander and Klein, 2002; McLaughlin et al., 2003). Semaphorins (Semas) that interact with their transmembrane Neuropilin and Plexin receptors, require cell-cell contact, although some Semaphorins are soluble ligands (Pasterkamp and Kolodkin, 2003). Semaphorins mediate both chemorepulsion and chemoattraction and help position the anterior commissure (Falk et al., 2005; Gu et al., 2003). Also, laminin and fibronectin in the extracellular matrix were discovered as some of the earliest molecules that promote axon growth (Lander, 1987).

1.2.3. Attraction versus repulsion.

There is growing evidence to support the hypothesis that growth cones make guidance decisions by measuring relative levels of attractive and repulsive molecules that they contact (Tessier-Lavigne and Goodman, 1996). Experimental manipulations of levels of guidance cues and receptors imply that an axon can alter its response to external cues

by changing the composition of guidance receptors present on the growth cone (Bashaw and Goodman, 1999; Lin and Goodman, 1994; Tessier-Lavigne and Goodman, 1996; Winberg et al., 1998). However, recent findings suggest that axon guidance is more complicated than the simple attraction and repulsion of axons to long- and short-range guidance molecules. It appears that axons can alter their response to guidance cues in a hierarchical manner depending on their position in the axon pathway. For example, commissural axons crossing the *Xenopus* spinal cord lose responsiveness to the chemoattractant Netrin-1 and gain responsiveness to the chemorepellent Slit only *after* crossing the midline when they start to express the Slit receptor Robo (Stein and Tessier-Lavigne, 2001). Slit is thought to silence netrin attraction by causing a direct interaction between Robo and DCC (the netrin receptor), enabling commissural axons to move on to their next target after reaching the attractive midline. Stein & Tessier-Lavigne's (2001) findings have sparked a debate over whether the observed Slit-Robo interactions during axon guidance are primarily the consequence of inhibition of netrin attraction or simply axon repulsion or a combination of the two (Bhat, 2005; Garbe and Bashaw, 2007; Hiramoto and Hiromi, 2006).

1.2.4. Extracellular matrix molecules influence axon guidance.

More complexity is thrown in by the heparan sulphates, chondroitin sulphates and their core glycoproteins. These highly diverse extracellular matrix molecules interact with axon guidance molecules and growth cones in various ways and the diversity of their carbohydrate chains appear to produce different axon guidance decisions even with the same guidance cue (Bulow and Hobert, 2004; Chung et al., 2001; Chung et al., 2000a; Chung et al., 2000b; Ichijo, 2004; McAdams and McLoon, 1995; Pratt et al., 2006). Bulow and Hobert (2004) proposed the term 'heparan sulphate code' to explain how heparan sulphate modifications of core proteins could be deployed in different brain regions along axonal pathways, resulting in the recruitment of specific groups of

guidance cues that influence axon navigation in key regions. This hypothesis arose from growing evidence for the use of heparan sulphate proteoglycans (HSPGs) as cofactors to recruit ligands to their receptors (Bernfield et al., 1999; Chung et al., 2000a; Guimond and Turnbull, 1999; Perrimon and Bernfield, 2000). Only last year it was discovered that heparan sulphate, a cell surface residue on extracellular matrix proteoglycans, binds to the Slit protein and functions to enhance Slit-Robo binding, which is relatively weak on its own (Hussain et al., 2006). Therefore, the complex panoply of axon navigation decisions is determined by the combinatorial action of signaling molecules (Yu and Bargmann, 2001) in the context of a molecular code inscribed into the extracellular substrate that growth cones navigate through. Deciphering the diverse proteoglycan codes and precise downstream signaling events offers great scope for future experimentation.

1.3. The visual system.

The retinotectal pathway is a well-characterised and popular model for axon guidance. This pathway is particularly useful for this thesis as *Foxg1* is expressed at various points along it. Retinal ganglion cells (RGCs) are projecting neurons found in the inner layer of the retina. These RGC axons carry visual information from the retinas, via the optic nerves and ventral midline of the brain, along the optic tracts that run dorsolaterally along the surface of the diencephalon to the left and right lateral geniculate nuclei in the thalamus and termination zones in the superior colliculi on both sides of the midbrain. RGC axons are presented with multiple navigational choices throughout their journey. A major choice point is the optic chiasm, positioned at the ventral surface of the hypothalamus, where retinal axons either cross to the contralateral side of the brain or remain uncrossed (ipsilateral). The optic chiasm itself provides cues for axons to cross or not (Mason and Sretavan, 1997). The simple, bilateral ‘choice’ of retinal axons at the optic chiasm means that any deviations from the norm are simple to

detect. The presence of an ipsilateral projection gives rise to binocular vision, enabling visual information from both eyes to be processed in the same region of the brain, which has advantages of improved depth perception. The trend in evolution has been from laterally-positioned eyes and complete RGC decussation at the optic chiasm (100% of retinal axons cross the midline) to frontally-placed eyes and partial decussation, in which a proportion of RGC axons project ipsilaterally, leading to the emergence of binocular vision that is exclusive to mammals and some predatory birds with forward-facing eyes (Jeffery, 2001). Therefore, observations in a mammal, such as the mouse, are more relevant to humans and other primates than observations in non-mammalian species, despite humans possessing a larger ipsilateral projection (almost 50%) than mice (~ 3% ipsilateral axons) due to their forward-facing eyes (Drager and Olsen, 1980; Fukuda et al., 1989; Polyak, 1957). Guidance molecules at the optic chiasm show strong evolutionary conservation between species, demonstrating the importance of this commissural tract and also the wide relevance of studies in a diversity of organisms from fruit flies and zebrafish to chicks and mice. The mouse was chosen for this thesis as it is the only animal with an uncrossed projection, lacking in birds and fish, for which appropriate mutants are available for experimental study. The ability to manipulate genes precisely and create gene knockouts, in which a gene is deleted, offers huge advantages for the study of normal gene function.

1.4. Development of the mouse optic chiasm.

1.4.1. Early stages of optic chiasm development.

At E9 in the mouse, Pax-2 is expressed in the ventral half of the optic stalk and the ventral midline of the forebrain, that will become the optic chiasm, is formed by neuroepithelial cells that express Shh (Echelard et al., 1993; Torres et al., 1996). At E11-E12, when the first RGC axons project towards the optic chiasm, Pax-2 expression

is present in both optic stalks and connecting midline neuroepithelium in a transverse line. Directly at the midline, Shh is absent (Torres et al., 1996) and this is thought to be the result of repression by Pax-2, limiting Shh expression to regions located caudal to decussating axons (Macdonald et al., 1997). In *Pax-2* null mice, all axons project ipsilaterally and Shh expression is continuous across the midline, leading to the hypothesis that Pax-2 provides a permissive corridor through a Shh domain that may normally repel axons or inhibit their growth (Torres et al., 1996). However, the ability of retinal axons of zebrafish *noi* mutants (*noi* being highly homologous to *Pax-2*), to cross *Shh*-expressing cells puts this hypothesis in doubt and calls for detailed examination of axon growth at the *Pax-2* null mouse chiasm.

1.4.2. The main stages of retinal axon projections through the optic chiasm.

The main stages of axon growth through the mouse optic chiasm are shown in Figure 1**.** The eyes and ventral diencephalon region are shown as if the observer is looking down upon the dorsal surface of horizontal slices through the level of the optic chiasm. (The dorsal-ventral axis is perpendicular to the page). At around embryonic day 12 (E12) in the mouse, shortly after RGC genesis begins, pioneering retinal axons arising from dorsocentral RGCs project from both eyes and converge on the midline of the ventral diencephalon to form the optic chiasm (Colello and Guillery, 1990) (Figure 1A). Some of these early pioneers cross into the contralateral tract, whilst others remain ipsilateral, entering the optic tract directly without approaching the midline (Colello and Guillery, 1990; Guillery et al., 1995; Marcus and Mason, 1995). These early ipsilateral projections are only transient and are eliminated later on during postnatal development (Insausti et al., 1984). E14 - E16 (Figure 1B) is the peak phase of RGC genesis and retinal axon growth through the optic chiasm and during this period the permanent ipsilateral projection develops (Colello & Guillery, 1990).

Figure 1. The main stages of RGC axon projections at the optic chiasm (adapted from Williams et al., 2006)

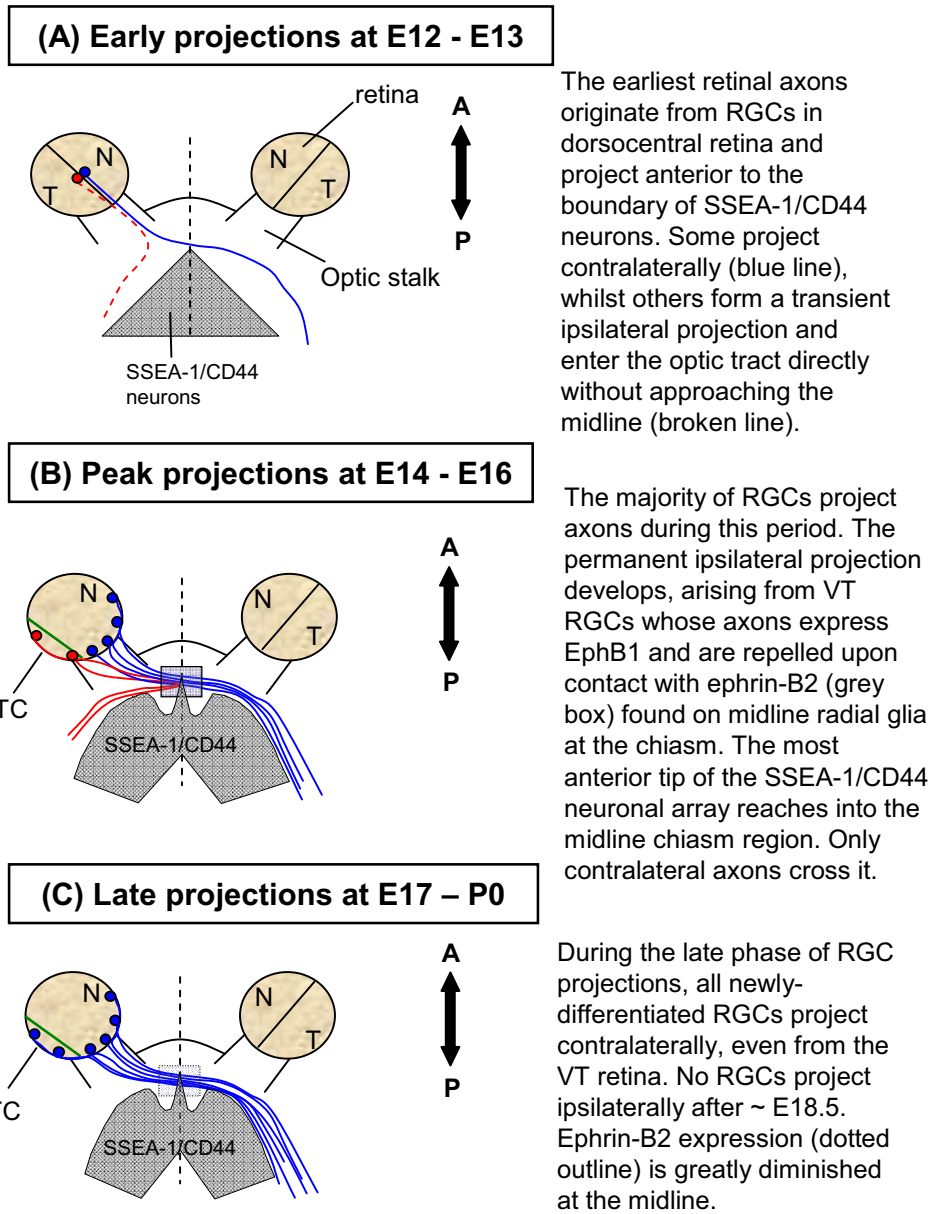

The earliest retinal axons originate from RGCs in dorsocentral retina and project anterior to the boundary of SSEA-1/CD44 neurons. Some project contralaterally (blue line), whilst others form a transient ipsilateral projection and enter the optic tract directly without approaching the midline (broken line).

The majority of RGCs project axons during this period. The permanent ipsilateral projection develops, arising from VT RGCs whose axons express EphB1 and are repelled upon contact with ephrin-B2 (grey box) found on midline radial glia at the chiasm. The most anterior tip of the SSEA-1/CD44 neuronal array reaches into the midline chiasm region. Only contralateral axons cross it.

During the late phase of RGC projections, all newly-differentiated RGCs project contralaterally, even from the VT retina. No RGCs project ipsilaterally after ~ E18.5. Ephrin-B2 expression (dotted outline) is greatly diminished at the midline.

Contralateral RGC axons arise from the entire retina, whereas permanent ipsilateral RGC axons arise from a small region of the peripheral ventrotemporal (VT) retina, called the 'ventrotemporal crescent' (VTC). The adult pattern of decussation is established by E15 - E16 with a 97:3 ratio of contralateral to ipsilateral axons (Drager, 1985; Drager and Olsen, 1980). At later stages (Figure 1C), from E17 to birth (at around E21), all RGC axons project contralaterally, including those from the VTC because ipsilateral RGC projections cease at E17.5 (Colello and Guillery, 1990; Drager, 1985; Marcus et al., 1995; Marcus & Mason, 1995).

1.5. Cells and molecules associated with axon divergence at the chiasm midline.

1.5.1. Ephrin-B2 and midline radial glia.

Glial structures play key roles in the formation of commissural tracts, particularly as sources of guidance cues, and the optic chiasm is no exception (Barresi et al., 2005; Lindwall et al., 2007; Silver, 1993; Steindler, 1993). All retinal axons appear to contact a midline specialization of radial glial cells prior to crossing the midline or remaining ipsilateral (Marcus et al., 1995). Figure 1 shows a diagram of the position of midline glia in relation to retinal axons in the developing optic chiasm. Midline glial cells express the axon guidance molecules Nr-CAM (Williams et al., 2006), Slit2 (Erskine et al., 2000) and Eph/ephrin subtype A and B receptors and ligands (Bertuzzi et al., 1999; Marcus et al., 2000). Ephrin-B2 is the only one of these molecules to date that has been shown to influence contralateral-ipsilateral axon divergence at the chiasm via the selective repulsion of VT RGC axons that express its receptor EphB1 (Nakagawa et al., 2000; Williams et al., 2003). RGC axons from other regions of the retina (dorsonasal, dorsotemporal and ventronasal) do not express EphB1 and are not repelled by ephrin-B2. Ephrin-B is absent from the ventral diencephalon of developing chick embryos

(Nakagawa et al., 2000), which lack a permanent ipsilateral projection, adding to evidence from *Xenopus* and mouse studies that ephrin-B2 is required for the uncrossed projection to form. Ephrin-B2 and EphB1 are also expressed in the human chiasm and temporal retina respectively (Lambot et al., 2005). Lambot et al. also showed that EphB1 expression occurs in the entire temporal half of the retina, mirroring the appearance of ipsilateral axons from all temporal RGCs and supporting the 50:50 contralateral:ipsilateral ratio in humans, suggesting that the uncrossed projection forms in a similar way to mice. Interestingly, a number of other EphB receptors (EphB1, EphB2 and EphB3) are expressed in the retina and these also share the ability to bind to ephrin-B2 (Birgbauer et al., 2000; Braisted et al., 1997; Hindges et al., 2002; Mann et al., 2002; Williams et al., 2003). Therefore, it is still unclear why ephrin-B2 does not bind to these other receptors in addition to EphB1, although one explanation is that ephrin-B2 has a higher affinity for the EphB1 receptor compared to the others (Flanagan and Vanderhaeghen, 1998). Alternatively, binding of ephrin-B2 to EphB1 may trigger 'ipsilateral-specific' downstream signaling events through specific EphB1 interactions with adaptor proteins such as Grb7 (Han et al., 2002) or the local synthesis of EphB1 protein in VT retinal axons *en route* to the chiasm may 'tag' them for an ipsilateral fate.

1.5.2. Chiasm neurons.

Another important cellular specialization in the ventral diencephalon, posterior to the optic chiasm, is a population of early-differentiating neurons that expresses a variety of cell surface molecules, including stage-specific embryonic antigen-1 (SSEA-1), and the cell surface protein CD44 (Kruger et al., 1998; Marcus and Mason, 1995; Sretavan et al., 1994; Sretavan et al., 1995). SSEA-1 and other molecules expressed by overlapping but slightly variable subsets of these neurons, such as chondroitin sulphate proteoglycans (Chung et al., 2000a, 2000b), Slit1 and Robo2 (Erskine et al., 2000) inhibit the growth of all retinal axons equally and may normally prevent retinal axons

deviating from their correct path rather than providing cues for axon divergence (Marcus et al., 2000). SSEA-1/CD44 neurons first appear at E12 in a 'V'-shape and are believed to provide an anatomical template or scaffold, guiding the earliest axons anteriorly around their borders to create the characteristic 'X'-shape of the chiasm (Erskine et al., 2000; Marcus and Mason, 1995; Mason and Sretavan, 1997; Runko and Kaprielian, 2002). At later stages, these neurons adopt a more elaborate conformation and borders of the SSEA-1/CD44 expression domain coincide with axon paths in the diencephalon (Lin et al., 2005). Recently, CD44 has been implicated in ipsilateral-contralateral pathfinding (Lin and Chan, 2003; Lin et al., 2005).

1.5.3. Slits, EphA and ephrin-As channel navigating axons.

A number of other molecules are expressed at and around the optic chiasm, such as ephrin-As expressed ventral and posterior to the chiasm (Marcus et al., 2000; Zhang et al., 1996), Slit1, expressed by a subset of SSEA-1/CD44 neurons and Slit2, expressed by midline radial glia (Erskine et al., 2000). Although blocking ephrin-A and EphA-binding reduced the inhibition of retinal axons to chiasm reaggregates *in vitro*, there was no differential effect on the growth of contralateral and ipsilateral axons (Marcus et al., 2000). Although the authors concluded that ephrin-A and EphA interactions are unlikely to control retinal axon divergence at the optic chiasm *in vivo*, this cannot be excluded entirely because divergence may require additional interactions or cues that are present *in vivo* but absent from the *in vitro* culture system used. Marcus et al. (2000) also proposed that ephrin-A - EphA repulsive interactions may prevent axons from entering inappropriate tissues and contribute to position-dependent sorting of retinal axons in the chiasm region, demonstrated by (Chan and Chung, 1999). In the case of *Slit1*$^{-/-}$*; Slit2*$^{-/-}$ double knockout mice, retinal axons form an ectopic chiasm anterior to the normal chiasm (Plump et al., 2002). These aberrantly-projecting axons originated from the entire retina and coupled with the observation of a normal ipsilateral projection in the *Slit1*$^{-/-}$*; Slit2*$^{-/-}$ mice, it appears unlikely that Slit1 and Slit2 are

important for retinal axon divergence, although a subtle role cannot be excluded. Rather, it appears that Slits are required to control the position at which retinal axons decussate in the ventral diencephalon and prevent axons from straying from their path (Thompson et al., 2006b; Thompson et al., 2006a).

1.6. Molecules controlling ipsilateral-contralateral divergence at the chiasm.

It is becoming increasingly evident from *in vivo* and *in vitro* experiments that the control of ipsilateral-contralateral pathfinding at the optic chiasm involves multiple attractive or repulsive factors that act sequentially or in concert in the eye, optic stalk, chiasm and possibly other regions along the retinofugal pathway (Bertuzzi et al., 1999; Chung et al., 2000b; Deiner et al., 1997; Deiner and Sretavan, 1999; Jeffery, 2001; Marcus et al., 1995; Marcus et al., 1999; Sretavan and Kruger, 1998; Sretavan and Reichardt, 1993; Wang et al., 1995; Wilson et al., 1997; Wizenmann et al., 1993; Zhang et al., 2000). *In vitro* work has shown that retinal axons are guided by both contact-mediated (Sretavan and Reichardt, 1993; Wang et al., 1995; Wizenmann et al., 1993; (Godement et al., 1994) and diffusible (Wang et al., 1996) cues and that the chiasm is generally inhibitory to axon growth. In the optic chiasm region alone, the midline location where contralateral and ipsilateral axons diverge coincides with an area in which several regulatory gene expression domains overlap (Marcus et al., 1999). The expression patterns of regulatory genes, such as Vax1, Vax2 and Pax2 that are expressed very early in development suggests that they are more likely to be involved in morphogenesis and regional patterning of the eye and ventral hypothalamus and so affect processes upstream of retinal axon divergence rather than in contralateral-ipsilateral divergence processes directly (Torres et al., 1996; Bertuzzi et al., 1999; Marcus et al., 1999). However, this does not mean that such an involvement does not occur.

Table 1 provides a summary of a few of the key molecules that are known to influence the contralateral-ipsilateral ratio in mice. This list is not intended to be exhaustive but rather provides a sample of notable findings in the literature. Figure 2 shows the contralateral-ipsilateral axon pathfinding defects at the chiasm in knockouts for a few of these molecules that are expressed in the retina. For each molecule a cartoon of the eye shows the location of RGCs that express that particular molecule. If the molecule is expressed by ipsilateral RGCs, these are shown in red. Contralateral RGCs are shown in blue. Foxd1 is the only molecule shown that is expressed both by contralateral RGCs more centrally and ipsilateral RGCs in peripheral VT regions (Herrera et al., 2004). Projection defects are shown for the mice in which the gene encoding the molecule has been knocked out. In the case of $Zic2^{kd/kd}$ mice, Zic2 expression levels were reduced substantially to 20% of the wild type level in a gene 'knockdown' (Nagai et al., 2000).

Table 1. Molecules that affect the ipsilateral projection.

Molecule	Axon guidance phenotype
Zic2 Zinc-finger transcription factor expressed by ipsilateral RGCs in VTC. Expressed around optic chiasm.	Reduced ipsilateral projection in *Zic2*$^{kd/kd}$ (abnormal chiasm) and *Zic2*$^{kd/+}$ mice (normal chiasm) (Herrera et al., 2003).
EphB1 Receptor tyrosine kinase expressed by ipsilateral RGCs in VTC & the majority co-label with Zic2.	Reduced ipsilateral projection in *EphB1* null mice (Williams et al., 2003).
Ephrin-B2 Expressed in midline radial glia at The optic chiasm midline. Expressed in dorsal (high) to ventral (low) gradient in retina.	Blocking ephrin-B2 function *in vitro*: VT RGC axons experience less repulsion by dissociated chiasm cells (ie) reduction in ipsilateral projection (Williams et al., 2003).
Foxd1 (BF-2)	*Foxd1* null mice: Increased ipsilateral

Forkhead box transcription factor expressed in the entire VT quadrant of the retina (not just the VTC). Expressed in posterior optic chiasm.	projection in majority of embryos. Stalling and misrouting guidance defects also observed. Disrupted chiasm shape (Herrera et al., 2004).
Islet-2 LIM-homeodomain transcription factor expressed by ~ 40% contralateral RGCs.	*Islet-2* null mice: Increased ipsilateral projection from more ipsilateral RGCs confined to VTC (Pak et al., 2004).
Nr-CAM Cell adhesion molecule expressed solely by contralateral RGCs.	*Nr-CAM* null mice: Increased ipsilateral projection from more ipsilateral RGCs in VT retina at late stages only (E18.5). (Williams et al., 2006).
Vax1 Homeodomain transcription factor expressed in the optic stalk and ventral hypothalamic midline.	*Vax1* null mice: No chiasm. Axons stall and form whorls in the hypothalamus (Bertuzzi et al., 1999).
Vax2 Homeodomain transcription factor expressed in the ventral retina.	*Vax2* null mice: Variable results in two different papers despite deleting the same portion of the Vax2 gene on the same genetic background. (1) Greatly reduced ipsilateral projection (Barbieri et al., 2002).

	(2) Normal or abnormally large ipsilateral projection (Mui et al., 2002).
Pax-2 Expressed by optic stalk and midline neuroepithelium from E11.	Increased ipsilateral projection in *Pax-2* null mice (Torres et al., 1996). Note: *Pax2* overexpression in neural tube of chick embryos (Thanos et al., 2004) and zebrafish *noi* mutants (Macdonald et al., 1997) caused a variety of chiasm abnormalities: increased ipsilateral routing, axon stalling, disturbances in axon crossing.
Brn3b POU-domain transcription factor expressed postmitotically in RGCs.	*Brn3b* null mice: Increased proportion of ipsilateral projections.
CD44 Cell surface carbohydrate moiety expressed by early-differentiating neurons in the ventral diencephalon.	*In vitro* brain slice culture: Reduced ipsilateral projection at E15 only (anti-CD44 antibodies applied at E15). Reduced contralateral projection at E13 only (Lin et al., 2005).
Chondroitin sulphate proteoglycans	*In vitro* brain slice culture: Absent ipsilateral projection at E14 and reduced ipsilateral

Expressed by early-differentiating neurons in the ventral diencephalon.	projection at E15 following enzymatic removal of chondroitin sulphate (Chung et al., 2000b). *In vitro*, chondroitin sulphate inhibits axons from VT retinal explants only (Cheung et al., 2005).
Shh Expressed by RGCs from E12 and in the ventral diencephalon anterior and posterior to axons.	Inhibition of chick retinal axon outgrowth (Trousse et al., 2001). Anti-Shh antibody treatment in E13 brain slice cultures: fewer contralateral retinal axons. At E15: increased ipsilateral projection (Hao et al., 2006).
Tyrosinase Key enzyme in melanin synthesis pathway. Mutated in albino mammals.	Albino mice: reduced ipsilateral projection from fewer, more peripheral VT RGCs. A greater proportion of RGCs in VTC project contralaterally (Marcus et al., 1996b). Non-mammalian albinos (frogs) have normal ipsilateral projections (Grant and Binns, 2003).

Figure 2. Molecules affecting the ipsilateral projection

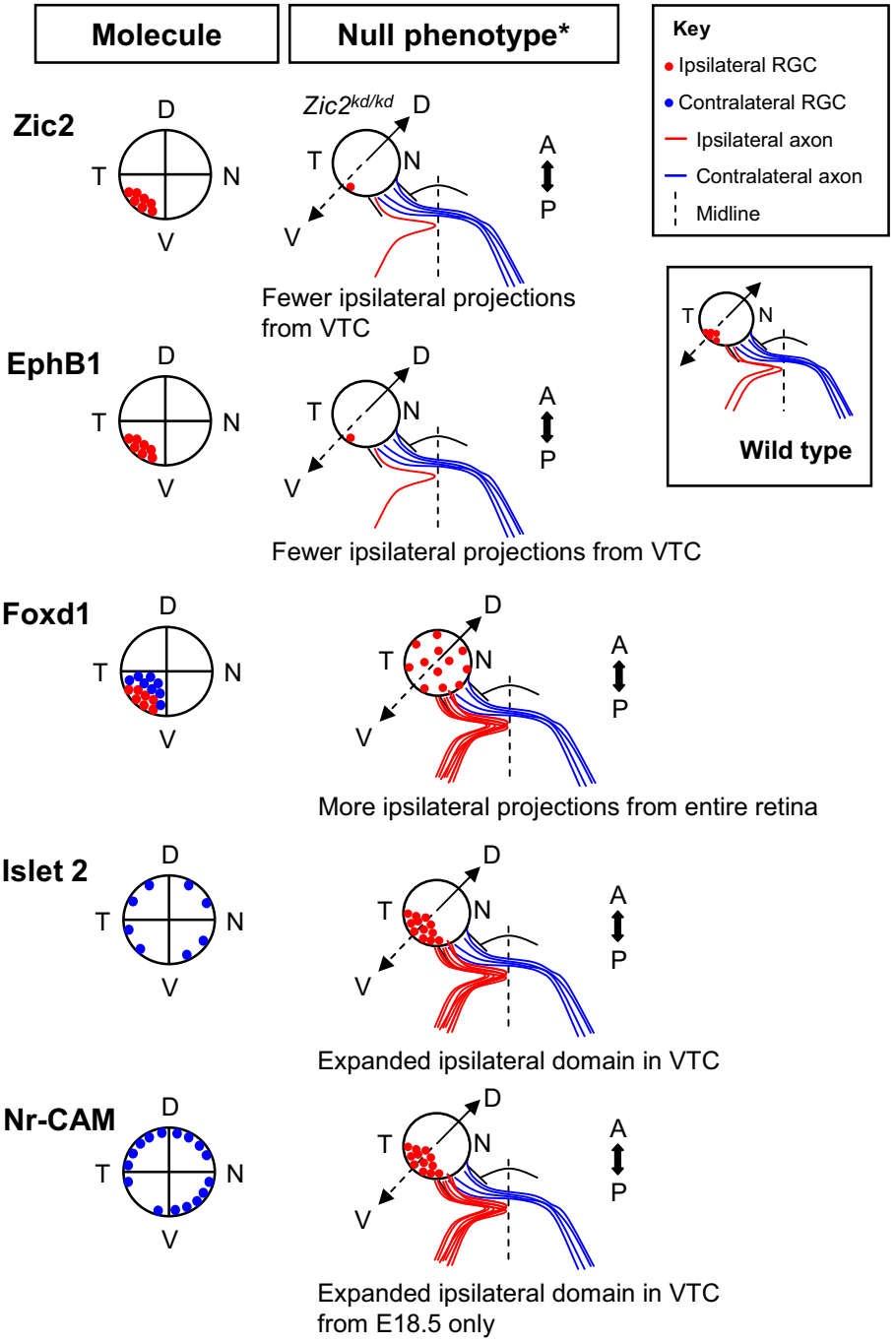

* Note that Zic2 null mice die at birth. The phenotype shown is that of a *Zic2*$^{kd/kd}$.

1.6.1. Zic2 and EphB1 in the ventrotemporal crescent.

The 'ventrotemporal crescent' (VTC) is the peripheral VT region of the retina from which ipsilateral RGCs and their axons arise. In the past decade, the transcription factor Zic2 was identified by *in vivo* and *in vitro* studies as an ipsilateral determinant that is expressed by VT RGCs that project ipsilaterally at the chiasm (Herrera et al., 2003). Zic2 is thought to mediate its effects via the VT-restricted expression of EphB1 that is repelled by ephrin-B2-expressing midline radial glia at the chiasm (Herrera et al., 2003; Williams et al., 2003). Although Zic2 is also expressed around the optic chiasm, the addition or removal of Zic2 from RGCs *in vitro* provided strong evidence that it influences the ipsilateral projection autonomously from within RGCs (Herrera et al., 2003).

1.6.2. Molecules associated with contralateral projections.

The cell adhesion molecule Nr-CAM, is expressed by RGCs that project contralaterally and its retinal expression mirrors the spatiotemporal changes in the origins of contralateral axons that occur throughout all stages of chiasm development. For instance, from E14 - E16, Nr-CAM is found in the entire retina apart from the VT Zic2-expressing region from E14 – 16 (Williams et al., 2006) but at later stages when all new RGCs project contralaterally, Nr-CAM is expressed in the entire retina including the VTC. Interestingly, *Nr-CAM* null mice display an increased ipsilateral projection specifically from more ipsilateral RGCs in the VT retina at E18.5 but not at earlier embryonic ages (Williams et al., 2006). Combined with *in vitro* findings that Nr-CAM mediates contralateral behaviour from within RGCs, the authors concluded that Nr-CAM promotes the crossing of contralateral RGC axons from the VTC only at late stages in chiasm formation. However, the functions of Nr-CAM protein in retinal axons and at the optic chiasm, where it is expressed in a high anterior to low posterior gradient, remain to be elucidated.

Another gene associated with the crossing of axons is the LIM-homeodomain transcription factor Islet-2 (Pak et al., 2004). Islet-2 (Isl2) is expressed by only a subset of contralateral RGCs with reduced expression in the VTC of the retina (Pak et al., 2004). In the VTC, Isl2-expressing RGCs are thought to suppress Zic2 and EphB1 expression, allowing them to project contralaterally.

Considering molecules at the chiasm, anti-CD44 and anti-Shh antibodies produced fewer contralateral retinal axons at the chiasm midline in slice cultures of the E13 brain (Lin et al., 2005; Hao et al., 2006), implying that CD44 and Shh normally promote the crossing of early axons. Interestingly, the same anti-Shh antibody treatment had no effect at E14 but at E15 the number of ipsilateral axons increased (Hao et al., 2006). The behaviour of E15 retinal axons to the removal of CD44 also changed but showed a reduction in the ipsilateral projection (Lin et al., 2005). These results suggest that CD44 and Shh have different effects on retinal axons depending on the developmental age. Interestingly, a previous study reported a general growth-inhibitory influence for Shh on chick retinal axons (Trousse et al., 2001) and the differences between these results and those of Hao et al. (2006) could be attributed to different *in vitro* experimental conditions. In support of this, the influence of Shh on retinal axons depends on its precise molecular interactions. For instance, Shh secreted from the floor plate acts as a chemoattractant for commissural spinal cord axons in the presence of Netrin-1 (Charron et al., 2003).

1.6.3. Genetic control of axon guidance.

Although recent studies have made substantial progress in identifying the molecules directing retinal axons at the optic chiasm, the genes responsible for regulating the expression of receptors on contralateral and ipsilateral axons and for determining how retinal axons interact and respond to these guidance cues is less well understood. Over the past decade, it has emerged that the distribution of axon guidance molecules and

hence axon paths correlate with domains of regulatory gene expression in zebrafish (Macdonald et al., 1994) and also in the mouse (Mastick et al., 1997; Tole and Patterson, 1995). These expression boundaries outline areas that are inhibitory to axons with the consequence that axons are funneled along appropriate routes that are permissive to growth.

Transcription factors, such as Foxg1, Foxd1, Zic2 and Isl2 exert their effects by activating or repressing downstream genes, which may in turn influence growth cone navigation cell-autonomously or cell-non-autonomously by regulating the expression of cell surface or diffusible molecules that act as pathway-derived guidance cues. It follows that the misexpression of certain regulatory genes (some examples are shown in Table 1) can lead to axon misrouting and this premise is supported by both *in vitro* and *in vivo* experiments (Herrera et al., 2004; Lin et al., 2005; Marcus et al., 1995; Pratt et al., 2002; Pratt et al., 2004; Sretavan et al., 1994). Recently, fascinating developments have revealed that transcription factors, such as Engrailed-2, Pax6 and Foxg1, multitask in their regulation of tissue morphogenesis in the developing embryonic brain as well as axon guidance (Brunet et al., 2005; Pratt et al., 2002; Pratt et al., 2004; Pratt et al., 2000).

This thesis will explore the influence of the forkhead box transcription factor *Foxg1* on retinal axon divergence at the optic chiasm based on previous observations in this laboratory of axon guidance defects in the retinotectal and thalamocortical tracts (Pratt et al., 2002, 2004).

1.7. Foxg1 (formerly known as *Brain Factor-1* [*BF-1*]) is a forkhead box transcription factor.

1.7.1. Overview of forkhead genes.

The *fork head* gene was first discovered in Drosophila (Weigel et al., 1989) and was found to encode a 'forkhead box' DNA binding domain that consists of 110 amino acids (Weigel and Jackle, 1990). Over the past two decades, *forkhead* genes have been identified across a wide range of phyla, forming a family of Forkhead box (Fox) transcription factors, whose members share the evolutionarily conserved Fox DNA binding domain (Carlsson and Mahlapuu, 2002). The forkhead transcription factors are also known as 'winged helix' transcription factors due to the butterfly-like structure of the loops (or 'wings') connecting the beta strands flanking one of the three alpha helices (Clark et al., 1993). The Fox DNA binding domain is highly conserved across species from *Drosophila* to mammals and chromosomal and phylogenetic analyses are suggestive of inter- and intra-chromosomal duplications (Lehmann et al., 2000; Lehmann et al., 2003). The Fox DNA binding domain binds specific DNA sequences, suggestive of a role for Fox proteins in transcriptional regulation (reviewed in Carlsson and Mahlapuu, 2002). Fox genes are expressed in a tightly regulated manner during development where they are involved in the formation of many different organs (Carlsson and Mahlapuu, 2002).

Foxg1 belongs to the *Fox* gene family and was found by its homology to the vertebrate *FoxA* subfamily (formerly known as hepatocyte nuclear factors (HNF3)) (Tao and Lai, 1992). There is strong *in vitro* evidence to show that Foxg1 acts as a transcriptional repressor by forming a complex with the Groucho transcriptional corepressors TLE and Hes that lack DNA-binding ability by themselves and also histone deacetylases to regulate expression of cell cycle inhibitors of the Cip/Kip family (Castella et al., 2000; Hardcastle and Papalopulu, 2000; Yao et al., 2001).

1.7.2. Expression of Foxg1 in the developing brain.

In vertebrates from *Xenopus* to humans, *Foxg1* displays a highly conserved pattern of expression in the anterior central nervous system (CNS) (Bourguignon et al., 1998; Murphy et al., 1994). *Foxg1* is first expressed at the 1-3 somite stage in developing mouse embryos in the anterior neural ridge (ANR) located in the anterior non-neural ectoderm (Dou et al., 1999). Between somite stages 5 - 8, Foxg1 expression spreads from the anterior neural plate rostrally to areas that eventually form the telencephalon, its derivatives and anterior eye structures (Dou et al., 1999; Shimamura et al., 1995). *Foxg1* expression is mainly restricted to anterior regions of the mouse forebrain: in the telencephalic neuroepithelial progenitors (Tao & Lai 1992), the nasal portion of the retina and optic stalk, the anterior hypothalamus and superior colliculus (Hatini et al., 1994; Xuan et al., 1995).

1.7.3. *Foxg1* null embryos exhibit forebrain defects.

Foxg1 is required for normal development of the forebrain and eyes, since the morphology of these structures is affected in *Foxg1*$^{-/-}$ embryos (Hanashima et al., 2004; Hanashima et al., 2002; Hatini et al., 1994; Huh et al., 1999; Xuan et al., 1995). The olfactory bulbs, nasal placodes and resulting nasal epithelium also fail to grow properly, whereas the otic vesicle, pharyngeal pouches and Rathke's pouch and their derivatives (inner ear, anterior foregut and the pituitary) appear unchanged from the wild type (Xuan et al., 1995).

One of the most noticeable abnormalities in *Foxg1* null mice is severe hypoplasia of the cerebral hemispheres (Dou et al, 1999). This hypoplasia appears to be caused by reduced proliferation and premature differentiation of telencephalic neuroepithelial cells between E10 and E18, reducing the size of the neural progenitor precursor pool (Hanashima et al., 2002; Martynoga et al., 2005; Takahashi et al., 1993; Xuan et al.,

1995). Recent *in vitro* and *in vivo* evidence has revealed that Foxg1 regulates cell cycle progression via transcriptional repression of the cell cycle inhibitor *p21Cip1* in telencephalic neuroepithelial cells leading to inhibition of TGF-beta-mediated cytostasis (Dou et al., 2000; Seoane, 2004). Therefore, *Foxg1* normally prevents premature growth arrest in telencephalic progenitor cells. Not surprisingly, deregulation of *Foxg1* has been associated with tumour growth. For example, the chick homologue of Foxg1, *qin*, was discovered as an oncogene (Li et al., 1997), and recently an increase in *FOXG1* copy number was linked to medulloblastoma brain tumours in humans (Adesina et al., 2007).

In addition to cerebral hemisphere hypoplasia, the ventral telencephalon of *Foxg1* null embryos is never specified (Dou et al., 1999), signified by the absence of ventral telencephalic markers Nkx2.1, Mash1 and Olig2 and expression of the dorsally-restricted telencephalic marker Pax6 in the entire mutant telencephalon from very early stages in development (Martynoga et al., 2005). Although, it was previously proposed that the inability of *Foxg1* mutants to specify ventral telencephalic tissue was due to loss of Shh from the ventral telencephalon (Huh et al., 1999), recent *in vivo* work in this laboratory suggests that *Foxg1* is required cell autonomously for the specification of the ventral telencephalon (Martynoga, unpublished).

1.7.4. Morphogenesis of the *Foxg1*$^{-/-}$ eye is affected.

Foxg1 and *Foxd1* (formerly *BF-2*) are among the first factors to be expressed in the nasal (*Foxg1*) and temporal (*Foxd1*) neuroretina and they also define the anterior and posterior chiasm region (Hatini et al., 1994; Yuasa et al., 1996). Consequently, *Foxd1* and *Foxg1* are thought to be responsible for establishing the nasal-temporal (or anterior-posterior) axis in the retina (Figure 3). Supportive evidence comes from the misexpression of Foxg1 in the temporal retina, which induces ephrin-A2/A5 expression (Takahashi et al., 2003).

Figure 3. *Foxg1* and *Foxd1* expression in the retina and chiasm

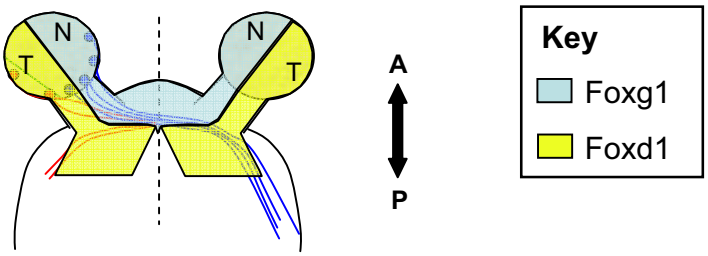

A schematic diagram looking down on a horizontal slice of the brain at the level of the optic chiasm. The mutually exclusive expression patterns of *Foxg1* (blue) and *Foxd1* (yellow) in the retina and chiasm region are marked. Contralateral RGC axons (blue lines) and ipsilateral RGC axons (red lines) are shown in relation to these expression domains. *Foxg1* is expressed in the nasal retina and optic stalk and the anterior optic chiasm region, including the midline where axons diverge. *Foxd1* is expressed in the temporal retina and optic stalk and it is absent from the midline. From E14.5, *Foxd1* expression is more limited to the VT retinal quadrant rather than the whole temporal retina (Herrera et al., 2004).

Furthermore, reversing the normal expression domains of *Foxd1* and *Foxg1* across the nasotemporal axis of the chick optic vesicle produces a disturbance in the retinotectal projection (Yuasa et al., 1996).

In addition to a putative role in retinal patterning, Foxg1 is also required for the normal morphogenesis of the eye (Hatini et al., 1994; Xuan et al., 1995; Huh et al., 1999). In *Foxg1* null embryos, the initial evagination of the optic vesicle occurs normally and eye defects first appear at E10.5 (Huh et al., 1999). *Foxg1*$^{-/-}$ embryos display abnormally-shaped eyes with a medially-elongated retina and retinal pigment epithelium (RPE), an abnormally small, misshapen lens and no optic stalks, such that the mutant retina contacts the ventral hypothalamus directly (Xuan et al., 1995; Huh et al., 1999). The elongated retina folds abnormally and this is most obvious in nasal regions (Xuan et al., 1995). The choroid fissure fails to close forming a ventral coloboma and is associated with an expansion of the optic vesicle proximally and the RPE failing to completely surround the optic cup in ventral and medial regions (Huh et al., 1999). The coloboma forms a channel that varies in width during development and between embryos, leaving the ventral optic cup open (Huh et al., 1999). *Foxg1*$^{-/-}$ embryos lack optic stalks and this is associated with reduced Pax2 expression and its restriction to the medial optic neuroepithelium and also the expansion of markers of the neural retina as well as the transcription factor Pax6. These all suggest that the absence of *Foxg1* favours the specification of a retinal fate rather than an optic stalk fate. These eye defects may be partly due to the absence of a ventral telencephalic supply of Shh in *Foxg1* null embryos (Huh et al., 1999). However, Shh ventral midline expression, which mediates proximodistal and dorsoventral eye patterning via regulation of *Pax* and *Vax* expression (Ekker et al., 1995; Lupo et al., 2005; Macdonald et al., 1995) is maintained in the absence of *Foxg1 in vivo* (Huh et al., 1999).

1.7.5. *Foxg1*$^{-/-}$ embryos display an increased ipsilateral projection.

The expression of Foxg1 in the source (RGCs), intermediate choice point (optic chiasm midline) and target (superior colliculi) cells of retinal axons in the retinotectal tract makes this transcription factor an ideal candidate for mediating axon guidance in the developing visual system. Recent work in this laboratory aimed to test whether *Foxg1* plays a role in axon guidance during mouse development. Mice in which the *Foxg1* coding sequences were replaced with either *cre recombinase* (Hebert and McConnell, 2000) or *LacZ* (Xuan et al., 1995) were used for anterograde tracing of retinal axons using the fluorescent dye dioctadecyltetramethylindocarbocyanine perchlorate (DiI). Surprisingly, despite abnormal development of the telencephalon and eyes of *Foxg1*$^{-/-}$ embryos, RGC axons were able to project from both eyes, cross at the optic chiasm, and reach thalamic targets as in wild type mice. However, a small proportion of retinal axons were misrouted from the optic tracts into the telencephalon, from which they are normally excluded (Pratt et al, 2002). Further investigation revealed that retinal axons from *Foxg1* null mice show a substantial increase in ipsilaterally projecting axons arising from both nasal and temporal RGCs (see Figure 4) (Pratt et al., 2004). The presence of a chiasm in *Foxg1* mutants suggests that the cause of the RGC pathfinding defect is more subtle than a complete loss of the crossed or uncrossed tract as previously described in *Pax2* and *Vax2* null mutants (Torres et al., 1996; Barbieri et al., 2002) or agenesis of the chiasm (Williams et al., 1994). Despite abnormal development of the eyes and forebrain, *Foxg1*$^{-/-}$ embryos exhibit a specific axon guidance defect, offering a tractable system with which to dissect the molecular mechanisms involved in the sorting of contralateral-ipsilateral retinal axons at the chiasm.

Figure 4. *Foxg1* null embryos display an increased ipsilateral projection

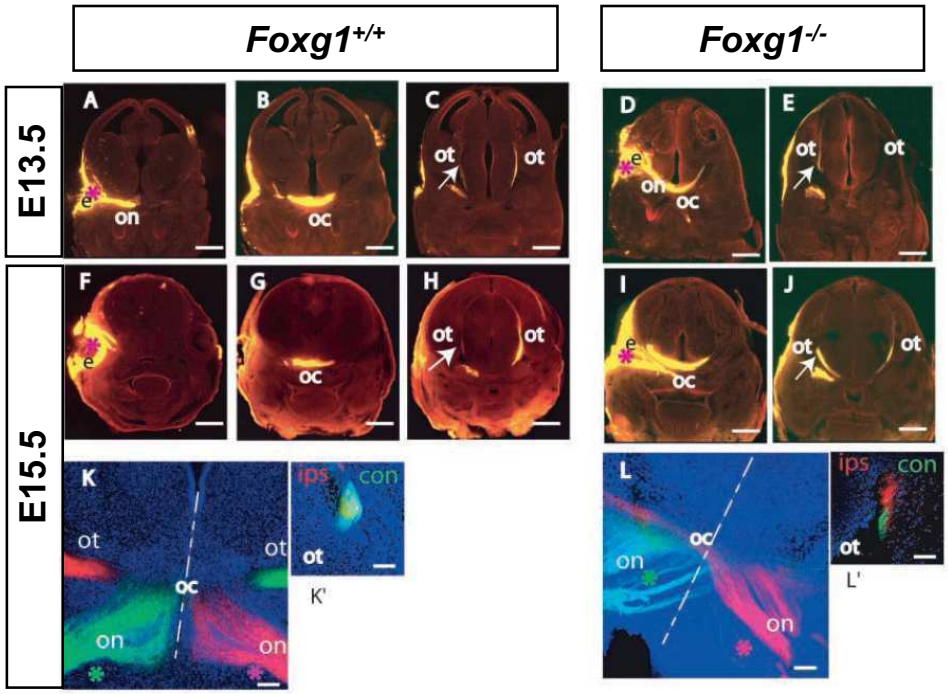

Figure from Pratt et al., 2004

RGC axon navigation in wild-type and *Foxg1*$^{-/-}$ embryos visualised by anterograde tract tracing at (A-E) E13.5 and (F-L) E15.5. For each age progressively more caudal sections of an individual embryo show injections of DiI (red asterisks) in (A, F) wild type retina and (D, I) *Foxg1*$^{-/-}$ retina, (B, G, D, I) labelling of optic nerve (on) and optic chiasm (oc) and (C, H, E, J) labelling of optic tracts (ot). (C, H) In the wild-type optic tracts, contralateral labelling is stronger than the ipsilateral labelling. (E, J) In the *Foxg1*$^{-/-}$ optic tracts, ipsilateral labelling appears stronger. (K, L) Double labelling experiments in which DiI was injected into one eye and DiA into the other eye of (K) an E15.5 wild type embryo and (L) an E15.5 *Foxg1*$^{-/-}$ embryo (ventral midline is marked by broken white line). (K', K'') Horizontal sections of the wild-type optic tracts, growing over the diencephalon, from the same embryo as in K showing that each optic tract is predominantly labelled with dye from the contralateral eye although some ipsilateral label is also detectable (appears yellow where dyes overlap). (L', L'') Horizontal sections of the *Foxg1*$^{-/-}$ optic tracts from the same embryo as in L showing abnormally high levels of label from the ipsilateral eye. Scale bars: A-E, 500µm; F-J, 650µm; K,L, 100µm.

1.8. AIMS

Foxg1 is expressed by many structures that projecting retinal axons encounter as they make their way to the optic chiasm, making it possible for Foxg1 to control growth cone navigation directly or indirectly, at any one or a combination of locations. Therefore, there are two important questions that this thesis aimed to address: (1) at which location(s) along the retinotectal pathway is Foxg1 required and (2) what type of mechanism is responsible for increasing the ipsilateral projection in *Foxg1* null embryos?

There are two main hypotheses regarding the location at which Foxg1 is primarily required for retinal axon guidance at the chiasm: -

(1) *Foxg1* expression in the retina is required for the correct navigation of RGC axons at the optic chiasm by determining their response to cells and molecules encountered along their route and at the chiasm midline.

(2) *Foxg1*-expressing cells at the optic chiasm may influence the ipsilateral-contralateral ratio of RGC axons by regulating the expression of axon guidance cues around the midline or providing appropriate contacts between growth cones and surrounding cells.

In order to distinguish between these two hypotheses, *in vitro* co-cultures consisting of wild type ↔ *Foxg1*$^{-/-}$ dorsonasal (source of contralateral axons) or ventrotemporal (source of ipsilateral axons) retinal explants and optic chiasm cells were used to identify whether *Foxg1* is primarily required in cells of the retina or chiasm for retinal axon divergence (Chapter 3).

Based on the co-culture findings, a candidate approach was then used to generate testable hypotheses about putative Foxg1 downstream effectors in order to elucidate the mechanism(s) by which Foxg1 influences the size of the ipsilateral projection. The expression patterns of regulatory genes and molecules known or suspected to affect axon guidance from within the eye (Chapters 4 and 5) and at the optic chiasm (Chapter 6) were investigated.

Since the position of progenitor cells in the developing retina determines whether they will differentiate into nasal, temporal, dorsal or ventral neurons and hence influence their axonal paths and final termination zones in the tectum (Dutting and Meyer, 1995; Dutting and Thanos, 1995), molecules involved in patterning the retina along the nasotemporal and dorsoventral axes were examined in *Foxg1*$^{-/-}$ and wild type embryos (Chapter 5).

Finally the expression pattern of Foxg1 protein was investigated using immunohistochemistry to examine whether its location mirrored *Foxg1* mRNA expression and whether it is found in axons (Chapter 7).

CHAPTER 2: Materials and Methods

More detailed materials and methods are included in the 'Methods' section for each individual Chapter.

2.1. Animals and *Foxg1* alleles.

All mice were housed and cared for under Home Office regulations. *Foxg1* heterozygous mice ($Foxg1^{+/-}$) are viable and were maintained by breeding pairs consisting of one wild type and one $Foxg1^{+/-}$ mouse.

To identify cells in which the *Foxg1* locus is transcriptionally active, we exploited the $Foxg1^{tm1M}$ (or $Foxg1^{lacZ}$) allele in which coding sequences are replaced by a *lacZ* cassette (Xuan et al., 1995). For lineage tracing, we used the $Foxg1^{tm1(cre)Skm}$ (or $Foxg1^{Cre}$) allele in which coding sequences are replaced by a Cre recombinase cassette (Hebert and McConnell, 2000). $Foxg1^{Cre}$ and $Foxg1^{lacZ}$ are predicted null alleles (Xuan et al., 1995; Hebert and McConnell, 2000). For lineage tracing, we used *Gtrosa26tm1Sho* (*R26RS*) reporter mice (Mao et al., 1999). Cre-mediated recombination in $Foxg1^{Cre}$;*R26RS* embryos irreversibly activates *lacZ* expression from the *ROSA26* locus (Mao et al., 1999; Hebert and McConnell, 2000). Lineage tracing experiments used the $Foxg1^{Cre}$ allele on an albino Swiss Webster background (as described by Hebert and McConnell, 2000). Other experiments used $Foxg1^{Cre}$ and/or $Foxg1^{lacZ}$ alleles on a mixed pigmented CBA/C57Bl6/Swiss Webster background. *Foxg1* homozygous mutants ($Foxg1^{Cre/Cre}$) and compound heterozygotes ($Foxg1^{Cre/lacZ}$) were identified by their hypoplastic telencephalon and distorted eyes. Heterozygous embryos (i.e. $Foxg1^{+/-}$) were identified by PCR genotyping, they were indistinguishable morphologically from wild type (Xuan et al., 1995; Huh et al., 1999) and we detected no RGC axon projection defects at the optic chiasm.

2.1.1. Mouse Genomic DNA Extraction.

1.Mouse tail tips (approx 0.5cm long) or ear clips (1 to 4 clips) or embryo hind quarters (1) digested overnight in 500µl tail tip lysis buffer (TTLB) containing 100µg/ml Proteinase K (Sigma).

2. Mix with 500µl PCIA (phenol: chloroform: isoamyl alcohol 50:49:1) for 20 minutes and centrifuge at 13K for 5 minutes. Remove the upper aqueous layer to a fresh tube (only recover 100 µl to 200 µl if interface viscous).

3.Add 1/10 volumes of sodium acetate pH5.5 and 2 volumes of 96% ethanol to the recovered aqueous portion. Mix until DNA strands visible. Spin 13K for 5 minutes and remove supernatant.

4.Wash pellet with 500µl 70% ethanol. Spin 13K for 1 minute and remove supernatant. Dry pellet for about 30 minutes at 37^{o}C.

5.Dissolve in 100µl ddH_20 with shaking overnight at 37^{o}C.

6.Use 1µl of DNA for subsequent PCR reactions.

Tail tip lysis buffer (TTLB)

200mM Tris pH8, 200mM NaCl, 5mM EDTA, 0.2% SDS

(Make up without SDS, autoclave, then add SDS)

2.1.2. Polymerase Chain Reaction (PCR) genotyping of *Foxg1* alleles.

Allele	Forward 5' Primer	Reverse 3' Primer	Product Size (bp)
Foxg1	5'-CTG ACG CTC AAT GGC ATC TA-3'	5'-TTT GAG TCA ACA CGG AGC TG-3'	438
Foxg1^{lacZ}	5'-TTG AAC TGC CTG AAC TAC CG-3'	5'-CCT GAC TGG CGG TTA AAT TG-3'	250
Foxg1^{Cre}	5'-CAT TTG GGC CAG CTA AAC AT-3'	5'-ATT CTC CCA CCG TCA GTAC G-3'	307

For all primers, cycling conditions were as follows: -

96°C for 2 minutes

[96°C for 30 seconds, 58.5°C for 30 seconds and 72°C for 30 seconds] for 35 cycles.

2.1.3. PCR Reaction Mix.

The following reaction mix was used for detection of all *Foxg1* alleles (see above).

Prepare 19µl mastermix per sample and prepare enough for *n*+1 samples.

2µl 10X Reaction Buffer (including 15mM $MgCl_2$)

1µl 5' Primer (10µM)

1µl 3' Primer (10µM)

0.4µl dNTP mix (Promega)

1µl DNA

0.2µl Taq Polymerase (1 unit)

14.4µl ddH_20

2.1.4. Agarose Gel Electrophoresis.

1) Prepare an agarose (Sigma) solution

1.5% agarose (for DNA fragments <600bp): 75g agarose in 50ml 1X TBE

2) Microwave on full power for 3 minutes, replacing evaporation losses with ddH_20

3) Add 1µl ethidium bromide (Fisher Scientific) at 10µg/ml, mix gently

4) Pour into a gel casting tray, immediately insert comb

5) Allow to set for 30 minutes

6) Prepare sample DNA by adding 2µl 10X loading buffer per 20µl PCR reaction

7) Load 10µl sample per well

8) Load 10µl (0.5µg) of DNA molecular weight marker XIV (Roche) in one well

9) Run gels at 80V for ~ 30 minutes, or until bands have resolved

10) Visualise by exposure to UV light

Molecular weight ladders: -
DNA molecular weight marker: for fragments <600bp

Working dilutions:
5µl DNA molecular weight marker
6µl 10X gel loading buffer
49µl ddH_20

2.2. Histology.

2.2.1. Fixation of Brain Tissue.

Following decapitation, embryonic heads were submerged in a solution of 4% paraformaldehyde in 1XPBS for 2 - 16 hours at 4°C with agitation. The heads were then washed with 1XPBS and either (1) dehydrated through a series of increasingly-concentrated ethanol solutions prior to embedding in paraffin wax, carried out using an automated tissue processor (Tissue-Tek VIP, Sakura) or (2) in the case of frozen sections, heads were placed in a 30% sucrose:PBS solution for cryoprotection and left overnight at 4°C with agitation until the heads sank. Heads were placed in OCT (Lamb), positioned in the horizontal, coronal or sagittal plane, frozen on dry ice and then stored at -80°C.

2.2.2. Microtome Sectioning of Wax Sections.

Wax-embedded heads were cut into 10µm-thick sections on a microtome (Reichert-Jung 2050) and sections floated onto poly-l-lysine (Sigma) slides. Sections were left to dry at 37°C for at least one hour prior to immunohistochemistry or haematoxylin and eosin staining.

2.2.3. Cryostat Sectioning.

Heads for cryostat sectioning were removed from storage at -80°C and equilibriated at -20°C to -26°C for one hour in the cryostat. 10µm-thick sections were cut on the cryostat and collected onto Superfrost Plus (BDH) slides. All sections were air-dried prior to storage at -80°C with a dessicant until use. Prior to immunohistochemistry, slides were thawed thoroughly at room temperature in their slide box.

2.3. Immunohistochemistry.

See individual chapters for detailed protocols for different antibodies.

2.3.1. Chromogenic endpoint.

A chromogenic endpoint was generally applied to wax sections. Sections were dewaxed in xylene and rehydrated through a series of solutions of descending ethanol concentration to water. Endogenous peroxidise activity was eliminated through incubation in dilute hydrogen peroxide solution. DNA was denatured and antigens unmasked by heat treatment in 10mM sodium citrate (pH6) in a microwave oven. Evaporation losses were replaced and slides cooled for at least 45 minutes prior to washing in 1XPBS. Blocking solutions varied according to the primary antibody used but generally contained 5 - 10% goat serum (NGS) in PBS with 0.1% Triton-X-100 (Sigma). Following incubation with the primary antibody, slides were washed 3X with 1XPBS followed by incubation with species-specific HRP-conjugated secondary antibodies for 1 hour at room temperature using a Envision^{+} Kit (Dako). Following several washes in 1XPBS, antibody staining was revealed using 3,3'-diaminobenzidine (DAB), which produces a brown precipitate. Slides were dehydrated through increasing concentrations of ethanol, cleared in two changes of xylene and then mounted under coverslips in DPX (BDH).

2.3.2. Fluorescent endpoint.

Immunofluorescence was performed as for those slides reacted with DAB except that dewaxing and rehydration steps did not need to be performed. Following incubation with the primary antibody, species-specific secondary antibodies conjugated to fluorescent molecules were used at 1:200 dilution: goat anti-mouse or goat anti-rabbit Alexafluor-488 or Alexafluor-568 (Molecular Probes). For double immunohistochemistry to detect two different primary antibodies, primary antibodies from two different species were chosen to avoid cross-reactivity and incubated together. This was followed by detection using Alexafluor-488 and -568 secondary antibodies. Nuclei were counterstained using the DNA dye TO-PRO-3 iodide (Molecular Probes) at 1:100 dilution in water. Sections were mounted under coverslips using Mowiol (see below) to prevent fading of fluorescence.

2.4. Preparation of Mowiol Mounting Medium.

This mountant solidifies once used and allows direct mounting of the coverslips onto glass slides. Once mounted, the coverslips can be viewed with immersion lenses as the coverslips will not move. The coverslips are also removeable by gently sliding off the side of the slide, using tweezers. The Mowiol can be removed by immersing the coverslips in ddH_20 for a few minutes.

1. Add 2.4g Mowiol (Calbiochem Cat no 475904) to
6g of Glycerol (Glycerol density =1.26g/ml – for 6g = 6/1.26 = 4.76mls)
(in a 50ml conical flask).

2. Stir with a pipette to mix.

3. Add 12ml dH_20 and leave stirring for several hours or overnight at room temperature.

4. Add 12ml 0.2M Tris (pH8.5)
(1M Tris = 121.14 g/l, 100nM = 12.114g/l
200nM = 24.228g/l or 2.423g/100ml)
and heat to 50°C for 1 – 2 hr or until Mowiol is completely dissolved.
Vortex occasionally.

5. Centrifuge at 2000rpm for 15 minutes.

6. Add 1,4-diazobicyclooctane (DABCO) Sigma(Antifade) to 2.5% (=0.72g)
Aliquot and store at -20°C.

7. Centrifuge before use to pull down any bubbles.

2.5. Microscopy.

2.5.1. Light Microscopy.

Slides were photographed using a Leica DMLB upright compound microscope connected to a Leica DSC480 digital camera, using Leica IM50 image management software.

2.5.2. Confocal Microscopy.

Fluorescent staining was viewed using a Leica DMRE compound microscope, part of a Leica TCS NT confocal system using 'Leica Lite' software. To view the co-cultures in 3D, a Zeiss Axiovert confocal microscope was used and viewed using the 'LSM Image Browser'. Alexafluor-488 staining was collected in the FITC (green) channel, Alexafluor-568 in the TRITC (red) channel and TO-PRO-3 in the Cy3 (far-red, pseudo-coloured blue) channel.

2.5.3. Image Analysis.

Some images were re-sized or cropped with Adobe Photoshop 7 software. When the brightness or contrast or images was adjusted to enhance detail, the changes were applied globally to the whole image.

2.6. Statistical Analysis.

Sigmastat (Systat Software Inc.) and Excel (Microsoft) were used for data analysis.

2.7. Staining for Bacterial LacZ (β-galactosidase).

2.7.1. Reagents.

LacZ Fixative (volumes for making 20ml)

4% paraformaldehyde in PBS	20ml
0.02% NP40	40µl of 10% stock
0.01% sodium deoxycholate	20µl of 10% stock
5mM EGTA	200µl of 0.5M stock
2mM $MgCl_2$	40µl of 1M stock

LacZ Wash (volumes for 100ml)

PBS	100ml
2mM $MgCl_2$	200µl of 1M stock
0.02% NP40	200µl of 10% stock
0.01% sodium deoxycholate	100µl of 10% stock

LacZ staining buffer (volumes for 10 ml)

PBS	10ml
2mM MgCl2	20µl of 1M stock
0.02% NP40	20µl of 10% stock
0.01% sodium deoxycholate	10µl of 10% stock
5mM Potassium ferricyanide	100µl of 0.5M stock
5mM Potassium ferrocyanide	100µl of 0.5M stock
1mg/ml X-gal	250µl of 40mg/ml stock in dimethylformamide (DMF) (kept in freezer).

LacZ stop solution (20mM EDTA in PBS)

20ml PBS + 800µl 0.5M EDTA

LacZ post-fix (2% Glutaraldehyde in PBS).

20ml PBS + 800µl 50% Glutaraldehyde.

2.7.2. Protocol.

All steps performed using a 20ml volume, except staining, which was performed in a 5ml volume.

1. Dissect embryos in ice cold PBS.
2. Fix with shaking at 4°C for 1 hour in LacZ Fixative
3. Wash 3 x 20 minutes (minimum) at room temperature shaking in LacZ Wash.
4. Stain in X-Gal at 37°C with shaking 1 hr to overnight (or longer) in the dark.
5. Wash in LacZ Stop Solution.
6. Postfix in LacZ postfix solution.
7. If cutting sections transfer to 50% ethanol and proceed with wax embedding [X-gal product leaches in organic solvents but persists].

E14.5 *Foxg* $^{lacZ/+}$ and *Foxg1* $^{lacZ/Cre}$ embryonic heads were dissected and fixed for 1 hour at 4°C in 4% paraformaldehyde, 0.02% NP40, 0.01% sodium deoxycholate, 5 mM EGTA, 2mM $MgCl_2$ in phosphate buffered saline (PBS). In some cases, heads were equilibrated in 30% sucrose/PBS and sectioned (10 mm) on a cryostat. Tissues were rinsed several times in wash buffer (2 mM $MgCl_2$, 0.02% NP40, 0.01% sodium deoxycholate in PBS), transferred to staining solution (wash buffer supplemented with 5 mM potassium ferricyanide, 5 mM potassium ferrocyanide and 1 mg/ml X-gal), and stained overnight (cryostat sections on slides) or for 2 days with agitation (wholemounts) at 37°C in darkness. Staining was stopped with 20 mM EDTA in PBS. Some wholemounts were sectioned with a vibratome (200 µm) or processed to wax, sectioned (10 µm) and mounted. Cryostat sections were counterstained with Nuclear Fast Red (Fisher).

2.8. Primary Cell Culture.

2.8.1. Dissociation of chiasm cells.

Papain dissociation system kit (Worthington Biochemical Corporation, #LK003160).

2.8.2. Collagen mixture for co-cultures.

Prepared by mixing the following reagents together on ice under sterile conditions. This mixture was made up fresh for each culture experiment.
180µl rat tail collagen type 1 (BD Biosciences, #354236)
180µl bovine collagen type 1 (BD Biosciences, #354231)
40µl 10X DMEM (Sigma, #D7777) - reconstitute powder using sterile ddH_20 and filter.
~ 10µl 0.8M sodium bicarbonate or enough to turn the mixture a pale pink colour

2.8.3. Earle's balanced salt solution ('EBSS').

Prepared by mixing the following reagents together under sterile conditions and stored for not more than two weeks at 4°C until use.

100 ml Earle's balanced salt solution 10X (Sigma, #E-7510)
0.22 g Na_2HCO_3 (Sigma, #S5761), final concentration 22 mg/ml
0.065 g glucose (Sigma, #G-7021), final concentration 6.5 mg/ml
900 ml double deionised water.
EBSS was oxygenated by bubbling with 95% O_2 and chilled on ice prior to use.

2.8.4. Serum-free culture medium.

Prepared by mixing the following reagents together under sterile conditions and stored for not more than two weeks at 4°C until use. Medium was warmed and equilibriated in a 37°C humidified incubator containing 5% CO_2 for at least one hour prior to use.

100 ml F12, Hams (Sigma, #N4888)
100 ml Dulbecco's modified Eagles' medium (DMEM) (Sigma, #D5671)
1 mg insulin (Sigma, #I6634), final concentration 5µg/ml
2 mg apo-transferrin (Sigma, #T1147), final concentration 10µg/ml
3 ml HEPES buffer (Sigma, #H0887)
0.24 g Na_2HCO_3 (Sigma, #S5761), final concentration 0.12mg/ml
3 ml antibiotics stock: 100 mg gentamycin (Sigma, #G1264) and 200 mg kanamycin (Sigma, #K1377) added to 20 ml sterile double deionised water, filter-sterilised and stored at -20°C.
2 ml putrescene stock: 100 µM stock, 161.1mg/100ml in sterile double deionised water, filter-sterilised and stored at -70°C (Sigma, #P5780), final concentration 16.11µg/ml

20µl progesterone stock: 20 µM stock, 6.29mg/100ml ethanol stored at -70°C (Sigma, #P8783), final concentration 6.29ng/ml
20µl Na_2SeO_3 stock: 30 µM stock, 5.2mg/100ml in sterile double deionised water, filter-sterilised and stored at -70°C (Sigma, #S5261), final concentration 5.2ng/ml
2 ml L-glutamine stock: 0.2M stock, 6.344g/100ml in sterile double deionised water, filter-sterilised and stored at -70°C (Sigma, #G2128), final concentration 25µg/ml.

2.8.5. Serum-free culture medium with methylcellulose.

5g of methylcellulose (Sigma, #M7027) was autoclaved and stirred in a 100 ml sterile bottle. 95 ml of DMEM/F12 was added to form a 5% solution and stirred over 3 days at 4°C.
1ml of methylcellulose was added to 9ml of serum-free culture medium for a final concentration of 0.5%.

CHAPTER 3: *Foxg1* chimeric co-cultures of retina and chiasm show that *Foxg1* is required both within dorsonasal retina and at the optic chiasm for the growth of nasal retinal axons over chiasm cells *in vitro*.

3.1. ABSTRACT

The chimeric co-culture experiment is a powerful tool with which to reveal the location where *Foxg1* is primarily required to mediate the contralateral versus ipsilateral routing of retinal axons at the chiasm midline. The expression pattern of *Foxg1* in the nasal retina and anterior chiasm raises the possibility that *Foxg1* influences the guidance of retinal axons from their origins in the RGC layer of the retina or at the point where they diverge ipsilaterally or contralaterally at the chiasm midline. The increase in ipsilateral projections from *Foxg1*$^{-/-}$ nasal retina could be the result of an autonomous requirement for *Foxg1* in nasal RGCs or a non-autonomous requirement outwith RGCs at the chiasm. Since the majority of the temporal retina normally does not express *Foxg1*, the increase in ipsilateral projections from Foxg1$^{-/-}$ temporal RGCs could either be the result of a non-autonomous requirement for *Foxg1* in temporal retina or at the chiasm. To deduce whether the axon guidance defect in *Foxg1* null embryos is principally due to a defect in the retina or the chiasm, DN and VT retinal explants were cultured with dissociated chiasm cells from E14.5 mouse embryos. Co-cultures were prepared consisting of retina and chiasm tissue from either wild type (*Foxg1*$^{+/+}$) or *Foxg1* heterozygous (*Foxg1*$^{+/-}$) embryos, which were used interchangeably and so collectively denoted as '*Foxg1*$^{+/\pm}$' embryos. These co-cultures reproduced previous findings that the growth of ventrotemporal axons *in vitro* is reduced by chiasm cells to a greater extent than axons from other regions of the retina, reflecting their avoidance of the chiasm midline and subsequent uncrossed trajectory *in vivo*. Axon outgrowth from DN

Foxg1$^{-/-}$ retina ↔ *Foxg1*$^{-/-}$ chiasm co-cultures was significantly lower compared to outgrowth from DN *Foxg1*$^{+/\pm}$ retina ↔ *Foxg1*$^{+/\pm}$ chiasm co-cultures, reflecting the increased avoidance of the chiasm by nasal axons observed in *Foxg1*$^{-/-}$ embryos (Pratt et al., 2004). A reduction was also observed in VT *Foxg1*$^{-/-}$ ↔ *Foxg1*$^{-/-}$ co-cultures compared to VT *Foxg1*$^{+/\pm}$ retina ↔ *Foxg1*$^{+/\pm}$ chiasm co-cultures, although this was not significant. The successful *in vitro* recapitulation of the *in vivo* behaviour of VT (uncrossed) and DN (crossed) axons co-cultured with chiasm were then used as references against which to compare axon outgrowth from chimeric *Foxg1*$^{+/\pm}$ ↔ *Foxg1*$^{-/-}$ co-cultures. These revealed that *Foxg1* is required both within the nasal retina and in chiasm cells for the guidance of nasal RGC axons. Axon outgrowth did not vary significantly among the various VT co-cultures, suggesting that *Foxg1* is not required by the temporal retina or at the chiasm for the guidance of VT axons. However, in order to confirm this, many more VT co-cultures would be needed due to the small amount of axon outgrowth produced by VT retina and the related difficulties in detecting small changes in axon outgrowth. Alternatively, VT retinal axons might normally be influenced by *Foxg1* expression in other tissues.

3.2. INTRODUCTION

Over the past decade, a number of molecules and regulatory genes have been identified in the eye, optic stalk and chiasm to play roles in controlling the ipsilateral or contralateral routing of retinal axons at the optic chiasm (Bertuzzi et al., 1999; Chung et al., 2000a; Chung et al., 2000b; Deiner & Sretavan, 1999; Herrera et al., 2004; Herrera et al., 2003; Jeffery 2001; Marcus et al., 1995; Marcus & Mason 1995; Marcus et al., 1999; Pak et al., 2004; Pratt et al., 2004; Sretavan et al., 1994; Sretavan et al., 1995; Sretavan & Reichardt, 1993; Sretavan & Kruger, 1998; Wang et al., 1995; Wang et al., 1996; Williams et al., 2006; Williams et al., 2003; Wizenmann et al., 1993; Zhang et al., 2000).

Foxg1 has been shown to affect the proportion of axons projecting ipsilaterally since in *Foxg1* null embryos there is an 8-fold increase in the ipsilateral projection (Pratt et al., 2004). During the peak period from E13 - E16 when RGCs project axons towards the chiasm, *Foxg1* is expressed by RGCs and tissues that retinal axons encounter as they navigate from their origins in the RGC layer of the retina, through the optic stalk and to the optic chiasm midline. The lens, retinal pigment epithelium, nasal retina, nasal optic stalk and anterior chiasm all express *Foxg1*. Therefore, *Foxg1* may control growth cone navigation at the ventral midline directly or indirectly, at any one or a combination of locations.

3.2.1. Hypotheses

This chapter aims to test the hypothesis that *Foxg1* is required in the retina or at the chiasm or both for the guidance of retinal axons. *Foxg1* expression is more widespread in the nasal retina compared to temporal retina (Hatini et al., 1994; Huh et al., 1999; Pratt et al., 2004; Chapter 5, this thesis). Therefore, *Foxg1* might direct the navigation of nasal axons autonomously from *Foxg1*-expressing nasal RGCs, determining the response of their growth cones to cells and molecules encountered along the route. However, *Foxg1*$^{-/-}$ embryos exhibit an increase in ipsilateral projections from both temporal and nasal RGCs (Pratt et al., 2004). This raises the possibility that *Foxg1* affects the guidance of temporal retinal axons non-autonomously from temporal RGCs that do not express *Foxg1*. In other words, *Foxg1* could exert its non-autonomous effects from within the temporal retina. An alternative hypothesis that would explain the increased ipsilateral projection from temporal retina and also nasal retina is that *Foxg1*-expressing cells around the optic chiasm influence the proportion of RGC axons projecting contralaterally or ipsilaterally, by providing an appropriate cellular and/or molecular environment around the midline.

3.2.2. *Foxg1* chimeras.

3.2.2.1. *In vivo*.

One method of determining whether *Foxg1* is required in the retina or at the chiasm to mediate the contralateral-ipsilateral projection of retinal axons would be to create *Foxg1* chimeric embryos consisting of wild type and $Foxg1^{-/-}$ cells. DiI labeling could then be used to label the paths taken by retinal axons at the chiasm and to backlabel axons to their origins in the retina. By examining whether $Foxg1^{-/-}$ RGCs in the nasal or temporal retina produce axons that cross the optic chiasm or remain ipsilateral and also by studying the behaviour of axons when confronted with chiasms consisting of mostly wild type or mostly $Foxg1^{-/-}$ cells, inferences could be drawn about the primary site of action of *Foxg1* and whether its effects are autonomous or non-autonomous. For example, if the defect lies in the $Foxg1^{-/-}$ chiasm, both wild type and $Foxg1^{-/-}$ retinal axons would be expected to project ipsilaterally in greater numbers than normal. In contrast, if the defect lies in the $Foxg1^{-/-}$ retina, $Foxg1^{-/-}$ retinal axons would be expected to project ipsilaterally in greater numbers, whereas wild type axons would not. Axons originating from the nasal and temporal retina might show differences in the proportion of ipsilateral axons that are misrouted depending on whether the absence of Foxg1 affects the guidance of axons from the entire retina or solely those axons from *Foxg1*-expressing RGCs. However, this *in vivo* approach is time-consuming and analysis could be complicated depending on the percentage contribution of $Foxg1^{-/-}$ cells in the retina or chiasm.

3.2.2.2. *In vitro Foxg1* chimeric co-cultures of retina and chiasm.

Instead of producing chimeras *in vivo*, an alternative approach was utilized using *in vitro* chimeric co-cultures of $Foxg1^{+/\pm} \leftrightarrow Foxg1^{-/-}$ retina and chiasm. Both $Foxg1^{+/+}$ and $Foxg1^{+/-}$ embryos were used to provide *Foxg1*-expressing 'control' tissue because

Foxg1 heterozygous brains are morphologically indistinguishable from wild type brains and have no reported retinal axon guidance defects. Wherever *Foxg1*$^{+/+}$ or *Foxg1*$^{+/-}$ embryos were used to provide tissue for culture, the notation '*Foxg1*$^{+/\pm}$' was used. Previous co-culture experiments have shown that the growth of axons from VT retinal explants is reduced to a greater extent than axons from the rest of the retina in the presence of dissociated chiasm cells (Herrera et al., 2004; Herrera et al., 2003; Marcus et al., 1995; Marcus and Mason, 1995; Marcus et al., 1996b; Wang et al., 1995). This has been interpreted as the *in vitro* equivalent of the *in vivo* avoidance of the chiasm by ipsilateral VT axons. In other words, axon outgrowth is a 'read-out' of crossing behaviour along a scale of low outgrowth, typical of VT ipsilateral axons, to high outgrowth, typical of contralateral axons from non-VT retina (see Figure 1). In order to decide whether axons from chimeric co-cultures behave like contralateral or ipsilateral axons from wild type embryos, axon outgrowth was compared to control co-cultures[1] of *Foxg1*$^{+/\pm}$ ↔ *Foxg1*$^{+/\pm}$ retina and chiasm that were used for calibration purposes. For example, a chimeric co-culture that produces high axon outgrowth similar to DN control co-cultures suggests that the axons behave like contralateral axons *in vitro.* In contrast, axons from chimeric co-cultures that grow as poorly as those in VT control co-cultures can be said to behave like ipsilateral axons *in vitro*. Similarly, *Foxg1*$^{-/-}$ ↔ *Foxg1*$^{-/-}$ co-cultures using DN and VT retina were prepared to test the hypothesis that they produce less axon outgrowth than DN and VT control co-cultures, reflecting the increased avoidance of the chiasm by nasal and temporal *Foxg1*$^{-/-}$ axons *in vivo*, shown by Pratt et al. (2004).

[1] For simplicity, the terms 'DN control co-cultures' or 'VT control co-cultures' are used in this chapter to refer to *Foxg1*$^{+/\pm}$ ↔ *Foxg1*$^{+/\pm}$ co-cultures using either DN or VT retina.

Figure 1. Co-cultures of retina and chiasm *in vitro* recapitulate *in vivo* axon projections at the optic chiasm.
(A, B) Schematic diagrams of the eyes, optic chiasm (midline depicted as a dotted line) and contralateral (blue lines) or ipsilateral (red lines) retinal axons as viewed from above. The paths of (A) contralateral-projecting RGC axons and (B) ipsilateral-projecting RGC axons *in vivo* are depicted. (C) A cartoon of a DN retinal explant (circle), cultured with chiasm cells (unfilled circles) showing contralateral RGCs that project numerous axons (green lines). This reflects the crossing of the chiasm midline by contralateral axons *in vivo*. (D) A cartoon of a VT retinal explant cultured with chiasm cells, showing only a single axon. This reflects the repulsion of ipsilateral axons from the chiasm midline *in vivo*.

Figure 1. *In vitro* outgrowth of retinal axons reflects *in vivo* contralateral/ipsilateral behaviour.

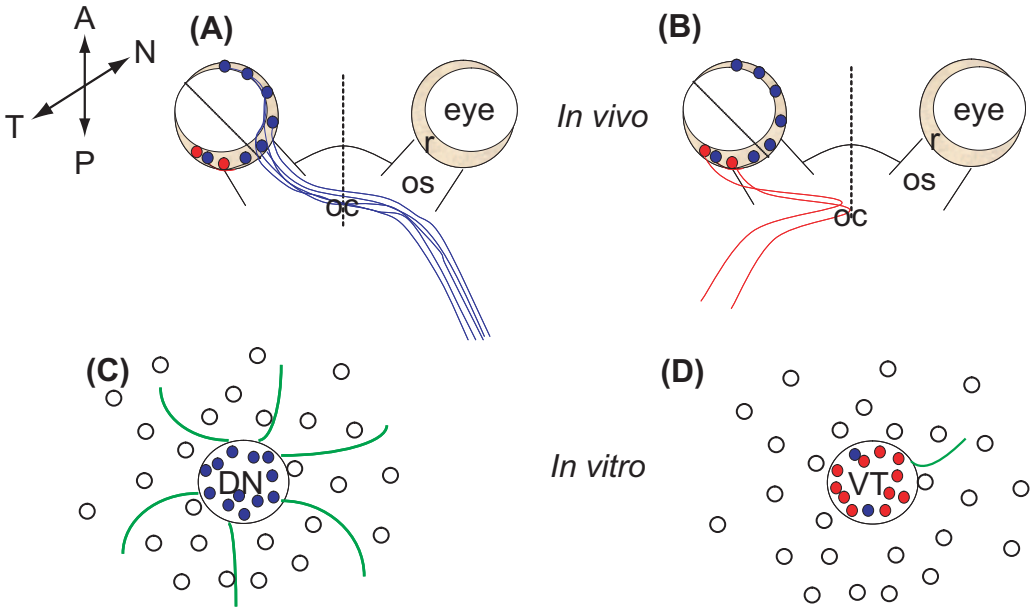

DN retinal explants produce high axon outgrowth in the presence of chiasm cells *in vitro* reflecting the contralateral path followed by their axons at the chiasm midline *in vivo*.

VT retinal explants produce low axon outgrowth in the presence of chiasm cells *in vitro* reflecting the ipsilateral path followed by their axons at the chiasm midline *in vivo*.

Key

- contralateral RGC
- ipsilateral RGC
- ventral midline
- contralateral axon
- ipsilateral axon
- neurofilament-positive neurite
- chiasm cell

Abbreviations: A, anterior; P, posterior; N, nasal; T, temporal; DN, dorsonasal; VT, ventrotemporal; r = retina, oc = optic chiasm, os = optic stalk

3.3. METHODS

3.3.1. Animals.

All experiments were carried out using *Foxg1*^{LacZ} (CBA) mated with *Foxg1*^{cre} (Swiss Stanford mice). Noon on the same day a plug was found was considered E0.5. Pregnant mothers were terminally anaesthetized in halothane 14 days after a plug was found and E14.5 embryos removed by caesarian section. *Foxg1*$^{+/+}$ and *Foxg1*$^{+/-}$ embryos were used to provide *Foxg1*-expressing tissue as their axon tracts and brain morphology are indistinguishable. They are both labeled 'control' or '*Foxg1*$^{+/\pm}$' in the Figures. Retina and chiasm co-cultures were prepared using embryos from the same litter to minimize variability between different co-culture combinations due to slight age differences. Only embryos with pigmented retinas were used for the dissections to facilitate dissection of the retina from the retinal pigment epithelium (RPE) and to eliminate possible variation in axon divergence caused by lack of pigmentation in albino embryos (Marcus et al., 1996b).

3.3.2. Retinal explants.

Co-cultures were prepared using a method similar to Wang et al. (1995). The co-culture method is outlined in Figure 2. *Foxg1*$^{-/-}$ embryos were identified phenotypically by their abnormal eye and brain morphology. E14.5 *Foxg1*$^{+/+}$/*Foxg1*$^{+/-}$ (designated '*Foxg1*$^{+/\pm}$') and *Foxg1*$^{-/-}$ embryos were decapitated in ice-cold oxygenated EBSS and retinas dissected free from the RPE, lens, vitreous and blood vessels in a sterile laminar-flow hood after making an orientating cut in the ventral pole. Equal-sized explants from peripheral dorsonasal or ventrotemporal retina were dissected in ice-cold EBSS. A 1:1 mixture of bovine dermis and rat tail collagen was prepared on ice by mixing 9 parts collagen to 1 part 10×DMEM/F12 medium. Bicarbonate was added to turn the collagen a pale pink/orange color. 10 - 20µl of collagen was pipetted and

Figure 2. Retina-chiasm co-culture method.
(A) Schematic overview of the method used for creating *Foxg1*$^{+/\pm}$ ↔ *Foxg1*$^{-/-}$ co-cultures of retina and chiasm. Retinas are depicted as circles and optic chiasms as rectangles. *Foxg1*$^{-/-}$ tissue is black and control *Foxg1*$^{+/\pm}$ tissue is white. *Foxg1*$^{+/\pm}$ ↔ *Foxg1*$^{-/-}$ co-cultures are shown. These combinations were prepared for DN and VT explants separately. (B) Dissection of DN and VT retinal explants. The eye is depicted as a circle with D-V and N-T axes. (1) A ventral orientating cut (red dashed line) was made slightly nasal to the D-V axis. (2) DN (blue) and VT retina (white) from the peripheral third of the retinal radius was dissected. (3) These retinal explants were further cut into roughly equal 200 - 400μm wide pieces. (4) Finally these retinal explants were positioned far apart from one another on a thin layer of collagen (shown in pink) and left for 2 hours prior to adding dissociated chiasm cells.

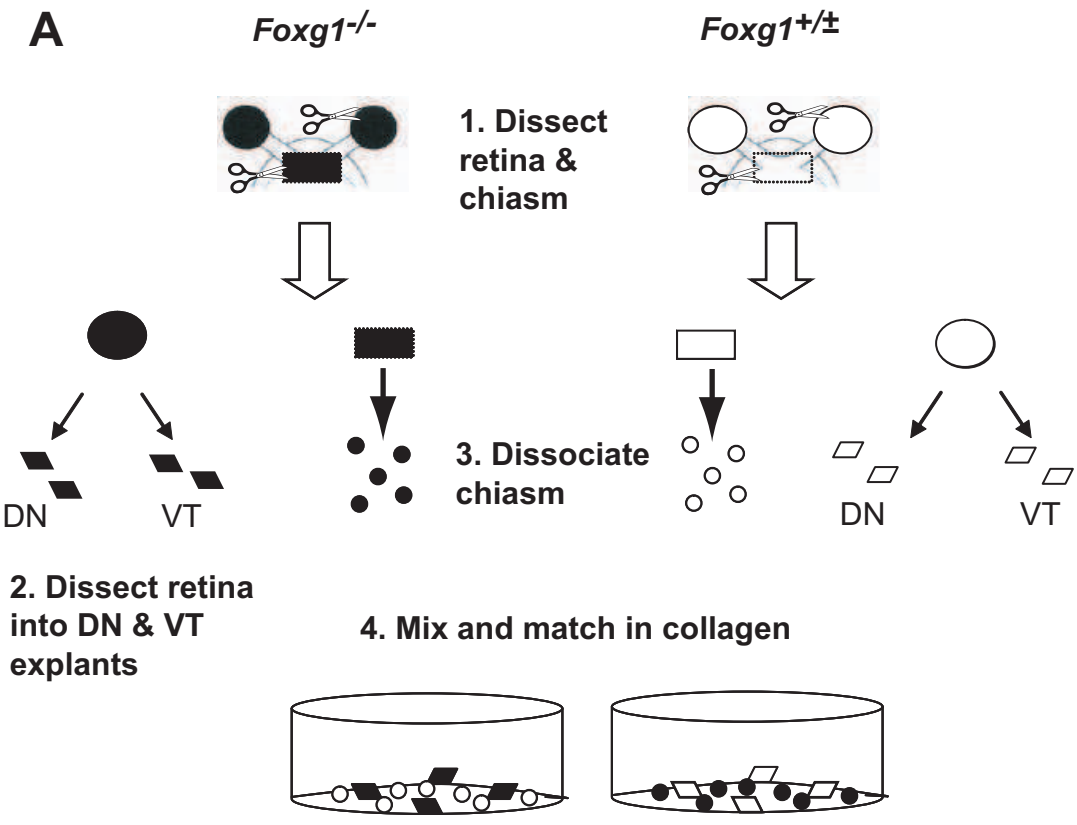

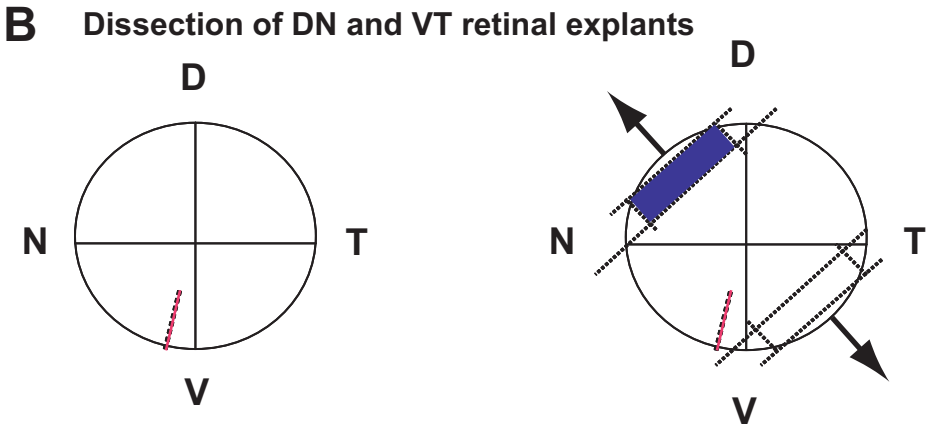

1. Ventronasal orientating cut

2. Dissection of DN & VT peripheral retina

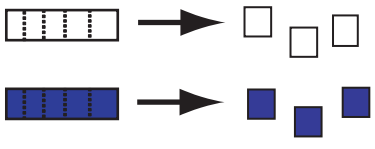

3. Retina cut into 200 - 400um wide pieces

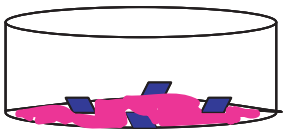

4. Explants positioned on thin layer of collagen gel

spread evenly onto circular glass coverslips pre-treated with poly-l-lysine (100 μg/ml) overnight at 4°C in Nunc four-well dishes. After allowing the collagen to set for 20 minutes in a 37ºC incubator (95% O_2: 5% CO_2), the retinal explants were placed on top of the collagen layer in a 20μl droplet of serum-free culture medium containing 0.5% methylcellulose to aid adhesion. The explants were placed in the 37ºC incubator where they were left for 2 hours to adhere to the collagen gel prior to adding chiasm cells.

3.3.3. Dissociation of chiasm cells.

Meanwhile, several *Foxg1*$^{+/\pm}$ and *Foxg1*$^{-/-}$ optic chiasms were dissected and dissociated using papain. Control (*Foxg1*$^{+/\pm}$) and *Foxg1*$^{-/-}$ optic chiasms were kept separate and care was taken to rinse dissecting instruments between dissections to avoid cross-contamination with cells or cellular substances that might influence the results. Dissociated chiasm cells were resuspended in a 1:1 mixture of rat-tail and bovine collagen to a density of 500 cells per mm^2 before adding to the retinal explants in a 5μl volume. The co-cultures were placed in a 37ºC incubator (95% O_2: 5% CO_2). After 2 hours, fresh serum-free culture medium without methylcellulose was added to the cultures, which were then replaced in the 37ºC incubator and left for 48 hours.

Retinal explants and dissociated chiasm cells were cultured in all eight possible combinations shown in Table 2 below.

Table 2. Co-culture combinations.

Non-chimeric co-cultures (*Foxg1*$^{+/\pm}$ ↔ *Foxg1*$^{+/\pm}$ and *Foxg1*$^{-/-}$ ↔ *Foxg1*$^{-/-}$)		**Chimeric co-cultures (*Foxg1*$^{+/\pm}$ ↔ *Foxg1*$^{-/-}$)**	
Retina	**Chiasm**	**Retina**	**Chiasm**
DN *Foxg1*$^{+/\pm}$	*Foxg1*$^{+/\pm}$	DN *Foxg1*$^{-/-}$	*Foxg1*$^{+/\pm}$
VT *Foxg1*$^{+/\pm}$	*Foxg1*$^{+/\pm}$	VT *Foxg1*$^{-/-}$	*Foxg1*$^{+/\pm}$
DN *Foxg1*$^{-/-}$	*Foxg1*$^{-/-}$	DN *Foxg1*$^{+/\pm}$	*Foxg1*$^{-/-}$
VT *Foxg1*$^{-/-}$	*Foxg1*$^{-/-}$	VT *Foxg1*$^{+/\pm}$	*Foxg1*$^{-/-}$

3.3.4. Neurofilament and Brn3a immunohistochemistry.

After 48 hours, the co-cultures were fixed using 4% paraformaldehyde in 1X PBS for 40 minutes at 4°C. The fixed cultures were washed on a shaker at 4°C with five changes of 1X PBS, each wash lasting 15 minutes except the last wash that was overnight. The following incubations or washes were all done on a shaker. The co-cultures were blocked in 10% goat serum, 0.2% PBSTx-100 for 90 minutes at room temperature. A mixture of primary antibodies: rabbit neurofilament (Biomol International) used at 1:200 and mouse Brn3a (Chemicon International) used at 1:300

diluted in the blocking solution was prepared. 250 µl of the primary antibody mixture was pipetted into each well and incubated overnight at 4°C. The primary antibody mixture was removed and cultures were washed six times with 0.1% PBSTx-100 at room temperature, each wash lasting 45 minutes. Secondary antibodies goat anti-mouse Alexa Fluor 546 and goat-anti-rabbit Alexa Fluor 488 were diluted in blocking solution to a final concentration of 1 in 500 each and 0.5 ml was pipetted into each well and incubated overnight at 4°C. The secondary antibody mixture was removed and cultures washed five times with 0.1% PBSTx-100 at room temperature. 0.5 ml of TO-PRO-3 diluted 1 in 2000 in blocking solution was added to each well for 1 hour at room temperature. The cultures were washed twice with 1xPBS and then covered with 9:1 glycerol: PBS before imaging.

3.3.5. Confocal microscopy.

Images of the cultures were obtained using a *Zeiss* inverted confocal microscope. Optical sections 4µm apart were scanned through each retinal explant in the red, blue and green channels allowing a 3D image to be reconstructed in the *LSM Image browser*.

3.3.6. Computer analysis

3.3.6.1. % axon coverage and fascicle width at varying distances from the retinal explant using *Image J*.

For each co-culture, only the green channel image was used to prevent the blue chiasm cells from being detected as a 'peak' (neurite) and interfering with the histogram analysis. The image was converted to black (background) and white (axons) for ease of measurement. 'Process'/Noise/Despeckle was built into the macro to remove some of the background 'speckle' effect that comes from chiasm cells picking up the green

secondary antibody. Macros were written to measure the width of each axon or fascicle at four set pixel distances perpendicularly outwards from the retinal explant surface: 25 pixels (23µm), 50 pixels (45µm), 75 pixels (68µm) and 100 pixels (91µm). To provide a measure of the degree of axon outgrowth, the width of each axon fascicle at each of the four distances from the explant was measured for each co-culture (see Figure 3). At each of the four distances from the explant, the widths of all the fascicles were summed to give a measure of the axon coverage at that distance. A large explant will have a greater surface area from which to extend axons and will tend to have a larger area covered by axons compared to a smaller explant of the same co-culture combination. The confounding factor of explant size was accounted for by expressing the total of all fascicle widths as a percentage of the length of the measuring line (i.e. percentage of the measuring line crossed or covered by axons).

Both computerized and manual methods were used to measure % axon coverage and the widths of fascicles or axons. The computerized method used the histogram of pixel intensity against distance along the measuring line provided by Image J. The width of each peak was measured along a horizontal line above the level of 'noise'. Since each peak represents a fascicle, the width of each peak represents the width of each fascicle. The height of each peak is the pixel intensity, which provides a measure of the number of axons making up that fascicle. A tall peak represents a high pixel intensity, which indicates that more axons are present in that fascicle.

To ensure that the peaks were 'real' rather than areas where there was high background staining from the secondary antibody, neurofilament-staining from chiasm cells or artifacts caused when acquiring the image, the histogram was compared to the original image and checked for correspondence. In the case of cultures with numerous axons or fascicles where an accurate visual comparison was impossible, individual fascicle widths were measured manually from the image. The computerized and manual methods were compared using one co-culture from each co-culture combination.

Figure 3. Measuring % axon coverage using Image J.
(A) Starting image. (B) Conversion of the green channel to black and white. For both manual and computerized counts, the explant border was traced using the segmented line tool (blue polygon). Four macros were written specifying that each point on the polygon should be expanded by 25, 50, 75 or 100 pixels. Each of these macros produced polygons radiating outwards from the explant border by 25, 50, 75 or 100 pixels. The 50 and 100 pixel polygons are shown in yellow. (C) For each of these distances, every time a neurite or fascicle crossed the yellow polygon, its width was measured (white line). (D) If a neurite did not grow outwards perpendicular to the explant border, the neurite width was measured manually where the polygon first touched the neurite (white line). Measurements were consistently done in the anti-clockwise direction. (E, F) Histograms produced by the computerized method. The x-axis represents the distance along the measuring polygon and the y-axis is the 'gray intensity' or white pixel intensity. Each peak is one axon or axon fascicle. The horizontal dotted line was positioned above the 'noise' or level of background staining, which was different for each explant. (F) Enlargement of rectangle shown in (E) with blue arrows showing widths of peaks (= fascicle width) measured. (G) Calculation for % axon coverage. ‘Circumference of measuring polygon’ was obtained from the maximum value of the x-axis on the histogram. Scale bars (A, B) = 100μm, (C, D) = 400μm.

Figure 3. Measuring % axon coverage

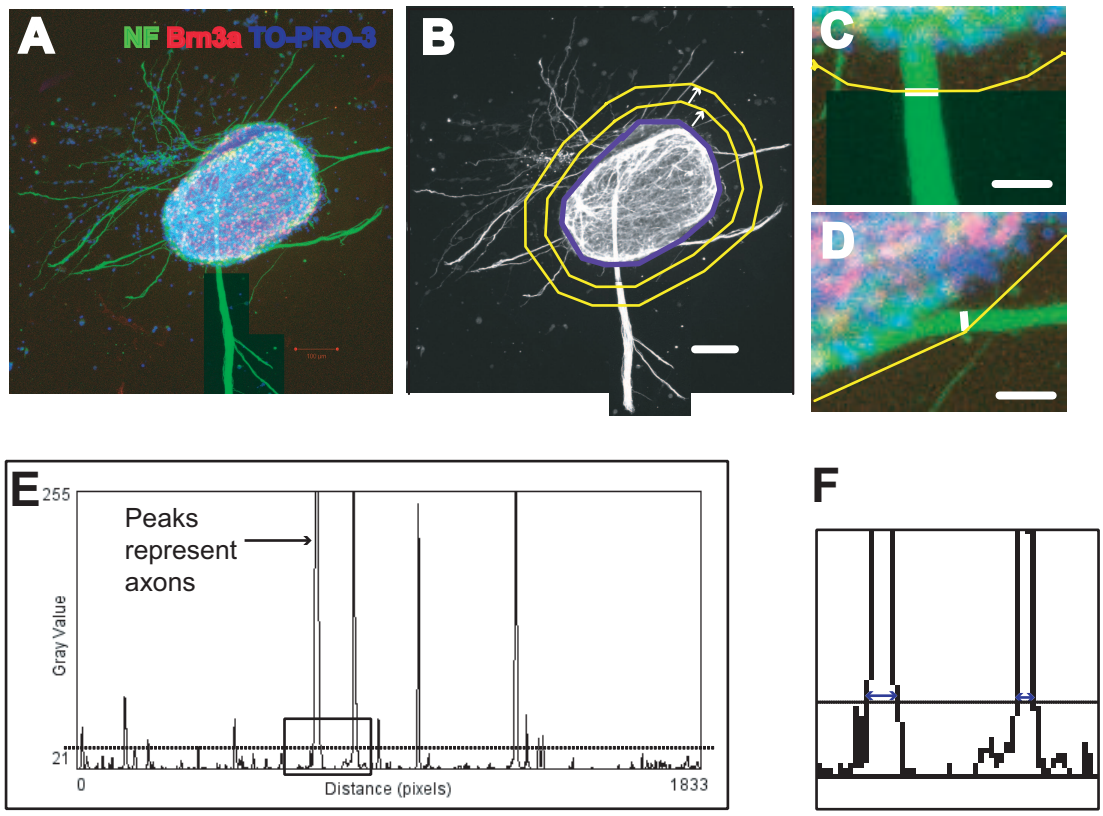

G **% axon coverage =** $\dfrac{\text{Sum of all neurite fascicle widths x 100}}{\text{Circumference of measuring polygon}}$

Both methods gave almost identical results for cultures with low background but variable results for high background images. Therefore, manual analysis was used in the latter cultures, constituting approximately two-thirds of cases. This enabled 'false' peaks resulting from background staining to be identified and excluded from the final analysis.

3.3.6.2. Axon/fascicle length.

To obtain a quantitative measure of neurite extension, the five longest neurites or fascicles were traced and their length measured using the overlay tool in the LSM Image browser. If fewer than 5 neurites were present, all of them were measured and used in the resulting analysis. For each explant, the mean of the 5 longest neurites for each culture was calculated and these means were used to produce a graph for each co-culture combination.

3.3.6.3. Chiasm density.

In order to show that all the co-cultures were plated with a similar density of optic chiasm cells, three 200µm by 100µm rectangles were drawn outwards from the retinal explant, with the 200µm edge perpendicular to the explant border. The placing of these rectangles was the same for each explant regardless of differences in size or shape. From the vertical line bisecting the explant, the first rectangle was placed 45 degrees diagonally to the right, the second rectangle at 180 degrees and the third 45 degrees diagonally to the left. The number of blue TOPRO3-positive chiasm cells was counted within these three measuring boxes and the average chiasm density calculated.

3.3.7. Statistical analysis.

SigmaStat was used to conduct ANOVAs on all DN and VT co-cultures as well as DN or VT co-culture combinations only. If a p-value of less than 0.05 was returned by ANOVA, multiple pairwise comparisons were conducted using the Tukey test, t-test or Dunn's test. For neurite length, p-values were calculated using the Tukey test on pools of mean longest neurite length for each explant, rather than pools of individual neurite lengths from all explants measured for each co-culture combination. The latter would break the assumption of independence of data points, since neurite lengths from the same explant are related or non-independent.

3.4. RESULTS

3.4.1. % axon coverage and longest neurite length did not vary between *Foxg1*-expressing and *Foxg1*$^{-/-}$ retina cultured in the absence of chiasm cells.

In order to eliminate the possibility that differences in axon outgrowth and length between the various retina-chiasm co-cultures could be caused by variability in the intrinsic axon outgrowth capabilities of *Foxg1*-expressing 'control' (*Foxg1*$^{+/\pm}$) versus *Foxg1*$^{-/-}$ retina, retinal explants were cultured under identical conditions to those used for co-cultures, except that chiasm cells were not added. Figure 4 shows typical confocal images of *Foxg1*$^{+/\pm}$ and *Foxg1*$^{-/-}$ explants from DN and VT retina. Fluorescent double immunohistochemistry reveals protein expression of the axon marker neurofilament (green) and the POU-homeodomain transcription factor Brn3a (red), expressed by postmitotic RGCs. Neurites were produced from all retinal explants. However, neurites from VT control explants appeared less fasciculated compared to the others. Neurite outgrowth was quantified for all retinal explants by measuring % axon coverage and the mean length of the five longest neurites for each culture.

Figure 4. *Foxg1*$^{-/-}$ retinal explants are capable of producing neurite outgrowth resembling that from *Foxg1*-expressing retina when grown in the absence of chiasm cells.
E14.5 control (*Foxg1*$^{+/\pm}$) and *Foxg1*$^{-/-}$ explants from DN and VT retina cultured in collagen without chiasm cells. (A, E, F) DN control, (B, G, H) VT control, (C, I, J) DN *Foxg1*$^{-/-}$ and (D, K, L) VT *Foxg1*$^{-/-}$ retinal explants. (A - D) Neurofilament immunohistochemistry revealed neurite outgrowth from all explants. (B) VT control retina projected the most neurites, which were less fasciculated compared to those from the other explants. (A) DN control retina projected the fewest neurites. (E - L) Brn3a immunohistochemistry for the retinal explants shown in A - D marked the nuclei of postmitotic RGCs (red), showing that they were present in all retinal explants. (F, H, J, L) High magnifications of Brn3a images E, G, I & K. Abbreviations: DN is dorsonasal retina, VT is ventrotemporal retina, control is *Foxg1*$^{+/+}$ or *Foxg1*$^{+/-}$ tissue, -/- is *Foxg1*$^{-/-}$ tissue, NF is neurofilament. Scale bars: A - H = 100μm, I - L = 10μm.

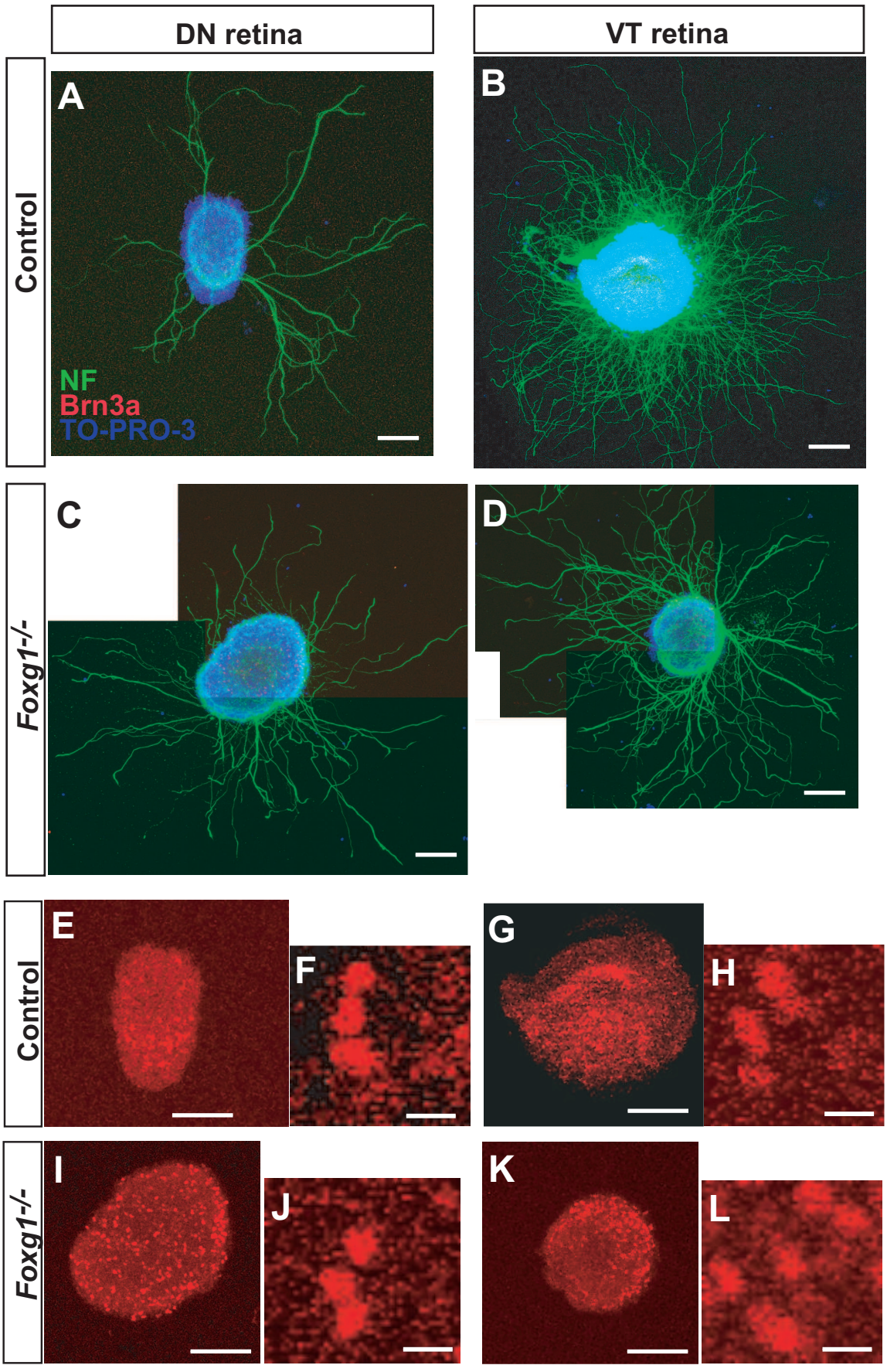
DN retina
VT retina
Control
Foxg1-/-
A
B
C
D
NF
Brn3a
TO-PRO-3
Control
Foxg1-/-
E
F
G
H
I
J
K
L

Figure 5 shows graphs of % axon coverage for *Foxg1*$^{+/\pm}$ and *Foxg1*$^{-/-}$ retinal explants at distances of 23µm (Fig. 5A) and 45µm (Fig. 5B) from the explant. T-tests were used to compare *Foxg1*$^{+/\pm}$ and *Foxg1*$^{-/-}$ explants from either DN or VT retina separately, to control for differences in axon outgrowth between these two retinal quadrants and to test for possible effects of the presence or absence of *Foxg1* on the behaviour of retinal axons in culture. Comparisons between *Foxg1*$^{-/-}$ and *Foxg1*$^{+/\pm}$ retinal explants within DN or VT retina separately, rather than comparisons between the two retinal quadrants, were used more frequently in the co-culture experiments. % axon coverage for *Foxg1*$^{+/\pm}$ and *Foxg1*$^{-/-}$ DN retinal explants at 23, 45, 68 and 91µm distances from the explants did not vary significantly (Figure 5C). Therefore, any differences observed in the DN co-culture experiments can be attributed to particular co-culture combinations rather than intrinsic differences in axonal outgrowth between *Foxg1*$^{+/\pm}$ and *Foxg1*$^{-/-}$ DN retina.

In contrast, t-tests comparing axon coverage between VT retinal explants revealed that *Foxg1*$^{-/-}$ retina had a significantly lower % axon coverage compared to *Foxg1*$^{+/\pm}$ retina at 23µm ($p = 0.045$) but not at any of the other distances. Since this difference is just below the critical p-value of 0.05 and occurred only at 23µm from the explant, it is unlikely that the difference in % axon coverage was large enough to obscure major differences between the various VT retina-chiasm co-culture combinations.

Comparisons of % axon coverage among all retinal explants failed to reveal significant differences between *Foxg1*$^{+/\pm}$ and *Foxg1*$^{-/-}$ explants for either DN retina or VT retina separately at distances of 23µm and 45µm from the explant (Figure 5D). *Foxg1*$^{+/\pm}$ and *Foxg1*$^{-/-}$ explants from VT retina exhibited significantly higher mean % axon coverage compared to DN *Foxg1*$^{+/\pm}$ explants at 45µm. This indicates that VT retina is capable of high axon outgrowth in the absence of chiasm cells and also shows that the outgrowth of axons from VT *Foxg1*$^{+/\pm}$ and VT *Foxg1*$^{-/-}$ retina is more prolific compared to DN retina.

Figure 5. Axon coverage and mean longest neurite length did not vary between dorsonasal control and *Foxg1*$^{-/-}$ explants cultured in the absence of chiasm cells.

Graphs showing % axon coverage for control (*Foxg1*$^{+/\pm}$) and *Foxg1*$^{-/-}$ retinal explants from DN and VT retina at distances of (A) 23µm and (B) 45µm from the retinal explant and (E) mean longest neurite length. (C) Table showing t-test results of % axon coverage when comparing DN or VT explants only. (D) Table showing % axon coverage results for the Tukey multiple pairwise comparisons test when comparing all DN and VT explants. (C, D) Statistically significant differences are highlighted in yellow. (A, B, D) Significant differences in % axon coverage were found when comparing mean values across all DN and VT explants. (A, B) VT control explants had a greater mean % axon coverage compared to DN control explants at both 23µm and 45µm. VT *Foxg1*$^{-/-}$ explants had a greater mean % axon coverage compared to DN *Foxg1*$^{-/-}$ explants at 45µm but not at 23µm. (C) Comparisons of DN control versus DN *Foxg1*$^{-/-}$ explants only did not reveal any significant differences by t-test at either 23µm or 45µm. Comparing VT control versus VT *Foxg1*$^{-/-}$ explants only revealed a significantly greater mean % axon coverage for wild type versus *Foxg1*$^{-/-}$ VT explants at 23µm ($p = 0.045$) but not at 45µm ($p = 0.593$). (D) Comparisons across all explants failed to show significant differences between DN control and *Foxg1*$^{-/-}$ explants or between VT control and *Foxg1*$^{-/-}$ explants (highlighted in pink). (E) Mean neurite length did not differ among retinal explants (ANOVA, $p = 0.184$). (F) Table showing non-significant t-test results for mean neurite length.

Abbreviations: DN is dorsonasal retina, VT is ventrotemporal retina, control is *Foxg1*$^{+/+}$ or *Foxg1*$^{+/-}$ tissue, -/- is *Foxg1*$^{-/-}$ tissue, N.S is not significant, error bars indicate standard error of the mean, n's are indicated in parentheses, * $p < 0.05$, ** $p < 0.005$.

A 23um from explant

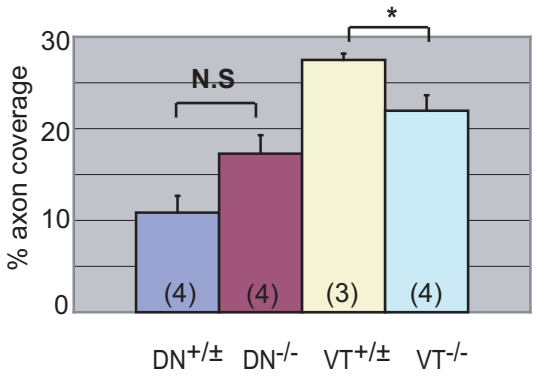

ANOVA (all) P < 0.001

B 45um from explant

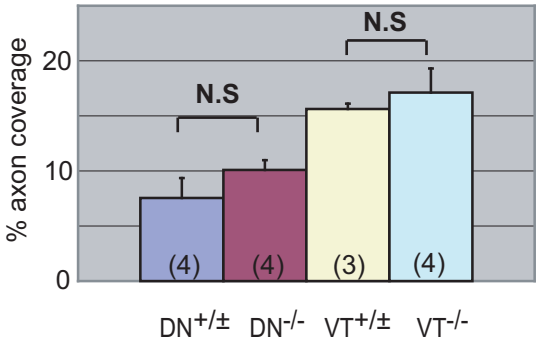

ANOVA (all) P = 0.004

C

T-test for DN or VT retinal explants only		
Comparison	23um p-value	45um p-value
DN +/± vs DN -/-	0.055	0.252
VT +/± vs VT -/-	0.045	0.593

D

Tukey test comparing all retinal explants		
Retinal explant	23um p-value	45um p-value
DN +/± vs DN -/-	0.084	0.666
VT +/± vs VT -/-	0.197	0.921
DN +/± vs VT +/±	< 0.001	0.027
DN +/± vs VT -/-	0.003	0.006
DN -/- vs VT +/±	0.01	0.152
DN -/- vs VT -/-	0.257	0.037

E

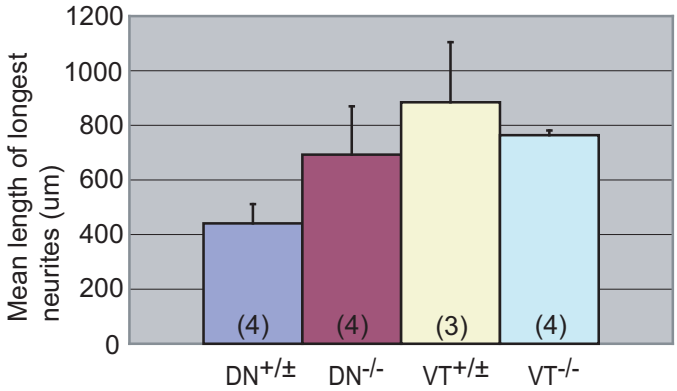

ANOVA (all) P = 0.184, not significant

F

T-test for DN or VT retinal explants only	
Comparison	p-value
DN +/± vs DN -/-	0.235
VT +/± vs VT -/-	0.544

Figure 5E shows a graph of mean lengths of the five longest neurites for *Foxg1*$^{+/\pm}$ and *Foxg1*$^{-/-}$ explants from DN and VT retina grown without chiasm. A one-way ANOVA failed to reveal any significant differences in mean longest neurite length among the various explants. T-tests comparing DN retinal explants and VT retinal explants separately produced non-significant results, confirming that neurites from *Foxg1*$^{+/\pm}$ and *Foxg1*$^{-/-}$ retinal explants do not differ in their extension capabilities in collagen alone (Figure 5F).

3.4.2. Non-chimeric control ↔ control co-cultures prepared from DN retina produced more extensive neurite outgrowth compared to DN *Foxg1*$^{-/-}$ ↔ *Foxg1*$^{-/-}$ co-cultures.

Figure 6 shows typical confocal images of co-cultures prepared using retina and chiasm exclusively from either *Foxg1*$^{+/\pm}$ or *Foxg1*$^{-/-}$ embryos. DN control co-cultures (*Foxg1*$^{+/\pm}$ ↔ *Foxg1*$^{+/\pm}$) displayed the most prolific neurite outgrowth in terms of length and number (Fig. 6A) in stark contrast to low outgrowth and short neurites in DN *Foxg1*$^{-/-}$ ↔ *Foxg1*$^{-/-}$ co-cultures (Fig. 6C).

VT control co-cultures and VT *Foxg1*$^{-/-}$ ↔ *Foxg1*$^{-/-}$ co-cultures all displayed low neurite outgrowth with short neurites (Fig. 6B & D). Neurites from all co-culture combinations contacted chiasm cells (white arrows outside explants in Fig. 6A, B, C, D). Neurites were observed to wrap themselves around all retinal explants but this was less prominent in DN control co-cultures. The green colour of the explant seen in Figure 6A was produced by many neurites growing outwards from the retina rather than wrapping around its surface. Brn3a-expressing RGCs were present and healthy in all retinal explants (Figures 6E – L). This was an important control, as explants with very few or apoptotic RGCs would produce fewer neurites. Excluding cultures with poor Brn3a immuno-staining from the analysis ensured that any variation between the *Foxg1*$^{+/\pm}$ ↔ *Foxg1*$^{+/\pm}$ and *Foxg1*$^{-/-}$ ↔ *Foxg1*$^{-/-}$ co-cultures was due to the presence or

Figure 6. Non-chimeric co-cultures: E14.5 dorsonasal control co-cultures displayed the most prolific outgrowth in terms of neurite length and number.

(A - D) Immunohistochemistry for the axonal marker neurofilament (green) and the RGC marker Brn3a (red) of retinal explants co-cultured with dissociated chiasm cells in collagen gel for 48 hours. The nuclear counterstain TO-PRO-3 (blue) reveals cells in the retinal explant and dissociated chiasm cells in the surrounding collagen gel. Note that image (A) is half the scale of the other images. Neurites contacted chiasm cells in all cultures (white arrows). (A) Control DN retina showed prolific neurite outgrowth into the surrounding *Foxg1*-expressing chiasm cells (blue cells outside the retinal border). (B) VT control co-cultures produced only a few short fasciculated neurites that extended into the surrounding chiasm cells. Many neurites wrapped themselves around the retinal explant (white arrow heads). (C, D) DN and VT $Foxg1^{-/-} \leftrightarrow Foxg1^{-/-}$ co-cultures displayed limited neurite outgrowth and neurites wrapped themselves around the explant. (D) An example of the maximum amount of neurite outgrowth observed for VT $Foxg1^{-/-} \leftrightarrow Foxg1^{-/-}$ co-cultures. (E - L) Brn3a immunohistochemistry for co-cultures A - D showed that RGCs were present in all explants. (E, F) DN control retina, (G, H) VT control retina, (I, J) DN $Foxg1^{-/-}$ retina and (K, L) VT $Foxg1^{-/-}$ retina. (I - L) Magnifications of images E - H. Abbreviations: control is $Foxg1^{+/+}$ or $Foxg1^{+/-}$ tissue, DN is dorsonasal retina, VT is ventrotemporal retina, NF is neurofilament. Scale bars: A = 200μm, B - E, G, I, K = 100μm, F, H, J, L = 10μm.

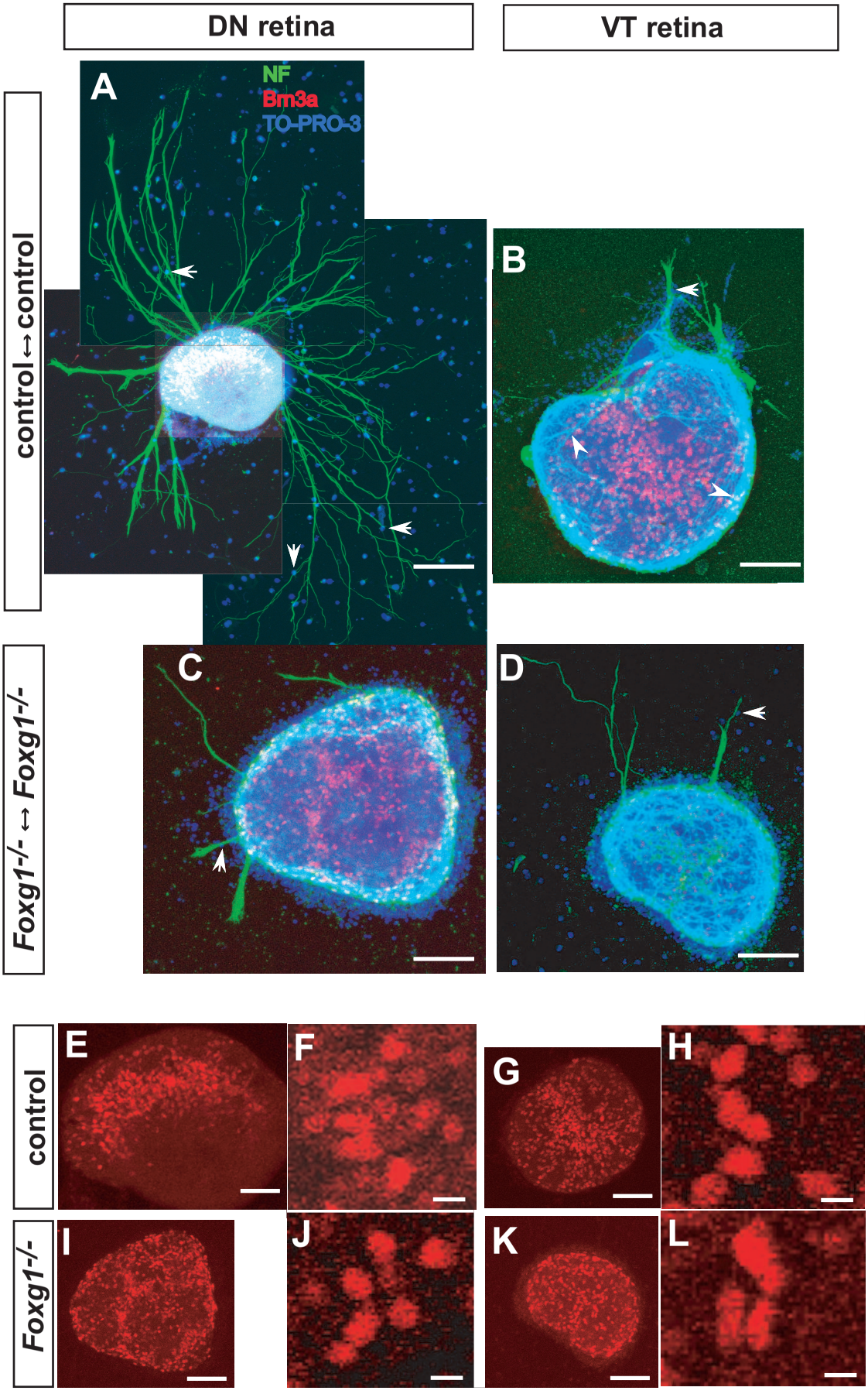
DN retina
VT retina
control ↔ control
Foxg1-/- ↔ Foxg1-/-
control
Foxg1-/-
A
NF
Bm3a
TO-PRO-3
B
C
D
E
F
G
H
I
J
K
L

absence of Foxg1 rather than differences in the numbers of viable RGCs within the retinal explant.

3.4.3. Chimeric co-cultures of *Foxg1*$^{+/\pm}$ ↔ *Foxg1*$^{-/-}$ retina and chiasm.

The main finding of the chimeric co-cultures *Foxg1*$^{+/\pm}$ ↔ *Foxg1*$^{-/-}$ was that DN *Foxg1*$^{-/-}$ retinal explants cultured with *Foxg1*$^{+/\pm}$ chiasm displayed the greatest neurite outgrowth compared to all other chimeric co-culture combinations. Figure 7 shows typical examples of all four possible chimeric co-culture combinations. DN *Foxg1*$^{-/-}$ retinal explants cultured with *Foxg1*$^{+/\pm}$ chiasm produced many long neurites that contacted chiasm cells frequently (Figure 7A). Conversely, neurites from all the other chimeric co-cultures were shorter and less numerous (Figures 7B – D). Neurites were observed to contact chiasm cells in all co-cultures (white arrows). Figures 7E – L show typical confocal images of retinal explants labeled using a Brn3a antibody, showing the presence of healthy RGCs in all co-cultures.

3.4.4. % axon coverage at varying distances from the retinal explant revealed differences among DN but not VT co-cultures.

Figure 8 shows mean % axon coverage at a distance of 23μm from the retinal explant for all DN (Fig. 8A) and all VT (Fig. 8B) co-culture combinations. % axon coverage differed significantly among all 8 co-culture combinations. The mean % axon coverage for DN control co-cultures (DN *Foxg1*$^{+/\pm}$ retina ↔ *Foxg1*$^{+/\pm}$ chiasm) was statistically higher compared to all other DN and VT combinations (Figure 8D). *Foxg1*$^{-/-}$ ↔ *Foxg1*$^{-/-}$ co-cultures had the lowest mean % axon coverage and there was no difference between DN and VT co-cultures. Analysing DN and VT co-cultures separately by ANOVA revealed significant differences among DN co-cultures only. Figure 8B shows that mean % axon coverage for all VT co-cultures was generally less than 3% (+/- standard error) and lower than all DN co-culture combinations.

Figure 7. Chimeric co-cultures: E14.5 Dorsonasal *Foxg1*$^{-/-}$ retinal explants co-cultured with *Foxg1*-expressing chiasm displayed more neurite outgrowth compared to all other chimeric co-cultures.

(A - D) Immunohistochemistry for the axonal marker neurofilament (green) and the RGC marker Brn3a (red) in *Foxg1*$^{-/-}$ ↔ control co-cultures. The nuclear counterstain TO-PRO-3 (blue) reveals cells in the retinal explant and dissociated chiasm cells in the surrounding collagen gel. Note that image (A) is half the scale of the other images. (A) DN *Foxg1*$^{-/-}$ retina cultured with control chiasm: many neurites extended for long distances into the surrounding chiasm cells from all sides of the explant. In cultures of (B) VT *Foxg1*$^{-/-}$ retina with control chiasm, (C) DN control retina with *Foxg1*$^{-/-}$ chiasm and (D) VT control retina with *Foxg1*$^{-/-}$ chiasm, neurites were shorter and fewer in number compared to (A). Neurites contacted chiasm cells in all co-culture combinations (white arrows). (E - L) Brn3a immunohistochemistry of retinal explants in co-cultures A - D showed that RGCs were present in all explants. (E, F) DN *Foxg1*$^{-/-}$, (G, H) VT *Foxg1*$^{-/-}$, (I, J) DN control and (K, L) VT control retinal explants. (I - L) Magnifications of images E - H. Abbreviations: control is *Foxg1*$^{+/+}$ or *Foxg1*$^{+/-}$ tissue, -/- is *Foxg1*$^{-/-}$ tissue, DN is dorsonasal retina, VT is ventrotemporal retina, NF is neurofilament. Scale bars: A = 200μm, B - H = 100μm, I - L = 10μm.

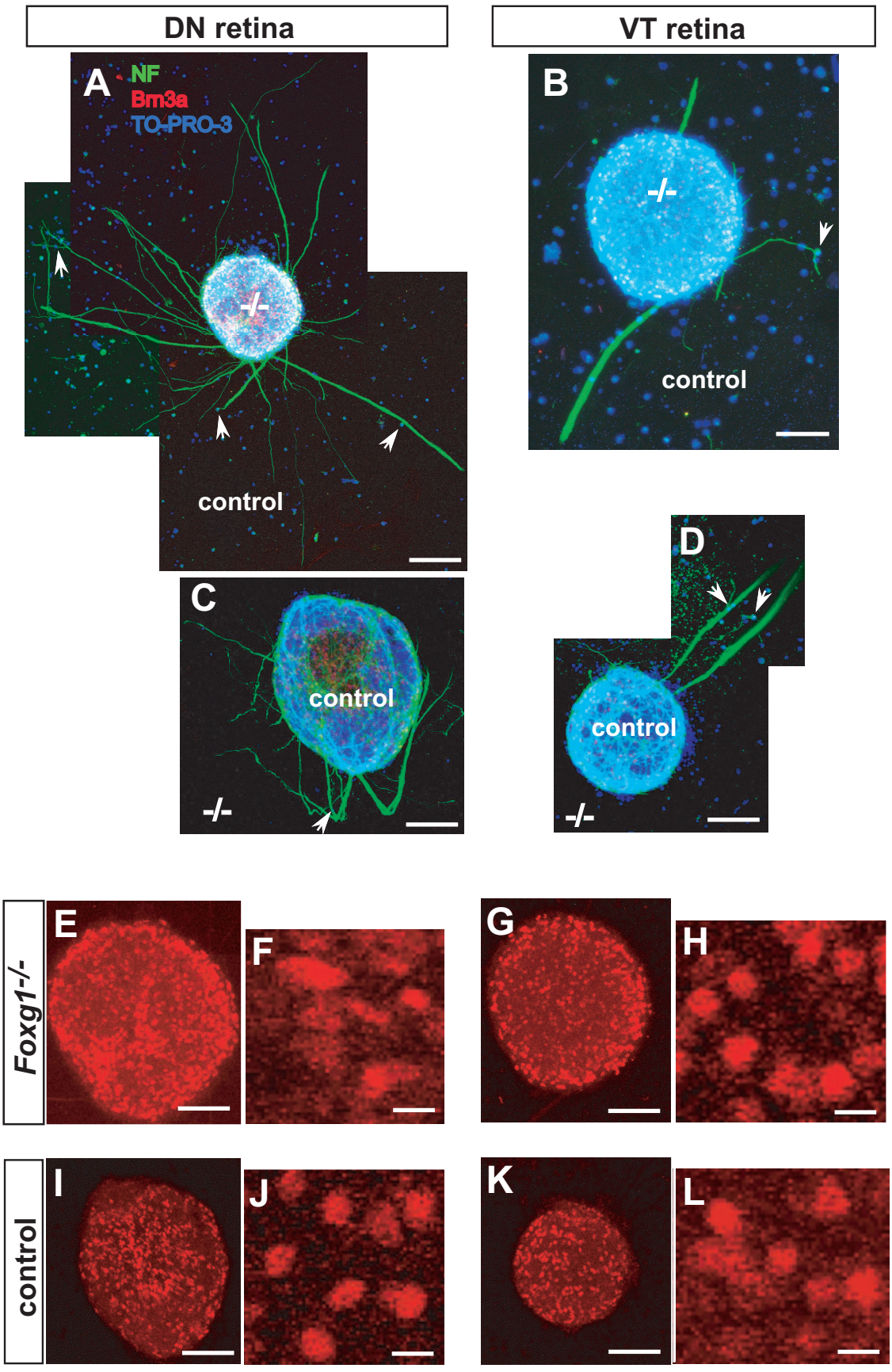
DN retina
VT retina
A
NF
Bm3a
TO-PRO-3
-/-
control
B
-/-
control
C
control
-/-
D
control
-/-
Foxg1-/-
E
F
G
H
control
I
J
K
L

Figure 8. % axon coverage differed among dorsonasal but not among ventrotemporal co-cultures at a distance of 23µm from the retinal explant.

% axon coverage for (A) DN and (B) VT co-cultures 23µm from the retinal explant. (A) % axon coverage differed significantly among the four DN co-culture combinations (ANOVA, $p < 0.001$). The mean % axon coverage for DN control co-cultures (first bar) was statistically higher ($p < 0.001$) compared to all other DN combinations. Cultures of DN *Foxg1*$^{-/-}$ retina with control chiasm (second bar) had a significantly higher mean % axon coverage than DN *Foxg1*$^{-/-}$ ↔ *Foxg1*$^{-/-}$ co-cultures (fourth bar, $p = 0.007$). (B) % axon coverage did not differ among the four VT co-culture combinations (ANOVA $p = 0.293$). (C) Table showing multiple pairwise comparisons among DN co-cultures only using the Tukey test. $P = 0.05$ is the critical value below which differences between means were considered statistically significant. (D) Table comparing all DN and VT co-culture combinations using the Tukey test. In (C) and (D), significant p-values were found for the same co-culture combinations and are highlighted in yellow. Abbreviations: DN is dorsonasal retina, VT is ventrotemporal retina, +/± is *Foxg1*$^{+/+}$ or *Foxg1*$^{+/-}$ tissue, -/- is *Foxg1*$^{-/-}$ tissue, oc is optic chiasm, error bars indicate standard error of the mean, n's are indicated in parentheses, ** $p < 0.001$, * $p = 0.007$.

% axon coverage for retina-chiasm co-cultures at a distance of 23um from the retinal explant

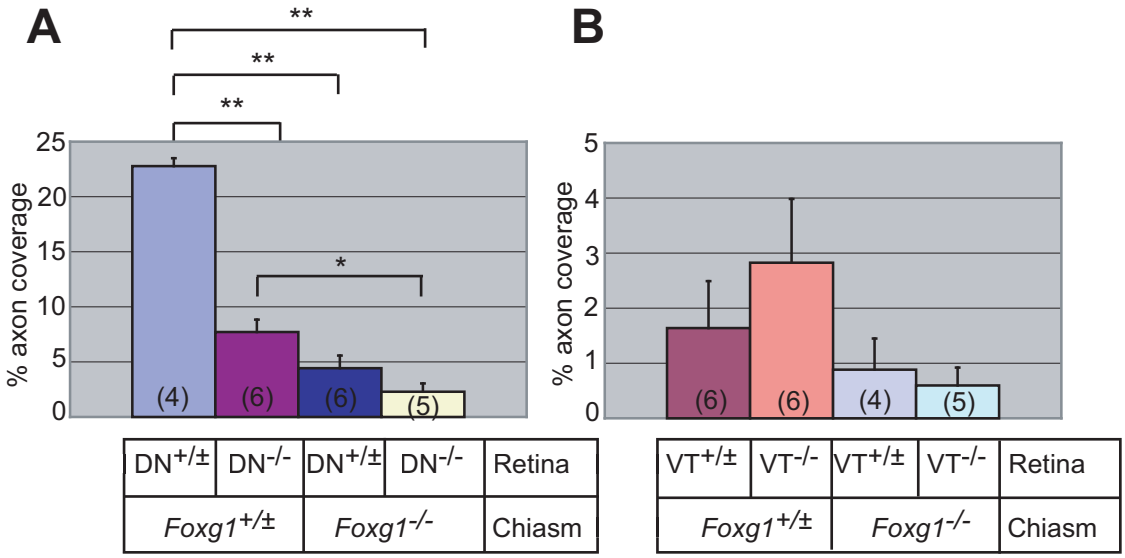

ANOVA (DN) P < 0.001

ANOVA (VT) P = 0.293

ANOVA (DN & VT) P < 0.001

C

Tukey test for DN co-cultures only	
Co-culture combination	p-value
DN +/±, +/± oc vs DN -/-, +/± oc	< 0.001
DN +/±, +/± oc vs DN +/±, -/- oc	< 0.001
DN +/±, +/± oc vs DN -/-, -/- oc	< 0.001
DN -/-, +/± oc vs DN -/-, -/- oc	0.007
DN -/-, +/± oc vs DN +/±, -/- oc	0.114
DN +/±, -/- oc vs DN -/-, -/- oc	0.464

D

Tukey test for all DN & VT co-cultures	
Co-culture combination	p-value
DN +/±, +/± oc vs all other combinations	< 0.001
DN -/-, +/± oc vs VT +/±, -/- oc	< 0.001
DN -/-, +/± oc vs VT +/±, +/± oc	< 0.001
DN -/-, +/± oc vs VT -/-, +/± oc	0.01
DN -/-, +/± oc vs DN -/-, -/- oc	0.006
DN -/-, +/± oc vs VT -/-, -/- oc	< 0.001
DN -/-, +/± oc vs DN +/±, -/- oc	0.192
VT -/-, -/- oc vs DN +/±, -/- oc	0.106

Multiple pairwise comparisons among the four DN retina-chiasm combinations produced the same results as for comparisons among all DN and VT co-cultures (Figures 8C, D).

The % axon coverage means for chimeric co-cultures DN *Foxg1*$^{+/\pm}$ retina ↔ *Foxg1*$^{-/-}$ chiasm and DN *Foxg1*$^{-/-}$ retina ↔ *Foxg1*$^{+/\pm}$ chiasm were not significantly different from one another. However, they were significantly lower than non-chimeric DN control co-cultures, demonstrating that *Foxg1*-expression in the retina and chiasm was unable to fully rescue axon outgrowth. However, co-cultures of DN *Foxg1*$^{-/-}$ retina ↔ *Foxg1*$^{+/\pm}$ chiasm (but not the reverse) had a significantly higher mean % axon coverage than DN *Foxg1*$^{-/-}$ ↔ *Foxg1*$^{-/-}$ co-cultures, suggesting that *Foxg1* expression in the chiasm can partially rescue neurite outgrowth from *Foxg1* null retina. Interestingly, although axon coverage for co-cultures of DN *Foxg1*$^{+/\pm}$ retina ↔ *Foxg1*$^{-/-}$ chiasm was greater compared to DN *Foxg1*$^{-/-}$ ↔ *Foxg1*$^{-/-}$ co-cultures, this difference was not statistically significant.

In summary, the % axon coverage for co-cultures of DN retinal explants with chiasm followed the order:-

Foxg1$^{+/\pm}$ retina ↔ *Foxg1*$^{+/\pm}$ chiasm > *Foxg1*$^{-/-}$ retina ↔ *Foxg1*$^{+/\pm}$ chiasm > *Foxg1*$^{-/-}$ retina ↔ *Foxg1*$^{-/-}$ chiasm

Figure 9 shows mean % axon coverage at a distance of 45μm from the retinal explant for each of the different co-culture combinations. As for 23μm, % axon coverage differed significantly among all 8 co-culture combinations and also among all DN co-culture combinations, whereas VT co-cultures (Fig. 9B) failed to reveal any differences. Multiple pairwise comparisons produced the same results as for 23μm from the explant (Figures 9C, D).

Figure 9. % axon coverage differed among dorsonasal but not among ventrotemporal co-cultures at a distance of 45µm from the retinal explant.

% axon coverage for (A) DN and (B) VT co-cultures 45µm from the retinal explant. (A) The % axon coverage differed significantly among the four DN co-culture combinations (ANOVA, $p < 0.001$). The mean % axon coverage for DN control co-cultures (first bar) was statistically higher ($p < 0.001$) compared to all other DN combinations. Cultures of DN *Foxg1*$^{-/-}$ retina with control chiasm (second bar) had a significantly higher mean % axon coverage than DN *Foxg1*$^{-/-}$ ↔ *Foxg1*$^{-/-}$ co-cultures (fourth bar, $p = 0.033$). (B) % axon coverage did not differ among the four VT co-culture combinations (ANOVA, $p = 0.345$). (C) Table showing multiple pairwise comparisons among DN co-cultures only using the Tukey test. $P = 0.05$ is the critical value below which differences between means are considered statistically significant. (D) Table comparing all DN and VT co-culture combinations using the Tukey test. In (C) and (D), significant p-values were found for the same co-culture combinations and are highlighted in yellow. Abbreviations: DN is dorsonasal retina, VT is ventrotemporal retina, +/± is *Foxg1*$^{+/+}$ or *Foxg1*$^{+/-}$ tissue, -/- is *Foxg1*$^{-/-}$ tissue, oc is optic chiasm, error bars indicate standard error of the mean, n's are indicated in parentheses, ** $p < 0.001$, * $p < 0.033$.

% axon coverage for retina-chiasm co-cultures at a distance of 45um from the retinal explant

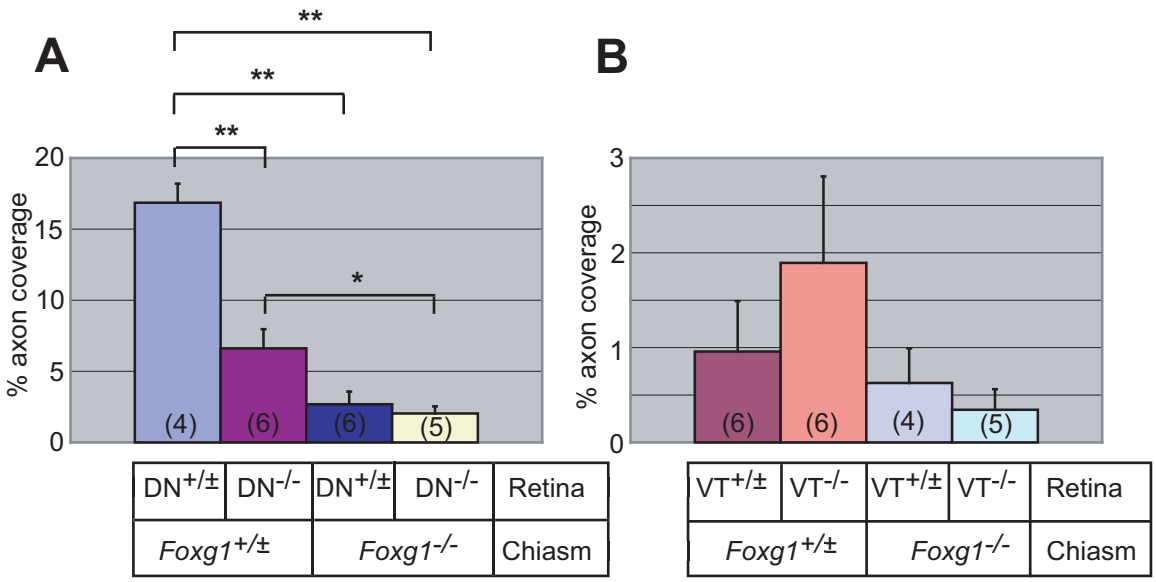

ANOVA (DN) P < 0.001

ANOVA (VT) P = 0.345

ANOVA (DN & VT) P < 0.001

C

Tukey test for DN co-cultures only	
Co-culture combination	p-value
DN +/±, +/± oc vs DN -/-, +/± oc	< 0.001
DN +/±, +/± oc vs DN +/±, -/- oc	< 0.001
DN +/±, +/± oc vs DN -/-, -/- oc	< 0.001
DN -/-, +/± oc vs DN -/-, -/- oc	0.033
DN -/-, +/± oc vs DN +/±, -/- oc	0.06
DN +/±, -/- oc vs DN -/-, -/- oc	0.972

D

Tukey test for all DN & VT co-cultures	
Co-culture combination	p-value
DN +/±, +/± oc vs all other combinations	< 0.001
DN -/-, +/± oc vs VT +/±, -/- oc	0.002
DN -/-, +/± oc vs VT +/±, +/± oc	< 0.001
DN -/-, +/± oc vs VT -/-, +/± oc	0.013
DN -/-, +/± oc vs DN -/-, -/- oc	0.031
DN -/-, +/± oc vs VT -/-, -/- oc	< 0.001
DN -/-, +/± oc vs DN +/±, -/- oc	0.086
VT -/-, -/- oc vs DN +/±, -/- oc	0.867

At 23μm and 45μm distances, even though DN *Foxg1*$^{-/-}$ retina cultured with *Foxg1*$^{+/\pm}$ chiasm produced greater axon coverages than DN *Foxg1*$^{+/\pm}$ retina cultured with *Foxg1*$^{-/-}$ chiasm, the difference in means was not statistically significant, although at 45μm this comparison produced a smaller p-value. Statistical analyses of % axon coverage at 68μm from the explant produced the same results as those found closer to the explant (data not shown). However, the significant difference between DN *Foxg1*$^{-/-}$ retina cultured with *Foxg1*$^{+/\pm}$ chiasm and DN *Foxg1*$^{-/-}$ ↔ *Foxg1*$^{-/-}$ co-cultures disappeared.

Moving further away from the explant to a distance of 91μm, the data did not follow a normal distribution (data not shown). Multiple pairwise comparisons revealed that the mean % axon coverage for DN control co-cultures was significantly higher compared to VT control co-cultures and VT *Foxg1*$^{-/-}$ ↔ *Foxg1*$^{-/-}$ co-cultures. However, all other differences in axon coverage that were present closer to the explant disappeared. One possible explanation is that very few axons remain at this distance, particularly for co-cultures with less axon outgrowth. Therefore, it becomes more difficult to accurately compare axon coverage between different co-cultures as the distance from the explant increases because axon length becomes a confounding factor. As a consequence, inferences were drawn from axon coverage measures obtained at the two distances closest to the explant (23μm and 45μm), which gave identical results.

Figure 10A shows % axon coverage for all DN co-culture combinations at increasing distances from the explant. All cultures showed a reduction in % coverage as the measuring distance increased from 23μm to 91μm. DN control co-cultures (blue diamonds on highest line) had the highest axon coverage over all distances measured and showed the steepest decline between 23μm and 45μm. Figure 10B is a summary graph for all 8 co-culture combinations at each of the four distances measured from the explant. VT co-cultures displayed the lowest % axon coverage means and at all distances from the explant one-way ANOVAs failed to reveal any significant differences in % axon coverage among the VT co-cultures.

Figure 10. % axon coverage for all co-cultures declined with increasing distance from the retinal explant.

(A) Graph showing % axon coverage for all dorsonasal retina-chiasm co-cultures at distances of 23, 45, 68 and 91μm from the retinal explant. All DN co-cultures showed an inverse relationship between axon coverage and distance from the explant. DN control co-cultures had significantly greater % axon coverages at all distances. The slopes of the lines are shallower for *Foxg1*$^{-/-}$ ↔ control and *Foxg1*$^{-/-}$ ↔ *Foxg1*$^{-/-}$ co-cultures reflecting the low number of neurites in these co-cultures.

(B) Summary graph of % axon coverage at varying distances from the retinal explant for all co-cultures. For each of the co-culture combinations, mean % axon coverage was highest closest to the explant and declined gradually as the distance from the explant increased. DN control co-cultures (first bar) had the highest mean % axon coverage overall. % axon coverage declined when *Foxg1* was absent from the DN retina (second bar) and was reduced further still when *Foxg1* was absent from the chiasm in the presence of *Foxg1*-expressing DN retina (third bar). DN *Foxg1*$^{-/-}$ ↔ *Foxg1*$^{-/-}$ co-cultures had the lowest mean % axon coverage out of all four DN combinations. All the VT co-cultures had low % axon coverage and none of them differed statistically from one another. Abbreviations: DN is dorsonasal retina, VT is ventrotemporal retina, +/± is *Foxg1*$^{+/+}$ or *Foxg1*$^{+/-}$ tissue, -/- is *Foxg1*$^{-/-}$ tissue, n's are indicated in parentheses.

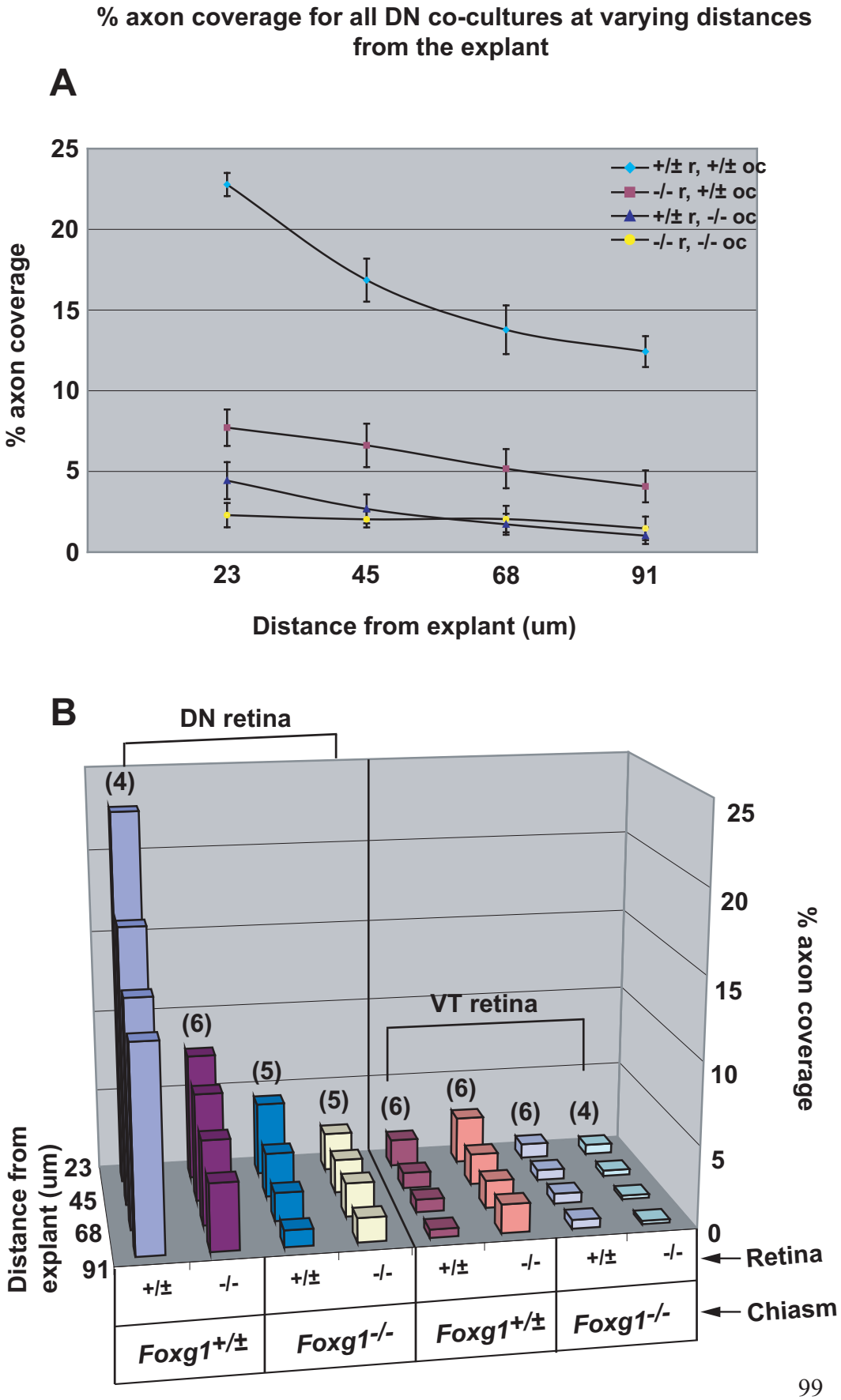
% axon coverage for all DN co-cultures at varying distances from the explant
A
% axon coverage
25
20
15
10
5
0
23
45
68
91
Distance from explant (um)
+/± r, +/± oc
-/- r, +/± oc
+/± r, -/- oc
-/- r, -/- oc
B
DN retina
VT retina
(4)
(6)
(5)
(5)
(6)
(6)
(6)
(4)
Distance from explant (um)
23
45
68
91
+/±
-/-
+/±
-/-
+/±
-/-
+/±
-/-
Foxg1+/±
Foxg1-/-
Foxg1+/±
Foxg1-/-
Retina
Chiasm
% axon coverage
25
20
15
10
5
0

3.4.5. The longest axons produced by dorsonasal *Foxg1*$^{-/-}$ retina cultured in the presence of *Foxg1*$^{+/\pm}$ chiasm were comparable in length to those from dorsonasal control co-cultures.

Figure 11 shows the mean length of the five longest neurites for DN and VT co-cultures. All 8 co-culture combinations had significantly different longest neurite lengths. The mean length of the five longest neurites was significantly greater for DN control co-cultures (Fig. 11A, 1st bar) compared to all other co-culture combinations apart from cultures of DN *Foxg1*$^{-/-}$ retina ↔ *Foxg1*$^{+/\pm}$ chiasm (Fig. 11A, 2nd bar), where there was no statistical difference (Figures 11A, D). In other words, removing *Foxg1* from the DN retina in the presence of *Foxg1*-expressing chiasm did not alter the maximum length to which neurites can extend compared to DN control co-cultures.

Comparisons among VT co-cultures failed to reveal any significant differences (Figure 11B). Statistical comparisons among DN co-cultures only (Fig. 11C) produced the same results as comparisons for all co-culture combinations (Fig. 11D), with one exception (asterisks in Figures 11C, D). Mean longest neurite lengths in cultures of DN *Foxg1*$^{+/\pm}$ retina with *Foxg1*$^{-/-}$ chiasm did not differ from *Foxg1*$^{-/-}$ ↔ *Foxg1*$^{-/-}$ co-cultures but were significantly shorter compared to those produced by DN control co-cultures. The mean length of the longest neurites was greater in cultures of DN *Foxg1*$^{-/-}$ retina with *Foxg1*$^{+/\pm}$ chiasm compared to DN *Foxg1*$^{-/-}$ ↔ *Foxg1*$^{-/-}$ co-cultures. However, this difference was only significant in statistical comparisons that encompassed all co-cultures but not significant in comparisons of DN co-cultures only, although the p-value of 0.057 is close to the critical value of p = 0.05. Therefore, the order of mean length for the 5 longest neurites from longest to shortest is: -

1. DN *Foxg1*$^{+/\pm}$ retina ↔ *Foxg1*$^{+/\pm}$ chiasm = DN *Foxg1*$^{-/-}$ retina ↔ *Foxg1*$^{+/\pm}$ chiasm
2. DN *Foxg1*$^{+/\pm}$ retina ↔ *Foxg1*$^{-/-}$ chiasm = DN *Foxg1*$^{-/-}$ retina ↔ *Foxg1*$^{-/-}$ chiasm

Figure 11. Dorsonasal *Foxg1*$^{-/-}$ retina cultured with *Foxg1*-expressing chiasm produced similar longest neurite lengths to DN control co-cultures.

Graphs showing mean lengths of the five longest neurites for (A) DN and (B) VT co-cultures. (B) Table comparing all DN co-cultures using the Tukey test, where $p < 0.05$ indicates a statistically significant result. (C) Table comparing all DN and VT co-culture combinations using the Tukey test. (B, C) Statistically significant results are highlighted in yellow. (A, B) Longest neurite means differed significantly among the four DN co-culture combinations (ANOVA, $p = 0.004$). The mean longest neurite length for DN control co-cultures (first bar) was significantly greater compared to all other DN combinations ($p \leq 0.016$), apart from DN *Foxg1*$^{-/-}$ retina cultured with control chiasm (second bar). (B, C) The longest neurites from cultures of DN *Foxg1*$^{-/-}$ retina with control chiasm did not differ significantly in length from those of DN control co-cultures (row highlighted in pink). (B) Longest neurite means did not differ among the four VT co-culture combinations (ANOVA, $p = 0.285$). (C) The mean lengths of the longest neurites for DN control co-cultures and cultures of DN *Foxg1*$^{-/-}$ retina with control chiasm were significantly greater compared to all VT combinations ($p \leq 0.006$). Cultures of DN *Foxg1*$^{-/-}$ retina with control chiasm had significantly higher mean longest neurite lengths compared to DN *Foxg1*$^{-/-}$ ↔ *Foxg1*$^{-/-}$ co-cultures ($p = 0.028$*). However, when comparisons were made solely between DN co-cultures (B), this difference disappeared but remained close to the critical p-value of 0.05 ($p = 0.057$*). The bracketed asterisk in (A) indicates this comparison. Abbreviations: DN is dorsonasal retina, VT is ventrotemporal retina, +/± is *Foxg1*$^{+/+}$ or *Foxg1*$^{+/-}$ tissue, -/- is *Foxg1*$^{-/-}$ tissue, error bars indicate standard error of the mean, n's are indicated in parentheses.

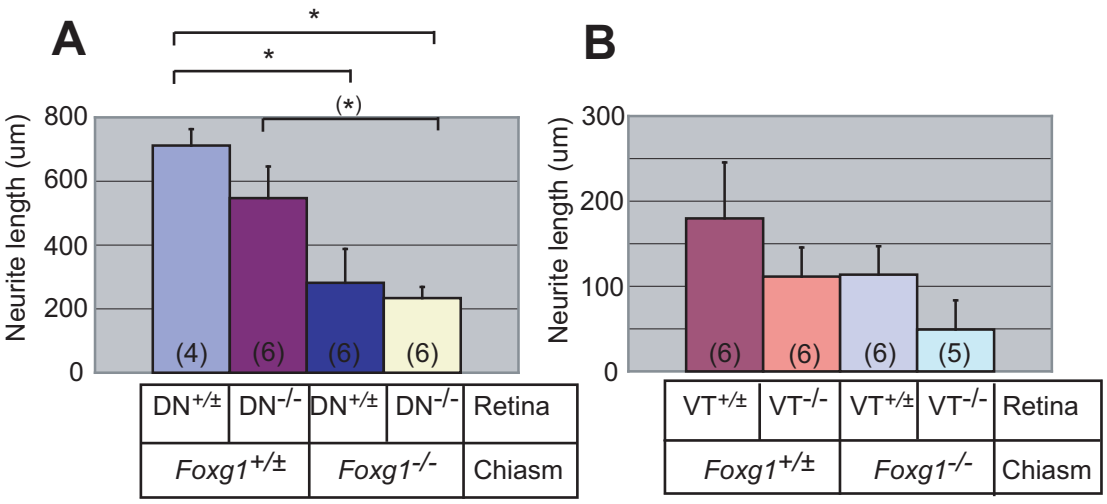

ANOVA P = 0.004

ANOVA P = 0.285

C

Tukey test for DN co-cultures only	
Co-culture combination	p-value
DN +/±, +/± oc vs DN -/-, -/- oc	0.007
DN +/±, +/± oc vs DN +/±, -/- oc	0.016
DN +/±, +/± oc vs DN -/-, +/± oc	0.577
DN -/-, +/± oc vs DN -/-, -/- oc	0.057*
DN -/-, +/± oc vs DN +/±, -/- oc	0.127

D

ANOVA (all) P < 0.001

Tukey test for all DN & VT co-cultures	
Co-culture combination	p-value
DN +/±, +/± oc vs DN -/-, -/- oc	< 0.001
DN +/±, +/± oc vs DN +/±, -/- oc	0.003
DN +/±, +/± oc vs DN -/-, +/± oc	0.736
DN +/±, +/± oc vs all other VT co-cultures	< 0.001
DN -/-, +/± oc vs DN +/±, -/- oc	0.098
DN -/-, +/± oc vs DN -/-, -/- oc	0.028*
DN -/-, +/± oc vs VT +/±, +/± oc	0.006
DN -/-, +/± oc vs VT -/-, +/± oc	< 0.001
DN -/-, +/± oc vs VT +/±, -/- oc	< 0.001
DN -/-, +/± oc vs VT -/-, -/- oc	< 0.001
DN +/±, -/- oc vs VT -/-, -/- oc	0.254

These results show that removing *Foxg1* from chiasm cells reduces the maximum length of DN *Foxg1*-expressing neurites. Also, the presence of *Foxg1* at the chiasm can fully rescue the extension of DN *Foxg1*$^{-/-}$ axons such that the longest neurites reach lengths equivalent to those found in DN *Foxg1*-expressing control co-cultures.

Figure 12A shows mean longest neurite lengths of retinal explants only alongside non-chimeric *Foxg1*$^{+/\pm}$ retina ↔ *Foxg1*$^{+/\pm}$ chiasm and *Foxg1*$^{-/-}$ retina ↔ *Foxg1*$^{-/-}$ chiasm co-cultures. Figure 12B shows the results of t-tests between retinal explants and their corresponding retina-chiasm co-culture, showing that DN *Foxg1*$^{-/-}$ ($p = 0.014$), VT control or '*Foxg1*$^{+/\pm}$' ($p = 0.005$) and VT *Foxg1*$^{-/-}$ ($p = 0.016$) explants all produced shorter neurites in the presence of chiasm cells. Interestingly, the lengths of the longest neurites produced by DN *Foxg1*$^{+/\pm}$ explants cultured alone were significantly shorter compared to those produced in combination with *Foxg1*$^{+/\pm}$ chiasm ($p = 0.021$). This indicates that DN *Foxg1*-expressing retinal neurites extend over greater distances when grown on a *Foxg1*$^{+/\pm}$ chiasm cell substrate.

3.4.6. Chiasm density.

The mean chiasm density did not vary significantly between different co-culture combinations (Figure 13). Therefore, any differences in axon outgrowth cannot be attributed to greater or lower densities of chiasm cells.

Figure 12. With the exception of dorsonasal control retina, chiasm cells reduced mean longest neurite lengths from DN and VT retinal explants. (A) A graph showing means for the length of the 5 longest neurites for retinal explants grown in the absence of chiasm cells in collagen alongside equivalent retina-chiasm co-cultures. (B) Tables of t-tests between adjacent pairs showed a significant reduction in mean longest neurite length when DN *Foxg1*$^{-/-}$, VT control and VT *Foxg1*$^{-/-}$ retinal explants were grown in combination with chiasm cells of the same genotype. However, DN control explants produced significantly longer neurites when grown in the presence of wild type chiasm cells ($p = 0.021$). Abbreviations: DN is dorsonasal retina, VT is ventrotemporal retina, control is *Foxg1*$^{+/+}$ or *Foxg1*$^{+/-}$ tissue, -/- is *Foxg1*$^{-/-}$ tissue, error bars indicate standard error of the mean.

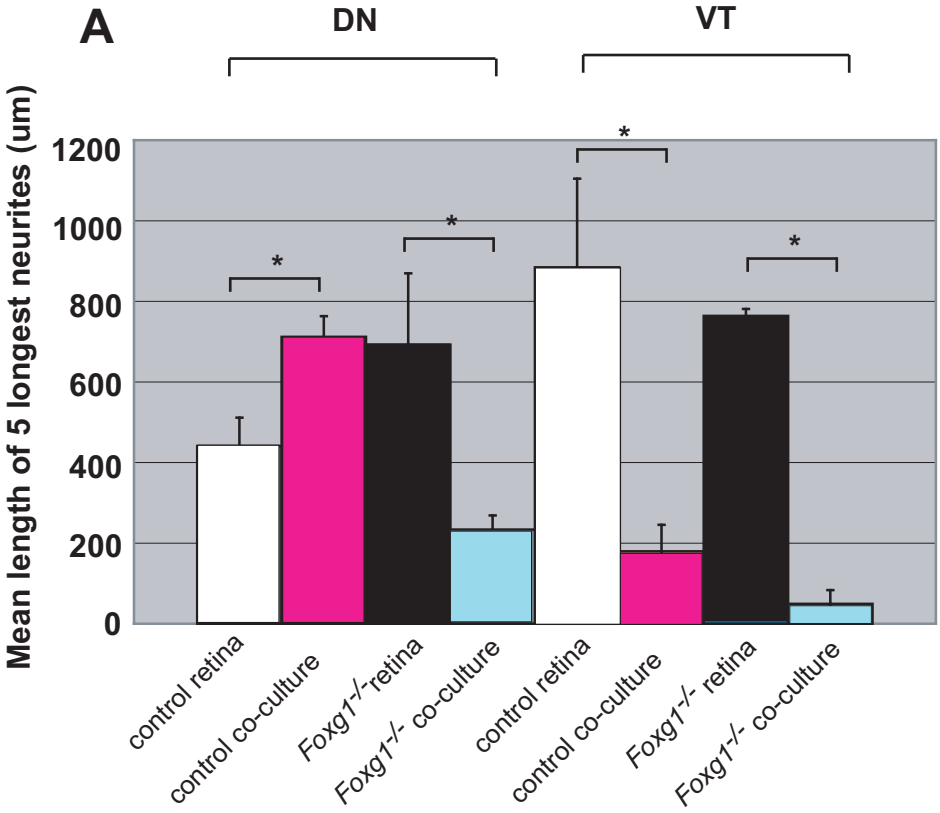

B

T-test	
Comparison	p-value
DN control vs DN control co-culture	0.021
DN *Foxg1*$^{-/-}$ vs DN *Foxg1*$^{-/-}$ co-culture	0.014
VT control vs VT control co-culture	0.005

Mann-Whitney	
Comparison	p-value
VT *Foxg1*$^{-/-}$ vs VT *Foxg1*$^{-/-}$ co-culture	0.016

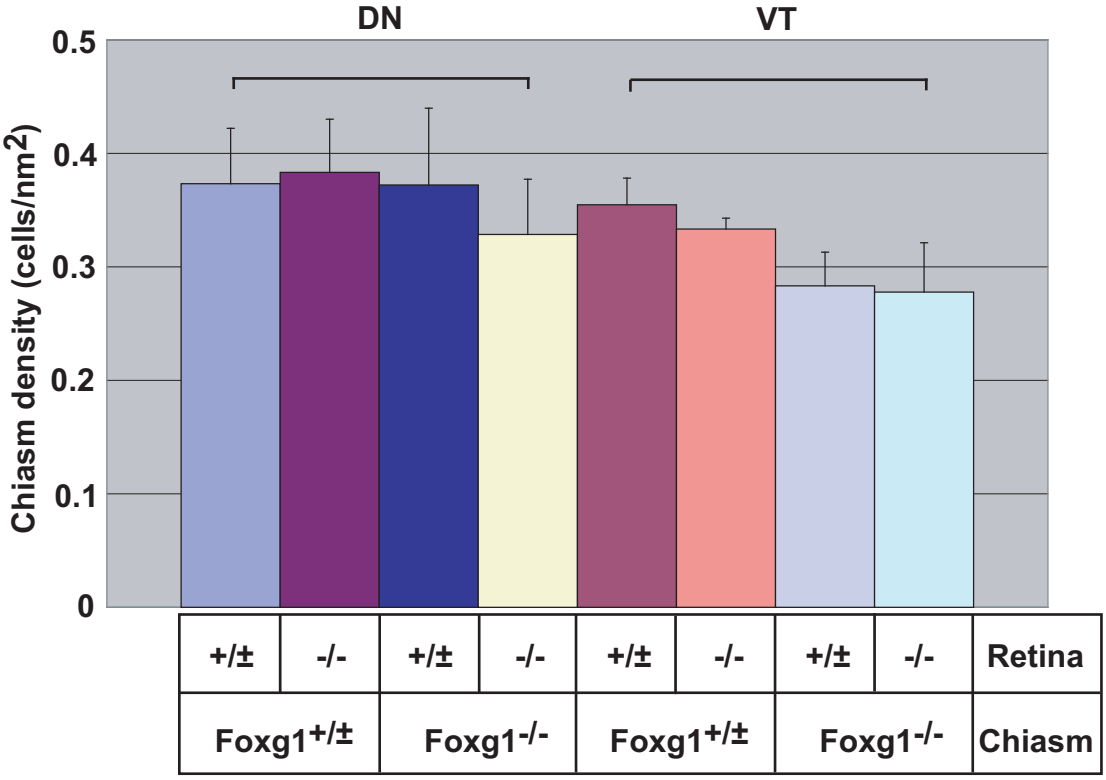

Figure 13. Chiasm cell density is the same across all co-cultures analysed.
The chiasm cell density for each co-culture combination does not differ ($p = 0.653$).

3.5. DISCUSSION

The chimeric co-culture experiment revealed that *Foxg1* is required both in the DN retina and in chiasm cells to mediate retinal axon laterality at the chiasm. The *in vitro* system was validated by preparing control co-cultures of *Foxg1*-expressing retina and chiasm. The axon outgrowth observed reproduced previous findings that in the presence of chiasm cells, VT axons are shorter and fewer in number compared to axons from DN retina (Herrera et al., 2004; Herrera et al., 2003; Marcus et al., 1995; Marcus and Mason, 1995; Marcus et al., 1996b; Wang et al., 1995). This reflects the avoidance of the chiasm region and subsequent ipsilateral path taken by VT retinal axons compared to the contralateral path across the chiasm midline followed by DN axons *in vivo*. % axon coverage from $Foxg1^{+/\pm} \leftrightarrow Foxg1^{+/\pm}$ VT and DN co-cultures was then used to define end-points on a scale from low outgrowth typical of ipsilateral axons to high outgrowth typical of contralateral axons. By comparing axon coverage (a measure of axon outgrowth) and neurite length of these control co-cultures to $Foxg1^{+/\pm} \leftrightarrow Foxg1^{-/-}$ chimeric co-cultures, conclusions could be made about the relative importance of *Foxg1* in the retina or the chiasm in producing contralateral axonal behaviour.

3.5.1. The behaviour of retinal axons from $Foxg1^{-/-} \leftrightarrow Foxg1^{-/-}$ co-cultures reflects the increased avoidance of the chiasm by nasal and temporal $Foxg1^{-/-}$ axons *in vivo*.

Axon coverage and longest neurite length were greatest in non-chimeric DN control co-cultures ($Foxg1^{+/\pm} \leftrightarrow Foxg1^{+/\pm}$), lowest in $Foxg1^{-/-} \leftrightarrow Foxg1^{-/-}$ co-cultures, with $Foxg1^{+/\pm} \leftrightarrow Foxg1^{-/-}$ co-cultures producing means between these two extremes. VT co-cultures mostly followed the same trend, with VT $Foxg1^{-/-} \leftrightarrow Foxg1^{-/-}$ co-cultures displaying lower axon coverage and shorter neurites compared to non-chimeric VT control co-cultures, although the difference was not statistically significant unlike for

DN cultures. The low degree of outgrowth observed in non-chimeric DN and VT *Foxg1*$^{-/-}$ ↔ *Foxg1*$^{-/-}$ co-cultures relative to non-chimeric control *Foxg1*-expressing co-cultures is reminiscent of the greater ipsilateral routing of *Foxg1*$^{-/-}$ nasal and temporal retinal axons *in vivo*. Statistical comparisons between DN and VT *Foxg1*$^{-/-}$ ↔ *Foxg1*$^{-/-}$ co-cultures failed to reflect the temporal bias in the source of ipsilateral projections in *Foxg1*$^{-/-}$ embryos, as in wild type embryos (Pratt et al., 2004). Nevertheless, there were hints of this difference shown by lower % axon coverage and shorter neurite lengths in *Foxg1*$^{-/-}$ ↔ *Foxg1*$^{-/-}$ co-cultures prepared using VT retina compared to those using DN retina. Overall, the axon outgrowth phenotypes of *Foxg1*$^{-/-}$ ↔ *Foxg1*$^{-/-}$ co-cultures provide accurate *in vitro* representations of the increased tendency of axons from the entire retina to project ipsilaterally at the chiasm.

3.5.2. *Foxg1* expression in the DN retina and chiasm is required for normal outgrowth of DN axons.

Overall, analyses of % axon coverage and longest neurite lengths produced similar trends and together showed that *Foxg1* is required in DN retina and in chiasm cells for high axon outgrowth from DN retina *in vitro*. Absence of *Foxg1* from DN retina significantly reduced axon coverage relative to non-chimeric DN control co-cultures, regardless of whether *Foxg1* was present at the chiasm suggesting an autonomous requirement for *Foxg1* in DN retina. However, *Foxg1* also acts non-autonomously outside DN retina because in DN *Foxg1*$^{-/-}$ retina ↔ *Foxg1*$^{+/\pm}$ chiasm co-cultures, axon coverage from DN *Foxg1*$^{-/-}$ retina was significantly greater compared to DN *Foxg1*$^{-/-}$ ↔ *Foxg1*$^{-/-}$ co-cultures. This requirement for *Foxg1* at the chiasm was strongly corroborated by observations that *Foxg1*-expressing chiasm can fully rescue maximum neurite lengths to non-chimeric control co-culture levels. In contrast, *Foxg1*-expressing DN retina (in *Foxg1*$^{+/\pm}$ retina ↔ *Foxg1*$^{-/-}$ chiasm co-cultures) could not increase neurite lengths or axon coverage relative to *Foxg1*$^{-/-}$ ↔ *Foxg1*$^{-/-}$ co-cultures.

In summary, the neurite length and axon coverage analyses showed the following: -

DN *Foxg1*$^{+/\pm}$ retina ↔ *Foxg1*$^{+/\pm}$ chiasm ≥ DN *Foxg1*$^{-/-}$ retina ↔ *Foxg1*$^{+/\pm}$ chiasm
DN *Foxg1*$^{-/-}$ retina ↔ *Foxg1*$^{+/\pm}$ chiasm > DN *Foxg1*$^{-/-}$ retina ↔ *Foxg1*$^{-/-}$ chiasm
DN *Foxg1*$^{+/\pm}$ retina ↔ *Foxg1*$^{-/-}$ chiasm = DN *Foxg1*$^{-/-}$ retina ↔ *Foxg1*$^{-/-}$ chiasm

Although this evidence shows that loss of *Foxg1* in the chiasm is sufficient to account for the drop in axon outgrowth and shorter neurites, the axon coverage findings show a clear role for *Foxg1* in the DN retina.

The fact that *Foxg1*-expressing chiasm fully rescued maximum neurite length but only partly rescued % axon coverage relative to non-chimeric DN control co-cultures may represent a real difference in the roles of *Foxg1* in mediating axon extension versus axon coverage. Alternatively, it could be a consequence of how the co-cultures were analysed. For a given co-culture, measurements of the five longest neurites only represented a small subpopulation of the total number of neurites in the whole co-culture. In contrast, % axon coverage encompassed all neurites and thus represented axon outgrowth from the whole culture. Moreover, there was considerable variability in longest neurite length between different explants within the same co-culture combination, particularly for DN *Foxg1*$^{+/\pm}$ retina ↔ *Foxg1*$^{-/-}$ chiasm co-cultures and all the VT co-culture combinations. Even when the mean neurite length was short, anomalously long neurites were often found. One explanation is that despite the repulsive environment presented to the retinal neurites by chiasm cells in culture, a couple of neurites can extend in a highly fasciculated manner over long distances by avoiding contact with chiasm cells. Despite these caveats, analyses of neurite length, combined with axon coverage data, are useful in determining the site of action of *Foxg1*.

3.5.3. *Foxg1* expression does not affect the outgrowth of VT retinal axons co-cultured with chiasm.

Axon coverage and longest neurite length did not differ among VT co-cultures. Taken at face value, these non-significant comparisons suggest that *Foxg1* does not play any role in the VT retina or at the chiasm in guiding VT RGC axons contralaterally or ipsilaterally. However, this is inconsistent with the DiI backlabeling observations of an increased ipsilateral projection from nasal and temporal retina in $Foxg1^{-/-}$ embryos (Pratt et al., 2004). A possible explanation for this inconsistency is that the co-culture method may not be sensitive enough to detect changes in the response of VT axons to $Foxg1^{-/-}$ or $Foxg1^{+/\pm}$ chiasm cells. This is plausible as the paucity of axons produced when VT retina is cultured with chiasm cells may make it hard to distinguish further reductions in axon coverage. For example, comparing co-cultures with three or four axons to those that show a reduction of one or two axons may not produce a statistically significant difference. It is possible that increasing the number of replicates for each VT co-culture combination may improve the power of the statistical test, enabling small changes to be detected. In order to distinguish between lack of sensitivity and a true result, more sensitive analyses of axon growth in VT co-cultures could be attempted, such as time-lapse video microscopy, growth cone turning assays or stripe assays consisting of $Foxg1^{-/-}$ and $Foxg1^{+/\pm}$ chiasm (Sretavan and Reichardt, 1993; Walter et al., 1987; Zheng et al., 1996).

Another possible reason that could lead to differential effects of *Foxg1* among the VT co-cultures being obscured is the presence of contralateral RGCs in the VT retinal explants. Although ipsilateral RGCs are concentrated in the VT crescent (VTC) that occupies approximately 20% of the entire retina, roughly 25% of RGCs in the VTC project ipsilaterally (Jeffery et al., 1981). Therefore, it was unavoidable that the VT retinal explants used for the co-cultures contained some contralateral RGCs. In order to eliminate ‘contaminating’ contralateral RGCs and provide a pure population of

ipsilateral RGCs for culture, a technique called immunopanning could be used (Butowt et al., 2000). This method has been used to isolate a pure population of chick RGCs for culture using monoclonal antibodies raised against Thy1 expressed exclusively by RGCs. It is conceivable that the same could be done using a marker of ipsilateral RGCs, such as the EphB1 receptor (Williams et al., 2003). However, this technique would dissociate RGCs into single cells and produce less retinal tissue. Therefore, changes to the *in vitro* co-culture method would have to be made.

3.5.4. *Foxg1*$^{-/-}$ retinal explants cultured without chiasm were not impaired in their ability to produce axons relative to *Foxg1*-expressing explants.

To exclude the possibility that intrinsic differences exist in the outgrowth or extension of neurites from *Foxg1*-expressing and *Foxg1*$^{-/-}$ retina that might explain the co-culture results observed, cultures of DN and VT retinal explants were prepared without chiasm cells. Comparisons of neurite extension and axon coverage between DN *Foxg1*$^{+/\pm}$ and DN *Foxg1*$^{-/-}$ retinal explants and between VT *Foxg1*$^{+/\pm}$ and VT *Foxg1*$^{-/-}$ explants failed to reveal significant differences, apart from a small difference in axon coverage between VT *Foxg1*$^{+/\pm}$ and VT *Foxg1*$^{-/-}$ explants observed at 23µm from the explant. However, this was not replicated at any other distance, nor was it seen in analyses of neurite extension. Consequently, any effect this might have had on axon coverage in the VT retina-chiasm co-cultures is considered negligible.

% coverage of axons from VT retina was greater compared to that from DN retina when cultured without chiasm cells. These data agree with a similar culture system in which VT wild type retina cultured alone in collagen produced significantly longer and more numerous axons than the other retinal quadrants (Wang et al., 1996). This is the opposite trend to that shown in the retina-chiasm co-cultures, where explants from non-chimeric DN control co-cultures produced significantly greater axon coverage

compared to all VT co-cultures. This indicates that *Foxg1*-expressing chiasm actually promotes the growth of contralateral (DN) axons and that the high axon coverage observed in DN *Foxg1*$^{+/\pm}$ retina ↔ *Foxg1*$^{+/\pm}$ chiasm co-cultures was not simply the result of differences in axon outgrowth between DN and VT retina. Rather this reflects previous findings that contralateral and ipsilateral retinal axons respond differently to chiasm cells and their diffusible molecules, with ipsilateral axons growing less well in their presence (Wang et al., 1995, Wang et al., 1996, Marcus et al., 1996b, Williams et al., 2006; Wizenmann et al., 1993). In conclusion, any variation in axon outgrowth or longest neurite lengths observed in the co-culture experiments could be completely attributed to the presence or absence of *Foxg1* for a particular combination of retina and chiasm.

3.5.5. DN retinal axons grow better in the presence of chiasm cells than in their absence whereas VT axons grow more poorly.

In the co-culture experiment described here, chiasm cells have a positive effect on axon outgrowth from DN retina but a negative effect on VT axon outgrowth relative to explants grown alone. The growth-promoting effect of chiasm on DN retinal axons is consistent with the co-culture results of Chan et al. (2002) in which DN but not VT neurites invaded neighbouring chiasm explants. Together, these results suggest that chiasm tissue not only provides inhibitory cues that reduce overall neurite outgrowth from VT but not DN retina but also contact-dependent attractive cues to axons from DN retina. It is possible that chiasm cells secrete a diffusible chemoattractant, such as netrin, that helps guide navigating retinal axons from the retina towards the ventral midline in order for them to contact midline radial glia. However, this remains hypothetical as no diffusible chemoattractants have been found at the chiasm. Although the diffusible protein netrin plays an important role in the navigation of commissural axons at the midline of the Drosophila ventral nerve cord and at the floor plate of the

vertebrate spinal cord (Kaprielian et al., 2001; Mitchell et al., 1996; Serafini et al., 1996; Shirasaki et al., 1996), netrins are not expressed at the chiasm midline in mice (Deiner et al., 1999). However, netrin-1 is present in the optic nerves and in ventral-lateral hypothalamic regions (Deiner & Sretavan, 1999). Therefore, it is conceivable that netrin-1 in these regions may interact with its receptor DCC and its repulsive receptor UNC-5, expressed on retinal axons to influence their navigation course (Anderson and Holt, 2002; Shewan et al., 2002).

More is known about molecules involved in contact-dependent attraction surrounding the chiasm. Cells of the ventral diencephalon are known to express surface molecules involved in cell-cell adhesion and axon extension, such as the L1 family of cell adhesion molecules expressed by RGCs and their axons (Lustig et al., 2001; Sretavan et al., 1994). One L1 family member is Nr-CAM that is expressed at the chiasm and also exclusively by contralateral RGCs and their axons and has been shown to promote contralateral behaviour *in vitro* and *in vivo* (Williams et al., 2006). However, Nr-CAM at the chiasm itself is unlikely to promote the growth of contralateral axons because wild type and *Nr-CAM*$^{-/-}$ chiasm reduced outgrowth of both DT (crossed) and VT (uncrossed) axons equally in retina-chiasm co-cultures and the same co-cultures showed that Nr-CAM acts primarily in the retina. Also, *in vivo* experiments using *Nr-CAM* null mice showed that Nr-CAM influences the guidance of late-born VT RGCs and is, therefore, an unlikely candidate for increasing ipsilateral projections in *Foxg1*$^{-/-}$ embryos. Chiasm cells express heparan sulphate, a sugar moiety on the transmembrane glycoprotein CD44 that promotes axon growth by sequestering heparin binding growth factors. CD44 itself has been reported to promote the growth of contralateral axons at the chiasm midline (Lin and Chan, 2003), although there is contradictory evidence that CD44 reduces neurite outgrowth from mouse retina (Sretavan et al., 1994). In summary, although there are a couple of molecules that appear to promote the growth of contralateral axons, it is unclear whether any of these are responsible for producing

the increased outgrowth of DN axons over chiasm cells observed in the co-cultures presented here.

3.5.6. Lack of *Foxg1 in vitro* produced axon outgrowth that resembled that of ipsilateral axons suggesting altered expression of ipsilateral determinants in the DN retina and at the chiasm.

In DN co-cultures lacking *Foxg1* in the DN retina or at the chiasm or both, % axon coverage was reduced, resembling that produced by VT axons from control co-cultures. The requirement for *Foxg1* in the retina and chiasm for contralateral axon outgrowth implies that changes occur in both of these tissues in *Foxg1*$^{-/-}$ embryos to increase ipsilateral behaviour by axons. In the DN retina, it is likely that expression of an ipsilateral determinant increases or alternatively a contralateral determinant could decrease. Similarly at the chiasm, the increased avoidance of the chiasm by Foxg1$^{-/-}$ retinal axons suggests an increase in a repulsive guidance cue or a reduction in an attractive cue.

The majority of research directed at understanding the role of the chiasm in contralateral-ipsilateral axon pathfinding has centred on repulsive or inhibitory factors rather than attractive cues. The reason for this is that during the peak period of retinal axon divergence in the mouse from E14 – E16, the chiasm is generally inhibitory. Molecules that are inhibitory to retinal axon growth in the chiasm region or ventral diencephalon include ephrin-B2 (Nakagawa et al., 2000; Williams et al., 2003), chondroitin sulphate proteoglycans (Tuttle et al., 1998); Chung et al., 2000a, 2000b), CD44 (Sretavan et al., 1994; Sretavan et al., 1995), SSEA-1 (Marcus and Mason, 1995; Sretavan et al., 1994) and slits (Thompson et al., 2006a, 2006b; Plump et al., 2002; Erskine et al., 2000; (Niclou et al., 2000; Ringstedt et al., 2000). However, the majority of these molecules have been shown to reduce axon growth from all retinal regions,

rather than VT axons selectively, supporting findings of the production of one or more diffusible repulsive cue(s) that affect all retinal loci equally (Chan et al., 2002; Wang et al., 1996). The effect of a diffusible cue on the different retinal explants could not be addressed in the co-cultures presented in this Chapter because it would involve keeping the chiasm intact and/or preventing it from contacting the retina. However, it is unlikely that this diffusible cue is responsible for changing the proportion of contralateral versus ipsilateral axons in *Foxg1*$^{-/-}$ embryos since it has been found to reduce axon outgrowth from wild type DN and VT retina equally (Chan et al., 2002; Wang et al., 1995).

In the past few years, a number of candidates have been identified that potentially influence ipsilateral-contralateral pathfinding (Herrera et al., 2003; Herrera et al., 2004; Pak et al., 2004; Williams et al., 2003; Williams et al., 2006). Previous studies have shown that contacts between retinal axons and cells or membranes from the chiasm region are crucial for suppressing the growth of ipsilateral but not contralateral axons (Chung et al., 2000a, 2000b; Wang et al., 1995; Wizenmann et al., 1993). Specifically, all axons contact a radial glial 'palisade' at the chiasm midline before either projecting ipsilaterally or contralaterally (Marcus & Mason 1995; Marcus et al., 1995). These midline radial glial cells express the evolutionarily-conserved molecule ephrin-B2, which is known to be responsible for the selective repulsion of EphB1- bearing ipsilateral axons in the amphibian *Xenopus* and mice (Nakagawa et al., 2000; Williams et al., 2003). Since contralateral axons do not express EphB1, they are not repelled when they contact their ligand ephrin-B2 at the chiasm midline. Therefore, it will be crucial to examine both ephrin-B2 at the chiasm and EphB1 expression in the retina of *Foxg1*$^{-/-}$ embryos. Another ipsilateral determinant is a zinc finger transcription factor involved in early neural patterning called Zic2 that is expressed in VT retina cotemporaneously and in the same RGCs as EphB1 (Williams et al., 2003). Zic2 has been shown to control the ipsilateral routing of RGCs both *in vitro* and *in vivo* (Herrera et al., 2003). Therefore, Zic2 is a prime candidate for increasing the ipsilateral

projection in *Foxg1*$^{-/-}$ embryos from the retina. In terms of contralateral determinants, Islet 2 (Isl2) expression is confined to RGCs that project contralaterally, although it is not expressed by all contralateral RGCs (Pak et al., 2004). *Isl2* null mice show an increased ipsilateral projection from a greater number of Zic2-expressing RGCs in the VTC. Therefore, Isl2 is another candidate molecule whose expression may be altered in the *Foxg1*$^{-/-}$ retina.

3.5.7. Extra-retinal tissues that express *Foxg1* may influence retinal axon guidance.

Although the co-cultures show a requirement for *Foxg1* in DN retina, they do not prove whether this is RGC-autonomous. It is possible that during eye development, *Foxg1*-expressing tissues, such as the lens and retinal pigment epithelium, influence the expression of genes in the retina that control its development (Dou et al., 1999). In the absence of *Foxg1,* retinal patterning may be disrupted through altered expression of patterning molecules or morphogens producing a retina that is more ipsilateral in character. Hence nasal RGCs that would normally project contralaterally would be respecified to project ipsilaterally. In this model, *Foxg1* is not required autonomously within nasal RGCs themselves but is required autonomously by the nasal retina. In the co-cultures, the retina had been dissected free from the RPE and lens. Therefore, throughout the *in vitro* 48-hour culture period, these extra-retinal tissues could not have influenced axon guidance directly. However, development of the retina occurs before the first axons leave the RGC layer and before E14.5, the age of the embryos used for the co-cultures. Therefore, extra-retinal tissues could have already patterned the retina in control and *Foxg1*$^{-/-}$ embryos, influencing the behaviour of retinal axons in culture. Since the co-cultures are not able to discriminate between an RGC- versus nasal retina-autonomous requirement, this hypothesis cannot be excluded.

3.5.8. Analyses of axon fasciculation, volume and surface area suffered from limitations and were not as representative as axon coverage.

For each co-culture, the widths of all axon fascicles were measured and the means calculated to provide a measure of axon fasciculation. Similarly the volume and surface area of axons extending into the surrounding chiasm cells were measured using the computer software *Volocity*. However, none of these analyses produced statistically significant results. This was surprising as it was hypothesized that chiasm cells would elicit greater fasciculation from VT (uncrossed) axons than from DN (crossed) axons due to greater inhibition of axon outgrowth by chiasm cells. VT axons might attempt to minimize the surface area of the axon in contact with optic chiasm cells or their secreted products whilst DN axons should show less fasciculation and greater surface areas and volumes because they are not as inhibited by chiasm cells.

Axon fasciculation analysis actually produced results opposite to those predicted. DN control co-cultures had the widest fascicles (instead of the predicted narrowest) and VT *Foxg1*$^{-/-}$ ↔ *Foxg1*$^{-/-}$ co-cultures had the narrowest fascicles (instead of the widest). A possible explanation could be the confounding influence of axon number. The more axons there are, the greater the probability that they will meet, bundle together and form fascicles as observed in DN control co-cultures. The fewer axons there are, the less likely they will be to fasciculate as they emerge from fewer locations along the explant surface, reducing the probability of one axon contacting another. Equally there are problems with measuring neurite volumes and surface area because they are confounded by the degree of fasciculation. For these reasons coupled with large variation between cultures of the same combination, fascicle width, axon volume and axon surface area were not considered reliable ways of analyzing axon outgrowth.

Examination of 3D reconstructions of the co-culture confocal images revealed that contacts between axons and chiasm cells were observed in all co-culture combinations.

However, it was unclear whether there was a reduction in the frequency of axon-chiasm contacts in cultures with less axon outgrowth, since contact frequency is expected to increase proportionally with increasing numbers of axons. This could be examined further using time-lapse video microscopy to observe the behaviour of growth cones in the proximity of chiasm cells.

The co-culture system used here does not attempt to fully recreate the complex environment found *in vivo* where there are many more factors, including the extracellular matrix and other tissues or diffusible molecules that almost certainly affect axon guidance. However, it reflects the observations seen by DiI tracing in wild type and *Foxg1*$^{-/-}$ embryos and more importantly it confirms previous findings using similar co-culture methods. The scope for manipulating the simple co-culture system, for example by adding molecules or blocking guidance cues or receptors present in the chiasm or retina, is immense. The unambiguous axon outgrowth phenotype of DN and VT retina co-cultured with chiasm means that any abnormalities are simple to identify and analyse, making this experiment a powerful tool for studying retinal axons at the chiasm.

CHAPTER 4: The number of cells expressing the ipsilateral determinant Zic2 is increased in the *Foxg1*$^{-/-}$ retina.

4.1. ABSTRACT

Previous studies have identified the zinc finger transcription factor Zic2 as an ipsilateral determinant that is expressed by postmitotic RGCs in the peripheral ventrotemporal (VT) retina. The aim of this chapter was to test the hypothesis that numbers of Zic2-expressing cells increase to match the unusually large ipsilateral projection originating from the entire *Foxg1*$^{-/-}$ retina. The *Foxg1*$^{-/-}$ nasal retina displayed an increase in the numbers of cells expressing Zic2 relative to the wild type but there was either no change or a slight decrease in the temporal retina. In wild type retinas, clusters of Zic2-expressing cells were mostly seen in VT retina and never in the nasal retina where *Foxg1* is normally expressed. This suggests that Foxg1 represses Zic2 in the nasal retina, thereby inhibiting ipsilateral projections in this region. In the nasal retina of *Foxg1* null embryos, it is hypothesized that the repression on Zic2 by Foxg1 is relieved. This results in increased Zic2 expression and ipsilaterally-projecting axons, most likely through induction of EphB1 receptors by Zic2, which are repelled by ephrin-B2 at the optic chiasm. Gain- and loss-of-function experiments would confirm whether Foxg1 can repress Zic2 *in vitro* and whether Foxd1 is involved in this process. Furthermore, studies of EphB1 expression in the *Foxg1*$^{-/-}$ retina would reveal whether its expression increases concomitantly with Zic2 in the nasal retina, bolstering evidence for EphB1's involvement in the ipsilateral program. In the *Foxg1*$^{-/-}$ eye, changes in Zic2 expression are biased towards the nasal retina compared with more subtle alterations in the temporal retina. This is compatible with a theory in which Foxg1

normally regulates Zic2 expression in nasal RGCs themselves, although a non-autonomous effect in temporal RGCs remains a possibility.

4.2. INTRODUCTION

4.2.1. An overview of the developmental roles of the Zic gene family.

Zic2 is a member of the Zic family of zinc-finger (ZF) proteins encoded by the Zic genes that are vertebrate homologues of the Drosophila *odd-paired* (*opa*) pair-rule gene (Aruga et al., 1996). The Zic or 'zinc finger protein of the cerebellum' genes were first discovered in the mouse cerebellum as a family of structurally-related genes that exhibited highly restricted patterns of expression (Aruga et al., 1996; Aruga et al., 1994). Five homologous *Zic* genes play evolutionarily conserved roles in human, mouse, frog, fish and ascidian development, including left-right axis formation, myogenesis, skeletal patterning and neurogenesis as well as a multitude of important functions in neural development (Aruga, 2004). These functions can be split into five main categories: cell fate determination in the ectoderm, neurulation, forebrain development, cerebellar patterning and retinal axon guidance.

Vertebrate *Zic1*, *Zic2* and *Zic3* are closely related forming a subgroup in phylogenic trees of the *Zic* gene family (Aruga et al., 1996). They are known as 'pre-patterning' genes as they are expressed before the earliest events in the development of the CNS. Zic1 - 3 proteins have highly similar amino acid sequences with partly overlapping expression patterns along the dorsal spinal cord and midbrain (Elms et al., 2004; Nagai et al., 1997). At later embryonic stages, *Zic1 - 3* are expressed in structures derived from the dorsal neural tube, notably the dorsal and ventral diencephalons and cerebellum (Inoue et al., 2004; Nagai et al., 1997). The restriction of Zic1, 2 and 3 to the dorsal part of the neural tube and its derivatives is due to the opposing actions of

BMP and Shh during neural tube development (Aruga et al., 2002). In the developing neural tube, Shh inhibits *Zic* gene expression ventrally, whereas dorsally, BMP4 and BMP7 act as positive regulators, demonstrated by overexpression studies in the chick spinal cord and in zebrafish (Aruga et al., 2002; Rohr et al., 1999).

Despite extensive knowledge of the various roles of Zic genes in development, their transcriptional targets and the signaling pathways through which Zic gene products exert their effects remain unknown. Nevertheless, some clues are emerging. Zic proteins play diverse roles during neural development, enhancing differentiation into neuroectoderm early in development but inhibiting neuronal differentiation later (Aruga et al., 2002). Inhibiting neuronal differentiation requires Notch signaling, which controls myriad developmental processes. This may in turn explain the numerous functions that Zic gene products play during development (Artavanis-Tsakonas et al., 1999; Kintner, 2002).

4.2.2. Zic transcription factors are possible modulators of hedgehog signaling.

Several lines of evidence suggest that Zic proteins have the potential to modulate hedgehog signaling. The zinc-finger domains of Zic and Gli transcription factors are highly homologous and recently it was shown that Zic proteins are capable of binding to specific Gli target DNA sequences in vitro, albeit with lower affinity than Gli proteins, suggesting possible interactions in vivo (Mizugishi et al., 2001). Moreover, recent findings elucidated that the ZF domains of Zic and Gli proteins can interact with one another, enhancing the nuclear localization of Gli and suggesting a role for Zic proteins as Gli cofactors (Koyabu et al., 2001). In this way, transcriptional regulation by Zic proteins may not always result from conventional sequence-specific binding. Although a Zic-Gli interaction has not been conclusively demonstrated in neural tissue, there is accumulating evidence for both opposing and cooperative interactions between

these two proteins through gain-of-function and loss-of-function analyses (Aruga et al., 1999; Brewster et al., 1998).

Further indications of a link between hedgehog signaling and Zic2 come from studies of mice with reduced Zic2 expression (Nagai et al., 2000). These *Zic2*$^{kd/kd}$ (Zic2 knockdown) mice possess a mutated Zic2 allele (*Zic2*^{kd}) whose expression is 21% of the wild type allele (Nagai et al., 2000). *Zic2*$^{kd/kd}$ mice experience a neurulation delay and subsequent neural tube closure defects resulting in spina bifida and a forebrain abnormality called holoprosencephaly (HPE) (Brown et al., 2001; Brown et al., 1998; Nagai et al., 2000) HPE is also a characteristic of *Shh* null mice (Chiang et al., 1996). HPE results from disrupted left-right forebrain patterning and produces phenotypes that range from severe cases in which there is a single ventricle or milder forms in which midline structures are malformed to varying degrees. Heterozygous loss-of-function mutations in ZIC2 are thought to be responsible for 3 – 4% of HPE cases in humans (Brown et al., 1998, 2001), although other genes, including SHH (Belloni et al., 1996; Roessler et al., 1996), SIX3 (Wallis et al., 1999) and TGIF (Gripp et al., 2000) also cause this forebrain phenotype. The convergent HPE phenotype of *Zic2* and *Shh* null mice suggests that Shh and Zic2 act in the same signaling pathway or that Shh regulates Zic2. Several observations are consistent with the idea that Shh inhibits or restricts Zic2 expression ventrally in the neural tube. For example, the Zic2-expressing region shifts ventrally in the spinal cord of *Shh* null mice (Brown et al., 2003) and also in mice with degeneration of the notochord, a structure that normally expresses Shh which then sets up ventral identity in the neural tubes (Nagai et al., 1997).

Despite the shared HPE phenotype, there are several differences between *Shh* and *Zic2* mutants. For instance, *Shh* mutants display facial deformities, such as cyclopia and midline clefts whereas *Zic2*$^{kd/kd}$ mice and *ZIC2*-deficient do not (Chiang et al., 1996; Roessler et al., 1996). Also, exencephaly and anencephaly occur in several *Zic2*$^{kd/kd}$ mice (Nagai et al., 2000) but these brain malformations are never observed in *Shh*

mutants. Therefore, further investigation is required to reveal the exact relationship between Zic2 and Shh specifically in forebrain development.

4.2.3. Zic2 determines the uncrossed retinal axon pathway.

In mouse embryos, Zic2 appears in the developing eye from E9.5 when it is expressed along with Zic1 and Zic3 in the optic vesicle and optic stalk. From E10.5, Zic2 is expressed in the proliferating ciliary marginal zone (CMZ) by retinal precursors (Nagai et al., 1997). Zic2 is expressed in ventrotemporal postmitotic RGCs from E14 - E17, the time-frame during which the permanent ipsilateral projection forms (Herrera et al., 2003). Since the ventrotemporal retina is the part of the retina that gives rise to ipsilateral retinal axons, Zic2 expression coincides spatially and temporally with the ipsilateral projection.

Simply observing a correlation between Zic2 expression and the appearance of ipsilateral retinal axons does not prove that Zic2 expression in VT RGCs is responsible for determining an uncrossed path at the chiasm. However, in the past few years, several lines of evidence have strongly implicated Zic2 as an ipsilateral determinant. Zic2 homozygous knockdown mice (Nagai et al., 2000) carry 2 copies of a mutated *Zic2*^{kd} allele (*Zic2*$^{kd/kd}$), which reduces Zic2 expression to 20% of the wild type level, display a severely reduced ipsilateral projection. However, *Zic2*$^{kd/kd}$ mice show morphological abnormalities of the ventral diencephalon and abnormal ephrin-B2 expression, so it is unclear whether the abnormal chiasm or lack of retinal Zic2 produced the guidance defect. In contrast, *Zic2*$^{kd/+}$ embryos, which have intermediate Zic2 expression levels between *Zic2*$^{kd/kd}$ and wild type embryos, have a chiasm that is normal anatomically and molecularly, yet still possess a reduced ipsilateral projection. Herrera et al. (2003) suggested that a reduction in Zic2 in the retina was probably the most likely explanation for this. The number of Zic2-positive cells is proportional to the degree of binocularity in different species (Herrera et al., 2003). For example, in the

stages when axons reach the chiasm (Thanos and Mey, 2001). Albino mice display a smaller ipsilateral projection compared to pigmented mice (Marcus & Mason, 1995) and this is reflected by a corresponding reduction in the number of Zic2-positive cells in the albino retina (Herrera et al., 2003). In addition in *Xenopus*, the subpopulation of VT RGCs that project ipsilaterally at metamorphosis expresses Zic2 mRNA (Herrera et al., 2003). Herrera et al. also showed that Zic2 is only expressed by uncrossed RGCs using dextran backlabeling from one optic tract combined with Zic2 immunohistochemistry at E16.5. Moreover, loss- and gain-of function *in vitro* experiments by the same authors further supported a role for Zic2 as an ipsilateral determinant acting primarily in the retina.

4.2.4. Hypotheses.

Given that Zic2 is expressed by VT ipsilateral RGCs and *Foxg1* null embryos display an increase in the numbers of ipsilateral RGCs, it is possible that there are greater numbers of Zic2-positive RGCs in *Foxg1*$^{-/-}$ retinas compared to those of wild types. Zic2 is also expressed in the developing ventral diencephalon from which the optic chiasm forms (Brown et al., 2003). Although all the evidence to date suggests that Zic2 expression in the retina primarily controls the size of the ipsilateral projection, it cannot be excluded that Zic2 expression at the optic chiasm also plays a role in retinal axon guidance. In this chapter, Zic2 expression was explored in the retina and optic chiasm of *Foxg1* null embryos using a Zic2-specific antibody and compared to age-matched wild type embryos to test the following hypotheses: -

Hypothesis 1: Numbers of Zic2-expressing cells increase in the *Foxg1*$^{-/-}$ retina in proportion to the increased ipsilateral projection.

Hypothesis 2: Zic2 expression is altered at the *Foxg1*$^{-/-}$ optic chiasm.

4.3. METHODS

4.3.1. Animals.

All experiments were carried out using embryos from *Foxg1*^{LacZ} (CBA) matings. Noon on the day the plug was found was considered E0.5. Embryos for Zic2 & Brn3a double fluorescence immunohistochemistry: pregnant females were sacrificed 13, 14, 15 and 16 days after the plug date. E13.5 – E16.5 embryos were fixed in 4% PFA in PBS for 2 hours, cryoprotected by immersion in 30% sucrose in PBS overnight, embedded in OCT compound, frozen on dry ice and stored at -80°C prior to sectioning on a Leica cryostat. Embryos for Brn3a immunohistochemistry on wax sections: pregnant females were sacrificed 14 or 16 days after the plug date giving E14.5 or E16.5 embryos. The decapitated heads were fixed in 4% PFA in PBS overnight, rinsed in 1XPBS and immersed in 50% ethanol prior to wax processing. After processing, heads were embedded horizontally in wax and sectioned into serial 10µm-thick sections on a microtome. Sections were mounted onto poly-l-lysine slides and dried overnight at 37ºC prior to Brn3a immunohistochemistry.

4.3.2. PCR genotyping.

Heterozygous embryos (*Foxg1*$^{+/-}$) were indistinguishable morphologically from wild type embryos (Xuan et al., 1995; Huh et al., 1999) and identified by PCR using specific primers that detected the *Foxg1*^{lacZ} allele: LacZ F2 5'-TTG AAC TGC CTG AAC TAC CG-3' and LacZ R2 5'-CCT GAC TGG CGG TTA AAT TG-3'. Only wild type embryos were used for quantitation purposes even though there appeared to be no difference in Zic2 or Brn3a expression between *Foxg1*$^{+/-}$ and wild type embryos. Wild type (*Foxg1*$^{+/+}$) embryos were identified by the absence of a PCR product using the *Foxg1*^{lacZ} allele-specific primers and used in all experiments. PCR cycling conditions

were 96°C for 2 minutes followed by [96°C for 30 seconds, 58.5°C for 30 seconds and 72°C for 30 seconds] for 35 cycles.

4.3.3. Zic2 DAB immunohistochemistry.

Zic2 immunohistochemistry was performed on 10µm-thick serially-collected cryostat sections cut horizontally through the eyes of E13.5 – E16.5 embryos using a rabbit monoclonal Zic2 antibody kindly donated by Stephen Brown, Columbia University, New York, at a concentration of 1 in 8000. The protocol used was identical to that for Zic2 and Brn3a double immunohistochemistry except that DAB was used to reveal the Zic2 primary antibody using a rabbit DAKO-EnVision+ Kit (Dako K4010). Slides were dehydrated through an ascending alcohol series (70% - 100%), immersed in two changes of xylene for 15 minutes each and mounted in DPX.

4.3.4. Brn3a DAB immunohistochemistry.

Brn3a immunohistochemistry was performed on 10µm-thick serial wax sections cut on a microtome. Sections were dewaxed by immersion in xylene and rehydrated through a descending series of ethanols from 100% to 70% and finally double distilled water. Endogenous peroxidase activity was blocked using a 9:1 ratio of methanol:30% hydrogen peroxide for 5 minutes. Antigens were retrieved by microwaving at medium-high in 10mM sodium citrate buffer pH5.5 in two 5 minute bursts replacing evaporation losses inbetween. Slides were rinsed 3 times in double distilled water and blocked for 1 hour at room temperature in 5% goat serum, 0.2% BSA, 0.1% TritonX-100 in PBS. A primary mouse monoclonal antibody for Brn3a (1 in 150) was applied for 1 hour at room temperature. Slides were rinsed in 1xPBS and a mouse DAKO-EnVision+ Kit was used to reveal the antibody staining using DAB. Following a sufficient DAB development time, slides were dehydrated through an ascending

alcohol series (70% - 100%), immersed in two changes of xylene for 15 minutes each and mounted in DPX.

4.3.5. Zic2 & Brn3a double immunohistochemistry at E14.5.

Zic2 and Brn3a double immunohistochemistry was carried out on 10µm-thick serially-collected cryostat sections cut horizontally through the eyes of E14.5 mouse embryos. Slides were thawed thoroughly at room temperature prior to fixing in ice-cold acetone for 10 minutes. Slides were rinsed in 3 changes of 1xPBS for 5 minutes each and endogenous peroxidase activity was blocked using 0.1% hydrogen peroxide in 1xPBS for 5 minutes. Antigens were retrieved by microwaving twice in 10mM sodium citrate buffer pH5.5 for 5 minutes each on 'medium'. Slides were rinsed in double distilled water and then blocked for 1 hour at room temperature in 5% goat serum, 0.2% BSA, 0.1% TritonX-100 in PBS. Primary antibodies: a mixture of rabbit monoclonal Zic2 antibody (1 in 8000) (Stephen Brown, Columbia University, New York) and mouse monoclonal Brn3a antibody (1 in 300) (Chemicon International) diluted in blocking solution was pipetted onto each section, covered in parafilm and left to incubate in a dark humidified chamber overnight at 4ºC and then for 30 minutes at room temperature. Slides were rinsed 3 times in 1xPBS for 5 minutes each. A mixture of secondary antibodies goat anti-rabbit IgG (H & L) AlexaFluor 488 and goat anti-mouse IgG (H & L) AlexaFluor 546 was applied to the sections at a concentration of 1 in 150 each and incubated for 1 hour in a dark humidified chamber at room temperature. Slides were rinsed 3 times in 1xPBS and counter-stained using TO-PRO-3 (1 in 2000). Slides were rinsed several times in 1xPBS, followed by a double distilled water wash prior to mounting in mowiol (Calbiochem).

4.3.6. Imaging and quantification.

Fluorescent images were obtained using a Leica confocal microscope. High power x40 magnification images were obtained in the red (Brn3a), green (Zic2) and blue (TO-PRO-3) channels. Montages were assembled and for each eye, the numbers of Zic2- and Brn3a-positive cells were counted in six evenly-spaced sections from most dorsal to most ventral. This was done by selecting the dorsal-most and ventral-most sections in which Brn3a-positive cells were visible. The intervening four sections were then chosen by dividing up the length between the dorsal- and ventral-most sections equally. Zic2 and Brn3a-expressing cells were counted in both wild type and Foxg1 null retinas and summed to obtain means. Nasal and temporal counts were kept separate. For Zic2 DAB immunohistochemistry, images were obtained using a Leica microscope and Zic2-positive cells counted in six evenly-spaced sections from most dorsal to most ventral. Nasal and temporal counts were kept separate.

4.3.7. Dextran backlabeling.

CBA females were mated with CBA males to obtain wild type embryos. Embryos were taken at E14.5, decapitated and the heads removed into ice-cold oxygenated EBSS in a Sylgard-coated dish. Under a dissecting microscope the lower jaw was removed. The head was turned upside down and one optic tract exposed. The tract was cut using microscissors and EBSS was removed from the dish. Filter paper was used to dry the cut optic tract as thoroughly as possible before inserting a pinch of dextran-rhodamine 3000 MW (Molecular Probes D3308) into the cut. The heads were placed into room-temperature oxygenated EBSS. The solution was bubbled gently for 3 hours at room temperature after which the heads were transferred to fresh, cold oxygenated EBSS. The embryos were stored covered overnight at 4ºC. The next day, heads were transferred to 4%PFA and fixed for 24 hours. The PFA was removed and 1xPBS added. Ipsilateral and contralateral retinas were dissected after making a ventral

orientating cut and the pigmented epithelium removed. 3 additional cuts were made from the periphery of the retina and each retina was flattened with the neural retina facing upwards on the slide. Zic2 immunohistochemistry was then performed as for cryostat sections and revealed using the goat anti-rabbit IgG (H & L) AlexaFluor 488. Retinas were cover-slipped using mowiol.

4.4. RESULTS

4.4.1. Zic2 is ectopically expressed in the nasal retina of *Foxg1*$^{-/-}$ embryos throughout the period when RGC axons navigate the optic chiasm.

Initially, Zic2 protein expression was investigated in the retinas of wild type and *Foxg1* heterozygous embryos (collectively called '*Foxg1*$^{+/\pm}$' in Figure 1) and *Foxg1* null embryos from E13.5 to E16.5. These embryonic ages were chosen because they correspond with the time when RGC axons navigate the optic chiasm. The Zic2 antibody used in all immunohistochemistry experiments was identical to that used by Brown et al. (2003). DAB immunohistochemistry confirmed previous findings (Herrera et al., 2003) that Zic2 protein is found in the peripheral VT region of the neural retina from E14.5 in wild type and *Foxg1* heterozygous embryos (Figure 1). The appearance of Zic2-expressing cells in the retina at E14.5 corresponds with the generation of the first permanent ipsilaterally-projecting RGCs from VT retina. Prior to this at E13.5, no clusters of Zic2-expressing cells were seen in the VT retina and Zic2-positive cells were mainly confined to the CMZ with some cells scattered throughout the retina (Figure 1A, B). At E15.5 and E16.5, the cluster of cells expressing Zic2 in peripheral VT retina became larger relative to the size of the retina, corresponding to more axons projecting ipsilaterally from this region (Figure 1I, M). In wild type and *Foxg1* heterozygous retinas from E13.5 to E16.5, no clusters of Zic2 expression were visible in dorsal regions of the retina.

Figure 1. Zic2 is ectopically expressed in the nasal retina of *Foxg1*$^{-/-}$ embryos throughout the period when RGC axons project and persists in ventrotemporal retina. (A – S) Zic2 immunohistochemistry revealed using DAB staining at E13.5 (A – D), E14.5 (E – H), E15.5 (I – L) and E16.5 (M – P) in dorsal and ventral sections of *Foxg1*$^{+/\pm}$ (*Foxg1*$^{+/+}$ or *Foxg1*$^{+/-}$) and *Foxg1*$^{-/-}$ retinas. All sections are 10µm cryostat sections cut in the horizontal plane with nasal pointing upwards. Zic2 is expressed in the ciliary marginal zone (CMZ) at all ages. Black dotted lines show the border between the CMZ and the neural retina and black arrows show the locations of Zic2-expressing cells. (A, B) In E13.5 *Foxg1*$^{+/\pm}$ retinas, Zic2-positive cells are scattered in all retinal layers but large clusters of cells are not seen outside the CMZ. (C) In *Foxg1*$^{-/-}$ ventral retina, strong Zic2 expression is seen in the temporal retina adjacent to the CMZ. (D) In dorsal *Foxg1*$^{-/-}$ retina, strong Zic2 expression is seen in cells of the nasal retina. (E, I, M) In E14.5 – E16.5 *Foxg1*$^{+/\pm}$ ventral retinas, a cluster of Zic2-positive cells is visible in the inner ventrotemporal retinal layer adjacent to the CMZ. (F, J, N) In E14.5 – E16.5 *Foxg1*$^{+/\pm}$ dorsal retinas, Zic2-expressing cells are found scattered in all retinal layers but there are no clusters of Zic2-expressing cells. (G, K) Ventral sections of E14.5 & E15.5 *Foxg1*$^{-/-}$ retinas show a cluster of Zic2-positive cells in temporal retina only near the CMZ. (O) In ventral E16.5 *Foxg1*$^{-/-}$ retinas, Zic2-expressing cells are scattered and less densely packed in temporal retina. Zic2-positive cells are also found in nasal retina (arrow-head). (H, L, D) Dorsal sections of E14.5 – E16.5 *Foxg1*$^{-/-}$ retinas show ectopic Zic2 expression in the nasal retina. (Q) High power magnification of the *Foxg1*$^{+/\pm}$ temporal retina of (M) showing a cluster of Zic2-positive cells. (R, S, T) High power magnifications of *Foxg1*$^{-/-}$ peripheral temporal retina in (O) and peripheral nasal and temporal retina in (P). Arrows point to regions of Zic2-expressing RGCs. (O) Scattered Zic2-expression (arrows point to a few Zic2-positive cells). (S) Cluster of Zic2-expressing cells in the nasal retina. (T) Clusters of Zic2-expressing cells are absent in temporal retina. Abbreviations: N = nasal, T = temporal. Scale bars: A – P = 200µm, Q – S = 100µm.

Figure 1. Developmental series of Zic2 expression in the retina from E13.5 - E16.5

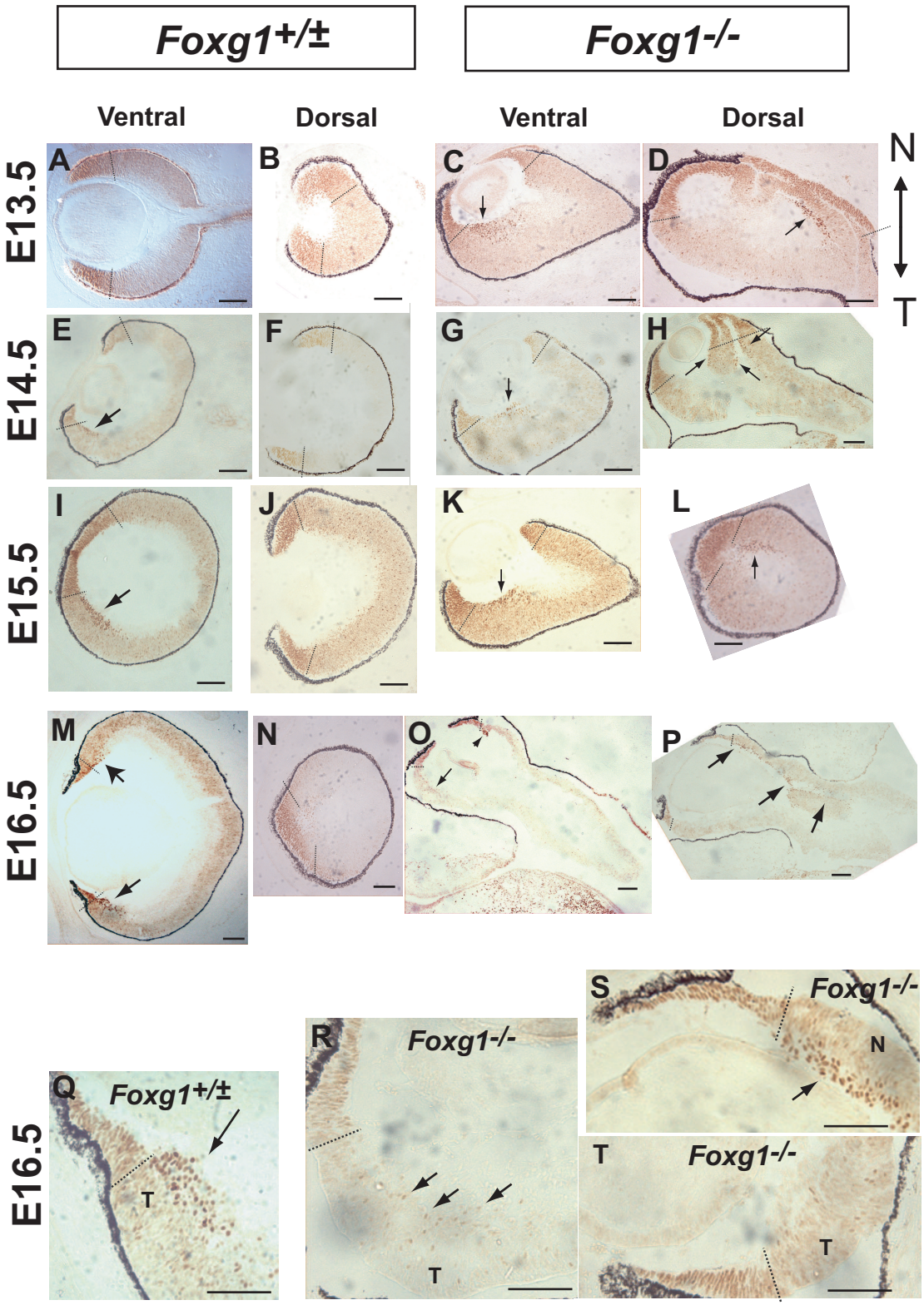

The most notable finding in *Foxg1* null dorsal sections from E13.5 to E16.5 was a cluster of Zic2-positive cells in the nasal peripheral retina. Zic2-expressing clusters were never observed in the nasal half of wild type or *Foxg1* heterozygous retinas, apart from small clusters of approximately a dozen or so Zic2-positive cells at E16.5 (Figure 1M). In *Foxg1*$^{-/-}$ retinas, this Zic2-expressing dorsonasal cluster became wider along the lateral-medial axis with increasing age, extending further into the extended retina (arrows in Figure 1P). In contrast to Foxg1-expressing retinas, Zic2 expression was observed one day earlier at E13.5 in temporal and nasal regions of *Foxg1*$^{-/-}$ retinas in addition to the CMZ (Figure 1C, D). In ventral sections in E13.5 to E15.5 *Foxg1*$^{-/-}$ retinas, Zic2 expression was observed in peripheral VT retina adjacent to the strongly-expressing CMZ as in Foxg1-expressing retinas. In E16.5 *Foxg1*$^{-/-}$ retinas, Zic2 expression was still present in the VT region but Zic2-expressing cells were more scattered laterally within the RGC layer in contrast to the tight clusters seen at earlier ages (arrows in Figures 1O, R). In addition, in ventral sections of E16.5 *Foxg1*$^{-/-}$ retinas, some Zic2-expressing cells were consistently observed in peripheral nasal retina (arrowhead in Figure 1O).

4.4.2. Qualitative analysis of Zic2 and Brn3a double fluorescence immunohistochemistry.

In order to investigate this Zic2-expressing cluster of cells in nasal *Foxg1*$^{-/-}$ retina in greater detail and to quantify the numbers of Zic2-positive cells in retinas that express Foxg1 compared to *Foxg1* null retinas, double immuhistochemistry for Zic2 and Brn3a, a marker of postmitotic RGCs, was performed on serial sections at E14.5. Although E14.5 is not the age of maximal Zic2 expression, which peaks around E15.5 to E16.5, the shape of the *Foxg1*$^{-/-}$ eye is not as distorted by extensive folding at this age, facilitating identification of the nasal-temporal axis.

4.4.2.1. Zic2 expression in E14.5 wild type retinas.

Ventral sections of wild type retinas showed a cluster of strongly Zic2-expressing cells in peripheral temporal retina adjacent to the Zic2-positive CMZ (Figures 2E, 2F, 5A - D). Temporally-located Zic2-expressing clusters of cells were also seen in the central retina around the level of the optic stalk (Figures 2C, 2D) and in sections just ventral to the optic stalk (Figures 4A - D). In all cases these clusters were located adjacent to the CMZ that expressed Zic2 consistent with previous reports (Nagai et al., 1997). In addition to the Zic2-positive clusters, scattered Zic2-expressing cells were found in the outer neuroblastic layer and more sparsely in the Brn3a-expressing RGC layer (Figures 4A, 4B, 5A, 5B). Zic2-expressing clusters were absent from dorsal sections of the wild type retina (Figures 2A, 2B, 3A - F). However, scattered Zic2-positive cells were observed throughout all layers of the dorsal retina with stronger expression in the outer neuroblastic layer (Figures 3A, B). Brn3a-labelled cells were found in the inner RGC layer of the retina. The clusters of Zic2-positive cells were located peripheral to the Brn3a-expressing RGCs and the majority failed to co-label.

4.4.2.2. Zic2 expression in E14.5 *Foxg1*$^{-/-}$ retinas.

In *Foxg1*$^{-/-}$ retinas, dorsal sections consistently showed a conspicuous cluster of Zic2-expressing cells in peripheral nasal retina adjacent to the CMZ (Figures 6A, 6B, 8A, 8E). In extremely dorsal sections, there was no obvious difference in the distribution of Zic2-positive cells, which were scattered sparsely among the nasal and temporal retina with strong expression in the CMZ (Figure 7A - F). The Zic2-expressing cluster of cells in nasal retina was also present in ventral sections of *Foxg1*$^{-/-}$ retinas (Figures 6D & E, 9A & E, 10A, B, E, F). The nasal Zic2-expressing cluster extended medially towards the midline into the extended retina (Figures 9A & E, 10A & E).

Figure 2. Dorsal to ventral series of Zic2 expression through an E14.5 wild type retina. Zic2 (green) and Brn3a (red) fluorescence immunohistochemistry in 10μm-thick sections of E14.5 wild type eyes from dorsal (A) to ventral (F). All sections are cut in the horizontal plane. Schematic diagrams above each image represent the eye as a sphere and indicate the dorsal-ventral position of the plane of section. Zic2 expressing cells are found predominantly in the ventro-temporal part of the retina. (A, B) Dorsally, no clusters of Zic2-expressing cells are present outside the CMZ. (C - F) In dorso-central to ventral sections, a cluster of Zic2-expressing cells is present in the temporal retina adjacent to the Zic2-positive CMZ. In all sections the RGC layer and outer layers contain scattered Zic2-positive cells throughout the retina. Abbreviations: A is anterior, P is posterior, N is nasal, T is temporal, D is dorsal, V is ventral. Scale bars: all 200μm.

Figure 2. Dorsal to ventral series of Zic2 expression in E14.5 wild type retina

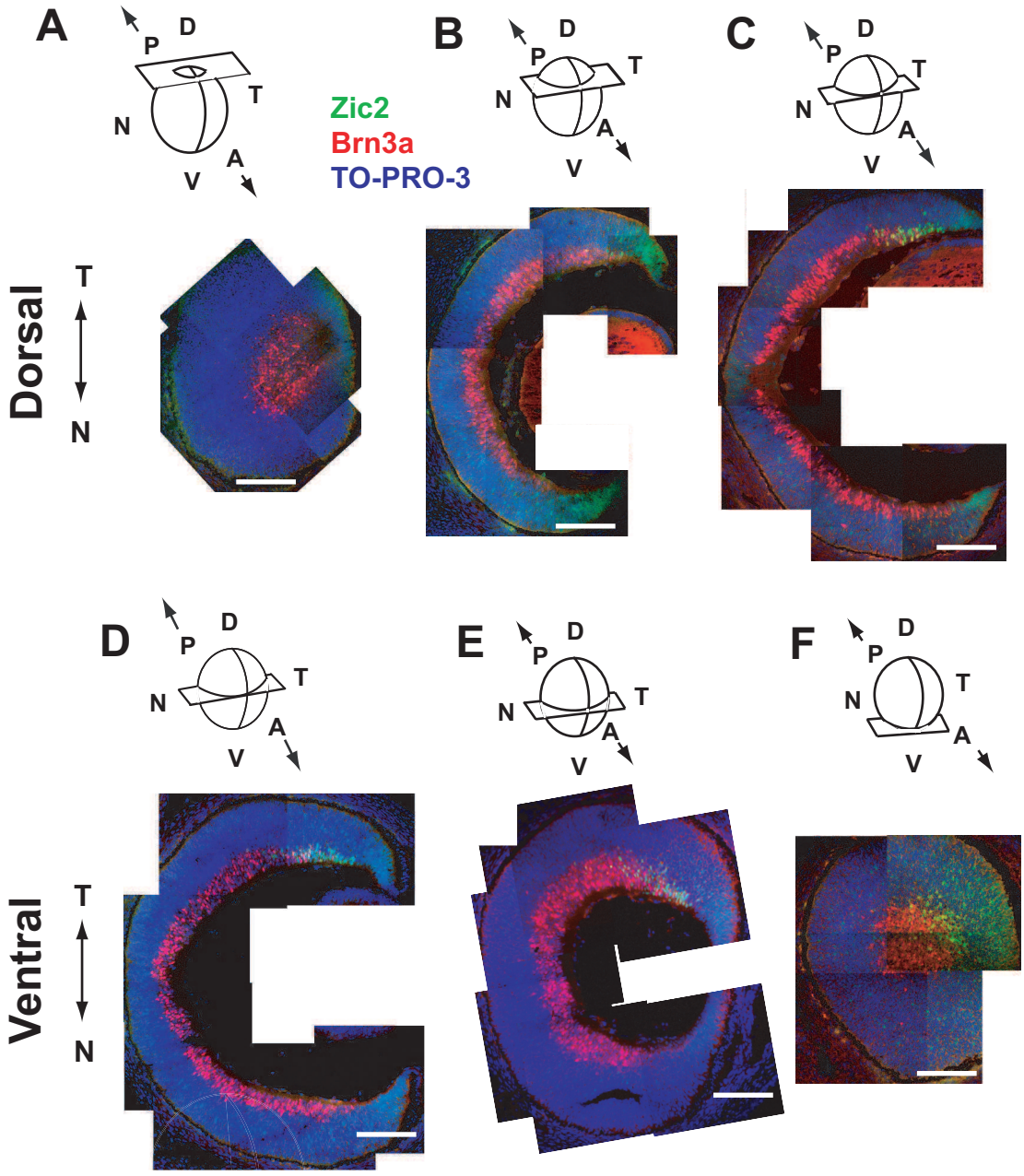

Figure 3. Cells expressing Zic2 are scattered sparsely throughout the dorsal retina of E14.5 wild type embryos. (A-F) Zic2 (green) and Brn3a (red) fluorescence immunohistochemistry in dorsal sections of E14.5 wild type eyes. All sections are cut in the horizontal plane. Schematic diagrams above each image represent the eye as a sphere and indicate the dorsal-ventral position of the plane of section. (C, E) and (D, F) High power magnifications of temporal and nasal retina nearest the CMZ from (A) and (B). (A) Dorsal section showing strong Zic2 expression in the CMZ in nasal and temporal retina. The CMZ borders are delineated by a white line. (C, E) Zic2-expressing cells are scattered around the whole retina and only a few are present within the Brn3a-expressing domain (some examples are indicated by white arrows). (B) Section ventral to (A) showing strong Zic2 expression in the CMZ. (D, F) Only a few Zic2-positive cells are found in the Brn3a-expressing RGC layer (white arrows). One double-labelled cell is visible in (D) (white arrow-head) but otherwise there is no double-labelling. Abbreviations: A is anterior, P is posterior, N is nasal, T is temporal, D is dorsal, V is ventral, CMZ is the ciliary marginal zone. Scale bars: A, B = 200μm, C - F = 100μm.

Figure 3. Zic2 expression in dorsal sections of E14.5 wild type retina

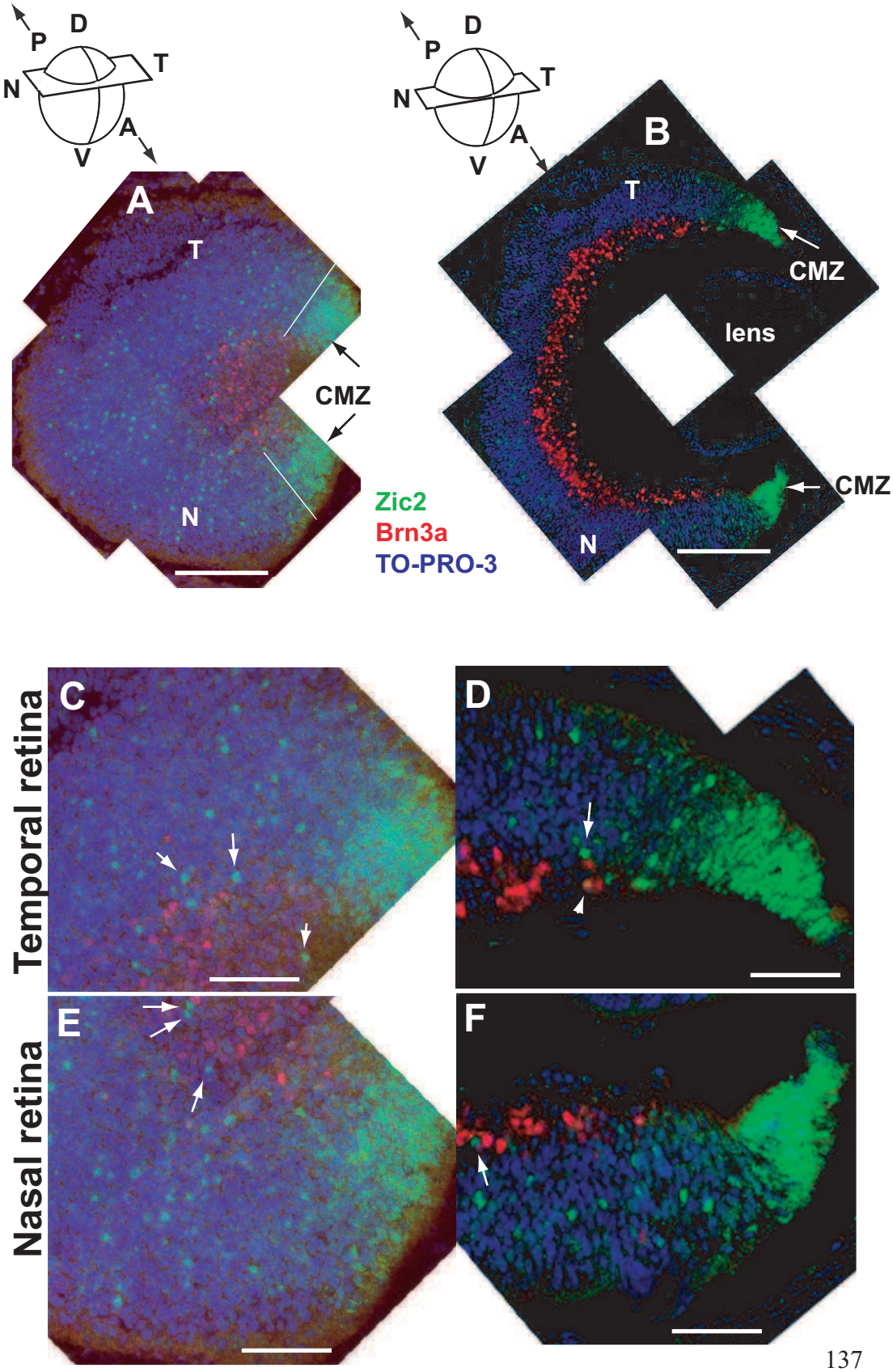

Figure 4. Zic2 expression is concentrated in the ventrocentral retina adjacent to the CMZ in the wild type. (A – F) Zic2 and Brn3a fluorescence immunohistochemistry in ventrocentral sections of E14.5 wild type eyes. (A, B) Sections just ventral to the central retina, although B is slightly more ventral than A. (A, B) Zic2-expressing cells are present in the temporal retina adjacent to the CMZ that expresses Zic2. (C, D) High power magnifications of the Zic2-positive cells in temporal retinas shown in (A) and (B). Yellow double-labelled cells that express both Zic2 and Brn3a are visible (white arrows indicate some examples). However, the majority of Zic2-positive cells do not express Brn3a. (E, F) High power magnifications of the nasal retinas of (A) and (B) showing only weak scattered Zic2 expression. Abbreviations: A is anterior, P is posterior, N is nasal, T is temporal, D is dorsal, V is ventral, CMZ is the ciliary marginal zone. Scale bars: A, B = 200μm, C – F = 100μm.

Figure 4. Zic2 expression in ventrocentral E14.5 wild type retina

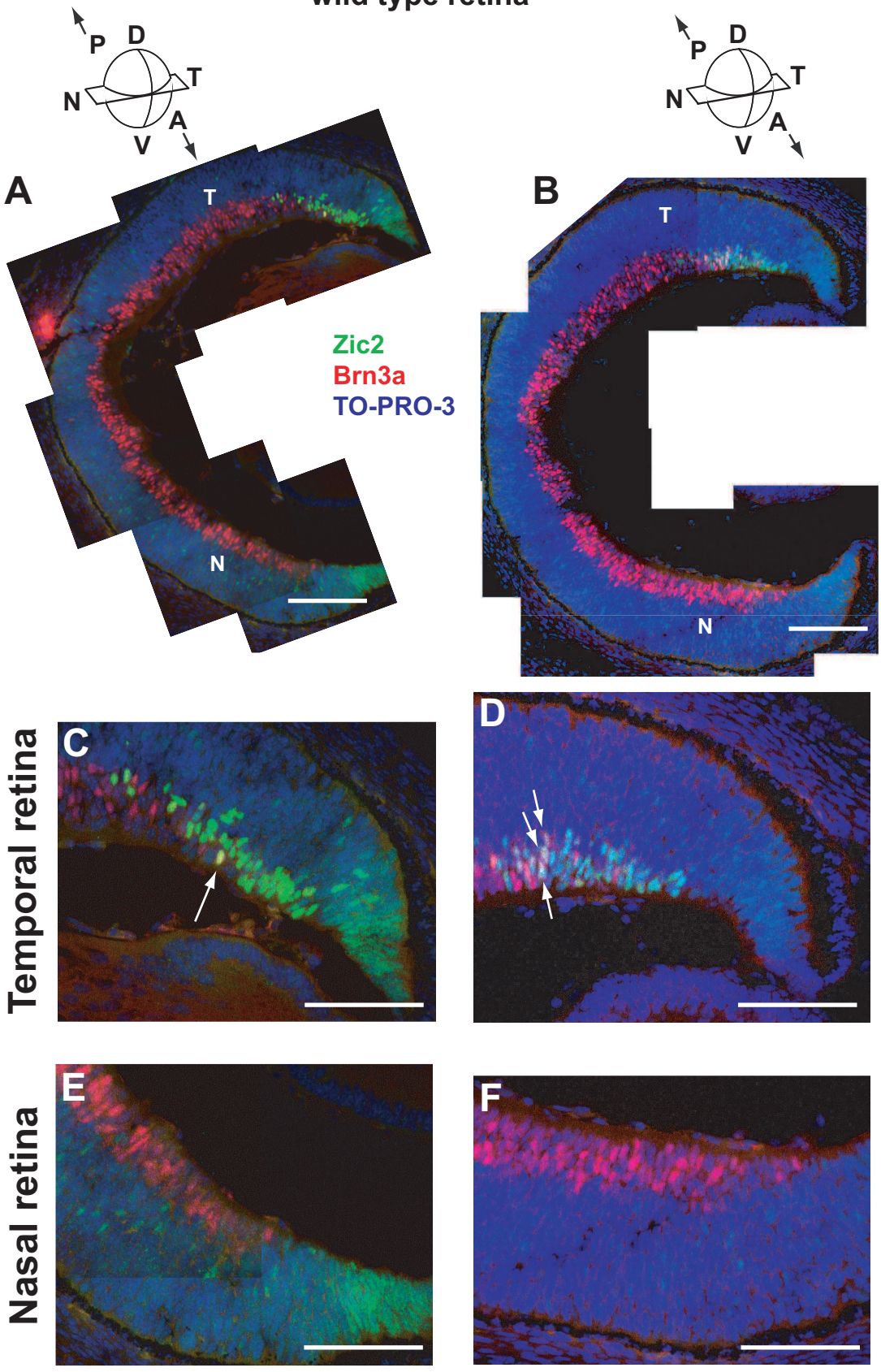

Figure 5. Zic2 is expressed in the ventrotemporal retina of E14.5 wild type embryos. (A-F) Zic2 and Brn3a fluorescence immunohistochemistry in ventral sections of E14.5 wild type eyes. (A) Ventral section showing a cluster of Zic2-expressing cells in temporal retina (white arrow). (B) Section ventral to (A) showing strong Zic2 expression in temporal retinal cells but weaker, scattered Zic2-positive cells in nasal retina. (C, E) and (D, F) High power magnifications of (A) and (B) respectively showing that Zic2 expression is predominantly found in temporal retina where a few double-labelled cells are found (white arrows indicate some examples). (E, F) Zic2 is expressed more weakly in fewer cells in nasal retina. Abbreviations: A is anterior, P is posterior, N is nasal, T is temporal, D is dorsal, V is ventral, CMZ is the ciliary marginal zone. Scale bars: A, B = 200μm, C - F = 100μm.

Figure 5. Zic2 expression in the ventrotemporal retina of wild type E14.5 embryos

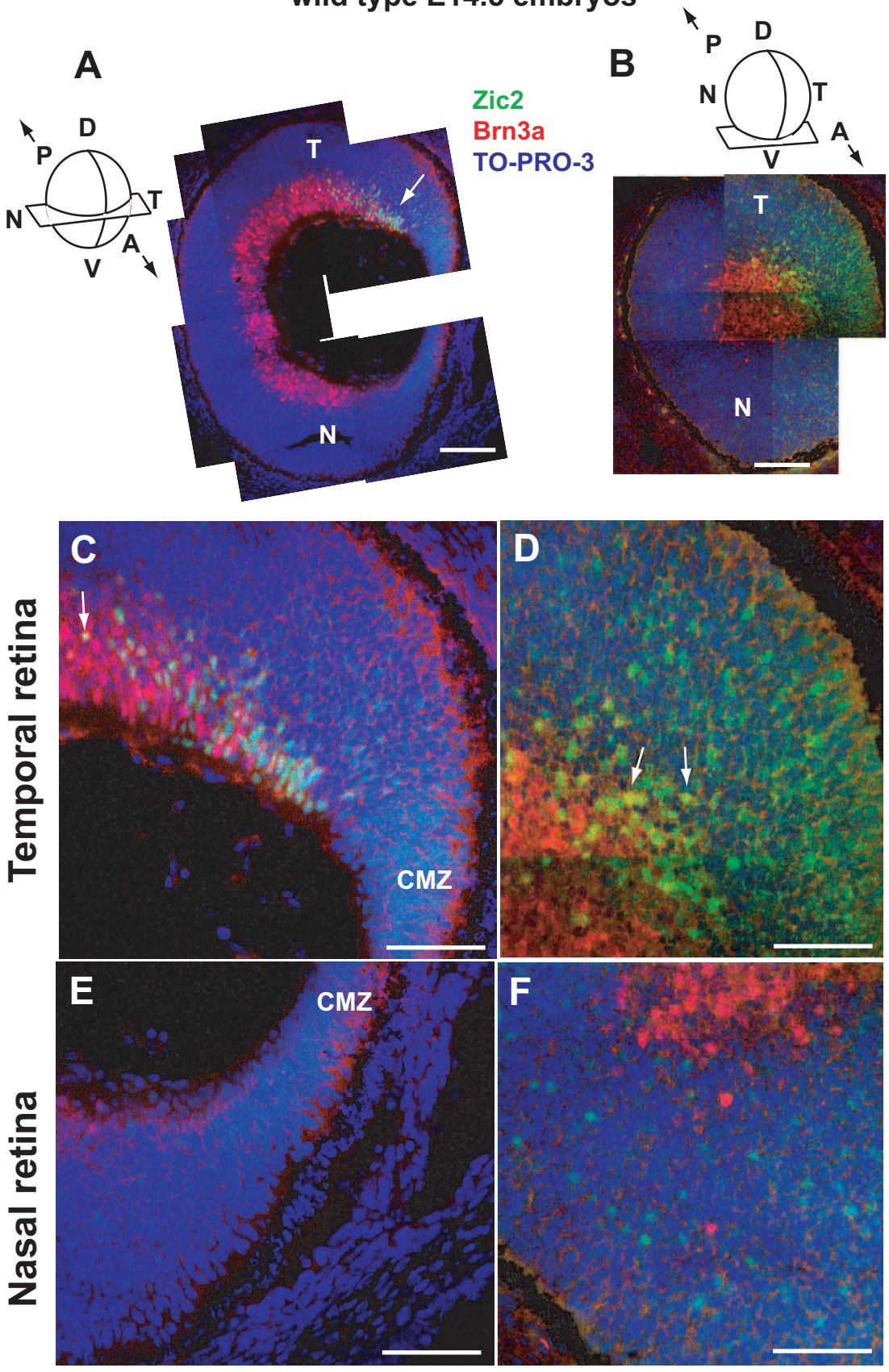

Figure 6. Dorsal to ventral series of Zic2 expression through the retina of an E14.5 *Foxg1*$^{-/-}$ embryo. Zic2 is expressed in ventrotemporal retina and also ectopically in nasal retina in E14.5 *Foxg1*$^{-/-}$ embryos. (A - F) Zic2 and Brn3a fluorescence immunohistochemistry in E14.5 *Foxg1*$^{-/-}$ eyes from dorsal (A) to ventral (F). In dorsal (A – C) and some ventral sections (D, E), Zic2-expressing cells are present in the nasal retina adjacent to the Zic2-positive CMZ and medially in the extended retina. (E, F) Ventrally, Zic2-positive cells cluster next to the CMZ in temporal retina. The RGC layer and outer layers contain scattered Zic2-positive cells throughout the entire retina. In dorsal and ventral sections the CMZ expresses Zic2 strongly.
Abbreviations: er = extended retina, A is anterior, P is posterior, N is nasal, T is temporal, D is dorsal, V is ventral. Scale bars: all 200μm.

Figure 6. Dorsal to ventral series of Zic2 expression in an E14.5 *Foxg1*$^{-/-}$ retina

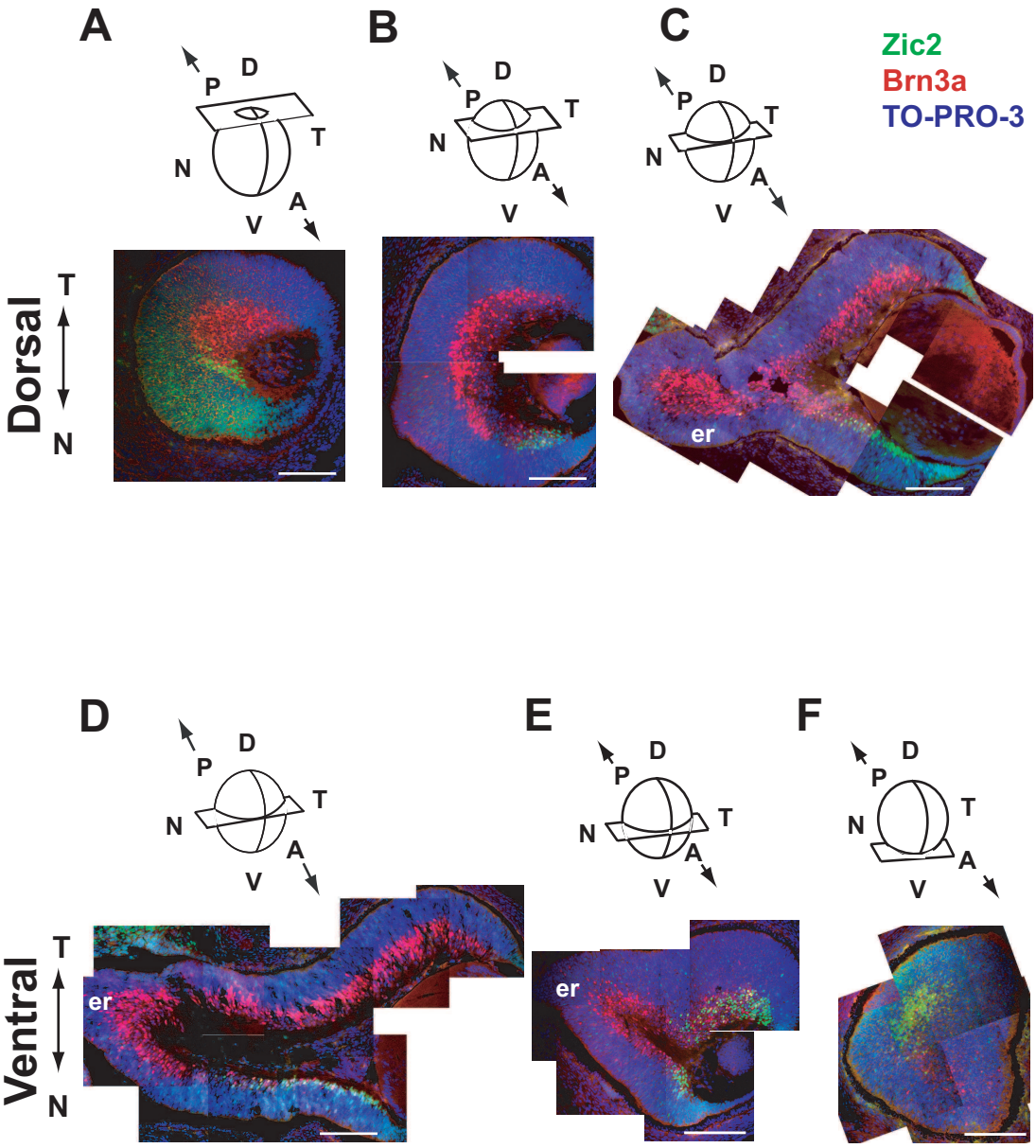

Figure 7. In extremely dorsal sections of E14.5 *Foxg1*$^{-/-}$ retina, Zic2 is expressed in cells scattered over the entire retina. Zic2 and Brn3a fluorescence immunohistochemistry in dorsal sections of E14.5 *Foxg1*$^{-/-}$ eyes. (A, B) Dorsally, Zic2 is expressed in the CMZ in peripheral nasal and temporal retina. (A) Dorsal section showing strong Zic2 expression in cells of the ciliary marginal zone. A white line indicates the boundary between the ciliary marginal zone and neural retina. Zic2 is expressed equally in nasal and temporal retina. Only a few Brn3a-positive cells are visible as the section is at the dorsal boundary of the RGC layer. (B) Section ventral to (A) showing RGCs expressing Zic2 and Brn3a equally in nasal and temporal retina. (C, E) and (D, F) High power magnifications of the temporal and nasal retina from (A) and (B) respectively. Abbreviations: A is anterior, P is posterior, N is nasal, T is temporal, D is dorsal, V is ventral, CMZ is the ciliary marginal zone. Scale bars: A, B = 200μm, C - F = 100μm.

Figure 7. Zic2 expression in E14.5 *Foxg1*$^{-/-}$ dorsal retina

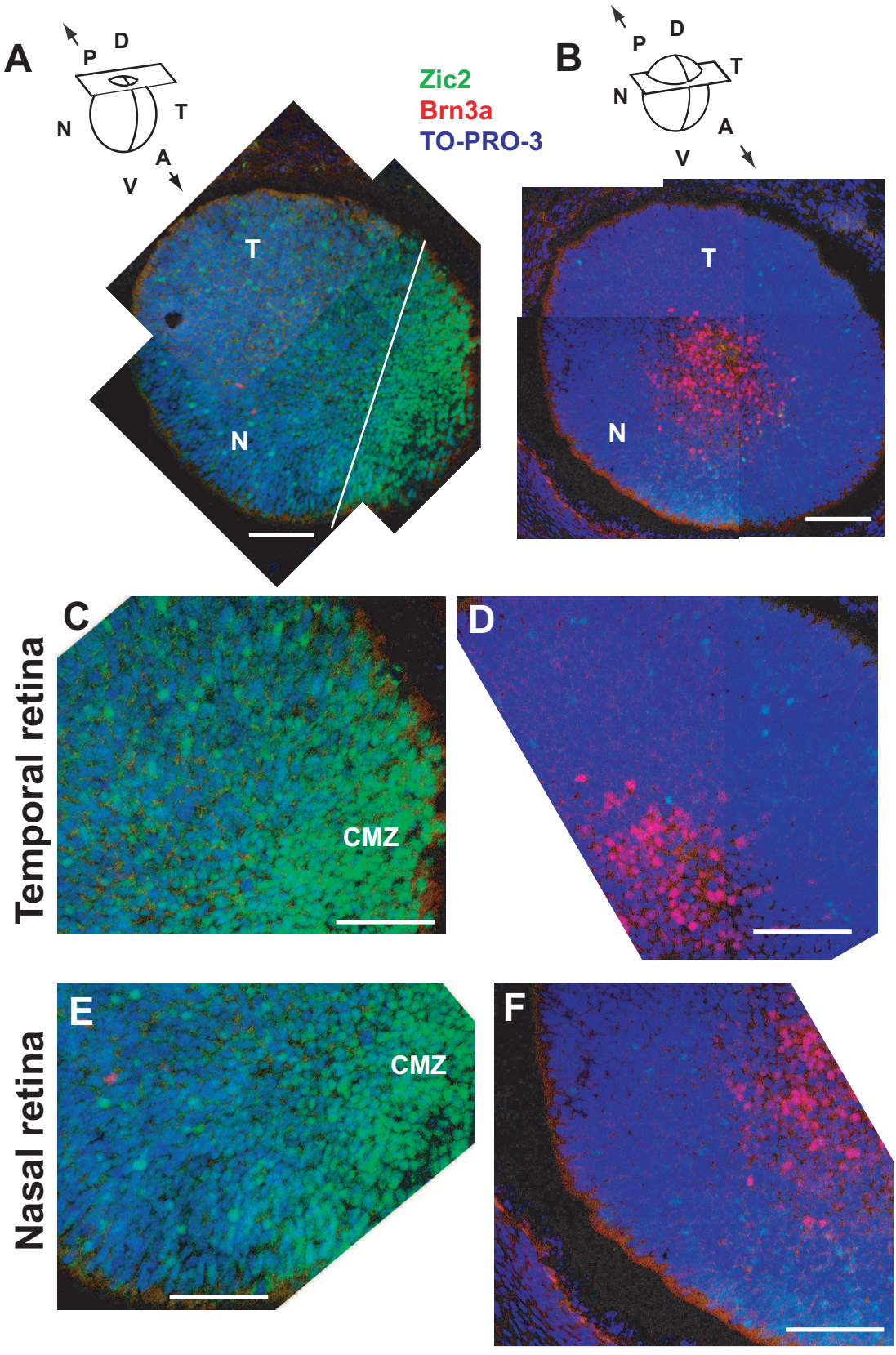

Figure 8. In dorsal sections of E14.5 *Foxg1*$^{-/-}$ retina, Zic2 protein is ectopically expressed in the nasal retina. (A - F) Zic2 and Brn3a fluorescence immunohistochemistry in dorsal sections of E14.5 *Foxg1*$^{-/-}$ eyes. In all dorsal sections, Zic2 is expressed in the CMZ in peripheral nasal and temporal retina. (A, B) Dorsal sections showing a cluster of Zic2-expressing cells in nasal but not temporal retina. (B) is ventral to (A). (C, E) and (D, F) High power magnifications of the temporal and nasal retina from (A) and (B) showing ectopic Zic2 expression in nasal retina. Some double-labeled cells (yellow) are visible in (E) & (F). Some examples are indicated using white arrows. Abbreviations: er is the extended retina, A is anterior, P is posterior, N is nasal, T is temporal, D is dorsal, V is ventral, CMZ is the ciliary marginal zone. Scale bars: A, B = 200μm, C - F = 100μm.

Figure 8. Zic2 expression in E14.5 *Foxg1*$^{-/-}$ dorsal retina

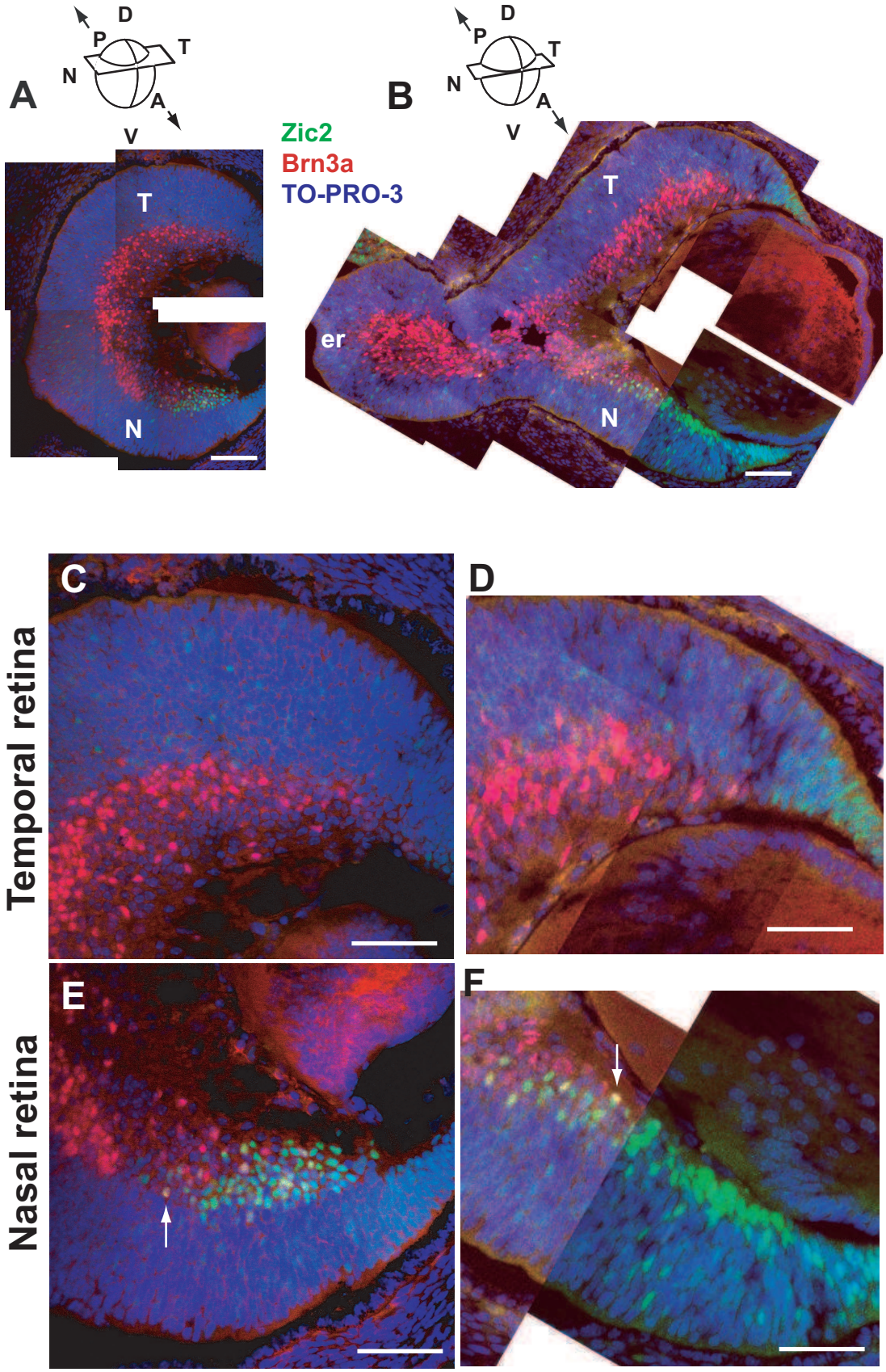

Figure 9. In ventral sections, Zic2 protein is ectopically expressed in the nasal retina of E14.5 *Foxg1*$^{-/-}$ embryos but is still present in temporal retina. (A - F) Zic2 and Brn3a fluorescence immunohistochemistry in ventral sections of E14.5 *Foxg1*$^{-/-}$ eyes. In all ventral sections, Zic2 is expressed in the CMZ. (A) Ventral section showing Zic2 expression predominantly in nasal retina extending medially into the extended retina. (C, E) High power magnifications of the temporal and nasal retina from (A) showing that Zic2-positive cells are more numerous in the nasal retina. (B) Section ventral to (A) showing Zic2 in temporal retina. (D, F) High power magnifications of temporal and nasal retina from (B) showing that there are Zic2-positive cells in temporal and nasal retina. Abbreviations: er = extended retina, N is nasal, T is temporal, D is dorsal, V is ventral. Scale bars: A, B = 200μm, C - F = 100μm.

Figure 9. Zic2 expression in E14.5 *Foxg1*$^{-/-}$ ventral retina

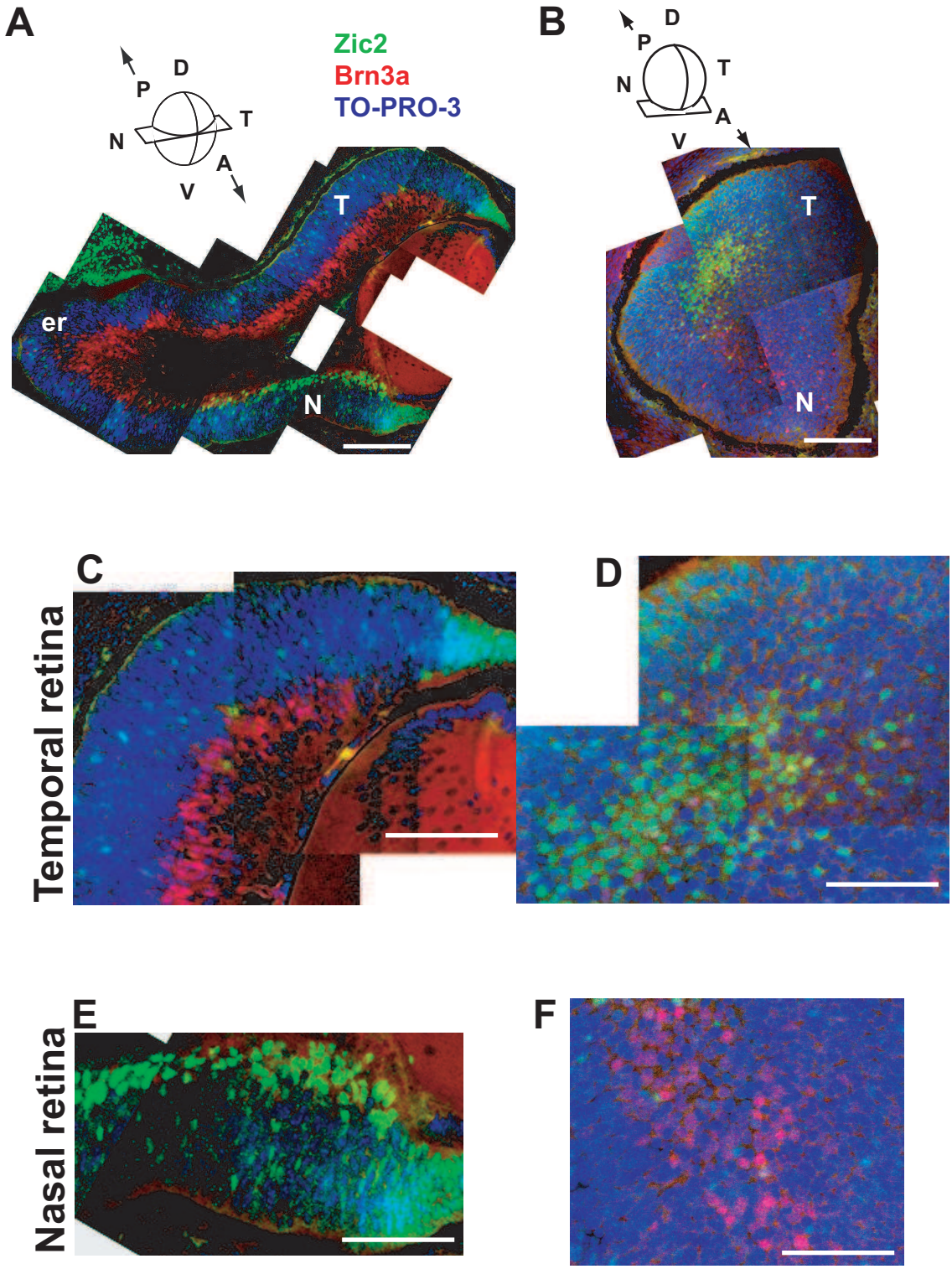

Figure 10. In ventral sections, Zic2 is ectopically expressed in the nasal retina of E14.5 *Foxg1*$^{-/-}$ embryos but is still present in temporal retina. (A - F) Zic2 and Brn3a immunohistochemistry in ventral sections of E14.5 *Foxg1*$^{-/-}$ eyes. In all ventral sections, Zic2 is expressed in the CMZ. (C, E) and (D, F) High power magnifications of the nasal and temporal retina nearest the CMZ in (A) and (B) respectively. (A) Section just ventral to the central retina. Zic2 is expressed in nasal retina including the extended retina. Expression is not as strong in temporal retina. (B) Section ventral to (A) showing the *Foxg1*$^{-/-}$ optic stalk. (D, F) Zic2-expressing cells are present in temporal retina as in wild type embryos but also ectopically in nasal retina. (D) White arrow points to one of a few double-labelled cells. Abbreviations: er is the extended retina, os indicates the *Foxg1*$^{-/-}$ correlate of the optic stalk, A is anterior, P is posterior, N is nasal, T is temporal, D is dorsal, V is ventral. Scale bars: A, B = 200μm, C - F = 100μm.

Figure 10. Zic2 expression in E14.5 *Foxg1*$^{-/-}$ ventral retina

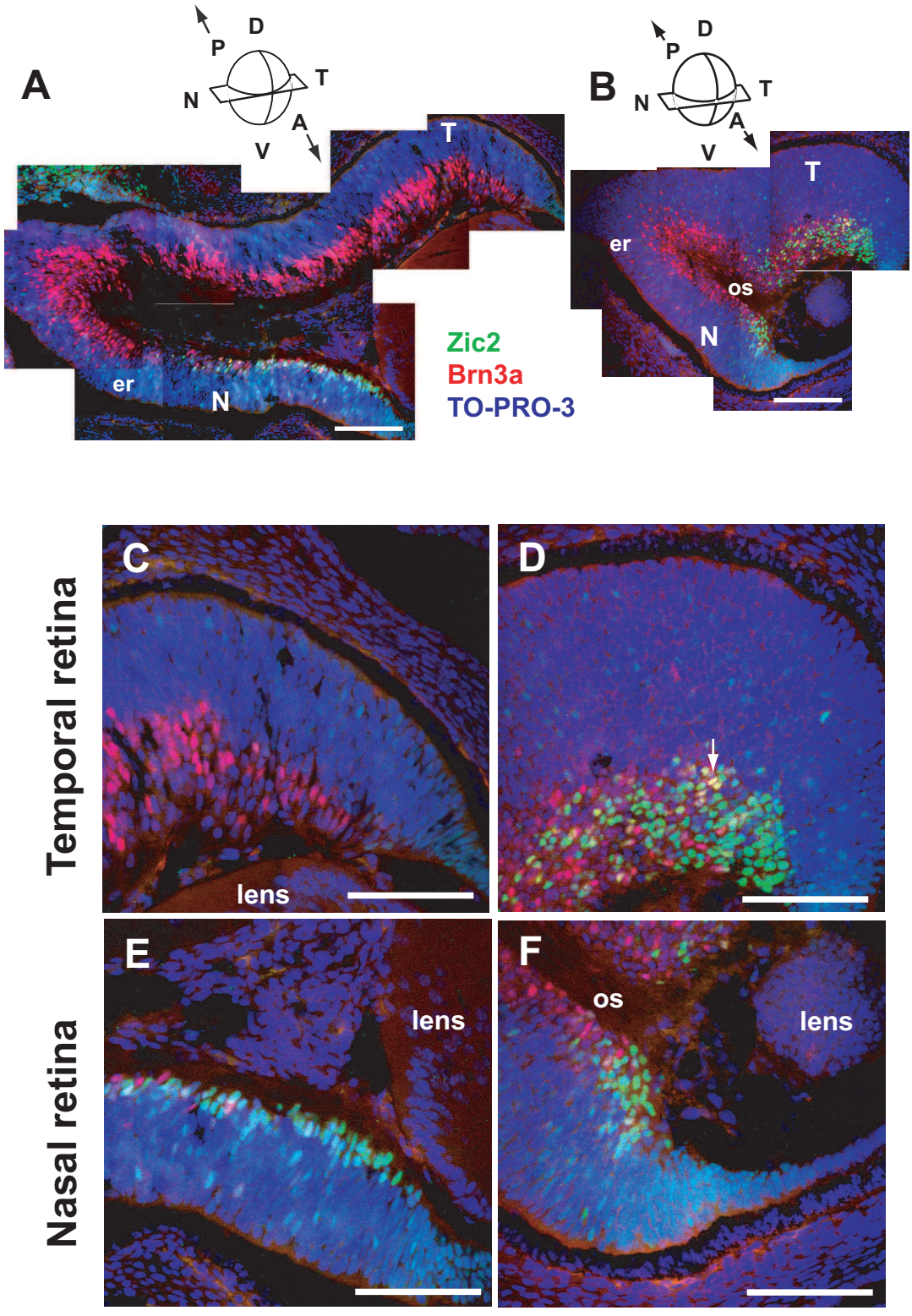

In extremely ventral sections, *Foxg1*$^{-/-}$ retinas displayed a Zic2-positive cluster in peripheral VT retina adjacent to the CMZ as in wild type retinas (Figures 9B & D, 10B & D). In all *Foxg1*$^{-/-}$ retinas examined, the CMZ expressed Zic2 as in the wild types. Scattered Zic2 expression was also visible throughout the rest of the retina, with stronger expression in the outer neuroblastic layer.

4.4.3. The number of Zic2-expressing cells is increased in the *Foxg1*$^{-/-}$ retina.

In order to quantify and compare the numbers of Zic2-positive cells in the wild type and *Foxg1* null retinas shown in Figures 2 - 10, the retinas were divided into six equally-spaced sections from dorsal to ventral (Figure 11A) and the numbers of Zic2-expressing cells counted and summed (Figure 11B). Numbers of Brn3a-expressing cells were counted in the same sections to provide a count of the numbers of RGCs. The nasal retina of *Foxg1*$^{-/-}$ embryos had a significantly greater number of Zic2-positive cells compared to wild type nasal retina (Figure 11B). However, there was no difference in the number of Zic2-expressing cells between *Foxg1*$^{-/-}$ and wild type temporal retinas. In the wild type, the temporal retina had significantly more Zic2-positive cells compared to the nasal retina as expected from previous studies. In order to control for differences in numbers of RGCs in each section that may have contributed to variation in the absolute Zic2 counts, the numbers of Zic2-positive cells were expressed as proportions of the numbers of Brn3a-expressing RGCs in each section. This produced the same trends as the absolute Zic2 counts, although the standard errors were reduced (Figure 11C). In *Foxg1*$^{-/-}$ embryos, the number and proportion of Zic2-positive cells in the nasal retina was greater than in the temporal retina. However, a significant difference was only found when Zic2-expressing cells were expressed as proportions of Brn3a-positive RGCs (Figures 11C, E).

Figure 11. Zic2-expressing cells are more numerous in E14.5 *Foxg1*$^{-/-}$ nasal retina compared to wild type retina. (A) Quantification method for fluorescence immunohistochemistry at E14.5. For each retina, numbers of Zic2- & Brn3a-positive cells were counted in 6 cryosections spaced at 80 – 100µm intervals through the retina from D (blue horizontal lines) to V (green horizontal lines). Counts for nasal and temporal retina were kept separate. Zic2 counts plotted in subsequent graphs are means for 4 (*Foxg1*$^{+/+}$) or 3 (*Foxg1*$^{-/-}$) retinas from different embryos. (B) There are significantly more Zic2-positive cells in *Foxg1*$^{-/-}$ nasal retina compared to wild type nasal retina. In wild type embryos, the temporal retina contains significantly more Zic2-positive cells than nasal retina. (C) The number of Zic2-positive cells expressed as a proportion of RGCs (Brn3a-positive cells) is significantly greater in *Foxg1*$^{-/-}$ nasal retina compared to both *Foxg1*$^{-/-}$ temporal retina and wild type nasal retina. The proportion of Zic2-positive RGCs is significantly greater in *Foxg1*$^{-/-}$ nasal retina than *Foxg1*$^{-/-}$ temporal retina. Means are counts of Zic2-positive cells in evenly-spaced sections from dorsal to ventral retina expressed as a percentage of the number of Brn3a-positive cells. (D, E, G) T-test comparisons for graphs (B, C, F). Statistically significant differences are highlighted in yellow. (F) The number of Zic2-positive cells expressed as a proportion of RGCs for the four retinal quadrants. The proportions of Zic2-expressing cells are significantly greater in *Foxg1*$^{-/-}$ DN and VN retinal quadrants. Abbreviations: N is nasal, T is temporal, DN is dorsonasal, VN is ventronasal, DT is dorsotemporal, VT is ventrotemporal, *Foxg1*$^{+/+}$ is wild type retina, *Foxg1*$^{-/-}$ is *Foxg1* null retina, Zic2+ve indicates Zic2-expressing cells, Brn3a+ve indicates Brn3a-expressing cells, error bars show SEM.

Figure 11. Quantification of Zic2-positive cells at E14.5

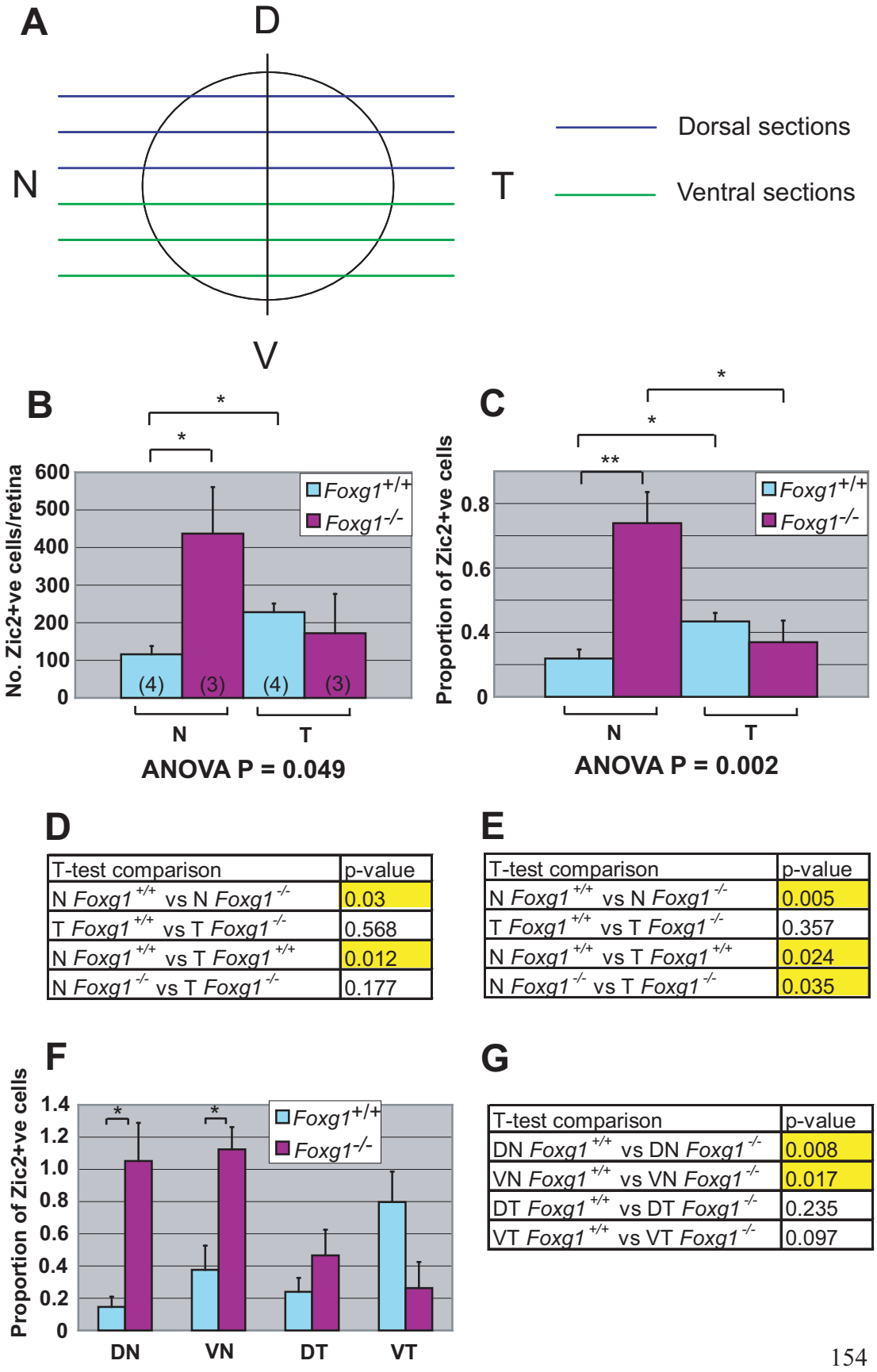

D

T-test comparison	p-value
N *Foxg1* $^{+/+}$ vs N *Foxg1* $^{-/-}$	0.03
T *Foxg1* $^{+/+}$ vs T *Foxg1* $^{-/-}$	0.568
N *Foxg1* $^{+/+}$ vs T *Foxg1* $^{+/+}$	0.012
N *Foxg1* $^{-/-}$ vs T *Foxg1* $^{-/-}$	0.177

E

T-test comparison	p-value
N *Foxg1* $^{+/+}$ vs N *Foxg1* $^{-/-}$	0.005
T *Foxg1* $^{+/+}$ vs T *Foxg1* $^{-/-}$	0.357
N *Foxg1* $^{+/+}$ vs T *Foxg1* $^{+/+}$	0.024
N *Foxg1* $^{-/-}$ vs T *Foxg1* $^{-/-}$	0.035

G

T-test comparison	p-value
DN *Foxg1* $^{+/+}$ vs DN *Foxg1* $^{-/-}$	0.008
VN *Foxg1* $^{+/+}$ vs VN *Foxg1* $^{-/-}$	0.017
DT *Foxg1* $^{+/+}$ vs DT *Foxg1* $^{-/-}$	0.235
VT *Foxg1* $^{+/+}$ vs VT *Foxg1* $^{-/-}$	0.097

The same data was divided into the four retinal quadrants: dorsonasal, dorsotemporal, ventronasal and ventrotemporal in order to investigate whether the increase in Zic2-labelled cells originated equally from the dorsal and ventral part of the nasal retina (Figure 11F). In *Foxg1*$^{-/-}$ embryos, the DN and VN retinal quadrants showed a significant increase in the number of Zic2-positive cells relative to equivalent wild type quadrants showing that increased Zic2 expression occurs in both the dorsal and ventral parts of the nasal retina (Figure 11G). None of the other retinal quadrants showed differences in the number of Zic2-positive cells. In wild type embryos, VT retina possessed the greatest number of Zic2-positive cells confirming previous studies and consistent with the role of Zic2 as an ipsilateral determinant. There were fewer Zic2-positive cells in the VT *Foxg1*$^{-/-}$ retina compared to wild type VT retina but this difference was not statistically significant.

4.4.4. Quantification of DAB immunohistochemistry.

Numbers of Zic2-positive cells were counted in the same way at E16.5 (Figures 12C, D) and also at E14.5 (Figures 12A, B) using DAB immunohistochemistry. Zic2 counts are shown as absolute numbers of Zic2-positive cells in six sections through the retina. These data are not expressed as proportions since the numbers of Brn3a-expressing cells were not counted in the same eyes used for the Zic2 counts, which would have produced variation. At E14.5, there are significantly greater numbers of Zic2-positive cells in nasal *Foxg1*$^{-/-}$ retina compared to nasal wild type retina (Figure 12A, E). In contrast, comparisons of the temporal retina revealed significantly fewer Zic2-expressing cells in *Foxg1*$^{-/-}$ embryos compared to wild types. Dividing the retina into quadrants revealed statistically significant differences in VN, DT and VT quadrants between wild type and *Foxg1*$^{-/-}$ embryos (Figure 12B, F). In VN and DT quadrants, *Foxg1*$^{-/-}$ retinas had greater numbers of Zic2-positive cells than equivalent wild type retinal quadrants, whereas comparisons of VT retina revealed fewer Zic2-expressing

Figure 12. Numbers of Zic2-expressing cells are greater in E14.5 and E16.5 *Foxg1*$^{-/-}$ nasal retina compared to wild type retina.
Graphs show means of numbers of Zic2-positive cells in evenly spaced sections through E14.5 and E16.5 wild type and *Foxg1*$^{-/-}$ retinas processed for Zic2 immunohistochemistry and revealed using DAB staining. The quantification method used was identical to that shown in Figure 11A. (B, D) Data in (A) and (D) shown divided into retinal quadrants. (A - D) Numbers of Zic2-positive cells in wild type and *Foxg1*$^{-/-}$ retinas at E14.5 (A, B) and E16.5 (C, D). Significant pairwise differences are marked with an asterisk. (A, C) At E14.5 and E16.5, the number of Zic2-positive cells is significantly greater in the nasal retina of *Foxg1*$^{-/-}$ embryos compared to wild type embryos. (E, F) T-tests between wild type and *Foxg1*$^{-/-}$ retinas for nasal and temporal retina (E) or retinal quadrants (F). Significant differences are highlighted in yellow. Abbreviations: N is nasal, T is temporal, DN is dorsonasal, VN is ventronasal, DT is dorsotemporal, VT is ventrotemporal, *Foxg1*$^{+/+}$ is wild type retina, *Foxg1*$^{-/-}$ is *Foxg1* null retina, Zic2+ve indicates Zic2-expressing cells, error bars show SEM.

Figure 12. Numbers of cells expressing Zic2 in E14.5 & E16.5 wild type and *Foxg1* null retinas

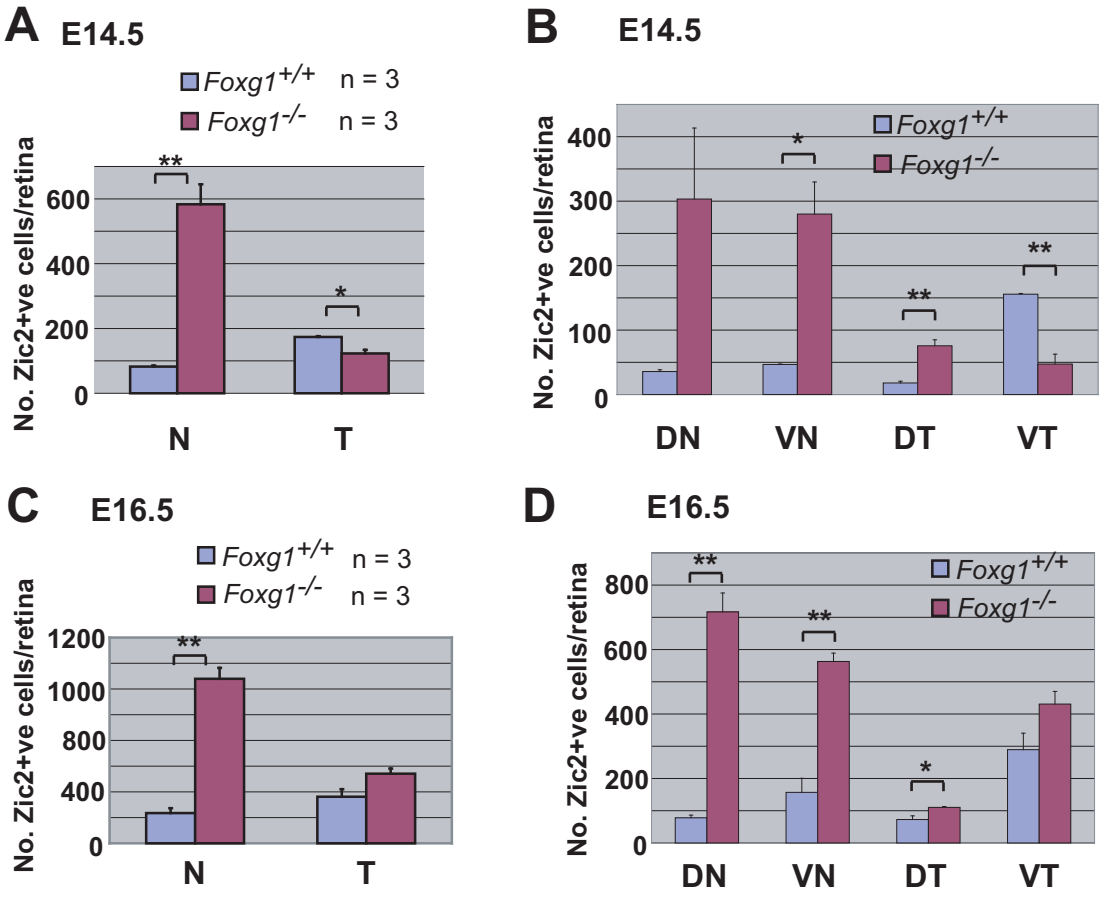

E

t-test comparison	p-values	
	E14.5	E16.5
N *Foxg1* $^{+/+}$ vs N *Foxg1* $^{-/-}$	0.001	< 0.001
T *Foxg1* $^{+/+}$ vs T *Foxg1* $^{-/-}$	0.011	0.065

F

Comparison	E14.5	E16.5
DN *Foxg1* $^{+/+}$ vs *Foxg1* $^{-/-}$	0.072	< 0.001
VN *Foxg1* $^{+/+}$ vs *Foxg1* $^{-/-}$	0.009	0.001
DT *Foxg1* $^{+/+}$ vs *Foxg1* $^{-/-}$	0.004	0.031
VT *Foxg1* $^{+/+}$ vs *Foxg1* $^{-/-}$	0.002	0.093

cells in the *Foxg1*$^{-/-}$ retina. Although DN *Foxg1*$^{-/-}$ retinal quadrants had greater numbers of Zic2-positive cells than equivalent wild type retinal quadrants, the difference was not significant. However, the standard error is very large for the DN *Foxg1*$^{-/-}$ Zic2 mean, which could have contributed to the insignificant p-value. Although the temporal retina shows differences that are not seen in the double fluorescence counts, the trend for each of the retinal quadrants and the nasal retina is the same for both DAB and fluorescence.

Quantification of Zic2 expression at E16.5 using DAB immunohistochemistry revealed the same results for the nasal retina at E14.5: significantly greater numbers of Zic2-positive cells were present in nasal *Foxg1*$^{-/-}$ retina compared to nasal wild type retina (Figure 12C). However, no difference was found between wild type and *Foxg1*$^{-/-}$ temporal retina. In *Foxg1*$^{-/-}$ embryos, both DN and VN retinal quadrants had significantly greater numbers of Zic2-positive cells (Figure 12D). The DT *Foxg1*$^{-/-}$ retina also showed a significant increase in Zic2-expressing cells compared to DT wild type retina. No difference in the numbers of Zic2-expressing cells was found in the VT retina at this age. Regardless of slight differences between the retinal quadrants that mainly affected temporal retina, all the data presented here reveal an increase in Zic2-expressing cells in the nasal retina of *Foxg1* null embryos at E14.5 and E16.5.

4.4.5. The number of RGCs does not differ between *Foxg1*$^{-/-}$ and wild type retina at E14.5 or E16.5.

In order to eliminate the possibility that the increased number of Zic2-expressing cells in the *Foxg1*$^{-/-}$ nasal retina was simply due to an increased number of RGCs, the numbers of postmitotic RGCs, identified using a Brn3a antibody, were counted in the same six sections through the retina used for quantifying Zic2 expression (Figure 13A, B).

Numbers of Brn3a-positive RGCs in the retina of wild type and *Foxg1*$^{-/-}$ embryos at E14.5 & E16.5

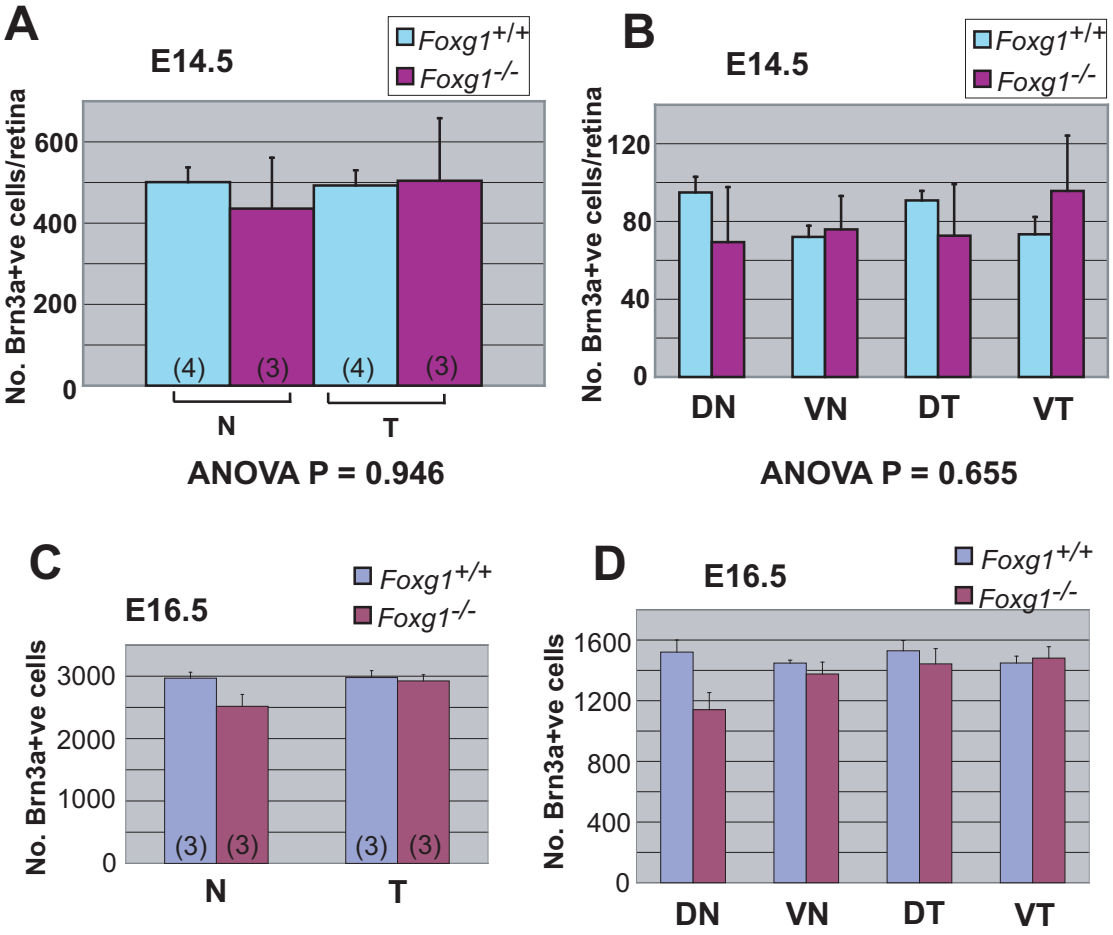

E

T-test comparison	p-value
N *Foxg1* $^{+/+}$ vs *Foxg1* $^{-/-}$	0.101
T *Foxg1* $^{+/+}$ vs *Foxg1* $^{-/-}$	0.736

F

T-test comparison	p-value
DN *Foxg1* $^{+/+}$ vs *Foxg1* $^{-/-}$	0.052
VN *Foxg1* $^{+/+}$ vs *Foxg1* $^{-/-}$	0.421
DT *Foxg1* $^{+/+}$ vs *Foxg1* $^{-/-}$	0.387
VT *Foxg1* $^{+/+}$ vs *Foxg1* $^{-/-}$	0.632

Figure 13. Numbers of Brn3a-expressing RGCs do not vary between wild type and *Foxg1*$^{-/-}$ retinas. All graphs show means of total numbers of Brn3a-positive cells in six evenly-spaced sections through a wild type or *Foxg1*$^{-/-}$ retina at E14.5 (A, B) and E16.5 (C, D). E14.5 counts are from Brn3a fluorescent immunohistochemistry and E16.5 counts are from DAB-revealed Brn3a immunohistochemistry. (E, F) T-test comparisons between *Foxg1*$^{+/+}$ and *Foxg1*$^{-/-}$ retina at E16.5. (A, C, E) Numbers of Brn3a-positive cells do not vary between *Foxg1*$^{+/+}$ and *Foxg1*$^{-/-}$ nasal and temporal retina. (A, B) At E14.5, one-way ANOVAs returned non-significant p-values. (B, D) Data in (A) and (C) split into retinal quadrants. (E, F) At E16.5, t-tests failed to produce significant differences. Abbreviations: N is nasal, T is temporal, DN is dorsonasal, VN is ventronasal, DT is dorsotemporal, VT is ventrotemporal, *Foxg1*$^{+/+}$ is wild type retina and *Foxg1*$^{-/-}$ is *Foxg1* null retina.

Although the Brn3a counts were more variable in *Foxg1* null retinas, the numbers of Brn3a-labelled cells between E14.5 wild type and *Foxg1*$^{-/-}$ retinas did not vary significantly. Similarly at E16.5, no significant differences were discovered between wild type and *Foxg1*$^{-/-}$ retinas (Figure 13 C, D). Therefore, an increase in the numbers of RGCs cannot account for the difference in Zic2 expression between wild type and *Foxg1*$^{-/-}$ nasal retinas. This is consistent with the finding that similar conclusions were drawn from the graphs showing Zic2-expressing cells as absolute counts or proportions (Figures 11B, C). Moreover, the numbers of Brn3a-positive cells did not differ between the nasal and temporal retina within either wild type or *Foxg1* null embryos confirming that the nasal-temporal axis imposed for the counts was valid.

4.4.6. Zic2 is expressed at the optic chiasm of wild type and *Foxg1*$^{-/-}$ embryos.

Zic2 is also expressed at the optic chiasm of E13.5 – E16.5 wild type and *Foxg1*$^{-/-}$ embryos throughout the period when RGC axons project (Figure 14). In wild type and *Foxg1*$^{-/-}$ retinas, Zic2 expression was strongest in lateral regions around the optic recess with a decreasing gradient towards the midline. The distorted shape of the *Foxg1*$^{-/-}$ chiasm hindered a straightforward comparison with chiasms from wild type embryos in the absence of quantitation using a method such as qRT PCR or counts of Zic2-expressing cells. Nevertheless, Chapter 6 of this thesis shows that many molecular and anatomical features of the chiasm region are preserved in *Foxg1* null embryos. In support of this, the Zic2 expression pattern at the *Foxg1*$^{-/-}$ chiasm shares certain features with that of wild type embryos, such as stronger lateral expression and a boundary between anterior Zic2-expressing and posterior Zic2-negative regions of the ventral hypothalamus. This anterior-posterior divide in Zic2 expression was examined further using Islet-1, which is expressed only in the most posterior chiasm regions, as well as in a few cells at the optic chiasm midline (Herrera et al., 2004).

Figure 14. Zic2 is expressed at the optic chiasm in wild type and *Foxg1* null embryos throughout the period when RGC axons project. Zic2 immunohistochemistry on horizontal sections of E13.5 – E16.5 optic chiasm revealed using DAB. All sections are taken at a similar dorsal-ventral location through the optic chiasm. Anterior is down. Arrows mark the midline. (A – D) E13.5, (E, F) E14.5 and (G, H) E16.5. (A, C, E, G) *Foxg1*$^{+/+}$ chiasm. (B, D, F, H) *Foxg1*$^{-/-}$ chiasm. (C, D) High power magnifications of (A) and (B) respectively. Abbreviations: er = extended retina. Scale bars: A, B = 500μm, C - G = 200μm.

Figure 14. Developmental series of Zic2 expression at the optic chiasm

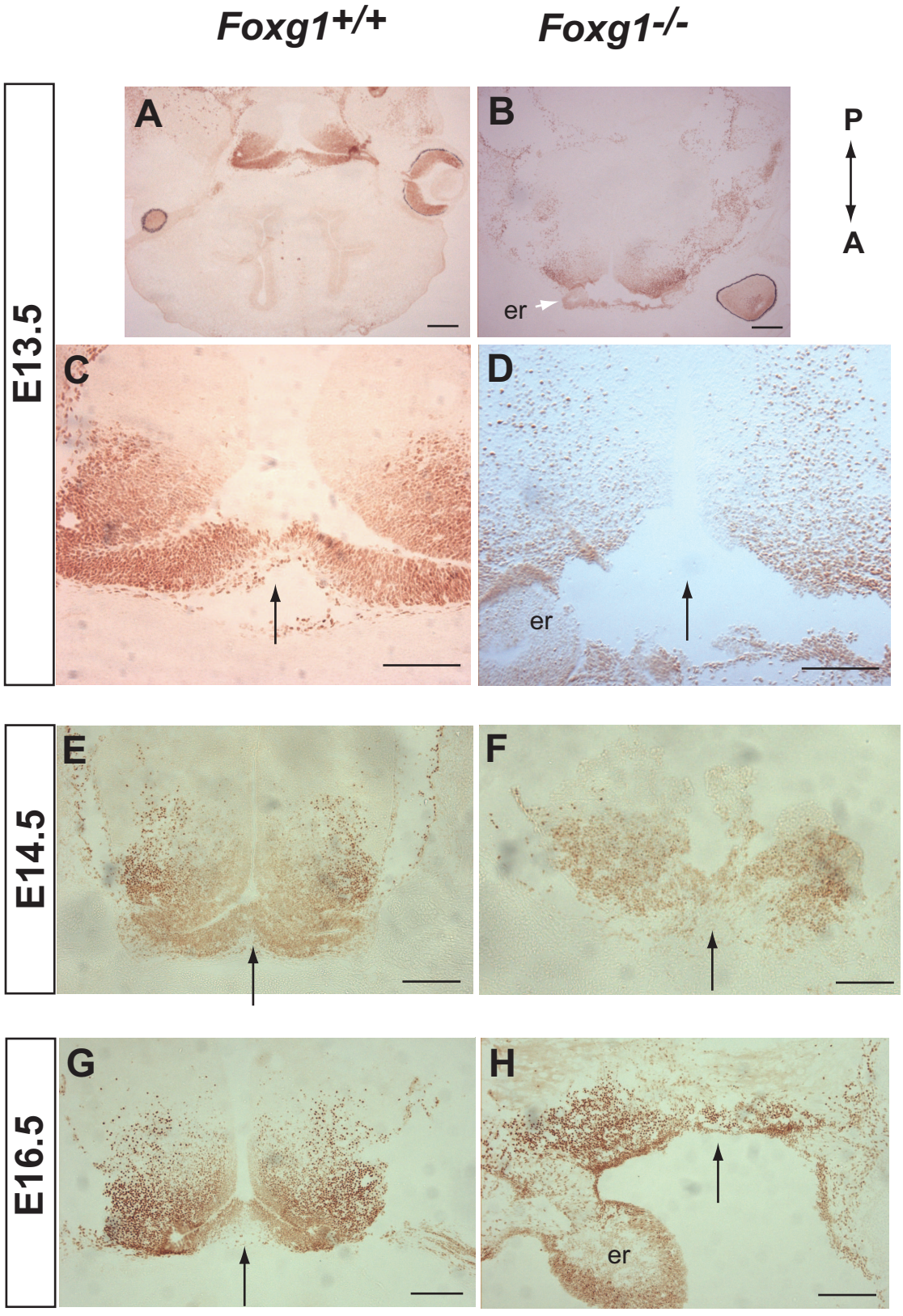

The function of Islet-1 at the chiasm is unknown but it is useful for orientation purposes. In *Foxg1*$^{-/-}$ embryos, the cortex is not present in this plane of section as it is much smaller (Figure 15A, B). Zic2 was not expressed in Islet-1-positive posterior chiasm regions in wild type embryos, indicated by the absence of Zic2 and Islet-1 double-labeled cells. In *Foxg1*$^{-/-}$ embryos, the Zic2-expressing region of the chiasm is located just posterior to where the extended retina attaches to the ventral hypothalamus. Islet-1 expression is absent from the *Foxg1*$^{-/-}$ posterior chiasm region (Figure 15B, D). The Zic2-expressing region extends further dorsally in *Foxg1* null embryos compared to the wild type but there is still a clear divide between the Zic2-positive anterior and Zic2-negative posterior region in the ventral chiasm as in the wild type. However, these results are based on a *Foxg1*$^{-/-}$ n of 1 and so more replicates are required before conclusions can be drawn. Zic2 was also expressed in other brain regions, including the thalamus with strong expression in the zona limitans intrathalamica (zli) (Figure 15A, B).

4.4.7. Zic2 is only found in ipsilaterally-projecting RGCs.

In order to show that Zic2-expressing cells in the retina project ipsilaterally but not contralaterally, dextran was used to backlabel one optic tract followed by Zic2 immunohistochemistry on the retina contralateral and ipsilateral to the dextran injection. This revealed that in wild type E14.5 embryos only ipsilateral RGCs are double-labeled and express Zic2, whereas contralateral RGCs are more numerous and Zic2-negative (compare Figures 16A and C). A similar result was found in an additional two dextran-backlabeled wild type embryos and the contralateral and ipsilateral eyes shown in Figure 16 are the clearest and most representative examples for this preliminary experiment.

Figure 15. Zic2 is expressed at the optic chiasm and thalamus in wild type and *Foxg1*$^{-/-}$ embryos at E14.5. (A – D) Zic2 (green) and Islet-1 (red) immunohistochemistry in 10µm-thick sagittal sections at the midline. (E) Schematic diagram of a sagittal section corresponding to (A – D). (A, C) wild type, (B, D) *Foxg1*$^{-/-}$. (A) In the wild type Zic2 is expressed at the optic chiasm but also in other parts of the brain including the thalamus. (C) High power magnification of (A) showing Zic2 expression dorsal to axons (white arrow) but anterior to Islet-1, which is expressed in posterior chiasm cells. (B) *Foxg1*$^{-/-}$ section showing the extended retina joining the ventral hypothalamus. (D) High power magnification of (B) showing Zic2 expression in the optic chiasm region (white arrow). Islet-1 is expressed in RGCs in the extended retina. Abbreviations: A = anterior, P = posterior, oc = optic chiasm, th = thalamus, ctx = cortex, r = retina, or = optic recess, zli = zona limitans intrathalamica. Scale bars: A, C, D = 200µm, B = 400µm.

Figure 15. Zic2 expression at the E14.5 optic chiasm

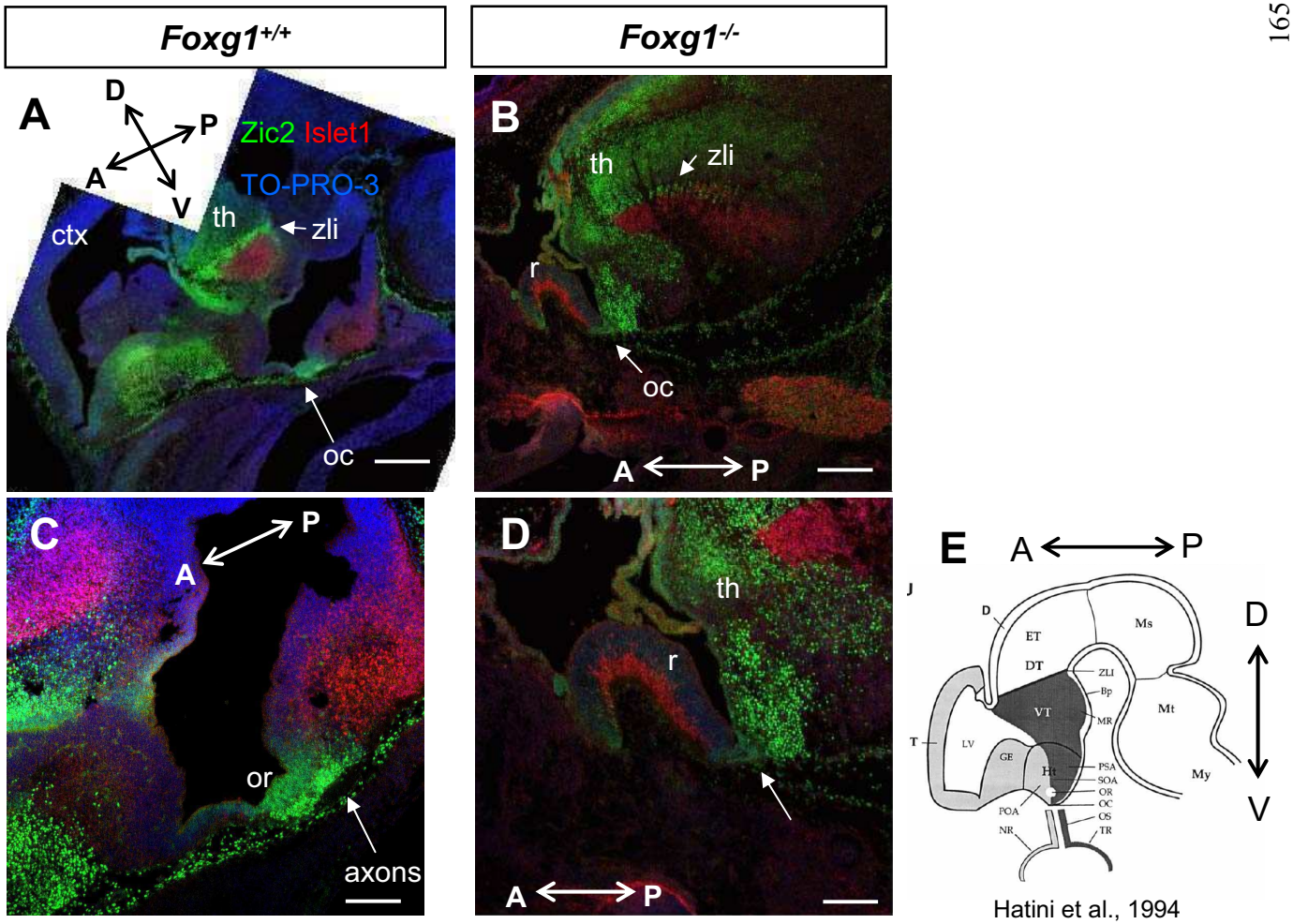

Hatini et al., 1994

Figure 16. Zic2 is only found in ipsilateral RGCs in E14.5 wild type retina. (A - C) Zic2 immunohistochemistry in the ipsilateral and contralateral retina following dextran backlabeling from one optic tract in an E14.5 wild type embryo. (A) The retina ipsilateral to the dextran injection shows only a few backlabeled RGCs limited to the ventrotemporal retina. Some backlabeled RGCs are Zic2-positive and appear yellow (examples shown with black arrows). (B) The dorsonasal part of the ipsilateral eye is Zic2-negative and no backlabeled RGCs are visible. There are a few backlabeled RGCs in dorsonasal retina (white arrow). (C) The retina contralateral to the dextran injection shows many backlabeled RGCs spread over the entire retina but none express Zic2. (D) Diagram showing the site of dextran injection into the optic tract and areas of the retina where backlabeled RGCs (red) and Zic2-expressing cells (green) and double-labeled cells (yellow) are found. Dorsal is up and anterior is pointing directly outwards perpendicular to the page. Abbreviations: D is dorsal, V is ventral, A is anterior, P is posterior, VN is ventronasal, VT is ventrotemporal, DN is dorsonasal, DT is dorsotemporal. Scale bars all 100μm.

Figure 16. Dextran backlabeling at E14.5 in a wild type embryo

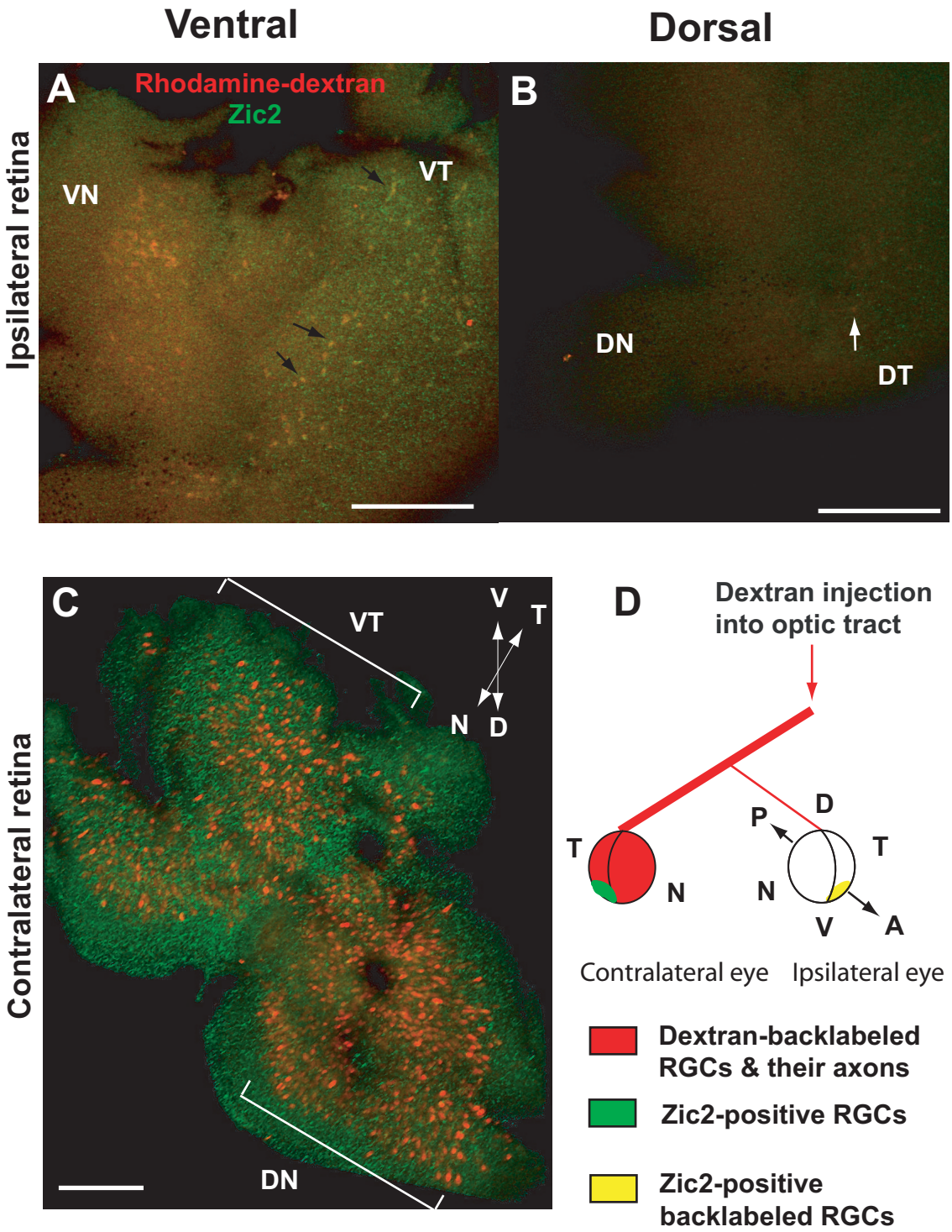

4.5. DISCUSSION

4.5.1. Significantly greater numbers of Zic2-expressing cells are present in the nasal *Foxg1*$^{-/-}$ retina.

Zic2 protein was found in the retinas of *Foxg1*-expressing and *Foxg1* null embryos throughout the period when retinal axons make a binary decision to cross the chiasm midline or remain ipsilateral. In the retina of wild type and *Foxg1* heterozygous embryos, Zic2 was expressed in a cluster of cells in the VT periphery of the retina, adjacent to the Zic2-expressing CMZ from E14.5 to E16.5, confirming previous findings (Herrera et al., 2003). Zic2-positive cells were also observed scattered throughout the remainder of the retina, including a sizeable number in the nasal retina but these were never found in clusters. *Foxg1*$^{-/-}$ embryos displayed an ectopic Zic2-expressing cluster in the nasal retina from E13.5 to E16.5. Although the VT Zic2 cluster was preserved in the retina of *Foxg1*$^{-/-}$ embryos, numbers of Zic2-expressing cells were greater in the nasal retina. Thus in the *Foxg1*$^{-/-}$ retina, Zic2 counts follow a N > T trend, which is the reverse of the wild type T > N. Quantification of the numbers of Zic2-expressing cells at E14.5 and E16.5 revealed that the nasal retina of *Foxg1*$^{-/-}$ embryos has significantly more Zic2-positive cells compared to that of an age-matched wild type embryo. This result was reproducible regardless of whether Zic2 expression was revealed by fluorescence or DAB. It follows that increased expression of the ipsilateral determinant Zic2 appears to be a likely cause of the increased ipsilateral projection from the nasal retina of *Foxg1* null embryos (see Figure 17).

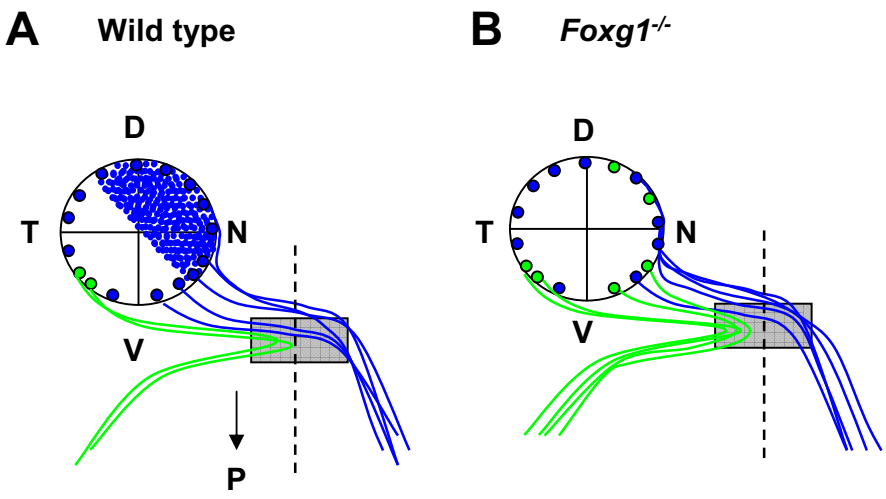

Figure 17. Proposed relationship between Zic2 expression and the ipsilateral projection in wild type and *Foxg1*$^{-/-}$ embryos. (A) Wild type, (B) *Foxg1*$^{-/-}$ retina. (A) Only RGCs from the VT crescent in the VT retinal quadrant express Zic2 (green circles) and project ipsilaterally at the chiasm midline (dashed line). *Foxg1* expression is indicated by blue stippling. (B) In *Foxg1*$^{-/-}$ retina, RGCs in the nasal hemiretina express Zic2 and their axons behave like those from VT retina by projecting ipsilaterally. RGCs in the VT crescent also express Zic2. Note: for simplicity, only a few projecting axons are illustrated.

Abbreviations: N, nasal; T, temporal; D, dorsal; V, ventral; P, posterior.

Key: Blue lines represent contralaterally-projecting RGC axons, green lines represent ipsilaterally-projecting RGC axons. Grey rectangle represents ephrin B2 expression at the optic chiasm.

When the numbers of Zic2-expressing cells were divided into the different retinal quadrants, fluorescence and DAB methods gave different results at E14.5. The fluorescence method revealed significantly greater numbers of Zic2-expressing cells per retina expressed as a proportion of the numbers of Brn3a-positive RGCs in dorsal and ventral locations within the *Foxg1*$^{-/-}$ nasal retina. However, counts using DAB only revealed the same finding in VN retina. Although numbers of Zic2-positive cells were greater in *Foxg1*$^{-/-}$ DN retina, the difference was not statistically significant from wild type DN retina. However, the variability in terms of the standard error in *Foxg1*$^{-/-}$ Zic2 counts was greatest for the DN quadrant compared to all other retinal quadrants for E14.5 fluorescence and DAB methods. This may be due to real variability in the DN quadrant of the *Foxg1*$^{-/-}$ retina compared to other regions of the retina or alternatively the low 'n' numbers (n = 3). If the latter is true and since the data follow a similar trend for DN retina for fluorescence and DAB Zic2 counts, it is plausible that increasing the numbers of *Foxg1*$^{-/-}$ retinas for Zic2 quantification using immunohistochemistry revealed by DAB may result in a significant difference in DN retina. At E16.5, significantly greater numbers of Zic2-positive cells were found in DN and VN *Foxg1*$^{-/-}$ retina, agreeing with the E14.5 fluorescence data.

Foxg1 is most widely expressed in the nasal half of the retina (Chapter 5, this thesis; Hatini et al., 1994; Huh et al., 1999; Pratt et al., 2004), which is the half of the retina that displays an increase in Zic2 expression in *Foxg1* null embryos. These results lend support to the hypothesis put forward earlier in this Chapter that the numbers of Zic2-expressing cells rise in proportion to the increased ipsilateral projection. However, an increase in Zic2 expression was only found in the nasal but not the temporal retina, from which many ipsilateral projections also arise in *Foxg1*$^{-/-}$ eyes. Consequently, a different explanation must be invoked to explain the increase in temporal ipsilateral projections. In summary, these results are consistent with a model in which Foxg1 normally suppresses Zic2 in the nasal retina. In *Foxg1*$^{-/-}$ embryos, Foxg1 is absent from the nasal retina, relieving the repression on Zic2 and thereby allowing Zic2 expression

to increase. The theory that Foxg1 acts cell autonomously to regulate Zic2 expression in nasal RGCs themselves is compatible with the data presented here but not proved by it.

4.5.2. Zic2 expression in the temporal retina.

The same trend for greater numbers of Zic2-positive cells in DT *Foxg1*$^{-/-}$ retina and fewer Zic2-positive cells in *Foxg1*$^{-/-}$ VT retina relative to equivalent wild type retinal quadrants was found for the fluorescence and DAB counts at E14.5. However, comparisons of the temporal retina of *Foxg1*$^{-/-}$ and wild type embryos revealed a significant difference with the DAB counts only. As mentioned previously for the nasal retina, it is impossible to tell whether the difference in statistical significance is due to intrinsic differences in the results obtained counting DAB- or fluorescently-labeled Zic2-positive cells or due to low 'n' numbers. One way to overcome this problem would be to increase the numbers of retinas analyzed using both fluorescence and DAB methods for revealing Zic2 expression.

At E16.5, there was no difference in Zic2 expression between the temporal retinas of wild type and *Foxg1*$^{-/-}$ embryos. Splitting up the temporal retina into dorsal and ventral regions revealed a significantly greater number of Zic2-positive cells in *Foxg1*$^{-/-}$ DT retina compared to the wild type, mimicking the trend in E14.5 embryos. E16.5 *Foxg1*$^{-/-}$ embryos showed no change in Zic2 counts in the VT retina relative to wild types. Interestingly, this is the only part of the retina in which a change in Zic2 expression was observed between E14.5 and E16.5. This suggests that there might be a developmental delay in the expression of Zic2 in the *Foxg1*$^{-/-}$ VT retina, which is apparent at E14.5 but disappears by E16.5. It would be fascinating to investigate this hypothesis further by examining Zic2 expression at E13.5 (when Zic2 expression appears in the retina), E15.5 and later on after E16.5 to observe temporal fluctuations in

Zic2 numbers in the VT retina in greater detail. Additionally, it would be prudent to investigate the onset of expression of various retinal markers, including *Brn3b* that is expressed in the earliest postmitotic RGCs from E11.5 (Pan et al., 2005), *Islet-1* that is expressed just after RGCs leave the cell cycle (Rachel et al., 2002) and also *Foxd1*, a forkhead box transcription factor whose expression is limited to the VT retina from E14.5 - E16.5 (Herrera et al., 2004). Interestingly, very low numbers of RGCs express Brn3a in the VTC, whereas Brn3b is expressed there to a greater extent (Quina et al., 2005). This could also account for the general lack of co-labeling between Brn3a and Zic2 in wild type and *Foxg1*$^{-/-}$ embryos. In all other regions of the retina, almost all RGCs expressing Brn3a also express Brn3b albeit at different levels. Brn3b was not used as an RGC marker in the experiments presented here because it is also expressed in RGCs in the neuroepithelial layer between E13.5 and E16.5, unlike Brn3a, which is expressed solely by RGCs in the ganglion cell layer (Pan et al., 2005).

The Zic2 counts for the temporal retina in *Foxg1* null eyes fail to explain the increased ipsilateral projections from the temporal half of the *Foxg1*$^{-/-}$ retina because they either show no change or a slight decrease in Zic2 expression. The increased proportion of temporal ipsilaterally-projecting retinal axons may be caused by a non-autonomous effect of *Foxg1*, since *Foxg1* is not normally expressed there. Alternatively, changes in the chiasm region or in other structures that temporal retinal axons encounter may result in their preference for an uncrossed trajectory. These results call for a more thorough study of possible non-autonomous effects of Foxg1 in the temporal retina and its resident RGCs.

4.5.3. The number of RGCs in E14.5 *Foxg1*$^{-/-}$ retina does not differ from the wild type at E14.5 or E16.5.

A possible explanation for the increase in Zic2-expressing cells in the *Foxg1*$^{-/-}$ retina is simply that there are more cells in the RGC layer relative to the wild type retina due to more extensive proliferation. Although the volume of the wild type and *Foxg1* null retina does not differ significantly at E15.5 (Pratt et al., 2004), it was not known whether the number of RGCs differed. Counts of RGCs expressing the postmitotic marker Brn3a showed that *Foxg1*$^{-/-}$ retinas have the same number of RGCs as age-matched wild type retinas at E14.5 and E16.5. This was true for the nasal and temporal retina and also for the different retinal quadrants rendering the possibility of a proliferative defect in the eye unlikely. Therefore, it was valid for Zic2 DAB counts to be shown without correcting for the number of RGCs. Moreover, within wild type or *Foxg1*$^{-/-}$ retinas, the numbers of Brn3a-positive cells did not differ between the nasal and temporal retina confirming that the nasal-temporal boundary imposed for the counts was valid.

4.5.4. Zic2 is expressed exclusively by ipsilateral RGCs.

The backlabeling experiment showed that only some ipsilateral RGCs express Zic2 and therefore, appear yellow or double-labeled. Contralateral dextran-backlabeled RGCs never co-labeled with Zic2, which concords with previous findings (Herrera et al., 2003). This also agrees with the fluorescence Zic2 images in which Zic2-positive cells rarely co-labeled with Brn3a-positive RGCs and were generally positioned at a more peripheral location (Figures 2 - 10). Double-labeled cells were usually found in the VT retina at the most peripheral extent of the Brn3a-expression domain, as for the dextran-backlabeled ipsilateral RGCs. Since RGCs are generated in a wave of differentiation from central to peripheral retina regulated by *Brn3-a*, *-b* and *-c*, this implies that Zic2-

positive cells are immature RGCs that have not yet begun to express certain RGC markers such as *Brn3a* (Pan et al., 2005; Xiang et al., 1995). Previous studies have shown that Zic2 is co-expressed with *Islet-1* (Herrera et al., 2003), which is expressed prior to *Brn3a* by postmitotic RGCs as they leave the cell cycle (Rachel et al., 2002).

In the future, it will be interesting to repeat this experiment using *Foxg1*$^{-/-}$ retinas to test the hypothesis that the increased ipsilateral projections in *Foxg1* null embryos are the result of increased Zic2 expression in the nasal retina. In other words, do Zic2-positive cells in the nasal *Foxg1*$^{-/-}$ retina follow an ipsilateral route rather than a contralateral one typical of Zic2-negative nasal retinal cells in the wild type? If this hypothesis is true, it is expected that *Foxg1*$^{-/-}$ retinas will show an increase in the number of double-labeled ipsilateral RGCs in the nasal retina relative to wild type retinas.

The main drawback with the dextran backlabeling experiment is that Zic2 is initially expressed in RGCs that project ipsilaterally but is subsequently downregulated once their axons reach the optic chiasm (Herrera et al., 2003). Therefore, backlabeled ipsilateral RGCs may not appear to express Zic2 even though they may have done so in the past. In addition, backlabeled RGCs are more mature and are located nearer to the central retina than Zic2-positive cells, which differentiate later by virtue of their peripheral location. In other words, Zic2-positive cells may have extended axons that have not reached the chiasm yet, or alternatively, they may not have extended axons at all. In order to investigate this more thoroughly, lineage-tracing would be required to identify retinal cells that have expressed Zic2 at any time in their lineage. Zic2 lineage tracing could be done using two mouse lines: (1) mice in which the coding sequences of Zic2 have been replaced with a cre recombinase cassette and (2) mice carrying a ROSA βgeo 26 reporter allele, '*R26R*' (Soriano, 1999). The R26R reporter allele consists of a stop codon flanked by *loxP* sites that is situated upstream of a βgeo cassette containing the *beta-galactosidase* gene. Mice carrying the R26R reporter allele express LacZ (βgeo) ubiquitously only after recombination due to recognition of *loxP*

sites and excision of the stop codon by cre recombinase. Therefore, when a Zic2-Cre heterozygous mouse is crossed with a ROSA26 reporter mouse, cre-mediated recombination occurs in tissues where Zic2 is active. This irreversibly activates beta-galactosidase expression that is visualized by LacZ staining, revealing any cells and their descendants that have expressed Zic2 at any time during development. Combined with backlabeling, lineage tracing would reveal whether RGCs that have expressed Zic2 project ipsilaterally, even if they have subsequently downregulated this transcription factor.

4.5.5. Zic2 expression at the wild type and *Foxg1*$^{-/-}$ optic chiasm.

The expression of Zic2 in the anterior chiasm region of wild type and *Foxg1*$^{-/-}$ embryos from E13.5 to E16.5 shows that Zic2 is present at the time retinal axons are projecting. Due to morphological differences between the wild type and *Foxg1*$^{-/-}$ ventral diencephalon, it is not possible to tell whether there are changes in Zic2 expression in the *Foxg1* null chiasm using Zic2 immunohistochemistry alone. This would require quantifying Zic2 protein expression at the chiasm using Western blotting or quantification of mRNA using qRT PCR. Nevertheless, the results show that Zic2 expression in the *Foxg1*$^{-/-}$ chiasm shares many properties with the wild type, such as stronger expression in lateral and anterior chiasm regions. All the *in vitro* and *in vivo* evidence to date suggests that Zic2 acts primarily in the retina to specify the ipsilateral routing of VT RGCs (Herrera et al., 2003, Pak et al., 2004, Williams et al., 2003, 2004). However, the possibility that Zic2 expression at the chiasm influences retinal axon pathfinding cannot be excluded.

4.5.6. Zic2 may influence ipsilaterality via EphB1.

EphB1 is an ephrin-B receptor that co-localises with Zic2 in VT retina from E14 – E17 when the permanent ipsilateral projection originates from VT retina (Pak et al., 2004). When EphB1-bearing VT retinal axons encounter ephrin-B2 at the optic chiasm, they are selectively repelled, whereas EphB1-negative retinal axons from other regions of the retina are not repelled (Williams et al., 2003). Although EphB1 has been implicated in mediating the behaviour of axons originating from Zic2-expressing RGCs, EphB1 is expressed prior to the onset of Zic2 expression from E12 – E13 in dorsocentral RGCs coinciding with the appearance of the first transient ipsilateral projections. This implies that EphB1 is regulated by transcription factors other than Zic2 at this early stage in the development of retinal projections (Williams et al., 2003). Nevertheless, evidence from EphB1 and *Isl2* null mice supports a link between EphB1 and Zic2. *EphB1* null mice display a marked reduction in the size of the ipsilateral projection, which resembles the phenotype of $Zic2^{kd/kd}$ mice (Williams et al., 2003). This phenotype is thought to be due to deletion of EphB1 in the retina because chiasm molecules associated with the ipsilateral projection, such as ephrin-B2, are all normal in *EphB1* null embryos. Also, in *Isl2* null mice that display an increased ipsilateral projection from VT RGCs, both Zic2 and EphB1 are upregulated in VT retina suggesting that they are both involved in the ipsilateral pathway (Pak et al., 2004). Although all the evidence to date suggests that Zic2 might control *EphB1* expression, it is equally possible that Zic2 specifies ipsilaterality independently of EphB1.

If Zic2 mediates its effects through EphB1, EphB1 should be expressed in the same nasal RGCs where Zic2 is ectopically expressed in *Foxg1* null embryos. The spatiotemporal pattern of EphB1 could be investigated using *in situ* hybridization and quantitatively by qRT PCR. Although, EphB1 antibodies exist, none have proved successful in immunohistochemistry in this or any other laboratory.

4.5.7. Hypotheses for the increase in Zic2 expression in nasal *Foxg1*$^{-/-}$ retina.

4.5.7.1. Foxg1 repression of Zic2.

Before hypothesizing about the possible interactions between Foxg1 and Zic2, it is important to understand how Zic2 is repressed in a subset of RGCs in the VT retina. The LIM homeodomain transcription factor Islet-2 (Isl2) is expressed in a subset of RGCs across the entire retina (Pak et al., 2004). There are a few Isl2-expressing RGCs in the VTC but they do not express Zic2 or EphB1, which are expressed by other RGCs in this region. In *Isl2* null mice the increased ipsilateral projections arise from a greater number of Zic2- and EphB1-positive RGCs in the VT retina, raising the possibility that Isl2 represses the ipsilateral genetic program via repression of Zic2 and EphB1 in the VT retina.

At present, it is unclear how Zic2 expression is regulated in the rest of the retina. One hypothesis that is compatible with the data presented here is that Foxg1 normally represses Zic2 in the nasal retina, where Zic2 is only weakly expressed, which would then prevent the expression of EphB1 in this region and thus prevent nasal RGC axons from projecting ipsilaterally (Figure 18). Zic2 is strongly expressed by RGCs in the VT retina because *Foxg1* is not expressed in this region and so cannot repress Zic2 (see Chapter 5). In *Foxg1*$^{-/-}$ retina, the absence of Foxg1 in nasal retina may relieve repression on Zic2, allowing cells in the nasal retina to express Zic2. Foxg1 has been shown to act as a transcriptional repressor *in vitro* (Dou et al., 2000; Yao et al., 2001), although no direct targets relating to retinal axon guidance have been identified. There is evidence for repression of Zic2 by Foxg1 in the ventral hypothalamus of *Foxd1*$^{-/-}$ embryos where Foxg1 and Zic2 occupy mutually exclusive expression domains (Herrera et al., 2004). However, there are no reports of this occurring in the retina.

Figure 18. Hypothetical model of transcriptional regulation of binocularity in RGCs. (A) Wild type retina. Foxg1-expressing RGCs project contralateral axons by repressing Zic2 in nasal retina this is hypothesised to diminish the expression of EphB1 receptors on axons. These axons are not repelled by ephrin-B2 at the chiasm. Zic2-expressing RGC axons in the VT retina project ipsilaterally. Zic2 expression in RGCs is thought to activate the expression of EphB1 receptors on axons that are repelled by ephrin-B2 at the chiasm. (B) In the wild type retina, Isl2 is thought to repress Zic2 in a subset of VT RGCs and thus repress the ipsilateral programme, leading to the production of contralaterally-projecting axons. Isl2 may generally repress the ipsilateral genetic programme in the rest of the retina, although the mechanism is unknown. (C) *Foxg1* null retina. Removing *Foxg1* relieves repression on Zic2, producing an increase in the number of Zic2-positive RGCs, which theoretically produces an increase in EphB1 receptors (vertical arrows), culminating in an increased ipsilateral projection. The VT retina still expresses Zic2, producing ipsilateral axons.

Abbreviations: D, dorsal; V, ventral; N, nasal; T, temporal; ipsi, ipsilateral; contra, contralateral; green indicates components of the ipsilateral program; blue indicates components of the contralateral program.

Figure 18

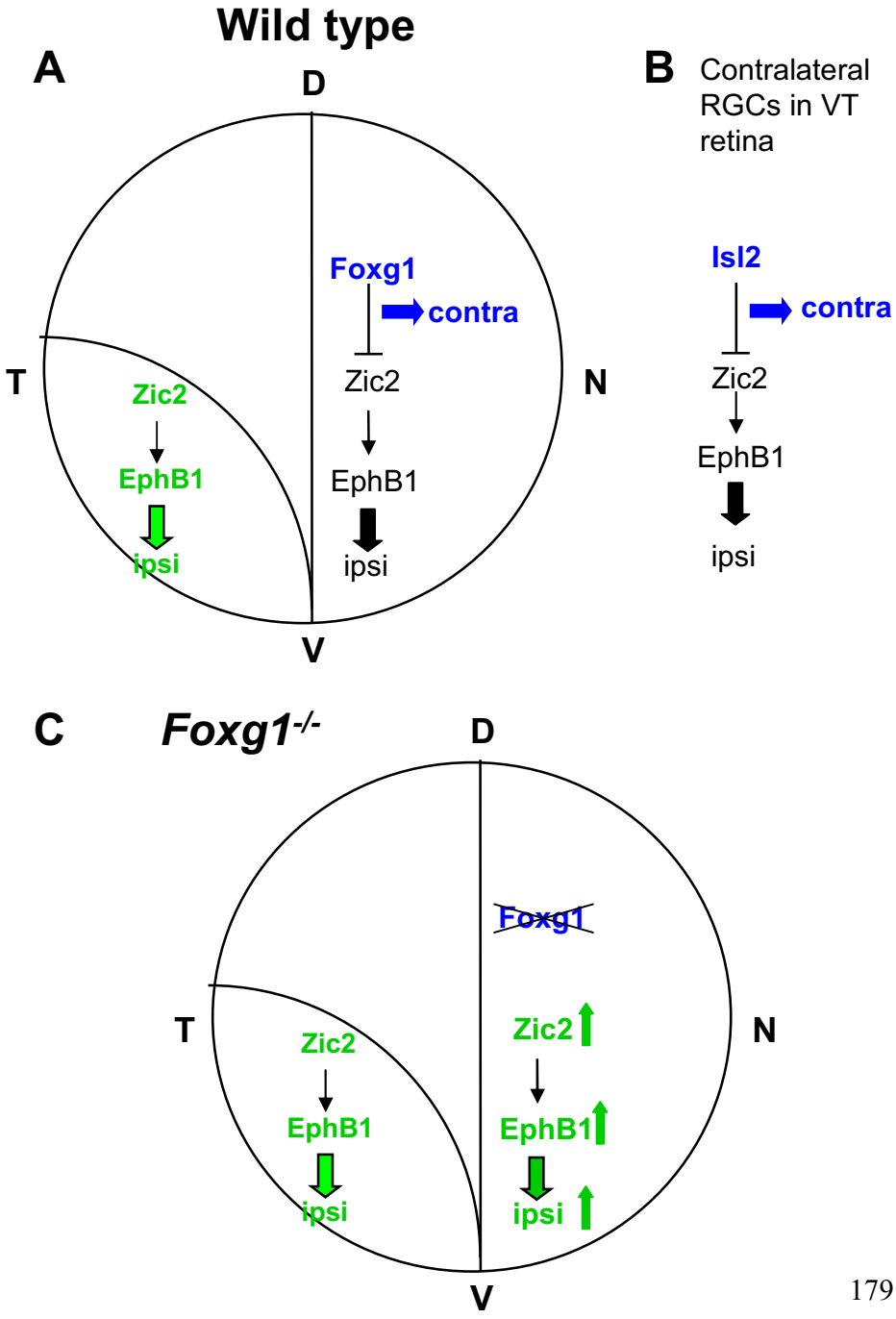
Wild type
A
D
T
N
V
Foxg1
contra
Zic2
EphB1
ipsi
Zic2
EphB1
ipsi
B
Contralateral RGCs in VT retina
Isl2
contra
Zic2
EphB1
ipsi
C
Foxg1-/-
D
T
N
V
Foxg1
Zic2
EphB1
ipsi
Zic2
EphB1
ipsi

In order to test whether Foxg1 is responsible for repressing Zic2, Foxg1 could be ectopically expressed in the VT retina, where it is normally absent, to see if Zic2 expression disappears or is reduced. Similarly, a Foxg1 expression construct could be used to transfect *Foxg1*$^{-/-}$ nasal retina, which ectopically expresses Zic2. If Foxg1 represses Zic2, it is expected that Zic2 levels would be reduced or eliminated. Finally Foxg1 expression could be knocked down specifically in the nasal retina of wild type embryos to test whether Zic2 expression increases in the absence of Foxg1 as in the *Foxg1*$^{-/-}$ retina. If this hypothesis is proved correct, elucidating the molecular mechanisms through which Foxg1 achieves this repression would then present the next challenge.

4.5.7.2. Foxd1 is required for Zic2 expression.

Another explanation for the increase in Zic2-positive cells in the nasal retina involves another Fox gene called Foxd1 (formerly known as 'BF-2'). Foxd1 is expressed in the ventrotemporal retina (Herrera et al., 2004) and its expression domain overlaps with that of Zic2, although it occupies a larger area. *Foxd1*$^{LacZ/LacZ}$ mice do not produce Foxd1 protein and expression of Zic2 and EphB1 is lost from the ventrotemporal retina entirely (Herrera et al., 2004). Although these *Foxd1* null mice exhibit an increased ipsilateral projection, which appears counter-intuitive given that Zic2 is an ipsilateral determinant, an expansion of Slit2 in the ventral diencephalon was assumed to repel more axons away from the midline. Therefore, Foxd1 may be required for the expression of Zic2 in VT retina since its absence abolishes Zic2 expression in this region. In *Foxg1* null embryos, Foxd1 expands into the nasal retina where Foxg1 is normally expressed (Huh et al., 1999). Therefore, if Zic2 requires Foxd1 for its expression, expansion of Foxd1 into *Foxg1*$^{-/-}$ nasal retina may lead to Zic2 expression here, leading to an increase in the number of Zic2-expressing cells.

However, there is an alternative explanation for the loss of Zic2 in *Foxd1* null embryos. In *Foxd1*$^{LacZ/LacZ}$ mice, Foxg1 expression expands into the VT retina, occupying the Foxd1 domain (Herrera et al., 2004). Therefore, if Foxg1 normally represses Zic2 expression, the absence of Zic2 in the VT retina of *Foxd1* null mice may be a consequence of repression by Foxg1, rather than loss of Foxd1 in VT retina.

Investigating whether Foxg1 represses Zic2 or whether Foxd1 is required for Zic2 expression would require gain- and loss-of-function *in vitro* experiments. Levels of *Foxd1* would have to be monitored in experiments that manipulate *Foxg1* and vice-versa since the expression domains of these two transcription factors expand whenever the other is absent (Huh et al., 1999; Herrera et al., 2004).

In summary, the increase in Zic2-expressing RGCs in the nasal retina of *Foxg1* null embryos provides a possible explanation for the increased number of ipsilaterally-projecting RGC axons, although this remains to be proven experimentally. Foxg1 normally represses Zic2 in the nasal retina, although it is unclear whether this repression is direct or indirect at present.

CHAPTER 5: Characterisation of the *Foxg1*$^{-/-}$ eye.

5.1. ABSTRACT

The aim of this chapter was to test the hypothesis that the increased ipsilateral projection in *Foxg1*$^{-/-}$ embryos might be caused by abnormal patterning of the *Foxg1*$^{-/-}$ retina leading to an expansion of ventral or temporal regions, which normally give rise to ipsilateral RGCs. The histology of the *Foxg1*$^{-/-}$ retina was also examined revealing that, despite its medial extension, the retina develops normally, forming the inner and outer retinal layers and an optic nerve-like structure. To examine whether dorsal, ventral, temporal or nasal patterning of the retina was altered in *Foxg1*$^{-/-}$ embryos, immunohistochemistry was used to detect EphB2 and ephrin-B2 proteins that are expressed in opposing dorsoventral (DV) gradients. The DV gradients of EphB2 and ephrin-B2 were maintained in the *Foxg1*$^{-/-}$ retina throughout the period when RGC axons project, implying that retinal patterning along this axis is not drastically altered. *Foxg1* itself was used as a nasal patterning marker in mice that contained one or two copies of a *Foxg1*^{lacZ} reporter allele, which allowed recognition of sites of *Foxg1* transcriptional activation. *Foxg1*$^{LacZ/+}$ embryos from E13.5 to E15.5 showed *Foxg1* activation in dorsonasal (DN) and dorsotemporal (DT) retina, with expression becoming increasingly restricted to nasal regions in the ventral retina. The spatial pattern of *Foxg1* activation in the *Foxg1*$^{LacZ/LacZ}$ retina differed from that in *Foxg1*$^{LacZ/+}$ embryos. In the *Foxg1*$^{LacZ/LacZ}$ dorsal retina, *Foxg1* activation was found in temporal regions that do not usually express *Foxg1* in the wild type whilst *Foxg1* activation was reduced in dorsonasal regions that normally express *Foxg1*. Ventrally, *Foxg1* activation was biased towards the nasal retina. The *Foxg1*$^{LacZ/LacZ}$ reporter mice and lineage tracing experiments indicated a slight increase in *Foxg1* transcriptional activation in the *Foxg1* null ventrotemporal (VT) retina compared to equivalent locations in the wild type retina. Although these findings are suggestive of abnormal nasotemporal (NT) retinal

patterning in the *Foxg1* null eye, further expression studies of molecules expressed along the NT axis are required to corroborate this.

5.2. INTRODUCTION

5.2.1. Eye development.

During neurulation, at approximately E9.5 in the mouse, optic vesicles evaginate from the forebrain and contact the overlying surface ectoderm, remaining attached to the diencephalon via the optic stalks. The optic vesicles then invaginate to form the optic cups. Determination of the eye fields is mediated by two members of the paired box (Pax) gene family: *Pax6* and *Pax2*. In mice and zebrafish, the evolutionarily conserved transcription factor *Pax6* is expressed throughout the optic vesicles in cells of the prospective retina, retinal pigment epithelium (RPE) and lens epithelium (Walther and Gruss, 1991). Loss-of-function mutations in *Pax6* produce a *Small eye* phenotype in mice (Hill et al., 1991), with heterozygotes showing reduced *Pax6* expression and microphthalmia, while homozygotes lack eyes, demonstrating the importance of *Pax6* in eye development. Sonic hedgehog (Shh) secreted from the ventral midline specifies the optic stalk (future optic nerve) proximally by inducing expression of *Pax2*, which then represses *Pax6* expression, limiting it to the optic cup that will form the neural retina and RPE (Macdonald et al., 1995; Walther and Gruss, 1991). Examination of the eyes of *Pax6* null mice suggests that Pax6 is involved in the development of retinal polarity along dorso-ventral and nasal-temporal axes via Vax2 (ventral) and Tbx5 (dorsal) and Foxg1 (nasal) and Foxd1 (temporal) (Baumer et al., 2002). Recently, Pax6 overexpression experiments in chick revealed that Pax6 regulates FGF8 and BMP4 expression to pattern the optic cup and also maintains a precise balance between these two signalling molecules for retinogenesis (Reza et al., 2007).

5.2.2. Hypothesis of altered retinal patterning in the *Foxg1*$^{-/-}$ eye.

The eyes of *Foxg1*$^{-/-}$ embryos develop abnormally, suggesting that Foxg1 plays a key role in patterning the developing eye (Xuan et al., 1995; Huh et al., 1999; Mui et al., 2002). Defects in the development of *Foxg1*$^{-/-}$ eyes are first observed at E10.5 (Huh et al., 1999). *Foxg1*$^{-/-}$ embryos lack a morphologically recognisable optic stalk and have abnormal ellipsoid-shaped eyes, with a medially-expanded retina, small lens and large ventral coloboma (failure of the choroid fissure to close) (Huh et al., 1999). The expanded optic vesicle connects directly with the brain due to the absence of an optic stalk. The RPE is also expanded medially. Pax6 retinal expression is expanded ventrally and medially in both anterior and posterior regions, whereas Pax2 that is normally restricted to the optic stalk and ventral pole of the optic cup is reduced to a few cells in the medial extent of the extended retina (Huh et al., 1999).

Retinogenesis proceeds in a fixed chronological order: retinal ganglion cells and horizontal cells are the first to differentiate at around E11, followed by cone-photoreceptors, amacrine cells, rod-photoreceptors, bipolar cells and finally Müller glia-cells (Drager, 1985; Young, 1985). Retinal progenitor cells are multipotent, meaning that they are able to generate any of the seven different retinal cell types up to the final cell division (Holt et al., 1988; Turner and Cepko, 1987; Wetts and Fraser, 1988). Retinal patterning along the dorsoventral and nasotemporal axes precedes the onset of retinogenesis (Hatini et al., 1994) and cell differentiation in the murine retina occurs in a central to peripheral wave (Prada et al., 1991). Consequently, the position of retinal progenitor cells in the retina determines which transcription factors are expressed by differentiated retinal cells, which then go on to dictate the behaviour of RGC axons at the optic chiasm and their topographic mapping onto the superior colliculus (Barbieri et al., 2002; Koshiba-Takeuchi et al., 2000; Schulte and Cepko, 2000; Schulte et al., 1999; Sperry, 1963; Yuasa et al., 1996).

Altered retinal patterning can lead to RGCs experiencing a different genetic and cellular environment culminating in aberrant projections. An increased ipsilateral projection could arise if there is an expansion in the absolute number of RGCs with molecular properties of ventral or temporal retina, since the VT quadrant gives rise to ipsilaterally-projecting RGCs (Colello and Guillery, 1990; Sretavan, 1990). This hypothesis appears more likely given the findings of Chapter 4 that showed an increase in the proportion of nasal RGCs expressing Zic2, which is primarily restricted to the VT retina (Herrera et al., 2003). Evidence against an increased number of VT RGCs without a corresponding reduction in RGC numbers in other parts of the retina comes from the finding that numbers of RGCs between the *Foxg1*$^{-/-}$ dorsal and ventral retina do not vary and are not significantly different from those of the wild type (presented in Chapter 4 of this thesis). Moreover, the overall volume of the *Foxg1*$^{-/-}$ eye is similar to that of an age-matched wild type eye (Pratt et al., 2004). However, these findings do not exclude the possibility of altered DV or NT patterning of the *Foxg1*$^{-/-}$ eye. This leads to the hypothesis for this chapter that the *Foxg1*$^{-/-}$ retina is more ventral or temporal in character, expanding the ipsilateral domain of the retina and reprogramming RGC axons from a contralateral to an ipsilateral fate in areas outside the VT crescent. This hypothesis could account for the rise in ipsilateral projections previously observed in the *Foxg1*$^{-/-}$ nasal and temporal retina (Pratt et al., 2004).

5.2.3. Nasotemporal polarity.

NT retinal polarity develops before DV axial polarity. At the optic cup stage, the transcription factor Foxg1 is expressed in the nasal optic cup and stalk whereas Foxd1 is expressed in the temporal optic cup and stalk (Figure 1) (Hatini et al., 1994). The expression domains of *Foxg1* and *Foxd1* are mutually exclusive and are separated by a gap (Hatini et al., 1994). Subsequently, the homeodomain transcription factors SOHo1 and GH6 are expressed in nasal retina and both repress EphA3, restricting its expression to the temporal retina (Schulte & Cepko, 2000).

Figure 1. Genetic regulation of retinal polarity

Adapted from McLaughlin et al., 2003

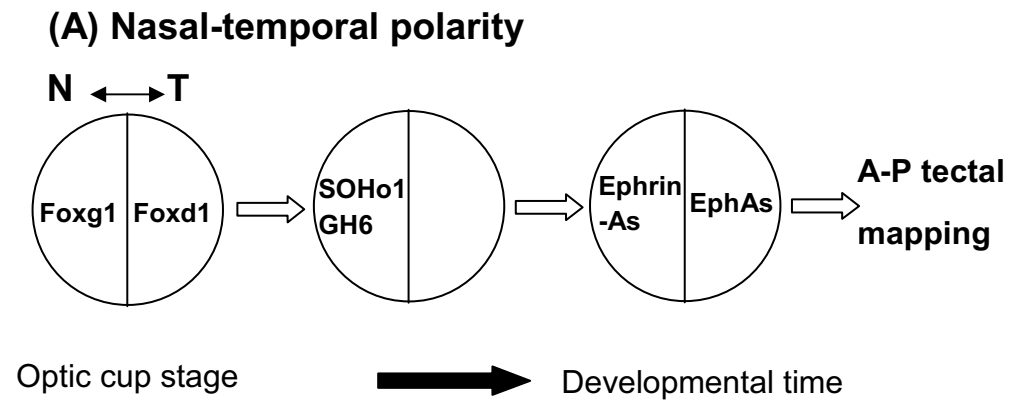

Figure 1. Genetic regulation of retinal polarity
The expression patterns of genes involved in establishing retinal patterning of the (A) NT and (B) DV axes are shown in a sequence from early development (left) to late development (right). Figure based on McLaughlin et al., 2003. Abbreviations: A, anterior; D, dorsal; L, lateral; M, medial; P, posterior; V, ventral.

Experiments in chick have shown that ectopic expression of *CBF1* (chick homologue of *Foxg1*), *SOHo1* or *GH6* in temporal retina and ectopic expression of *CBF2* (chick *Foxd1* homologue) in nasal retina results in retinotectal mapping defects along the anterior-posterior axis (Yuasa et al., 1996). Therefore, *Foxg1* and *Foxd1* play crucial roles in guiding nasal and temporal axons to their appropriate anterior-posterior termination zones in the superior colliculus.

The restricted expression of *Foxg1* in the nasal retina enables its use as a nasal retinal marker. The mice used in this Chapter were $Foxg1^{lacZ}$ knock-in mice in which the coding sequences of *Foxg1* were replaced by a *lacZ* cassette (Xuan et al., 1995). The $Foxg1^{lacZ}$ reporter allele reveals sites where *Foxg1* is transcriptionally active via the production of lacZ protein, which turns X-galactosidase or 'lacZ' staining solution blue. *Foxg1* transcriptional activation has been examined previously at E12.5 showing that the anterior-posterior patterning of the $Foxg1^{lacZ/LacZ}$ optic vesicle resembles that of $Foxg1^{LacZ/+}$ embryos, with lacZ staining confined to the anterior half of the optic vesicle as shown schematically in Figure 2 (Huh et al., 1999).

In this Chapter, later embryonic ages were examined using the same $Foxg1^{LacZ}$ reporter mice to observe whether this anterior-posterior divide in lacZ staining was maintained. $Foxg1^{lacZ/+}$ embryos possess only one copy of the *Foxg1* allele but are indistinguishable from $Foxg1^{+/+}$ embryos and have normal eyes as reported previously (Huh et al., 1999). Therefore, they were suitable as controls.

Figure 2. *Foxg1* activation in the *Foxg1*$^{LacZ/LacZ}$ eye

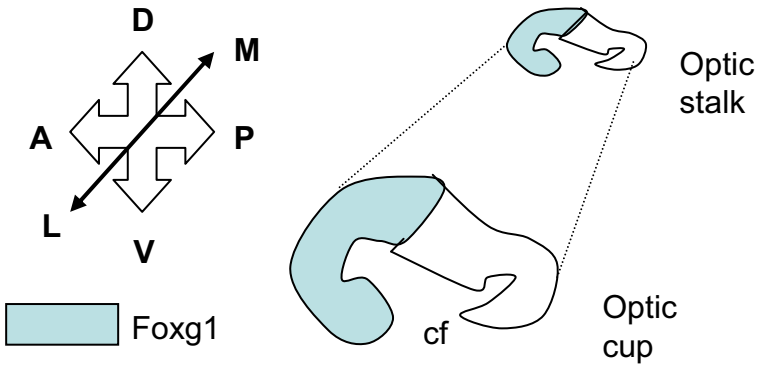

Figure 2. *Foxg1* activation in the *Foxg1*$^{lacZ/lacZ}$ eye.
A schematic diagram of sagittal sections through the optic cup extended retina of a *Foxg1*$^{lacZ/lacZ}$ eye at E12.5. The anterior and posterior lips of the invaginated optic vesicle fail to fuse normally to form the choroid fissure (cf). The blue shading indicates the anterior domain of the optic vesicle where *Foxg1* has been deleted in the *Foxg1* null retina. Abbreviations: A = anterior, D = dorsal, L = lateral, M = medial, P = posterior, V = ventral. Figure based on Huh et al., 1999.

5.2.4. Dorsoventral polarity.

The results of chick gain-of-function analyses and mouse loss-of-function analyses suggest that dorsoventral (DV) patterning is complex. However, the following gene interactions are well characterized. DV polarity is initially set up by Shh, retinoic acid and BMPs (Chow and Lang, 2001; Peters, 2002). Ventroptin is expressed in ventral retina, whilst BMP4 is confined to dorsal retina. Both ventroptin and BMP4 are mutually repressive and regulate the spatial distribution of downstream target genes along the DV axis (Sakuta et al., 2001). Dorsally, BMP4 activates Tbx5 but represses Vax2. Tbx5 in turn activates transcription of ephrin-Bs but represses EphBs in the dorsal retina, whilst Vax2 activates EphBs but represses ephrin-Bs in the ventral retina (Schulte et al., 1999; Koshiba-Takeuchi, 2000). EphB2, EphB3 and EphB4 are expressed in a low-to-high gradient from dorsal to ventral (Birgbauer et al., 2000; Connor et al., 1998; Henkemeyer et al., 1996; Hindges et al., 2002; Holash and Pasquale, 1995). In contrast, ephrin-B1 and ephrin-B2 are expressed in a complementary high-to-low gradient from dorsal to ventral (Marcus et al., 1996; Birgbauer et al., 2000; Hindges et al., 2002).

5.2.5. EphBs and ephrin-Bs are important mediators of axon guidance.

The polarised expression of EphBs and ephrin-Bs is highly conserved across species from fish (Brennan et al., 1997), amphibians (Mann et al., 2002), birds (Connor et al., 1998; Holash et al., 1997), mammals (Barbieri et al., 2002; Birgbauer et al., 2000, Marcus et al., 1996) and marsupials (Vidovic and Marotte, 2003; Vidovic et al., 1999). This evolutionary conservation fits with the discovery that Ephs and ephrins from both subclasses A and B play roles in retinotopic mapping from lower to higher vertebrates: subclass B members mediate latero-medial tectal mapping from DV retinal gradients (Braisted et al., 1997; Hindges et al., 2002; Mann et al., 2002; O'Leary and

McLaughlin, 2005) and subclass A members mediate antero-posterior topographic mapping from NT retinal gradients (Drescher et al., 1997; McLaughlin et al., 2003).

In addition to their roles in retinotectal mapping, some subclass B Ephs and ephrins appear to mediate retinal axon guidance at the mouse optic chiasm (Williams et al., 2003). Recently, it was shown that repulsion between EphB1 receptors expressed on VT retinal axons and ephrin-B2 at the optic chiasm midline produced ipsilateral projections in the mouse (Williams et al., 2003). Nevertheless the EphB1 - ephrin-B2 interaction could not provide a global mechanism for all ipsilateral axons due to the presence of a few residual ipsilateral axons in *EphB1* null mice. Williams et al. showed that *EphB1* and *EphB2* mRNAs are most strongly expressed in the peripheral VT retina where ipsilateral RGCs are located in the mouse and *Xenopus*. Murine *EphB2* is expressed more widely in the ventral retina than VT-restricted *EphB1* and so *EphB2* was chosen as the ventral marker in this chapter. EphB2's ligand ephrin-B2 is expressed at the chiasm in developing mouse and *Xenopus* embryos where it has been linked to the ipsilateral projection as mentioned earlier (Nakagawa et al., 2000; Williams et al., 2003). However, it is also expressed in a dorsoventral gradient that is strongest in the dorsal part of the retina. Due to their clear polarised DV expression gradients, EphB2 and ephrin-B2 were chosen to study DV patterning in this Chapter.

5.3. METHODS

5.3.1. *Foxg1* alleles and genetic background.

To identify cells in which the *Foxg1* locus is transcriptionally active we exploited the $Foxg1^{tm1M}$ (or $Foxg1^{LacZ}$) allele in which coding sequences are replaced by a LacZ cassette (Xuan et al., 1995). We also used the $Foxg1^{tm1(cre)Skm}$ (or $Foxg1^{Cre}$) allele in which coding sequences are replaced by a Cre recombinase cassette (Hebert and

McConnell, 2000). *Foxg1*^{Cre} and *Foxg1*^{LacZ} are predicted null alleles (designated *Foxg1*$^{-/-}$) (Xuan et al., 1995; Hebert and McConnell, 2000).

For lineage tracing, *Gtrosa26tm1Sho* (*R26RS*) reporter mice were used (Mao et al., 1999). Cre-mediated recombination in *Foxg1Cre*;*R26RS* embryos irreversibly activates *lacZ* expression from the *ROSA26* locus (Mao et al., 1999; Hebert and McConnell, 2000). Lineage tracing experiments used the *Foxg1Cre* allele on an albino Swiss Webster background (as described by Hebert and McConnell, 2000). Crosses used: - Cross 1: R26RS$^{+/+}$ reporter mice x Foxg1$^{Cre/+}$ mice produced progeny with genotypes R26RS$^{+/-}$; Foxg1$^{+/+}$ and R26RS$^{+/-}$; Foxg1$^{Cre/+}$ (presence of Foxg1^{Cre} detected by PCR). Cross 2: R26RS$^{+/-}$; Foxg1$^{Cre/+}$ (progeny of Cross 1) x Foxg1$^{Cre/+}$ mice produced R26RS$^{+/-}$; Foxg1$^{Cre/Cre}$ (*Foxg1* null) and R26RS$^{+/-}$; Foxg1$^{Cre/+}$ ('wild type' expression of *Foxg1*).

Other experiments used *Foxg1*^{lacZ} and/or *Foxg1*^{Cre} alleles on a mixed pigmented CBA/C57Bl6/Swiss Webster background. *Foxg1* homozygous mutants (*Foxg1*$^{Cre/Cre}$) and compound heterozygotes (*Foxg1*$^{Cre/lacZ}$) were identified by their hypoplastic telencephalon and distorted eyes. Heterozygous embryos (i.e. *Foxg1*$^{+/-}$) were identified by PCR genotyping: they were indistinguishable morphologically from wild type (Xuan et al., 1995; Huh et al., 1999) and no RGC axon projection defects were observed at the optic chiasm.

Dissections: Pregnant females were terminally anaesthetized and embryos removed by caesarian section in ice-cold PBS. Embryos were taken at E13.5, E14.5, E15.5 and E16.5.

5.3.2. PCR genotyping *Foxg1* alleles.

Tails were removed from the embryos to obtain tissue for genotyping. The $Foxg1^{LacZ}$ allele was detected with primers LacZ F2 5'-TTG AAC TGC CTG AAC TAC CG-3' and LacZ R2 5'-CCT GAC TGG CGG TTA AAT TG-3'. The $Foxg1^{Cre}$ allele was detected using primers NLSCreFor 5'-CAT TTG GGC CAG CTA AAC AT-3' and NLSCreRev 5'-ATT CTC CCA CCG TCA GTA CG-3'. Cycling conditions: 96°C for 2 minutes followed by [96°C for 30 seconds, 58.5°C for 30 seconds, and 72°C for 30 seconds] for 35 cycles.

5.3.3. H & E staining.

Wax-embedded heads from E13.5 and E15.5 embryos were cut into 10µm-thick coronal sections, collected onto poly-l-lysine-coated slides and dried overnight in a 37ºC incubator. Wax sections were dewaxed in two changes of xylene and then dehydrated through a series of alcohol solutions: 100%, 95%, 90%, 70% and finally distilled water. Haematoxylin and eosin (1% aqueous) solutions were filtered prior to use. Sections were immersed in the filtered Harris Hematoxylin for 2 minutes followed by a rinse in tap water until the water turned clear. Sections were immersed in eosin stain for 3 minutes, dipped in tap water, transferred to potassium aluminium sulphate for 2 minutes and then rinsed in tap water. Sections were dehydrated in a series of ascending alcohol solutions (70%, 90%, 95%, 100% x2), cleared in 2 changes of xylene and mounted using DPX.

5.3.4. LacZ staining.

E14.5 $Foxg1^{lacZ/+}$ and $Foxg1^{lacZ/lacZ}$ embryonic heads were dissected and fixed for 1 hour at 4°C in 4% paraformaldehyde, 0.02% NP40, 0.01% sodium deoxycholate, 5mM EGTA, 2mM $MgCl_2$ in phosphatebuffered saline (PBS). In some cases, heads were

equilibrated in 30% sucrose/PBS and sectioned (10μm) on a cryostat and collected onto Superfrost Plus slides. Tissues were rinsed several times in wash buffer (2 mM MgCl2, 0.02% NP40, 0.01% sodium deoxycholate in PBS), transferred to staining solution (wash buffer supplemented with 5 mM potassium ferricyanide, 5 mM potassium ferrocyanide and 1 mg/ml X-gal), and stained overnight (cryostat sections on slides) or for 2 days with agitation (wholemounts) at 37°C in darkness. Staining was stopped with 20 mM EDTA in PBS. Wholemounts were processed to wax, sectioned (10μm) using a microtome and mounted onto poly-l-lysine-coated slides. Cryostat sections were counterstained with Nuclear Fast Red.

5.3.5. Immunohistochemistry.

EphB2 and ephrin-B2 immunohistochemistry was performed essentially as described by Batlle et al. (2002). E13.5 and E16.5 embryo heads were fixed in 4% paraformaldehyde in phosphate buffer high salt (PBHS) (0.04M phosphate, 0.03M NaCl, pH7.0) at 4^{o}C with shaking overnight and processed to wax. 10μm sections were cut and floated onto polylysine coated glass slides. After rehydration, endogenous peroxidase activity was blocked with 90% methanol: 3% hydrogen peroxide and antigens unmasked by microwaving in 10mM sodium citrate buffer (pH6.0). Sections were then reacted with primary antibody overnight and a bridge rabbit anti-goat antibody before final detection using the Envision^{+} (Rabbit) Kit (Dako K4010) following the manufacturers instructions. Primary antibodies were goat anti-mouse ephrin-B2 (R&D Systems AF496) used at 1:500; goat anti-mouse EphB2 (R&D Systems AF467) used at 1:1000; rabbit anti-goat (Dako Z0228) used at 1:400. Antibody incubation and pre-incubation blocking were carried out in 1% bovine serum albumin in PBS at room temperature. Following a diaminobenzidine colour reaction, sections were dehydrated and mounted.

5.4. RESULTS

5.4.1. Morphology of the *Foxg1*$^{-/-}$ eye.

The morphology of the *Foxg1*$^{-/-}$ eye was examined at E15.5 during the peak period of retinal axon projections. The aim was to test the hypothesis that the *Foxg1*$^{-/-}$ retina displays severe anatomical abnormalities, particularly of the RGC layer, which might contribute to the increased ipsilateral routing of RGC axons. Haematoxylin and eosin staining revealed that the organisation of the *Foxg1* null retina resembles that of the wild type: it possesses an optic fibre layer (OFL) where RGC axons collect and fasciculate *en route* to the optic chiasm, a RGC layer, a denser outer retinal layer and retinal pigment epithelium (Figure 3C, D). Although *Foxg1*$^{-/-}$ eyes lack a clear optic stalk structure, axons were visible leaving the retina medially through an optic nerve-like channel (Figure 3F) that resembles the wild type optic nerve (Figure 3A) but is instead surrounded by retinal tissue that is extended towards the midline (arrows in Figure 3F). Anteriorly, the *Foxg1*$^{-/-}$ retina is tilted towards the ventral surface of the brain and displays a distinctive coloboma ventrally where the optic vesicle has failed to close (Figure 3H, I, J), leaving a gap in the RPE and retina. In comparison to an anterior wild type section where the RGC axons form a neat OFL (Figure 3G), the *Foxg1*$^{-/-}$ axons and RGCs fill a wider area that extends medially (Figure 3I). It is unclear whether folding of the retina in these anterior sections resulted in the eye being sectioned in a different plane to the wild type. Apart from these anterior-most regions, the *Foxg1*$^{-/-}$ retina retains features of the wild type retina, particularly in extremely posterior sections (Figure 3K).

Figure 3. Morphology of the *Foxg1*$^{-/-}$ eye.
Haematoxylin (purple) and eosin (pink) staining of coronal 10µm-thick wax sections of (A, D, G) wild type and (B, C, E, F, H, I, J, K) *Foxg1*$^{lacZ/lacZ}$ E15.5 embryos. Haematoxylin labels cell nuclei, whereas eosin stains the cytoplasm, axons and cell membranes. (A) Wild type eye showing axons leaving the eye through the optic nerve (on). (B) Posterior section of a *Foxg1*$^{lacZ/lacZ}$ eye showing the medial bulge in the retina that becomes more severe anteriorly. (E) *Foxg1*$^{lacZ/lacZ}$ eye showing axons medially (arrow). (F) *Foxg1*$^{lacZ/lacZ}$ eye sectioned just posterior to (E) showing axons leaving the retina medially through an optic nerve-like structure. Arrows point to the medial extension of the retina that is visible dorsal to the retinal axons. (C, D) High power magnification of boxed areas in (B) and (A) respectively showing the optic fibre layer (OFL) where axons from the RGC layer accumulate and fasciculate as they leave the eye. (G) Wild type anterior eye showing RPE surrounding the entire retina. (H, I) Anterior sections of a *Foxg1*$^{lacZ/lacZ}$ eye showing a ventral gap in the RPE and retina called a coloboma (col) where the optic vesicle has failed to close. Also note the ventral rotation of the eyes in these anterior sections. (I) Section anterior to (H): axons (a) occupy an area medially behind the lens and dorsal to the coloboma and the RGC layer is less organised. (J) Section anterior to (I) showing a wider gap in the RPE and retina. (K) Posterior *Foxg1*$^{lacZ/lacZ}$ eye with a continuous RPE. Abbreviations: r, retina; l, lens; RGCs, retinal ganglion cells; col, coloboma; on, optic nerve; rpe, retinal pigment epithelium; OFL, optic fibre layer; a, axons. Scale bars: A, B, E – H, 200µm; C, D 100µm.

Figure 3. Morphology of the E15.5 eye

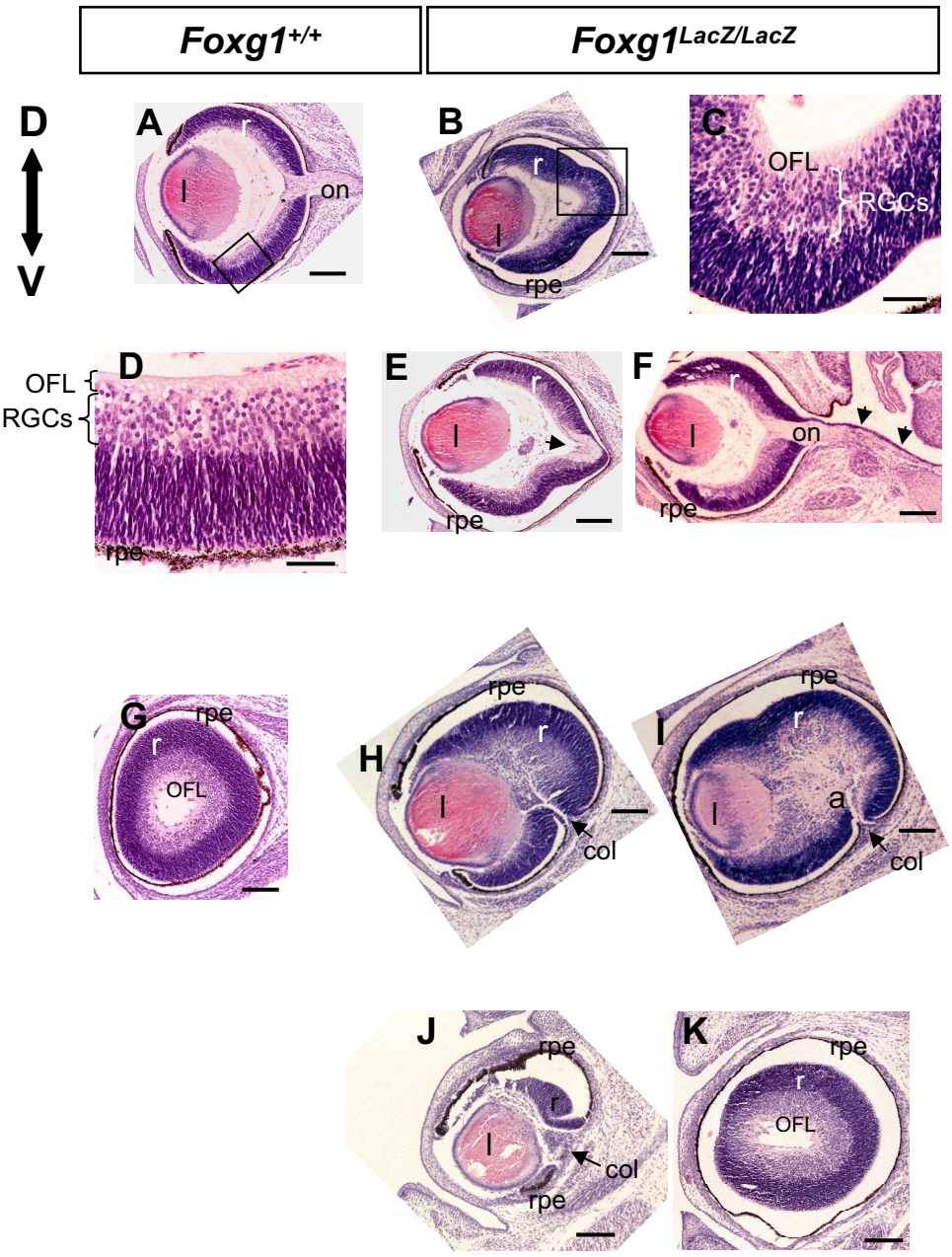

5.4.2. Transcriptional activation of *Foxg1* in *Foxg1*^{LacZ} reporter mice.

5.4.2.1. Transcriptional activation of *Foxg1* in the E14.5 *Foxg1*$^{lacZ/+}$ retina.

In dorsal-most sections through the E14.5 *Foxg1*$^{lacZ/+}$ retina, lacZ staining was found throughout all layers of the nasal and temporal retina but was slightly more prominent nasally in all E14.5 retinas examined (Figure 4A). Moving ventrally, strong lacZ staining was still observed nasally in all retinal layers but a lacZ-negative region was seen in the temporal retina (Figure 4D, G, J). In increasingly ventral retinal sections of *Foxg1*$^{lacZ/+}$ embryos, the lacZ-negative region expanded progressively towards nasal or anterior regions (Fig. 4M, P) until staining was absent from the entire retina (Fig. 4S). In dorsal and ventral sections, lacZ staining was found in all layers of the nasal retina. However, staining was most intense in the RGC layer (Figure 5C) compared to the outer retinal layers. The E13.5 and E15.5 *Foxg1*$^{lacZ/+}$ retina exhibited the same lacZ staining pattern as for E14.5 (data not shown).

5.4.2.2. Morphological variation between *Foxg1*$^{lacZ/lacZ}$ eyes.

For a given embryonic age, *Foxg1*$^{lacZ/lacZ}$ eyes exhibited morphological variation in the degree of folding and medial extension of the retina between different embryos from different litters, between embryos from the same litter and even between the eyes of the same embryo, adding to previous observations of variability between *Foxg1* null eyes (Huh et al., 1999). Figure 4 shows an example of morphological variation within the same *Foxg1*$^{lacZ/lacZ}$ embryo. Equally-spaced dorsal to ventral sections through one eye are shown in Figures 4B, E, H, K, N, Q, T and an equivalent dorsal to ventral series through the other eye is shown in Figures 4C, F, I, L, O, R, W. In *Foxg1*$^{lacZ/+}$ embryos, the symmetry of the retina made the nasal-temporal divide simple to place, along a line that bisected the optic stalk. In dorsal sections, the *Foxg1*$^{lacZ/lacZ}$ retina tended to be more symmetrical, facilitating placement of the nasal-temporal dividing line.

Figure 4. Transcriptional activation of *Foxg1* in the retina at E14.5. X-gal staining (blue) of E14.5 *Foxg1*$^{lacZ/+}$ embryos (A, D, G, J, M, P, S) and *Foxg1*$^{lacZ/lacZ}$ embryos (B, C, E, F, H, I, K, L, N, O, Q, R, T, U - W). Adjacent *Foxg1*$^{lacZ/lacZ}$ images in each row represent eyes from the same embryo at equivalent dorsal-ventral levels that appear different due to a slight asymmetry in the sectioning. All sections are 10µm-thick horizontal cryostat sections and nuclei are counterstained with Nuclear Fast Red (pink). *Foxg1*$^{lacZ/+}$ embryos possess one functional copy of the *Foxg1* allele and are phenotypically normal. *Foxg1*$^{lacZ/lacZ}$ embryos cannot produce Foxg1 protein. The *Foxg1*^{lacZ} reporter allele reveals sites where *Foxg1* is transcriptionally active via the production of lacZ protein, which turns X-gal blue. (A) In the *Foxg1*$^{lacZ/+}$ eye, extremely dorsal sections reveal lacZ staining throughout all layers of the nasal and temporal retina. (D, G) Dorsal sections through the same *Foxg1*$^{lacZ/+}$ eye show lacZ staining predominantly in the nasal retina but also a lacZ-negative region in temporal retina that becomes larger as sections move ventrally. (J) In central *Foxg1*$^{lacZ/+}$ sections the nasal half of the retina is lacZ-positive. (M, P) Moving ventrally, the nasal lacZ-stained area becomes smaller and increasingly restricted to the anterior-most region of the nasal retina until it disappears in extremely ventral sections (S). (B, C) In *Foxg1*$^{lacZ/lacZ}$ embryos, extremely dorsal retinas show scattered *lacZ* staining mainly in the temporal retina with a few nasal lacZ-positive cells. (E, F, H) Dorsal *Foxg1*$^{lacZ/lacZ}$ sections ventral to (B, C) show strong lacZ staining in the temporal retina, particularly in the inner RGC layer. Less staining is present nasally. (I, K, L) In dorsocentral sections, lacZ staining is prominent in the temporal RGC layer but appears more scattered and less concentrated in outer retinal layers. Staining is strong throughout all layers of the nasal medially-extended retina and also near the nasal ciliary marginal zone (I, L). (N, Q) Ventrally, temporal staining decreases, whilst nasal staining in the medial loops of the extended retina remains strong. (O, R) Ventral *Foxg1*$^{lacZ/lacZ}$ eyes cut at a slightly different angle to (N, Q) such that nasal staining in the medially extended retina is present in more dorsal sections (I, L). (T, W) In ventral-most sections of *Foxg1*$^{lacZ/lacZ}$ eyes, there are very few lacZ-stained cells. High power magnifications of (T) showing (U) temporal and (V) nasal retina with arrows pointing to some lacZ-positive cells. Scale bars: 200µm in A – T & W, 50µm in U, V. Abbreviations: N, nasal; T, temporal; l, lens; er, extended retina; a, retinal axons; tel, telencephalon; rpe, retinal pigment epithelium; vhy, ventral hypothalamus.

Figure 4. *Foxg1* activation in the retina at E14.5

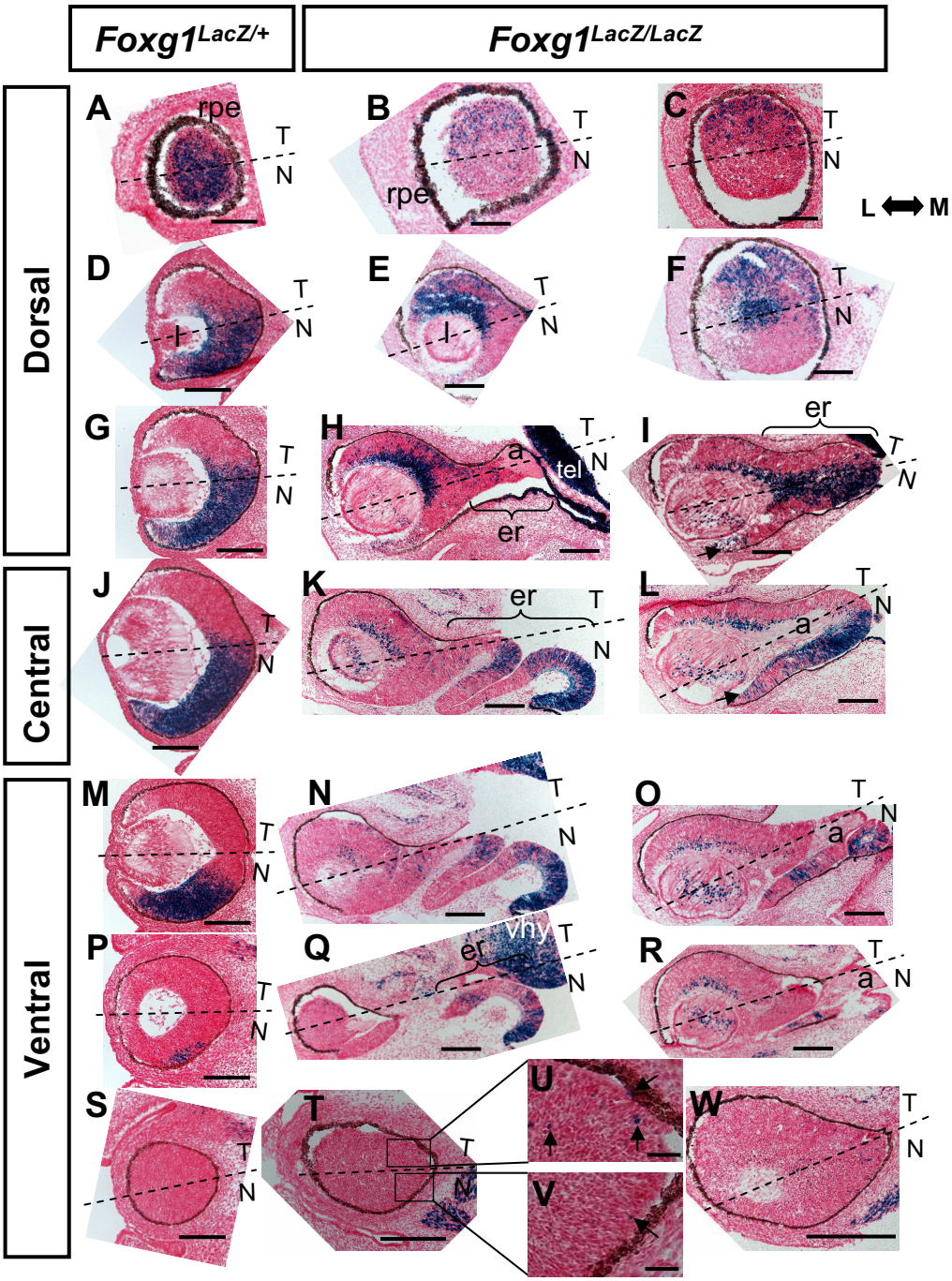

Figure 5. *Foxg1* activation in the E14.5 retina.
X-gal staining of E14.5 *Foxg1*$^{lacZ/+}$ embryos (A – C) and *Foxg1*$^{lacZ/lacZ}$ embryos (D - I) counterstained with Nuclear Fast Red. All sections are horizontal cryostat sections. (A) *Foxg1*$^{lacZ/+}$ section just dorsal to the level of the optic stalk showing lacZ staining throughout the nasal retina with a few scattered cells temporally. High power magnifications of the (B) temporal and (C) nasal retina that are depicted as boxed regions in (A). (B) LacZ-positive cells are scarce in the temporal RGC layer of the retina. (C) In nasal retina, lacZ-positive cells are found throughout all retinal layers but staining is particularly strong (very dark blue) in the RGC layer. The white dotted line delineates the border between the RGCs and outer retinal layers. (D) An equivalent dorsal *Foxg1*$^{lacZ/lacZ}$ section to (A) showing lacZ staining temporally. (E) High power magnification of boxed area in the temporal retina of (D) showing strong lacZ staining in the RGC layer but more scattered weaker staining in outer layers. (F) *Foxg1*$^{lacZ/lacZ}$ section ventral to (D). High power magnifications of (G) nasal and (H) temporal retina that are boxed in (F). (G) LacZ-positive stripes, one to a few cells wide, spanning the extended retina are visible nasally. (H) Temporally, LacZ-expressing cells are found mainly in the RGC layer but also in the outermost retinal layer. (I) *Foxg1*$^{lacZ/lacZ}$ nasal region of the medial extended retina showing dense lacZ staining spanning the retina.
Scale bars: 200µm in A, D, F; 100µm in B, C, E, G, H, I. Abbreviations: N, nasal; T, temporal; l, lens; er, extended retina; r, retina; rpe, retinal pigment epithelium; RGCs, retinal ganglion cells.

Figure 5. *Foxg1* activation in the E14.5 retina

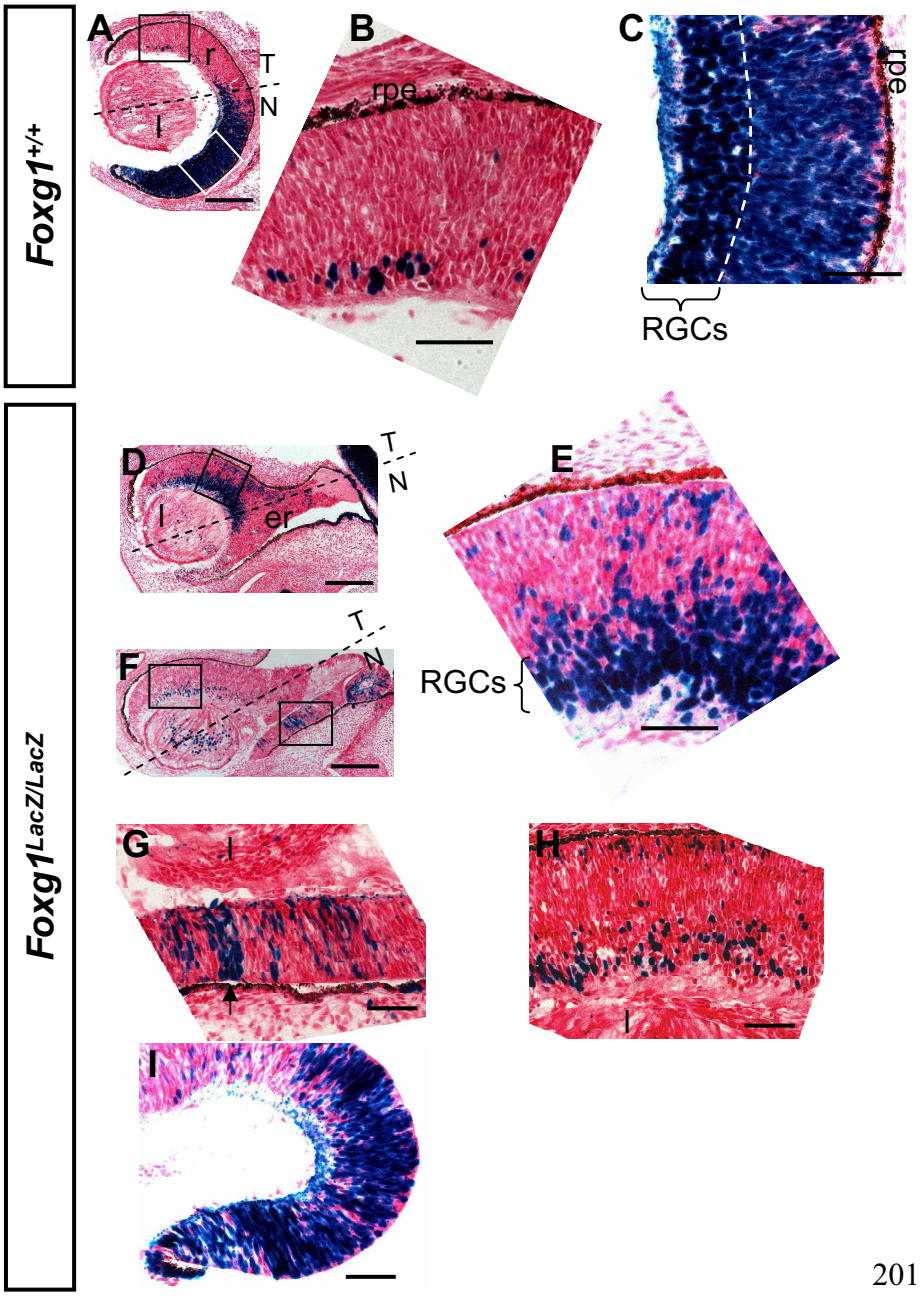

However, in ventral sections, the medial folding of the anterior retina was more pronounced in all embryos examined. In these instances, the dividing line between nasal and temporal retina was placed at roughly a 60 degree angle to the anterior-posterior axis of the brain.

5.4.2.3. Transcriptional activation of *Foxg1* in the E14.5 *Foxg1*$^{lacZ/lacZ}$ retina.

The variation in the appearance of the *Foxg1*$^{lacZ/lacZ}$ retina meant that the lacZ staining pattern in eyes sectioned at equivalent dorsal-ventral locations also showed a degree of variability. Nevertheless, the lacZ staining patterns of different *Foxg1*$^{lacZ/lacZ}$ eyes from E13.5 to E15.5 showed common reproducible features that did not appear random. In the E14.5 *Foxg1*$^{lacZ/lacZ}$ dorsal retina, scattered lacZ staining was found in the temporal retina with less dense staining nasally. This is essentially a mirror image of the *Foxg1* activation pattern in *Foxg1*$^{lacZ/+}$ dorsal retina (compare Figures 4A, D with Figures 4B, E). Dorsally, the most intense lacZ expression was found in the RGC layer, resembling that found in the *Foxg1*$^{lacZ/+}$ nasal retina, with sparser, weaker staining in the outer retina (Figure 5E). Moving ventrally but remaining in the dorsal retina, *Foxg1*$^{lacZ/lacZ}$ embryos displayed strong, dense lacZ expression in the temporal RGC layer with weaker, more scattered expression in outer layers (Figures 4E, F, H). In the same sections, lacZ-positive cells were rarely found in the nasal retina. *Foxg1* activation in the ventral *Foxg1* null retina resembled that of the *Foxg1*$^{lacZ/+}$ retina with lacZ staining becoming increasingly restricted to the nasal medially-extended retina, whereas staining in temporal RGCs decreased (Figures 4K, L, N, O, Q). *Foxg1* activation spanned the nasal extended retina whereas in temporal retina, lacZ-expressing cells were mainly found in the inner retinal layer (Figures 5G, H, I). Radial lacZ-positive stripes one to a few cells wide were observed nasally in the extended retina (Figures 5F, G) and the medial loop of the nasal extended retina consistently displayed intense lacZ staining (Figures 4K, N, Q & 5I). In extremely ventral sections, very few lacZ-positive

cells were observed in the nasal or temporal retina (Figures 4T, U, V, W). There appeared to be a slight temporal bias in the location of these sparse cells (compare Figures 4U & V). In both *Foxg1*$^{lacZ/+}$ and *Foxg1*$^{lacZ/lacZ}$ embryos, lacZ staining was also observed in the lens, telencephalon, optic chiasm midline (see Chapter 6) and superior colliculus.

At E13.5 (Figure 6) and E15.5 (Figure 7), lacZ staining of *Foxg1*$^{lacZ/lacZ}$ embryos revealed a similar pattern of *Foxg1* activation compared to E14.5 *Foxg1*$^{lacZ/lacZ}$ retinas. The morphology of the *Foxg1* null eye at E15.5 resembled that of the eye at E14.5 more closely compared to E13.5. Morphological variability between eyes within the same embryo is demonstrated at E15.5 in a dorsal-ventral series through one eye in Figures 7C, F, I, L, O and an equivalent series through the other eye in Figures 7D, G, J, M, P. Dorsal-most sections exhibited strong lacZ staining in posterior temporal retina with less dense staining nasally at E15.5 (Figs. 7C, D) and E13.5 (Fig. 6A). Moving ventrally through the E15.5 (Figs 7E - J) and E13.5 (Figs. 6C, D) eye, lacZ staining was consistently strong in the inner RGC layer of the nasal and temporal retina with scattered staining in other retinal layers. Ventral sections of the E15.5 retina showed a reduction in both the number and density of lacZ-positive cells situated in temporal retina (Figs. 7L, M). This was not apparent at E13.5, where strongly *lacZ*-expressing cells were still found in ventrotemporal regions (Figs. 6I, J). However, in the E13.5 central retina, a nasal bias in staining was observed particularly in the medial part of the extended retina (Figs. 6H, I). In the E13.5 and E15.5 ventral retina, temporal lacZ-expressing cells were mainly found in the RGC layer with outer layers containing fewer lacZ-positive cells (Figs. 6H, I, J & 7L, M). However, the E13.5 retina displayed stronger temporal staining than at E15.5. Ventronasally, the medially extended retina stained strongly for lacZ at both ages (Figs. 6G, H, I & 7M, P). In ventral-most sections, only a few *lacZ*-expressing cells were found scattered throughout the nasal and temporal retina (Figs 6K & 7O) and there appeared to be a slight temporal bias in their location (Figs. 6K, L, M) as for ventral E14.5 retinas.

Figure 6. Transcriptional activation in the E13.5 *Foxg1*$^{lacZ/lacZ}$ retina.

X-gal staining of E13.5 *Foxg1*$^{lacZ/lacZ}$ embryos counterstained with Nuclear Fast Red. All sections are horizontal cryostat sections. Sections are ordered in a dorsal-ventral series from (A) most dorsal to (K) most ventral. (A) Extremely dorsal section showing lacZ staining scattered throughout temporal retina and partly in the nasal retina. (B) Section ventral to (B) showing staining laterally in temporal and nasal regions. (C) Strong lacZ staining is present in the nasal retina (arrows) and in the inner RGC layer of the peripheral temporal retina. Scattered staining is found in outer temporal retinal layers. (D) LacZ staining predominates in the inner retinal layers in both temporal and nasal regions. (E) Section ventral to (D) showing axons (a) leaving the eye and growing medially along the extended retina. (F, G) High power magnifications of boxed areas in (E). (F) Temporally, scattered lacZ-positive cells are found mainly in the inner retinal layers with a few in the outermost layers. (G) Nasally, strong, dense lacZ staining is concentrated in the medial extended retina. (H, I) Ventral sections showing strong, dense staining throughout the nasal retina. Strong staining is found in the inner temporal retina layers but medial regions are mostly lacZ-negative. (J) Section ventral to (I). In temporal regions, lacZ staining spreads into all retinal layers but remains strongest in the inner retina. Nasal regions have less stain. (K) Extremely ventral section. (L, M) High power magnifications of temporal and nasal retina shown as boxed regions in (K). LacZ-positive cells are observed more frequently in temporal retina (L) than nasal retina (M). Abbreviations: N, nasal; T, temporal; l, lens; rpe, retinal pigment epithelium; a, axons. Scale bars: 200µm in B, C, D, E, H, I; 100µm in A, F, G, J, K; 50µm in L, M.

Figure 6. *Foxg1* activation in the E13.5 *Foxg1*$^{LacZ/LacZ}$ retina

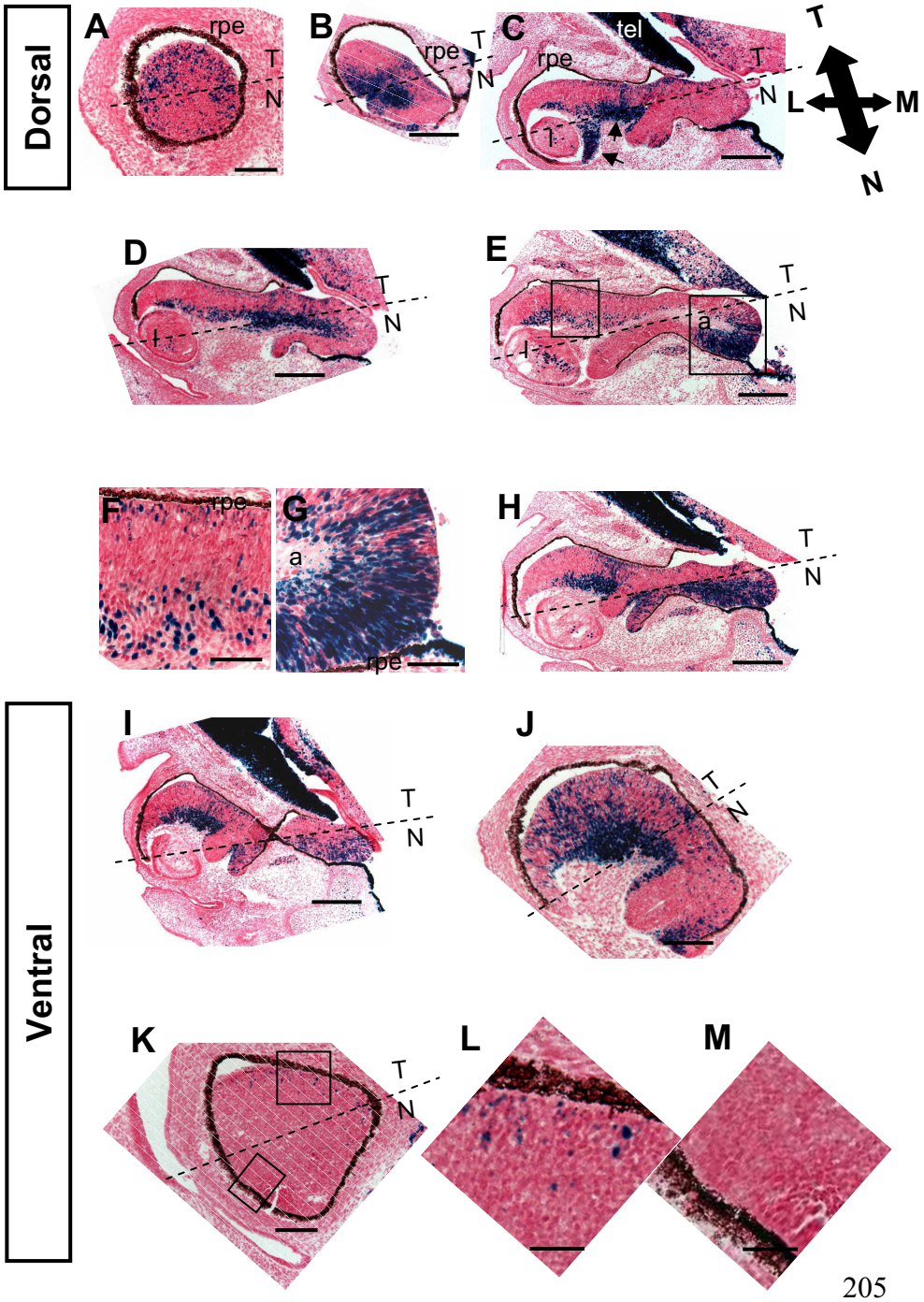

Figure 7. Transcriptional activation of *Foxg1* in the *Foxg1*$^{lacZ/lacZ}$ eye at E15.5.

X-gal staining of 10μm-thick cryostat sections through a E15.5 *Foxg1*$^{lacZ/lacZ}$ embryo. Brown DAB staining indicates the location of Zic2 protein expression, which is expressed strongly in the anterior dorsal thalamus, particularly medially, parts of the ventral thalamus and also in the retina. All sections are cut horizontally. (A, C, F, I, L) Dorsal to ventral sections through a *Foxg1*$^{lacZ/lacZ}$ brain at E15.5. In these images the right eye (magnified in E, H, K, N) is ventral to the left eye (magnified in B, D, G, J, M). (A, B) Dorsal section showing scattered *lacZ* staining in the nasal and temporal retina. (C – E) Dorsal and (F – H) dorsocentral retinal sections showing staining in nasal and temporal regions including the medially-elongated retina (er). *LacZ* staining is particularly strong in the RGC layer in all sections. (I – K) Ventral sections showing staining predominantly in the nasal extended retina, including the RGC layer (arrows in J & K). The nasal staining bias is more obvious in section (K), which is ventral to (J). Scattered *lacZ*-positive cells are mainly present in the RGC layer of the temporal retina. (L – N) Ventral retinal sections. (M) Scattered lacZ-positive cells in the inner nasal and temporal layer. (N) Section ventral to (M) showing staining mainly in the nasal extended retina. (P) Ventral section to (N) showing scattered lacZ staining mainly in the temporal retina (R) but not in nasal retina (Q). Abbreviations: A, anterior; P, posterior; D, dorsal; V, ventral; er, extended retina; l, lens; tel, telencephalon; th, thalamus. Scale bars: 400μm in A, C, F, I, L; 100μm in B, D, E, G, H, J, K, M, N.

Figure 7. *Foxg1* activation in the E15.5 *Foxg1*$^{LacZ/LacZ}$ retina

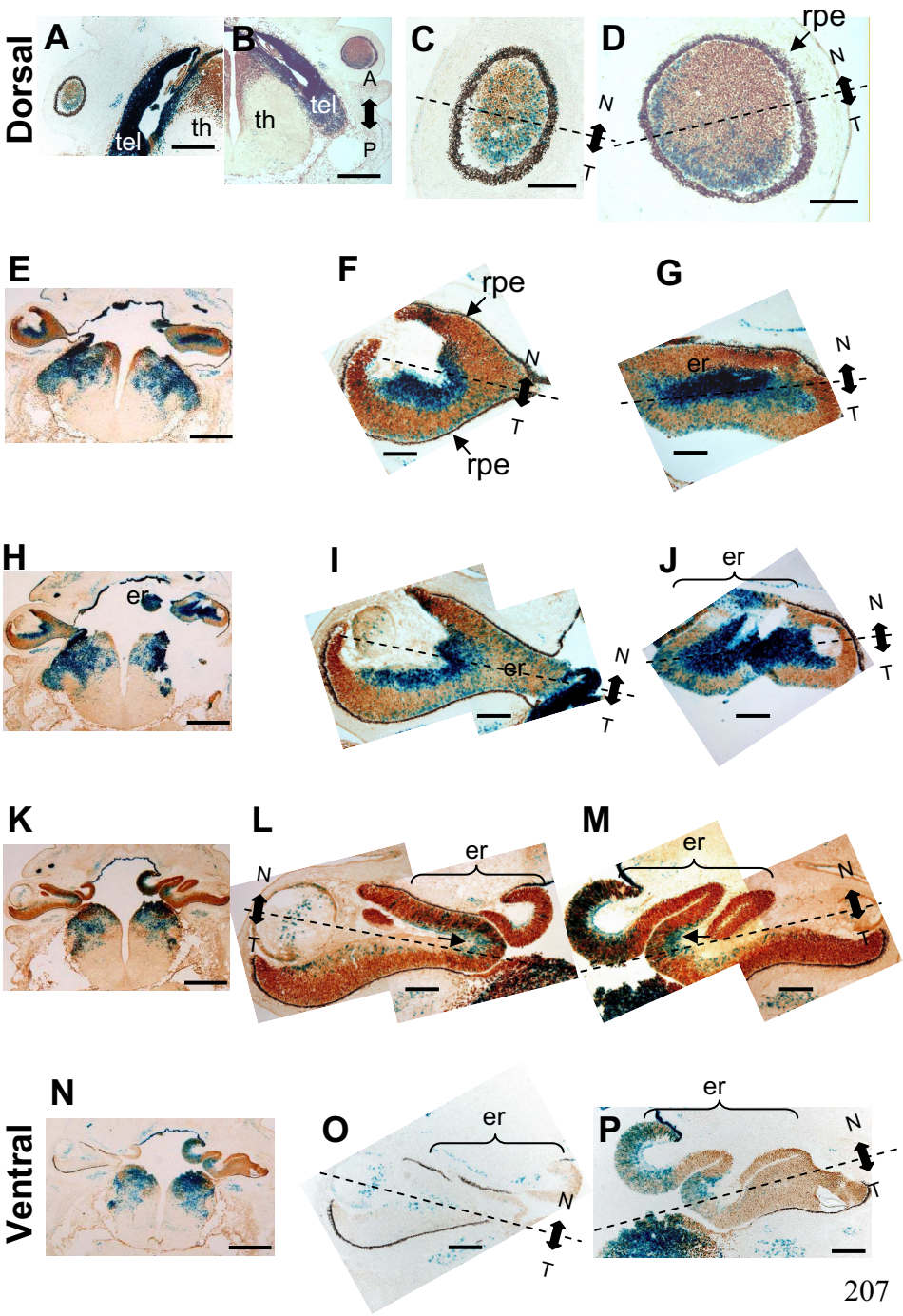

In summary, these results indicate that in *Foxg1*$^{lacZ/+}$ embryos that are phenotypically indistinguishable from wild types, *Foxg1* is expressed in nasal and temporal parts of the dorsal retina, with most widespread expression dorsonasally. The *Foxg1* expression domain becomes increasingly restricted to nasal regions in the ventral retina. In *Foxg1*$^{lacZ/lacZ}$ eyes, *Foxg1* activation is more widespread in the temporal retina but less widespread in dorsonasal regions compared to *Foxg1*$^{lacZ/+}$ embryos.

5.4.3. Lineage tracing of *Foxg1* expression in the retina.

LacZ-staining of retinal sections from mice carrying the *Foxg1*^{lacZ} allele revealed only a snapshot of *Foxg1* transcriptional activation at a given time-point or developmental stage. Therefore, lacZ-negative cells could have activated *Foxg1* at a previous point in time during development but subsequently turned it off. In order to discover whether a given retinal cell or any of its descendants had ever expressed *Foxg1,* lineage tracing was performed using floxed ROSA26 reporter mice (Mao et al., 1999). This line of mice contains a β galactosidase-neomycin phosphotransferase fusion gene (βgeo)-trapped ROSA26 locus modified such that βgeo is ubiquitously expressed only after Cre-mediated excision of loxP-flanked DNA sequences. ROSA26 mice were crossed with *Foxg1*$^{Cre/+}$ mice that express cre recombinase in cells where the *Foxg1* promoter is active (Hebert & McConnell, 2000). LacZ staining of the embryos was used to reveal cells & their descendants in which *Foxg1* was activated at any time during their lineage due to cre-mediated recombination and excision of a stop codon upstream of the *βgeo* reporter allele. The matings generated compound heterozygous embryos that contained ROSA26 and one or two copies of the *Foxg1*^{Cre} allele. *Foxg1*$^{Cre/+}$ embryos are phenotypically normal and lacZ staining revealed cells and their descendants that have expressed *Foxg1* at any time during their lineage. *Foxg1*$^{Cre/Cre}$ embryos cannot produce functional Foxg1 protein due to the insertion of a cre recombinase cassette in the *Foxg1* coding sequence (Hebert & McConnell, 2000). Therefore, lacZ staining of *Foxg1*$^{Cre/Cre}$

embryos revealed cells in which the *Foxg1* promoter has ever been active and would normally produce Foxg1 protein.

5.4.3.1. *Foxg1* expression in *Foxg1*$^{Cre/+}$; *ROSA26* embryos.

In the dorsal retina, *Foxg1*$^{Cre/+}$; *ROSA26* embryos displayed lacZ staining nasally (Figs. 8A-D, I, J). In the most dorsal sections, lacZ staining was seen in the nasal and temporal retina (Fig. 8A). A lacZ-negative region appeared in the lateral part of the temporal retina (Fig. 8B, I) and this expanded medially as sections became increasingly ventral (Figs. 8C, D, J). In the dorsotemporal retina, radial columns of *lacZ*-expressing cells, that were mostly one- to two-cells wide, were observed spanning the retina from the inner to outer layers. These radial stripes are likely to be radial clones of cells arising from single lacZ-positive retinal progenitors (Reese et al., 1999). Examination of serial sections revealed that these radial stripes were not confined to one part of the retina. In the central retina at the level of the optic stalk, half of the retina was lacZ-positive and half was mostly lacZ-negative apart from a few, scattered lacZ-stained cells. The lens (Figs. 8C, D, E) and nasal part of the optic stalk (Fig. 8K) also exhibited strong staining. Ventral to the optic stalk, nasal lacZ staining was reduced gradually as sections became more ventral (Figs. 8F - H, L, M, N) and the boundary between lacZ-positive and -negative regions shifted nasally (anteriorly). LacZ-stained cells were observed scattered in the temporal retina as in dorsal sections. In ventral-most sections, both the nasal and temporal retina displayed scattered lacZ-positive cells, although there was a nasal bias in their distribution (Fig. 8N). In the nasal retina, lacZ-staining of the retina was particularly prominent in the outer-most layer and also the inner retinal layer where RGCs are found (Figs. 8J, K, L).

Figure 8. Lineage tracing of retinal cells that have expressed Foxg1 using E14.5 *Foxg1$^{Cre/+}$; R26RS* embryos.
X-gal staining of horizontally-sectioned *Foxg1$^{Cre/+}$; R26RS* eyes reveals retinal cells and their descendants that have expressed *Foxg1* at any time during their development. Staining is widespread in dorsal sections but becomes increasingly restricted to the anterior-most nasal retina in ventral sections. (A – H) Dorsal to ventral series of X-gal-stained sections through a *Foxg1$^{Cre/+}$; R26RS* eye. (I – M) High power magnifications of (B), (D), (E) and (G). (A) Dorsal-most section showing uniform staining for lacZ in nasal and temporal retina. (B, C, D, I) Sections ventral to (A) showing uniform staining in the nasal retina. The lacZ-negative region in the temporal retina grows progressively larger as the sections become more ventral. (B, I) Small areas of lacZ-negative regions in the posterior-most temporal retina (indicated with an arrow in I. (J) Radial columns of lacZ-positive cells spanning the temporal retina (arrows indicate some examples). (E, K) Section at the level of the optic stalk showing staining in the nasal retina and optic stalk and in a few radial columns temporally (arrows indicate some examples). (F, G, L) Ventral sections show lacZ staining increasingly restricted to the anterior-most nasal retina as the lacZ-negative region becomes larger. (H, M) Ventral-most section showing the complete absence of lacZ-staining in the retina. In (M) the dotted line outlines the lacZ-negative retina. Scale bars: 400μm in A – H; 150μm in I – M. Abbreviations: A, anterior; P, posterior; N, nasal; T, temporal; l, lens; ne, nasal epithelium; os, optic stalk.

Figure 8. Lineage tracing at E14.5 using

***Foxg1*$^{Cre/+}$; *R26RS* embryos**

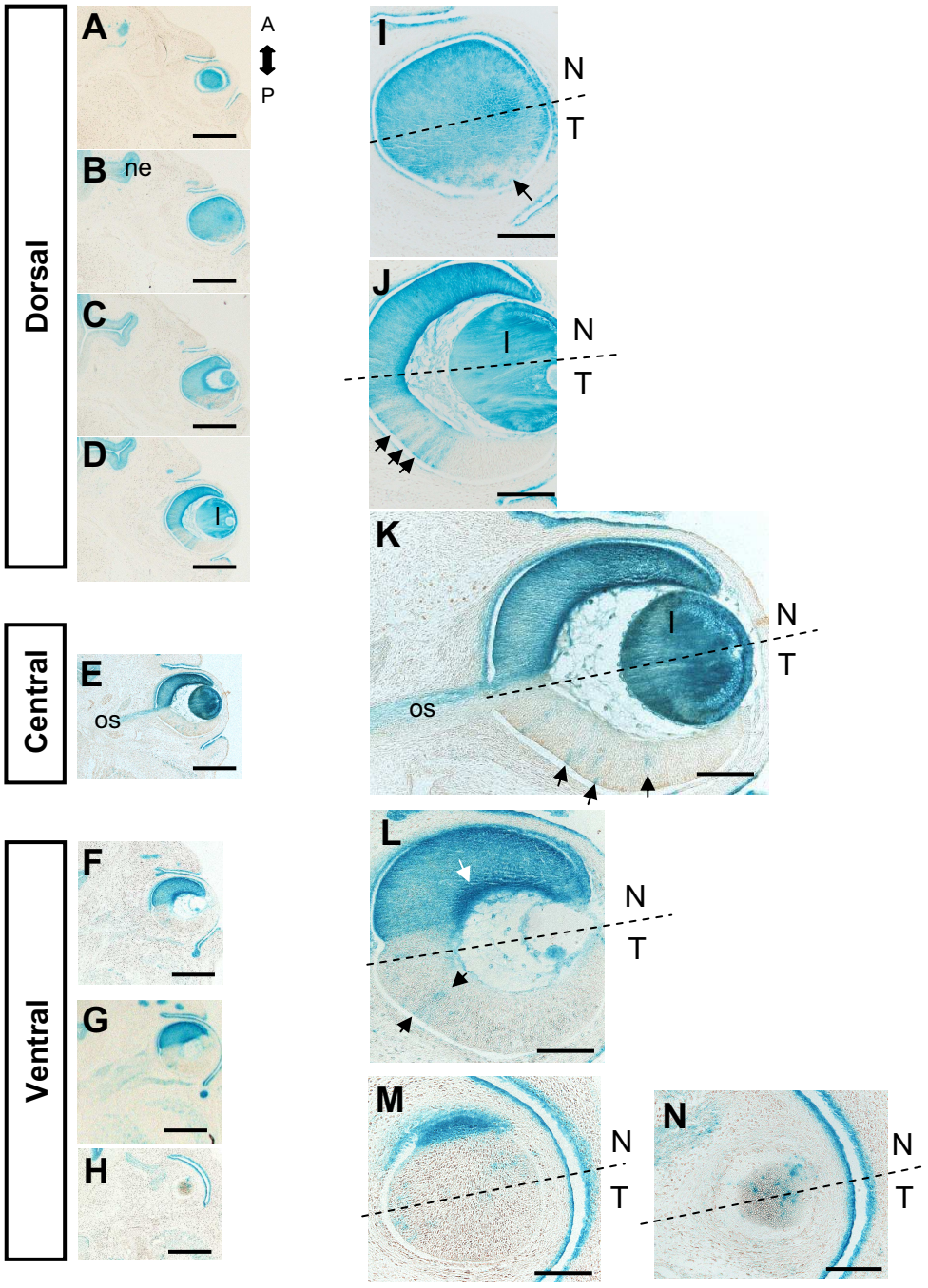

5.4.3.2. *Foxg1* activation in *Foxg1*$^{Cre/Cre}$; *ROSA26* embryos.

In dorsal-most sections, lacZ staining in *Foxg1*$^{Cre/Cre}$; *ROSA26* embryos resembled that seen in *Foxg1*$^{Cre/+}$; *ROSA26* embryos with strong LacZ-staining in the whole of the dorsal retina (Fig. 9A, B). In dorsal sections, lacZ staining was seen throughout the nasal retina including the medially extended retina but lacZ-negative regions were observed in the lateral regions of the temporal retina, adjacent to the CMZ (arrowheads in Figs 9C - F). In the central retina, temporal LacZ-positive radial stripes were observed and lacZ-staining was found throughout the nasal retina as in *Foxg1*$^{Cre/+}$; *ROSA26* embryos (compare Figs. 9H & 8K). This lacZ-staining pattern was maintained in ventral sections: the nasal retina exhibited strong lacZ-staining throughout, whereas radial stripes of *lacZ*-expressing cells were present temporally (Figs. 9I - L). In the most medial parts of the extended retina, lacZ staining was strong throughout both nasal and temporal regions (Figs. 9B - M). In ventral-most sections, scattered *lacZ*-expressing cells were found in nasal and temporal retina, whereas the medially extended retina showed strong lacZ-staining throughout (Fig. 9M).

To summarise the lineage-tracing findings, cells in the ventrotemporal retina that would not normally express *Foxg1* show *Foxg1* activation in *Foxg1* null embryos.

Figure 9. Lineage tracing of *Foxg1* activation in retinal cells of E14.5 *Foxg1*$^{Cre/Cre}$*; R26RS* embryos.

Foxg1$^{Cre/Cre}$*; R26RS* embryos cannot produce Foxg1 protein. X-gal staining of horizontally-sectioned *Foxg1*$^{Cre/Cre}$*; R26RS* eyes reveals retinal cells and their descendants in which *Foxg1* has been transcriptionally active at any time during their development. All sections are horizontal. (A - M) Sequence through the eye from most dorsal (A) to most ventral (M). Sections C, G, H, M are counterstained with Nuclear Fast Red. (A - F) Dorsal sections showing widespread lacZ staining over the entire retina. (A) Most dorsal section showing uniform lacZ staining. (C - F) Weaker staining is seen dorsolaterally (marked by arrowheads). (G, H) Sections of central retina showing staining predominantly in nasal retina. In temporal retina, radial columns of lacZ stained cells are observed (a few are marked with arrows in (H)). (I - M) Ventral sections showing staining predominantly in the nasal retina. In the ventral retina, lacZ staining is more patchy. (M) High power magnification of ventral-most retina showing patchy lacZ staining in the retina with strong staining in the extended retina. Abbreviations: l, lens; r, retina; er, extended retina; hy, hypothalamus.

Figure 9. Lineage tracing at E14.5 using *Foxg1*$^{Cre/Cre}$; *R26RS* embryos

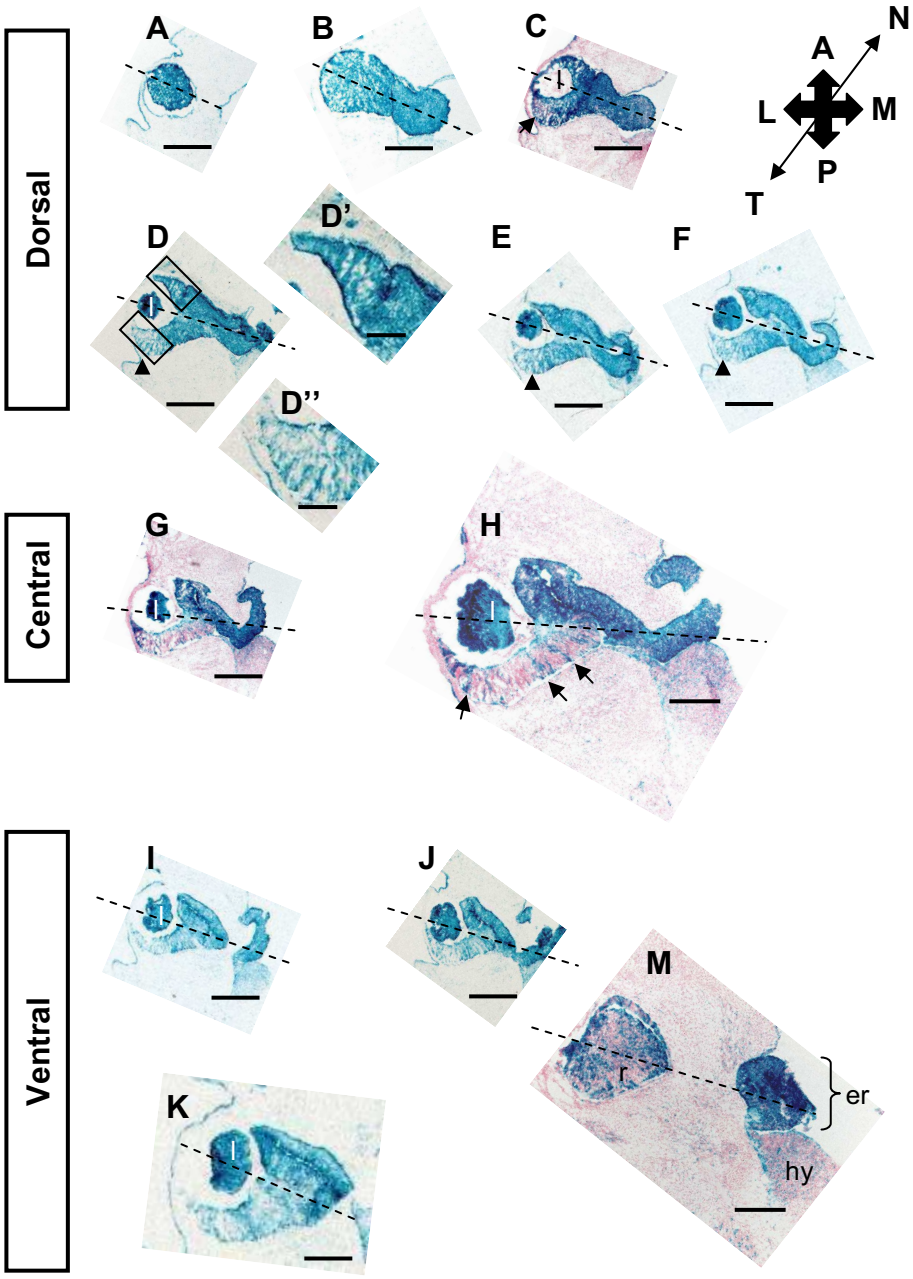

5.4.4. Dorsoventral polarity.

Dorsoventral polarity was investigated using EphB2 and ephrin-B2 at E13.5 and E16.5 since these developmental ages span the peak period during which many RGCs project. Contralateral RGC axons start to project approximately one to two days earlier than ipsilateral RGC axons (Colello & Guillery, 1990; Guillery et al., 1995; Marcus et al., 1995). At E13.5 contralateral RGCs have already started to project their axons towards the chiasm, whereas the formation of the permanent ipsilateral projection is still in its early stages (Sretavan, 1990). By E16.5, many contralateral and ipsilateral RGC axons have traversed the chiasm midline.

In the E13.5 wild type retina, EphB2 was expressed in a ventral$^{[high]}$ to dorsal$^{[low]}$ gradient (Fig. 10E), whereas its ligand ephrin-B2 was expressed in a complementary dorsal$^{[high]}$ to ventral$^{[low]}$ gradient (Fig. 10A). These dorsoventral gradients were present in the *Foxg1*$^{-/-}$ retina at the same age with the medial extended retina showing levels of EphB2 and ephrin-B2 intermediate between the dorsal- and ventral-most regions (Figs. 10C, G). At E16.5, the wild type and *Foxg1*$^{-/-}$ retina exhibited the same dorsal$^{[high]}$ to ventral$^{[low]}$ ephrin-B2 gradient as at E13.5 with strongest expression in the dorsolateral retina (Figs. 10B, D, D'). At the same age in wild type (Fig. 10F) and *Foxg1*$^{-/-}$ embryos (Fig. 10H, H'), EphB2 was expressed equally in the dorsal and ventral retina, with slightly higher levels ventrolaterally, suggesting that the ventral retina is not expanded in *Foxg1* nulls. In wild type and *Foxg1*$^{-/-}$ E16.5 embryos, the optic chiasm and optic tracts stained strongly for EphB2 protein suggestive of EphB2 expression by navigating RGC axons (Fig. 10I, K). In addition, the wild type optic nerve displayed EphB2 expression as did the *Foxg1*$^{-/-}$ elongated retina.

Figure 10. The expression patterns of EphB2 and ephrin-B2 are maintained in the developing retina of *Foxg1*$^{-/-}$ embryos. Ephrin-B2 (A – D) and EphB2 immunohistochemistry (E – L) in wild type (A, B, E, F, I, K) and *Foxg1*$^{-/-}$ embryos (C, D, G, H, J, L). Figures published in Pratt et al., 2004. (A – H) Coronal sections (dorsal is pointing upwards); (I – L) horizontal sections (posterior is pointing upwards). Ephrin-B2 is expressed in a dorsolateral$^{[High]}$ to ventrolateral$^{[Low]}$ gradient at E13.5 in the developing retina of a (A) wild type and (C) *Foxg1*$^{-/-}$ embryo. The gradient is maintained at E16.5 in both (B) the wild type and (D, D') the *Foxg1*$^{-/-}$ retina. (D') section anterior to (D) showing a more pronounced ephrin-B2 gradient compared to (D). EphB2 is expressed in a complementary ventrolateral$^{[High]}$ to dorsolateral$^{[Low]}$ gradient in the E13.5 retina in both (E) the wild type and (G) the *Foxg1*$^{-/-}$ retina. At E16.5, these gradients are more shallow than at E13.5 in both the (F) wild type and (H, H') *Foxg1*$^{-/-}$ retina. (H') is anterior to (H) and shows a greater difference between strong EphB2 expression ventrolaterally and weak expression dorsolaterally. (E, F, I) The optic nerve (on) stains strongly for EphB2 protein consistent with EphB2 expression by navigating RGC axons. (I, K) In the wild type at E16.5, EphB2 is expressed in the optic nerve as it leaves the retina (r) and approaches the optic chiasm (oc) to emerge into the optic tract (ot) (boxed area in I). (J, L) In the *Foxg1*$^{-/-}$embryo, EphB2 is expressed in the elongated retina (er), at the optic chiasm and in the optic tract as it emerges from the chiasm (boxed area in J). (I – L) White dashed line indicates the position of the midline. Abbreviations: er, extended retina; l, lens; r, retina; rpe, retinal pigment epithelium; on, optic nerve; ot, optic tract; oc, optic chiasm. Scale bars: 100µm in A - H; 200µm in I - L. [Note: E16.5 immunohistochemistry (Figures B, D, F, H, I - L) was performed by Dr Thomas Pratt].

Figure 10

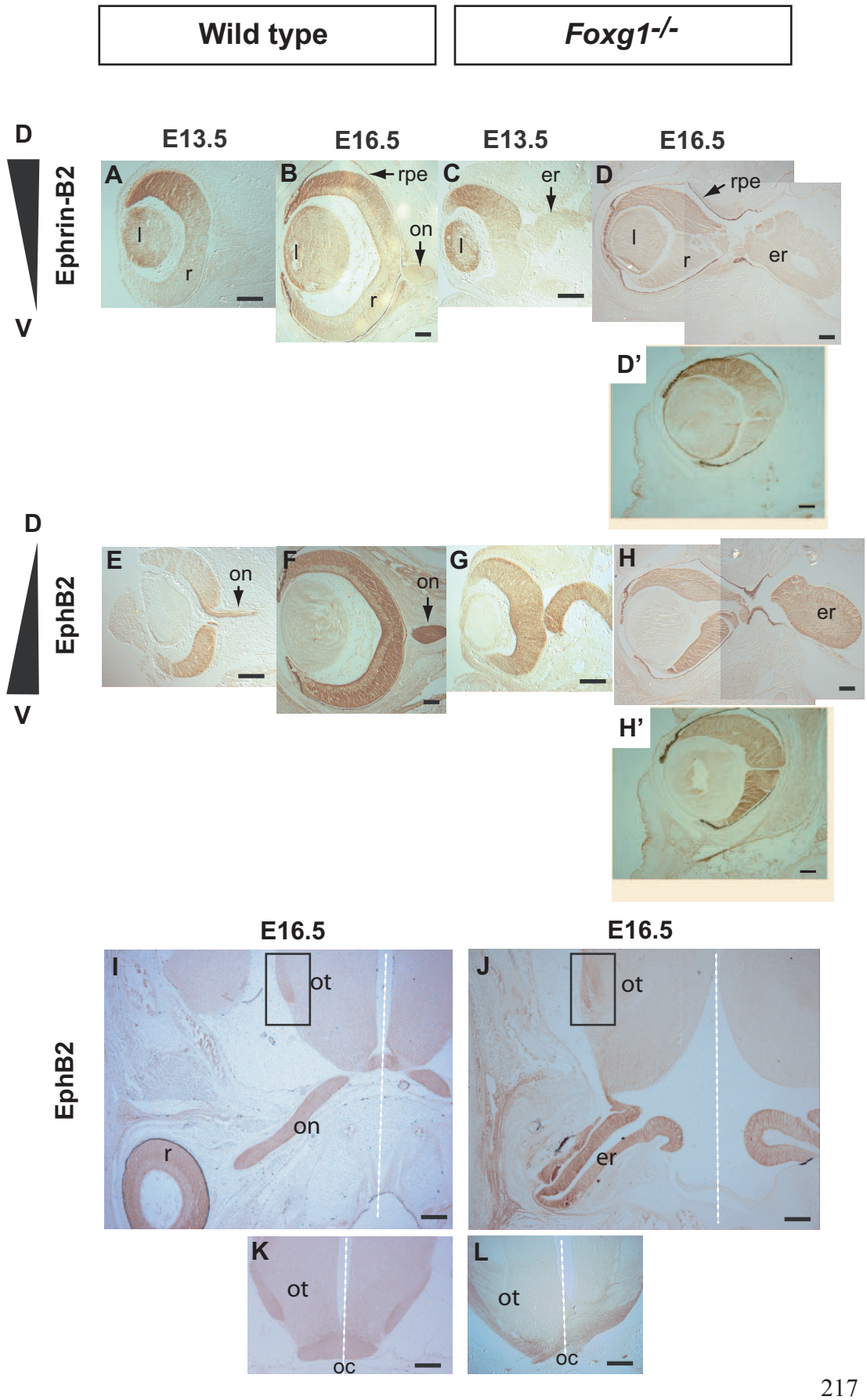
Wild type
Foxg1-/-
D
V
Ephrin-B2
E13.5
E16.5
E13.5
E16.5
A
B
rpe
C
er
D
rpe
l
r
on
l
r
l
r
er
D'
D
V
EphB2
E
on
F
on
G
H
er
H'
EphB2
E16.5
E16.5
I
ot
on
r
J
ot
er
K
ot
oc
L
ot
oc

5.5. DISCUSSION

5.5.1. The morphology of the *Foxg1*$^{-/-}$ retina retains many normal features.

Despite abnormal folding of the *Foxg1*$^{-/-}$ retina anteriorly, in more posterior regions, cellular differentiation of the retinal layers into the inner RGC layer and outer layers resembled the wild type (this Chapter and Huh et al., 1999). In addition, despite lacking a normal optic stalk, *Foxg1*$^{-/-}$ retinal axons were observed leaving the retina from a medial opening in the eye where they formed an optic nerve-like structure that channeled axons towards the midline of the brain. These observations agree with and add detail to findings from previous DiI tracing experiments in this laboratory showing that retinal axons leave the eyes and form optic tracts (Pratt et al., 2002). These similarities with the wild type are remarkable considering the squashed, elongated appearance of the *Foxg1*$^{-/-}$ retina.

Nevertheless, the *Foxg1* null retina showed retinal abnormalities in anterior regions, particularly surrounding the ventral coloboma where the optic cup failed to close, as reported previously (Huh et al., 1999). The RGC layer occupied a wider area in this region. However, since the abnormal folding of the retina primarily occurs in anterior regions, this could lead to sectioning through the RGC layer at a different angle from that of the wild type. A better way of visualizing the RGC layer would be to fluorescently label Brn3a or Brn3b proteins that are expressed in almost all RGCs in the intact *Foxg1*$^{-/-}$ eye. The eye could then be scanned in 3-dimensions using confocal microscopy and a 3-dimensional image of the RGC layer reconstructed on a computer. This would eliminate sectioning difficulties and determine whether the anterior regions of the retina show greater abnormalities in the organization of the RGC layer. If 3-dimensional images reveal anterior defects in the RGC layer, a hypothetical cause of this could be defective retinal patterning along the AP axis because anterior regions normally express *Foxg1* in the wild type (Hatini et al., 1994; Xuan et al., 1995; Huh et

al., 1999; Dou et al., 1999). In contrast, the organisation of the posterior retina, which does not normally express *Foxg1*, resembled the wild type more closely.

In agreement with previous studies, the retinal pigment epithelium does not completely surround the extended retina, particularly in ventral and medial regions (Huh et al., 1999). It is not known whether the absence of RPE along some regions of the *Foxg1* null retina affects its development and thus presents a tantalizing area for future research. Similarly the slight ventral rotation of the $Foxg1^{-/-}$ eye and the abnormally small lens, both of which have been previously described (Hatini et al., 1994; Xuan et al., 1995; Dou et al., 1999; Huh et al., 1999), could potentially affect the expression of regulatory genes both within and outside the retina, contributing to its abnormal development. Since it is difficult to separate primary defects that are directly caused by the absence of *Foxg1* from secondary defects that are knock-on effects resulting from the primary abnormalities in $Foxg1^{-/-}$ embryos, it would be informative to conditionally knock out *Foxg1* in the eye after it has developed normally. This is a project that is currently being pursued in this laboratory and promises to open more avenues of research that are not possible using *Foxg1* null embryos alone.

5.5.2. $Foxg1^{LacZ}$ reporter mice reveal differences in *Foxg1* activation in the $Foxg1^{-/-}$ eye.

In $Foxg1^{lacZ/+}$ embryos, when RGC axons are navigating the optic chiasm, lacZ staining revealed that transcriptional activation of *Foxg1* occurs predominantly in the nasal retina with strong *Foxg1* expression in RGCs, which project axons to the optic chiasm. *Foxg1* expression was most widespread in dorsal retina, covering nasal and temporal regions. *Foxg1* was only expressed in a few cells in the rest of the temporal retina and lineage tracing revealed that most temporal cells and their descendants never express *Foxg1*. These observations hint at the possibility of a cell autonomous role for *Foxg1* in the guidance of retinal axons from the nasal retina, whereas this is not as plausible for

the temporal retina, the majority of whose cells do not express *Foxg1* throughout development.

The *Foxg1* expression pattern described here is similar but not identical to that found previously using $Foxg1^{LacZ}$ reporter mice (Huh et al., 1999) and by *in situ* hybridisation (Hatini et al., 1994). However, most of these previous descriptions state that *Foxg1* is limited to the nasal retina until E12.5 (Figure 11A), whereas this chapter presents new findings of fairly substantial *Foxg1* expression in the dorsotemporal retina from E13.5, with the border between *Foxg1*-positive and *Foxg1*-negative regions running at an angle to the NT axis (Figure 11Bi). The difference could be due to spatiotemporal changes in *Foxg1* expression between E12.5, the latest age described in earlier studies, and E13.5-E14.5 (this Chapter). Alternatively, previous studies may have used a slightly different plane of section, such that the NT axis is angled relative to the one shown here. Regardless of these differences, this is the first comprehensive description of *Foxg1* expression through the entire retina at E14.5.

All the $Foxg1^{lacZ/lacZ}$ retinas examined for this chapter displayed morphological variation, between and within embryos, consistent with previous reports (Huh et al., 1999). Nevertheless, consistent trends in the lacZ staining patterns were observed. A schematic diagram of the pattern of *Foxg1* activation is shown in Figure 11Bii. $Foxg1^{lacZ/lacZ}$ retinas displayed a similar *Foxg1* activation pattern to $Foxg1^{LacZ}$ heterozygotes in mid - ventral retinal sections where nasal *lacZ* staining predominated. Therefore, nasotemporal polarity appeared to be maintained in some retinal locations. The presence of blue lacZ-positive cells showed that cells that would normally express *Foxg1* were present in $Foxg1^{-/-}$ retinas, ruling out a simple deletion of nasal cells. However, $Foxg1^{lacZ/lacZ}$ embryos displayed more extensive *Foxg1* activation in the temporal retina, particularly in dorsal parts but also ventrally, whereas DN regions displayed reduced *Foxg1* activation relative to $Foxg1^{lacZ/+}$ embryos. Similar observations were made in the lineage tracing experiments with *Foxg1* null embryos.

Figure 11.

(A) *Foxg1* expression pattern described in the literature (optic cup stage until ~ E12.5)

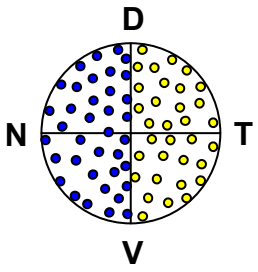

Early in eye development until ~ E12.5, *Foxg1* (blue) is expressed in the nasal half of the retina and *Foxd1* (yellow) is expressed in a complementary pattern in the temporal retina. Together these transcription factors are thought to set up nasal-temporal polarity (Hatini et al., 1994; Huh et al., 1999).

.

(B) *Foxg1* activation at E14.5

***Foxg1*$^{LacZ/+}$**

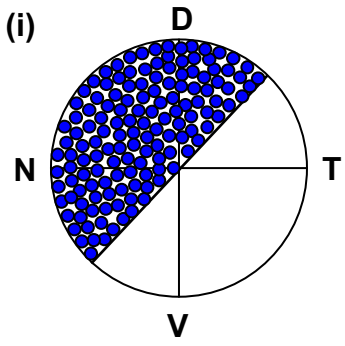

Foxg1 expression (blue) is more widely expressed in dorsal retina compared to ventral retina. The boundary between *Foxg1*-positive and *Foxg1*-negative regions is slanted at an angle to the vertical DV axis. Dots represent RGCs.

***Foxg1*$^{LacZ/LacZ}$**

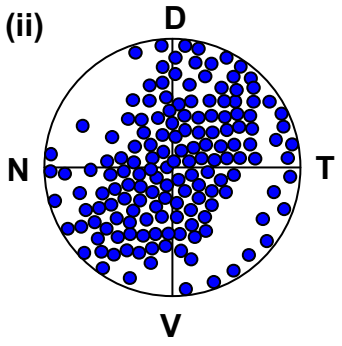

Compared to the *Foxg1*$^{LacZ/+}$ retina, there is no clear divide between *Foxg1*-expressing and non-expressing regions. The area over which *Foxg1* is activated is reduced in DN retina but increased in the DT and VT quadrants. The VN region shows more variable activation possibly due to greater morphological abnormalities in this part of the retina.

Together, these findings suggest that cells in the temporal retina that would not normally express *Foxg1* activate *Foxg1* in the *Foxg1*$^{-/-}$ retina. Also, cells in the dorsonasal retina that would normally express *Foxg1* in *Foxg1*$^{lacZ/+}$ embryos do not activate *Foxg1* in the *Foxg1*$^{-/-}$ retina. It is unclear whether the temporal cells that ectopically activate *Foxg1* have been mis-specified as 'nasal' cells through defective nasal-temporal patterning or whether they are nasal cells that have migrated abnormally into temporal regions. Similarly in the DN retina, cells that fail to activate *Foxg1* may have been mis-specified as 'temporal' cells or they may have migrated from *Foxg1*-negative temporal regions. Ideally, a migratory defect would be investigated by fluorescently labeling a single cell in the nasal retina within the developing eye, *in vitro* or *in vivo*. Abnormal migration into temporal regions would be visible by fluorescence in the temporal retina.

The alternative explanation to a migratory defect in the *Foxg1* null retina is that NT patterning is altered. This is not an unexpected occurrence, since the misexpression of *Foxg1* and *Foxd1* homologues in the chick (*CBF1* and *CBF2*) affects their mutual expression domains and also the expression of other nasal and temporal patterning genes: EphA3, SOHo1, GH6, ephrin A2 and ephrin A5 (Takahashi et al., 2003). In order to confirm whether patterning of the retina along the nasal-temporal axis is affected by the absence of *Foxg1* as suggested by the *Foxg1*^{LacZ} reporter mice, it would be prudent to investigate the nasal-temporal expression patterns of molecules in the retina. This would also confirm whether *lacZ* expression in *Foxg1* null embryos faithfully reports regions in which *Foxg1* is active, as previously found in *Foxg1*$^{lacZ/+}$ reporter mice (Xuan et al., 1995). Without further investigation of nasal-temporal patterning, it remains possible that *Foxg1*^{LacZ} is ectopically expressed in the *Foxg1*$^{lacZ/lacZ}$ retina, which would provide misleading evidence for NT disruption. This seems unlikely given that lacZ staining in *Foxg1*$^{lacZ/lacZ}$ embryos was observed in tissues that would normally have expressed *Foxg1* during development, notably in the telencephalon, lens, ventral hypothalamus (see Chapter 6), RPE, nasal epithelium and

superior colliculus (this Chapter and Hatini et al., 1994; Huh et al., 1999). These findings provide evidence against but cannot exclude the possibility of ectopic *Foxg1* activation in the *Foxg1*$^{lacZ/lacZ}$ retina. Ephrin-A5 is restricted to the nasal retina and it would be interesting to see whether its expression pattern resembles that of *Foxg1*. This would be interesting given that CBF1 in chick has been shown to control retinal ephrin-A5 via a DNA-binding-dependent mechanism (Takahashi et al., 2003). It would also be sensible to examine the expression patterns of molecules present in the temporal retina, such as Foxd1 and EphA5/EphA6, the latter of which are expressed in a low nasal to high temporal gradient.

Overall, these results warrant a more in-depth investigation of nasotemporal patterning, since increased specification of temporal regions could promote more axons to remain ipsilateral at the chiasm.

5.5.3. Expression gradients of EphB2 and ephrin-B2 are maintained along the dorsoventral axis in *Foxg1* null embryos.

The EphB2 and ephrin-B2 dorsal-ventral expression gradients were maintained in *Foxg1*$^{-/-}$ embryos at E13.5 and E16.5. Thus it is unlikely, but not impossible, that the ventral region of the *Foxg1*$^{-/-}$ retina is expanded. It remains feasible that EphB2 and ephrin-B2 are expressed normally in the absence of *Foxg1*, whereas the expression of other ventral markers may be affected. This could be investigated by examining the expression of other dorsally and ventrally expressed molecules, such as the dorsal marker Tbx5 and ventral marker Vax2. In fact the bi-axial patterning of the retina is an over-simplistic view as several regulatory genes, such as Vax2 and ventroptin, involved in retinal polarity are not expressed solely along the DV or NT axis. This is reflected in ectopic expression studies of ventroptin or Tbx5 in the chick where both DV and NT maps are affected, consistent with their normal expression gradients along both of these

axes (Sakuta et al., 2001). Therefore, regulatory transcription factors expressed in the retina combine in various ways that are still not fully understood to regulate the expression of DV and NT guidance molecules.

5.5.4. Summary.

In summary, despite the abnormal squashed and medially-elongated appearance of the *Foxg1*$^{-/-}$ eye, the retinal layers appear to form normally in their correct locations, apart from defects in the RGC layer anteriorly that might be either sectioning artifacts caused by retinal folding or secondary consequences of retinal patterning defects and which might affect axon routing. DV polarity appeared to be maintained in the *Foxg1*$^{-/-}$ retina based on the dorsoventral expression gradients of two molecules known to play roles in retinotectal mapping. Cells that would normally express *Foxg1* were not present in the same nasal-temporal pattern as for wild type embryos, although a nasal bias in *Foxg1* activation was observed in more ventral retinal locations. This might suggest either defective nasal-temporal patterning of the retina or aberrant migration, both leading to a retina in which cells with nasal characteristics are found in temporal regions and vice-versa. Evidence against a complete breakdown of nasal-temporal polarity comes from the co-culture findings that demonstrated significant differences among cultures comprised of DN retina and chiasm cells but not among VT retina combinations prepared from wild type and *Foxg1*$^{-/-}$ tissue (see Chapter 3). Also, Pratt et al. (2004) showed that a greater proportion of ipsilateral projections still originated from the temporal retina as in wild types. Moreover, expression of Zic2 was predominantly affected in the nasal region of the *Foxg1*$^{-/-}$ retina whereas its temporal expression was broadly maintained (Chapter 4). Thus it appears that the absence of *Foxg1 in vivo* and *in vitro* mainly affects the molecular characteristics and axon routing of RGCs from the nasal retina in which *Foxg1* is normally expressed. Nevertheless, further investigation

into nasal-temporal patterning is required to determine whether the *Foxg1*$^{-/-}$ retina shows temporal abnormalities.

CHAPTER 6: Characterization of the *Foxg1*$^{-/-}$ optic chiasm.

6.1. ABSTRACT

The co-culture findings in Chapter 3 show that the optic chiasm of *Foxg1*$^{-/-}$ embryos is more inhibitory and/or less attractive to nasal retinal axons. This could occur through the increased expression of a repulsive guidance cue, reduced expression of an attractive cue or simply through abnormal morphology of the chiasm region. Therefore, the aim of this Chapter was to examine the cellular and molecular morphology of the *Foxg1*$^{-/-}$ chiasm and the expression of key molecules known to influence the guidance of retinal axons at the chiasm. Throughout the period when retinal axons project, the *Foxg1* activation pattern and morphology of the *Foxg1*$^{-/-}$ chiasm region retained many wild type features. In *Foxg1*$^{-/-}$ embryos the expression patterns of the transcription factor Nkx2.2, and of cell surface molecules stage-specific embryonic antigen-1 (SSEA-1) and CD44 that are expressed by a population of chiasm neurons, were not dissimilar from the wild type. Ephrin-B2, which is required for the formation of the ipsilateral projection, was present at the *Foxg1*$^{-/-}$ chiasm midline as for the wild type. In summary, key chiasm cells and molecules were present in the *Foxg1*$^{-/-}$ chiasm and failed to show obvious abnormalities in spatial or temporal expression. Nevertheless, this does not rule out a change in the expression of other guidance cues at or surrounding the optic chiasm, nor does it rule out the possibility of *Foxg1*$^{-/-}$ retinal axons interacting with chiasm molecules in a different manner to wild type axons.

6.2. INTRODUCTION

6.2.1. Overview of retinal axon navigation at the developing mouse optic chiasm.

The aims of this chapter were to determine whether the *Foxg1*$^{-/-}$ chiasm architecture is maintained and whether molecules expressed by cells at or surrounding the optic chiasm in *Foxg1*$^{-/-}$ embryos are present in the wild type conformation. The first retinal axons arising from the dorsocentral (DC) retina start to project towards the chiasm from E12 in the mouse (Colello & Guillery, 1990). These pioneer axons grow towards the ventral midline of the hypothalamus and enter the chiasm region via the optic stalks. The first axons project both contralaterally and ipsilaterally in a stochastic manner, although the ipsilateral projection is only transient at this stage and uncrossed axons enter the optic tract directly rather than contacting midline cells (Colello & Guillery, 1990; Guillery et al., 1995; Marcus et al., 1995). From E13 - E15, many RGC axons project towards and across the chiasm. Since RGC differentiation proceeds radially outwards from dorsocentral to peripheral retina (Drager, 1985; Reese and Colello, 1992), contralateral projections from RGCs located over the entire retina form prior to E14.5, when permanent ipsilateral projections begin to arise from the VT retina (Colello & Guillery, 1990). During the peak phase of retinal axon divergence between E14 and E16, *in vitro* and live imaging (Godement et al., 1994; Sretavan & Reichardt, 1993) has revealed that the chiasm region is generally inhibitory to axons and that this inhibition can be attributed to cells (Wang et al., 1995), membranes (Wizenmann et al., 1993) and the secretion of a diffusible factor that inhibits axon growth from all retinal regions (Wang et al., 1996).

A midline specialisation of radial glial cells contacts all retinal axons in the chiasm region (Marcus et al., 1995). Contacts between navigating growth cones and glial processes have been shown to be crucial for the formation of the permanent ipsilateral

projection from VT retina. Recently, it was shown that repulsion between EphB1 receptors on VT axons and ephrin-B2 present on midline radial glia is the main mechanism by which the permanent uncrossed projection develops (Nakagawa et al., 2000; Williams et al., 2003). It is only after contacting the midline radial glia that axons 'decide' whether to cross into the contralateral tract or remain ipsilateral. Videos of axons in brain preparations revealed that the growth of retinal axons through the chiasm is retarded, during which their growth cones increase in complexity as their filopodia constantly extend and retract (Godement et al., 1994; Sretavan & Reichardt, 1993). The slowing of axons as they enter the chiasm is probably due to the growth-inhibitory chiasm environment. Ipsilateral axons have complex filopodia that become simpler upon entering the ipsilateral optic tract. Constant growth cone remodelling and complex growth cone morphology is thought to be associated with axons sampling and integrating diffusible and cell surface guidance cues prior to committing themselves to a given trajectory.

6.2.2. SSEA-1 & CD44.

Stage-specific embryonic antigen-1 (SSEA-1) and CD44 are cell surface carbohydrate moieties on glycoproteins and glycolipids that are expressed by a specialized group of early-differentiating neurons immediately posterior to the developing optic chiasm and both molecules have been implicated in influencing the paths taken by navigating retinal axons throughout development of the retinofugal pathway (Sretavan et al., 1995; Sretavan et al, 1994; Marcus & Mason, 1995; (Kruger et al., 1998); Lin et al., 2005). SSEA-1 is thought to be essential for the formation of the characteristic 'X'-shape by retinal axons at the chiasm (Mason & Sretavan, 1997; Erskine et al., 2000; Runko & Kaprielian, 2002). At E12.5, SSEA-1 neurons are expressed in an inverted 'V'-shape, with the tip of the 'V' pointing anteriorly. RGC axons grow towards, contact and then travel along the surfaces of SSEA-1-positive neurons but not through them. As development proceeds, axons are added progressively to more anterior locations, such

that the bundle of axons develops from posterior to anterior (Sretavan et al., 1994; Marcus & Mason, 1995). From E13 – E16, the expression pattern of SSEA-1 becomes more elaborate, concomitant with the peak period of axon growth through the optic chiasm (Lin et al., 2005). At these later ages, SSEA-1-expressing neurons are increasingly found adjacent to retinal axons at the chiasmatic midline and along the region where axons enter the optic tracts and therefore, are present in the appropriate locations to influence axon growth.

SSEA-1 neurons have been shown to provide repulsive guidance cues to retinal axons *in vitro* (Sretavan et al., 1994; Marcus & Mason, 1995) and the addition of SSEA-1 to retinal explants is capable of inhibiting neurite outgrowth equally from both dorsonasal and ventrotemporal regions. Therefore, an expansion of the SSEA-1 population anteriorly might repel a greater proportion of retinal axons into the ipsilateral tract and reduce the proportion that is able to cross the midline. This possibility was addressed by immunohistochemical detection of SSEA-1 during early chiasm development at E13.5 and later at E15.5, when more axons have passed through the chiasm.

The cell surface transmembrane glycoprotein CD44 occupies a more restricted area compared with SSEA-1 and is expressed by more central chiasm neurons (Lin et al., 2005). The expression domains of SSEA-1 and CD44 overlap at the chiasm midline, including the raphe of midline glia but laterally, chiasm neurons express only SSEA-1. Eliminating CD44-immunoreactive neurons by complement-mediated antibody ablation prevents axons from entering the chiasm (Sretavan et al., 1995). However, this study eliminated the CD44-bearing neurons and did not address the effects of CD44 itself on retinal axons. *In vitro* experiments in the mouse demonstrated that CD44 inhibits outgrowth of axons from retinal explants (Sretavan et al., 1994). In semi-intact retinofugal pathway explants, anti-CD44 antibodies reduced the contralateral projection but left the ipsilateral projection unaffected at E13 (Lin et al., 2003). In E15 explants, anti-CD44 treatment reduced the uncrossed projection but left the contralateral projection unaffected. The authors concluded that at early stages in retinofugal development, CD44

promotes the midline crossing of axons but at later stages, CD44 is required for the formation of the permanent ipsilateral projection. Therefore, one hypothesis for the increased ipsilateral projection of *Foxg1*$^{-/-}$ embryos is that increased CD44 expression in the ventral diencephalon at E15.5 produces a chiasm environment that is less conducive to axon crossing. This hypothesis was tested by investigating CD44 protein expression using a monoclonal CD44 antibody.

6.2.3. Nkx2.2.

A number of regulatory genes are expressed in the diencephalon in cells surrounding or located at the chiasm midline, some of which have been implicated in controlling the trajectory of retinal axons at the midline (Marcus et al., 1999). One such molecule is the transcription factor Nkx2.2, which is expressed by cells and radial glia at the midline of the optic chiasm where axons decussate and also in the SSEA-1/CD44-expressing neuronal array (Marcus et al., 1999). Nkx2.2 protein expression was investigated at the *Foxg1*$^{-/-}$ chiasm to see whether Nkx2.2-expressing chiasm cells were present in their correct locations. Abnormalities in the distribution of Nkx2.2-expressing cells, such as disorganisation or an expansion/reduction, may suggest abnormal interactions between retinal axons and key cells at the chiasm, which might alter their trajectory.

6.2.4. Ephrin-B2.

Ephrin-B2 is expressed by midline radial glia at the mouse optic chiasm (Williams et al., 2003). In *Xenopus* and mice, the appearance or upregulation of ephrin-B2 expression around the chiasm region has been linked to the appearance of the ipsilateral projection (Nakagawa et al., 2000; Williams et al., 2003). In a semi-intact visual pathway explant, inhibition of ephrin-B2 activity by soluble EphB4-Fc completely abolished the formation of ipsilateral projections showing that ephrin-B2 is necessary for the ipsilateral projection to form (Williams et al., 2003). Williams et al. (2003) also showed that ephrin-B2 is

selectively inhibitory to VT retinal axons, which express EphB1 that is responsible for their repulsion by ephrin-B2-expressing radial glia at the chiasm midline. At E13.5 in the mouse, when ipsilateral projections from the VT retina start to enter the chiasm region, ephrin-B2 is weakly expressed at the chiasm. Ephrin-B2 expression increases up until E16.5 during the key period when the majority of RGCs project axons towards the optic chiasm (Williams et al., 2003). It follows that an increase in expression of ephrin-B2 at the optic chiasm may repel a greater proportion of RGC axons into the ipsilateral optic tract.

6.3. METHODS

6.3.1. Mice.

To identify cells in which the *Foxg1* locus is transcriptionally active we exploited the *Foxg1*^{tm1M} (or *Foxg1*^{LacZ}) allele in which coding sequences are replaced by a LacZ cassette (Xuan et al., 1995). *Foxg1*^{LacZ} is a predicted null allele (designated *Foxg1*$^{-/-}$) (Xuan et al., 1995; Hebert and McConnell, 2000). *Foxg1* homozygous mutants (*Foxg1*$^{LacZ/LacZ}$) were identified by their hypoplastic telencephalon and distorted eyes. Heterozygous embryos (i.e. *Foxg1*$^{LacZ/+}$) were identified by PCR genotyping: they were indistinguishable morphologically from wild types (Xuan et al., 1995; Huh et al., 1999) and no RGC axon projection defects were observed at the optic chiasm.

Dissections: Pregnant females were terminally anaesthetized and E13.5, E14.5 or E15.5 embryos removed by caesarian section in ice-cold PBS.

PCR genotyping Foxg1 alleles: Tails were removed from the embryos to obtain tissue for genotyping. The *Foxg1*^{LacZ} allele was detected with primers LacZ F2 5'-TTG AAC TGC CTG AAC TAC CG-3' and LacZ R2 5'-CCT GAC TGG CGG TTA AAT TG-3'.

Cycling conditions: 96°C for 2 minutes followed by [96°C for 30 seconds, 58.5°C for 30 seconds, and 72°C for 30 seconds] for 35 cycles.

6.3.2. H & E staining.

Wax-embedded embryo heads were cut into 10µm-thick coronal sections, collected onto poly-l-lysine-coated slides and dried overnight in a 37ºC incubator. Wax sections were dewaxed in two changes of xylene and then dehydrated through a series of alcohol solutions: 100%, 95%, 90%, 70% and finally distilled water. Haematoxylin and eosin (1% aqueous) solutions were filtered prior to use. Sections were immersed in the filtered Harris Hematoxylin for 2 minutes followed by a rinse in tap water until the water turned clear. Sections were immersed in eosin stain for 3 minutes, dipped in tap water, transferred to potassium aluminium sulphate for 2 minutes and then rinsed in tap water. Sections were dehydrated in a series of ascending alcohol solutions (70%, 90%, 95%, 100% x2), cleared in 2 changes of xylene and mounted using DPX.

6.3.3. LacZ staining.

E14.5 *Foxg1*$^{lacZ/+}$ and *Foxg1*$^{lacZ/LacZ}$ embryonic heads were dissected and fixed for 1 hour at 4°C in 4% paraformaldehyde, 0.02% NP40, 0.01% sodium deoxycholate, 5 mM EGTA, 2mM $MgCl_2$ in phosphatebuffered saline (PBS). In some cases, heads were equilibrated in 30% sucrose/PBS and sectioned (10µm) on a cryostat and collected onto Superfrost Plus slides. Tissues were rinsed several times in wash buffer (2 mM MgCl2, 0.02% NP40, 0.01% sodium deoxycholate in PBS), transferred to staining solution (wash buffer supplemented with 5 mM potassium ferricyanide, 5 mM potassium ferrocyanide and 1 mg/ml X-gal), and stained overnight (cryostat sections on slides) or for 2 days with agitation (wholemounts) at 37°C in darkness. Staining was stopped with 20 mM EDTA in PBS. Wholemounts were processed to wax, sectioned (10µm) using a microtome and

mounted onto poly-l-lysine-coated slides. Cryostat sections were counterstained with Nuclear Fast Red.

6.3.4. Immunohistochemistry.

Ephrin-B2: immunohistochemistry was performed on wax sections essentially as described by Batlle et al. (2002). E13.5 and E16.5 embryo heads were fixed in 4% paraformaldehyde in phosphate buffer high salt (PBHS) (0.04M phosphate, 0.03M NaCl, pH7.0) at 4^{o}C with shaking overnight and processed to wax. 10µm sections were cut and floated onto polylysine coated glass slides. After rehydration, endogenous peroxidase activity was blocked with 90% methanol: 3% hydrogen peroxide and antigens unmasked by microwaving in 10mM sodium citrate buffer (pH6.0). Sections were then reacted with primary antibody goat anti-mouse ephrin-B2 (R&D Systems AF496) (1:500 dilution) overnight, followed by incubation with a bridge rabbit anti-goat antibody (Dako Z0228) used at a 1:400 dilution, before final detection using the Envision^{+} (Rabbit) Kit (Dako K4010) following the manufacturers instructions. Antibody incubation and pre-incubation blocking were carried out in 1% bovine serum albumin in PBS at room temperature. Following a diaminobenzidine colour reaction, sections were dehydrated, cleared in xylene and mounted using DPX.

SSEA-1 and Nkx2.2: immunohistochemistry was performed as described previously on 10µm wax sections (SSEA-1: Marcus & Mason, 1995; Nkx2.2: Pratt et al., 2004) except that detection of the primary antibody was carried out using the Envision^{+} (Mouse) Kit (Dako K4006) following the manufacturer's instructions. Primary antibodies were mouse monoclonal anti-Nkx2.2 antibody (Developmental Studies Hybridoma Bank, USA 74.5A5) used at 1:30 and mouse monoclonal anti-SSEA1 antibody (Developmental Studies Hybridoma Bank, USA MC-480). Following a diaminobenzidine colour reaction, sections were dehydrated, cleared in xylene and mounted using DPX.

SSEA-1 and CD44: Standard immunohistochemistry protocols were followed. E15.5 embryo heads were fixed overnight in 4% paraformaldehyde in PBS, processed to wax, and sectioned at a thickness of 10μm. Sections were dewaxed in xylene and rehydrated through an alcohol series. Endogenous peroxidase activity was blocked with 90% methanol: 3% hydrogen peroxide. Antigens were unmasked by microwaving in 10mM sodium citrate buffer, pH 6, before reacting overnight with the primary antibody. Double-immunofluorescence immunohistochemistry was performed on wax sections blocked for 1 h at room temperature with 2% goat serum in 1% bovine serum albumin and PBS using the following primary antibodies: mouse monoclonal anti-stage-specific embryonic antigen 1 (anti-SSEA1) antibody (MC-480; Developmental Studies Hybridoma Bank) used at 1:50 and rat anti-CD44 IgG (IM7; PharMingen, San Diego, CA) used at 1:50. The primary incubation was performed overnight at 4°C. After several washes in PBS, slides were incubated in goat anti-rat Alexa Fluor 488 and goat anti-mouse Alexa Fluor 568 fluorescent secondary antibodies (A-11006, A-11004; Invitrogen), used at 1:150, for 45 min in the dark. Slides were washed with PBS, counterstained with 1:2000 TOPRO3 (Invitrogen), mounted in Mowiol and visualized using a Leica TCSNT confocal microscope.

6.4. RESULTS

6.4.1. Optic chiasm morphology is relatively normal in *Foxg1* null embryos.

Haematoxylin and eosin tissue staining was used to reveal the cellular morphology of the ventral hypothalamus and chiasm region at E15.5, the peak time at which axons cross the midline. Anterior to posterior sections through the chiasm failed to show any obvious disruptions to the cellular organisation. In anterior sections, the palisade of cells at the floor of the third ventricle was present in an equivalent location in wild type and *Foxg1* null embryos (Figs. 1A, B). The anterior chiasm of wild type and *Foxg1*$^{-/-}$ embryos consistently revealed a group of midline cells bordered dorsally by the third ventricle and ventrally by the pial surface, and these cells appeared to contact retinal axons. Mid-chiasm (Figs. 1C, D) and posterior chiasm (Figs. 1E, F) sections failed to show major differences in chiasm anatomy, although *Foxg1*$^{-/-}$ retinal axons appeared to be less fasciculated than those of the wild type, particularly in posterior regions (Fig. 1F). This resembles the wider area occupied by DiI at the *Foxg1*$^{-/-}$ chiasm (Pratt et al., 2004). In *Foxg1*$^{-/-}$ and wild type mid-chiasm sections, cells at the floor of the third ventricle dorsal to the axons appear to be the cell bodies of midline radial glia that are known to be located in this region (Marcus et al., 1995). However, specific markers for radial glia would need to be used to confirm this. The *Foxg1*$^{-/-}$ retinal axons approached the ventral midline of the hypothalamus in a similar manner to wild type axons (compare Figs. 1A & B and 1G & H). The most obvious difference was that the *Foxg1*$^{-/-}$ retinal axons were visible over a wider latero-medial area compared to wild type axons, presumably due to the lack of an optic stalk in the former.

Figure 1. Morphology of the optic chiasm at E15.5.
Haematoxylin (purple) and eosin (pink) staining through the E15.5 optic chiasm from posterior to anterior in a (A, C, E, G, I) wild type and (B, D, F, H, J) *Foxg1*$^{LacZ/LacZ}$ embryo. Note that in *Foxg1*$^{LacZ/LacZ}$ sections, the right side is slightly anterior to the left and in wild type sections, the left is slightly anterior to the right. All sections are wax and cut in the coronal plane with dorsal pointing upwards. Arrows point towards the midline. Anterior chiasm sections in a (A) wild type and (B) *Foxg1*$^{-/-}$ embryo showing axons approaching the midline laterally. A group of midline cells contact wild type and *Foxg1*$^{-/-}$ retinal axons. Mid-chiasm (C, D) and posterior chiasm (E, F) sections do not show major differences in chiasm anatomy. Cell bodies at the floor of the third ventricle and dorsal to retinal axons are observed in wild type and *Foxg1*$^{-/-}$ chiasms. (D, F) In the *Foxg1*$^{LacZ/LacZ}$ chiasm, axons tend to be less fasciculated than in the wild type. Low power images of (G, I) wild type and *Foxg1*$^{-/-}$ brains (H, J). (G, H) Anterior to the chiasm, axons (marked with an asterisk) are visible lateral to the midline. (H) The *Foxg1*$^{-/-}$ hypoplastic telencephalon (tel) lacks ventral regions that are present in the wild type (vtel in (G)). (J, H) Axons at the posterior chiasm. (H) *Foxg1*$^{-/-}$ axons occupy a wider area dorsoventrally and laterally. Abbreviations: D, dorsal; V, ventral. Scale bars: A – F: 100μm, G, H, I, J: 200μm.

Figure 1. Morphology of the chiasm at E15.5

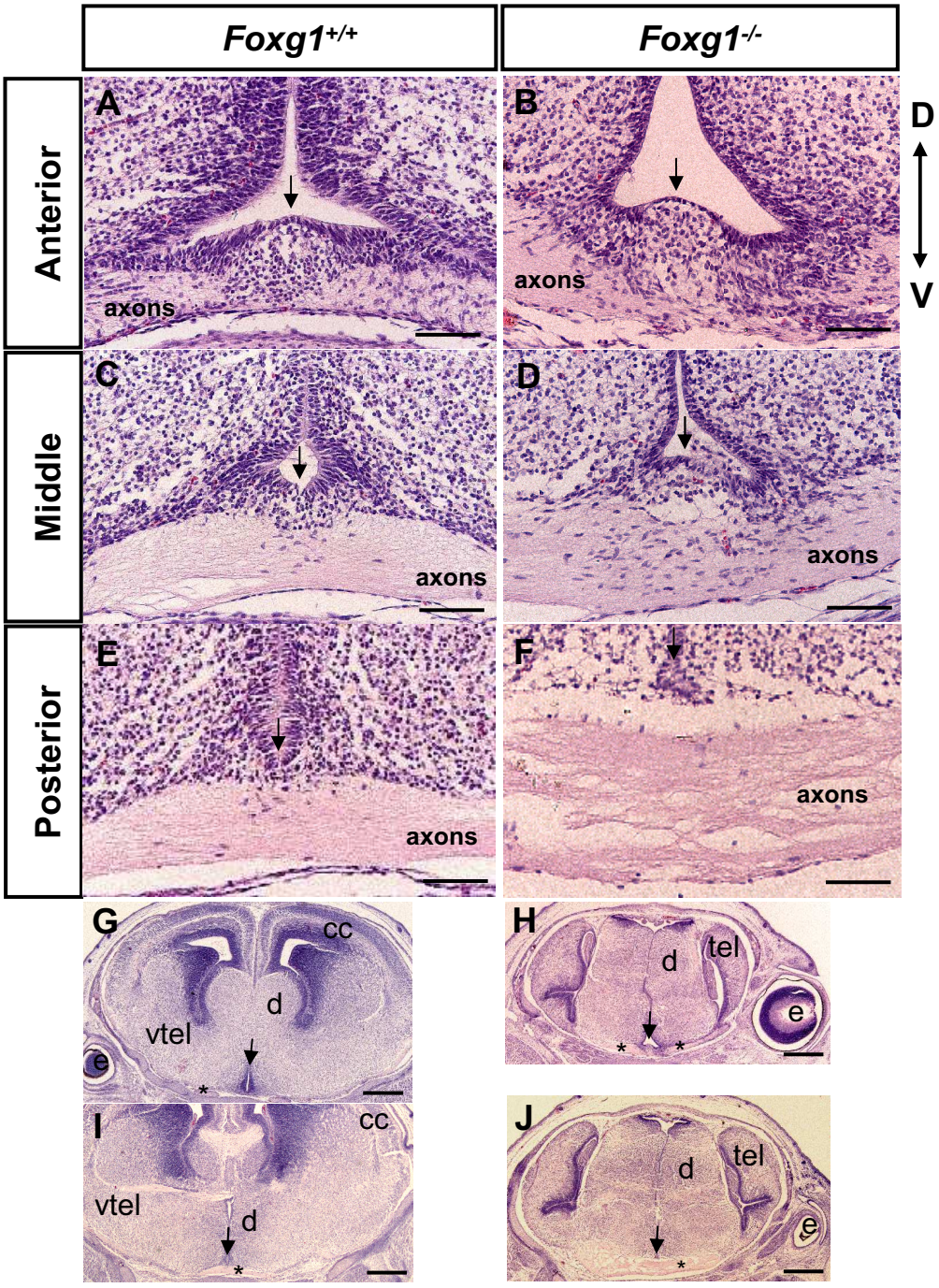

6.4.2. *Foxg1* activation occurs in similar chiasm regions in *Foxg1*$^{-/-}$ and wild type embryos.

Reporter mice carrying the *Foxg1*^{LacZ} reporter allele were used to investigate *Foxg1* activation at the optic chiasm of *Foxg1*$^{LacZ/LacZ}$ embryos. In sagittal sections at the brain midline, E14.5 *Foxg1*$^{LacZ/+}$ embryos displayed strong uniform lacZ staining in anterior forebrain regions, including the telencephalon, ganglionic eminences, nasal epithelium, Rathke's pouch and anterior hypothalamic regions (Figure 2A). Equivalent *Foxg1*$^{LacZ/LacZ}$ sections showed staining in the hypolastic telencephalon, Rathke's pouch, anterior hypothalamus and also a structure previously described as the vestigial ventral telencephalic neuroepithelium (Figure 2B). In both *Foxg1*$^{LacZ/+}$ and *Foxg1*$^{LacZ/LacZ}$ embryos, *Foxg1* activation occurred in the anterior chiasm, revealed by strong lacZ staining (Figures 2C, D). *Foxg1* activation was considerably reduced in the posterior *Foxg1*$^{LacZ/+}$ and *Foxg1*$^{LacZ/LacZ}$ chiasm, although scattered *lacZ*-expressing cells were visible. *Foxg1*$^{LacZ/+}$ embryos displayed a clearer boundary between the posterior and anterior *lacZ*-expressing region compared to *Foxg1*$^{LacZ/LacZ}$ embryos. In order to investigate *Foxg1* activation in greater detail and to obtain a clearer 3-dimensional representation, lacZ staining was performed on horizontal and coronal cryostat sections at E14.5 (Figure 3). Confirming the sagittal lacZ staining results, *Foxg1* activation was mainly restricted to anterior chiasm regions in both *Foxg1*$^{LacZ/+}$ and *Foxg1* null embryos (Figure 3). *Foxg1* activation in the anterior *Foxg1*$^{LacZ/LacZ}$ chiasm was reduced relative to *Foxg1*$^{LacZ/+}$ embryos latero-medially (compare Figures 3C, E, G to 3D, F, H). However, lacZ staining was stronger in postero-lateral regions of the *Foxg1*$^{LacZ/LacZ}$ hypothalamus. In more ventral regions, fewer lacZ-expressing cells were visible in both the *Foxg1*$^{LacZ/+}$ (Figure 3I) and *Foxg1*$^{LacZ/LacZ}$ (Fig. 3J, K) chiasm and lacZ-positive cells extended posteriorly along the midline.

Figure 2. *Foxg1* activation at the optic chiasm

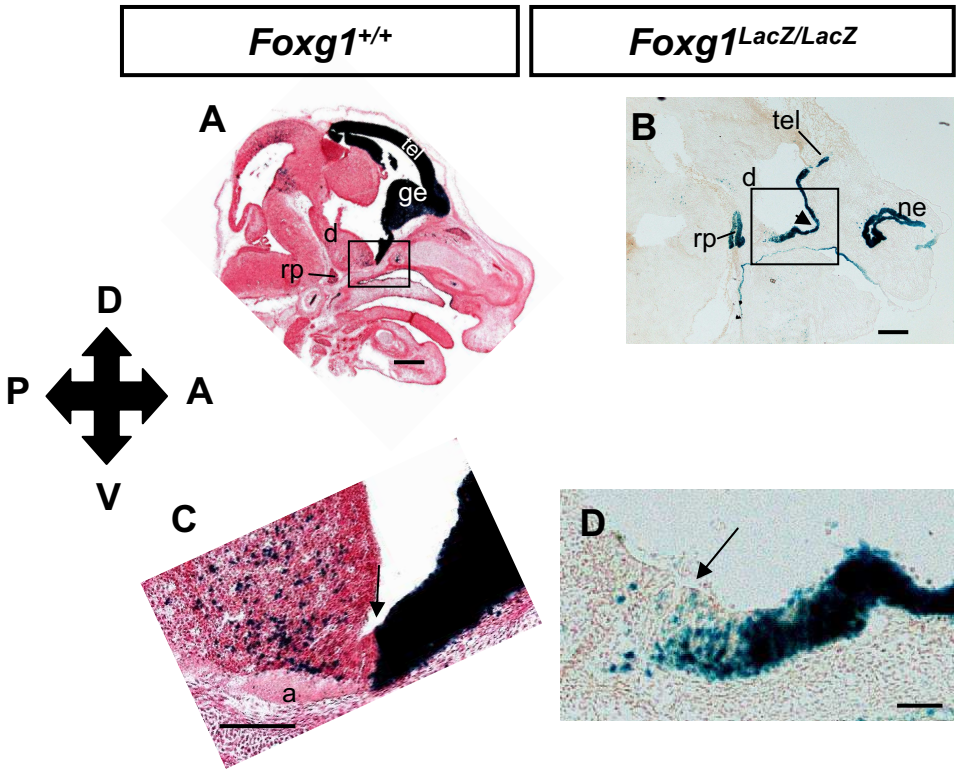

Figure 2. *Foxg1* activation at the optic chiasm.
X-gal staining of E14.5 cryostat sections from a (A, C) *Foxg1*$^{LacZ/+}$ and (B, D) *Foxg1*$^{LacZ/LacZ}$ embryo cut in the sagittal plane through the optic chiasm midline. *Foxg1*$^{LacZ/+}$ sections are counterstained with Nuclear Fast Red. (A) *Foxg1*$^{LacZ/+}$ midline section showing lacZ staining mainly in anterior brain regions: the telencephalon (tel), ganglionic eminences (ge), ventral diencephalon and Rathke's pouch (rp). (B) Equivalent *Foxg1*$^{LacZ/LacZ}$ section to (A) showing lacZ staining in the telencephalon, telencephalic neuroepithelium (arrow head), nasal epithelium (ne) and Rathke's pouch (rp). (C, D) High power magnifications of the optic chiasm midline shown as boxed areas in (A) and (B). (C) In the *Foxg1*$^{LacZ/+}$ chiasm, strong lacZ staining is present anteriorly and separated from the weaker staining posterior chiasm region by a sharp boundary delineated by an arrow. (D) In the *Foxg1*$^{LacZ/LacZ}$ chiasm, lacZ staining is found anteriorly but not posteriorly after the arrow. The boundary between lacZ-positive and lacZ-negative regions appears less clear than in the *Foxg1*$^{LacZ/+}$ chiasm. Abbreviations: a, axons; d, diencephalon; D, dorsal; V, ventral, A, anterior; P, posterior. Scale bars: 100μm in A - C; 50μm in D.

Figure 3. *Foxg1* activation at the optic chiasm.
X-gal staining of E14.5 cryostat sections from (A, C, E, G, I, L, O) *Foxg1*$^{LacZ/+}$ and (B, D, F, H, J, K, M, N, P) *Foxg1*$^{LacZ/LacZ}$ embryos. Serial horizontal sections through the same embryo: (A, C, E, G, I) *Foxg1*$^{LacZ/+}$ and (B, D, F, H, J, K) *Foxg1*$^{LacZ/LacZ}$. Serial coronal sections through the same embryo: (L, O) *Foxg1*$^{LacZ/+}$ and (M, N, P) *Foxg1*$^{LacZ/LacZ}$. All sections are counterstained with Nuclear Fast Red. Black arrows point to the chiasm midline. (A) *Foxg1*$^{LacZ/+}$ and (B) *Foxg1*$^{LacZ/LacZ}$ low power magnification images to show the plane of section. All *Foxg1*$^{LacZ/LacZ}$ images are ventral to (B). All *Foxg1*$^{LacZ/+}$ images are ventral to (A) apart from (C), which is a high power magnification of the chiasm region. (C – H) Strong lacZ staining is visible in cells in the anterior chiasm region in both (C, E, G) *Foxg1*$^{LacZ/+}$ and (D, F, H) *Foxg1*$^{LacZ/LacZ}$ embryos. LacZ staining in the *Foxg1*$^{LacZ/LacZ}$ chiasm occupies a narrower lateral – medial area compared to equivalent wild type sections. Fewer lacZ-expressing cells are seen ventrally in both the (I) *Foxg1*$^{LacZ/+}$ and (J, K) *Foxg1*$^{LacZ/LacZ}$ chiasm and lacZ-positive cells are found extending posteriorly along the midline. (K) is a high power magnification of the ventral chiasm midline in a section ventral to (J). (D, F, K) Axons (a) are visible laterally and anteriorly to the lacZ-positive cells in the *Foxg1*$^{LacZ/LacZ}$ chiasm but are not obvious in the *Foxg1*$^{LacZ/+}$ chiasm, presumably due to the intensity of lacZ staining obscuring them. In coronal sections in the (L) *Foxg1*$^{LacZ/+}$ and (M) *Foxg1*$^{LacZ/LacZ}$ anterior chiasm, lacZ staining is present at the midline dorsal to the axons and also among the dorsal-most part of the axon bundle. (N) is posterior to (M) and shows a narrowing of the lacZ staining region relative to (N). In posterior chiasm regions, (O) *Foxg1*$^{LacZ/+}$ and (P) *Foxg1*$^{LacZ/LacZ}$ embryos display fewer lacZ-expressing cells at the midline. Scale bars: A - J: 200μm, K – P, 50μm. Abbreviations: A, anterior; p, posterior; D, dorsal; V, ventral; hy, hypothalamus; a, axons; os, optic stalk; oc, optic chiasm, r, retina. Note: Figures (L) and (O) were kindly provided by Dr Thomas Pratt.

Figure 3. *Foxg1* expression at the E14.5 optic chiasm

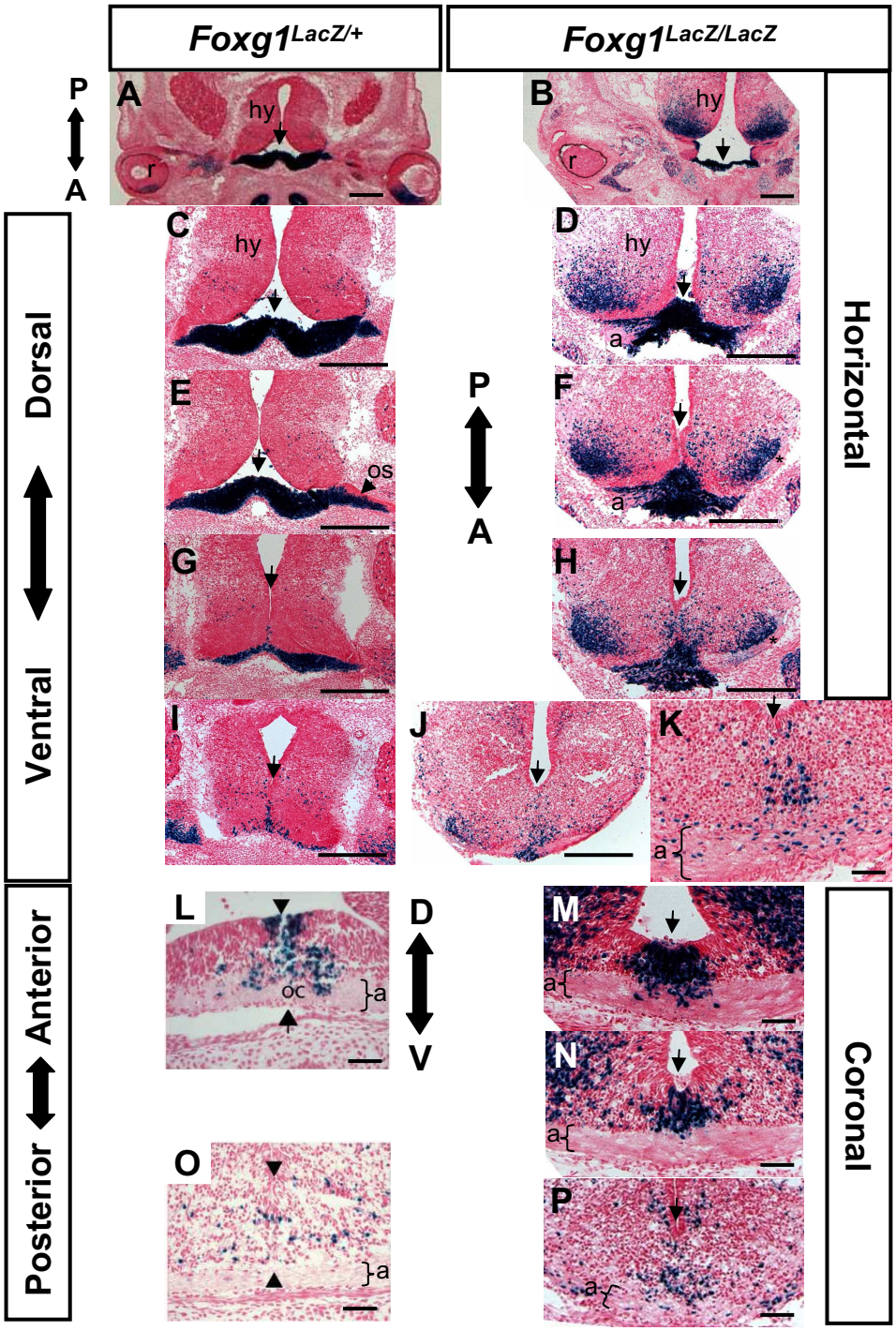

In horizontal sections, axons (pale pink) were visible adjacent to the lacZ-positive cells laterally in the *Foxg1*$^{LacZ/LacZ}$ chiasm (Figs. 3D, F) and also posteriorly along the lateral thalamus (asterisks in Figs. 3F, H). Axons were not visible in *Foxg1*$^{LacZ/+}$ embryos, presumably due to the intensity of lacZ staining obscuring them and the tighter fasciculation of wild type axons relative to *Foxg1* null axons. In coronal sections through the *Foxg1*$^{LacZ/+}$ and *Foxg1*$^{LacZ/LacZ}$ anterior chiasm, lacZ-positive cells were visible at the midline dorsal to the axons where they were found amongst the dorsal-most regions of the retinal axon bundle (Figs. 3L, M). In posterior chiasm regions, *Foxg1*$^{LacZ/+}$ and *Foxg1*$^{LacZ/LacZ}$ embryos displayed fewer *lacZ*-expressing cells at the midline (Figs. 3N, O, P).

6.4.3. SSEA-1 and CD44 are expressed at the *Foxg1*$^{-/-}$ optic chiasm in similar locations to the wild type.

At E13.5, SSEA1-positive neurons were arrayed posterior to the future optic chiasm in wild type (Figs. 4A, C, D) and *Foxg1*$^{-/-}$ (Figs. 4B, E) embryos in an inverted 'V' shape, with no evidence of an anterior expansion in the mutant. In the *Foxg1*$^{-/-}$ chiasm, the population of SSEA-1 neurons extended towards the lateral walls of the diencephalon as in the wild type (Figs. 4 C, D, E). Also, the cellular morphology of SSEA-1-positive neurons did not differ between *Foxg1*$^{-/-}$ and wild type chiasms (Figs. 4F, G). The posterior domains of SSEA-1 expression appeared to be wider in the *Foxg1* null diencephalon (Fig. 4E) compared to wild type embryos (Fig. 4C). One explanation for a wider SSEA-1 expression domain is that the molecular patterning of the posterior chiasm region is altered in *Foxg1*$^{-/-}$ embryos. Alternatively, the spatial expression pattern of SSEA-1 may be distorted as a result of abnormal morphological development of the *Foxg1*$^{-/-}$ ventral diencephalon.

Figure 4. SSEA-1 expression at the optic chiasm. SSEA-1 protein expression at the (A, C, D, F) wild type and (B, E, G) *Foxg1*$^{-/-}$ chiasm at E13.5. Sections are horizontal, anterior is up. Immunohistochemistry was performed using antibodies for SSEA-1. Downward-pointing arrows point towards the midline. (A) Wild type section through the optic chiasm showing SSEA-1-positive neurons arrayed in an inverted 'V'-shape. SSEA-1 expression is also evident in the optic nerves (on). (B) SSEA-1 expression in the *Foxg1*$^{-/-}$ optic nerve (on*). Note that the plane of section is slightly tilted such that the left side is ventral to the right. The SSEA-1-positive 'arm' of the 'V' is visible on the right side, but is less clear on the left, which is further ventral. (C, D) Wild type and (E) *Foxg1*$^{-/-}$ sections dorsal to (A) and (B) showing strong bilaterally symmetrical SSEA-1 expression posterior to the third ventricle. Expression extends postero-laterally in (C) and (E). Midline arrows in (C) and (E) point to the tip of the 'V'. (D) Wild type section dorsal to (C) showing SSEA-1 expression laterally on neuronal processes (black arrow) that is also visible in *Foxg1* nulls, shown by short arrows in (B) and (E). (F, G) High magnification showing the morphology of SSEA-1 neurons in (F) wild type and (G) *Foxg1*$^{-/-}$ posterior chiasm. (H) Wild type section showing SSEA-1 expression in cells of the optic stalk (see arrow). Abbreviations: on, optic nerve; os, optic stalk; r, retina; l, lens. Scale bars: A, B, C, D, E, H: 100μm; F, G: 50μm.

Figure 4. SSEA-1 expression at the optic chiasm

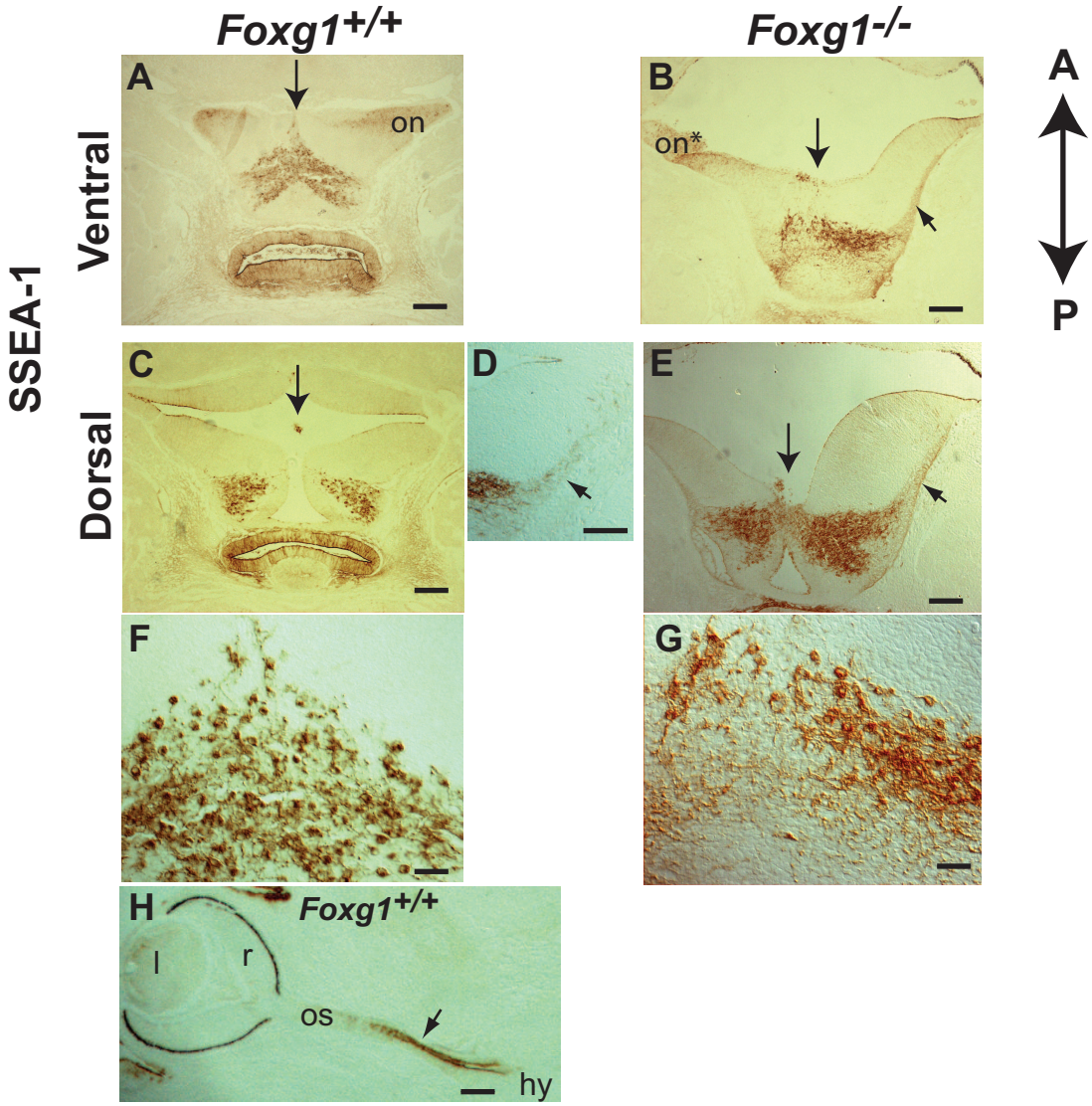

In coronal sections, at E15.5, SSEA-1 was expressed on cell surfaces and neuronal processes in the wild type and *Foxg1*$^{-/-}$ anterior lateral hypothalamus (Figs. 5C, F). CD44 expression was weakly expressed dorso-laterally to SSEA-1. In a section just posterior to the point where axons decussate, SSEA-1 and CD44 were observed on neuronal processes at the midline, dorsal to retinal axons (Figs. 5I – N). CD44 expression appeared to be slightly stronger in *Foxg1*$^{-/-}$ embryos and occupy a wider region, although this may be related to morphological differences between the *Foxg1* null and wild type diencephalon. In general, SSEA-1 and CD44 did not co-localise apart from small areas where their expression domains overlapped. In the posterior wild type and *Foxg1*$^{-/-}$ chiasm, SSEA-1 and CD44 expression was reduced at the midline but expression remained laterally (Figs. 5O – Z). High power magnifications showed that CD44 expression on cell surfaces and neuronal processes was present medially in comparison to SSEA-1 that was located in more lateral regions (compare Figs. 5V, Y to 5U, X). Examination of serial sections of wild type and *Foxg1*$^{-/-}$ embryos at E15.5 failed to show obvious differences in SSEA-1 expression. However, CD44 expression appeared to be slightly stronger in *Foxg1*$^{-/-}$ mid-chiasm sections than in wild types (compare Figs. 5J, M & 5P, S).

6.4.4. Nkx2.2 expression is maintained at the *Foxg1*$^{-/-}$ chiasm.

The transcription factor Nkx2.2 was chosen as a suitable optic chiasm marker because RGC axons normally grow through a domain of Nkx2.2 expression at the midline (Marcus et al., 1999). As for SSEA-1 and CD44, perturbations in Nkx2.2 expression might suggest abnormal development of the *Foxg1*$^{-/-}$ chiasm. Nkx2.2 expression was found at the wild type (Fig. 6E, G, I) and *Foxg1*$^{-/-}$ (Fig. 6F, H, J) optic chiasm. In *Foxg1* nulls there was no obvious spatial shift in the expression pattern of Nkx2.2, indicating that cells in the *Foxg1*$^{-/-}$ optic chiasm are able to express the regulatory gene Nkx2.2 normally. In conclusion, expression of Nkx2.2 as well as SSEA-1 appears relatively

Figure 5. SSEA-1 and CD44 expression at the optic chiasm.
SSEA-1 (red) and CD44 (green) immunohistochemistry at the optic chiasm of (A, C-E, I – K, O – Q, U – W) wild type and (B, F – H, L – N, R – T, X - Z) *Foxg1*$^{-/-}$ embryos at E15.5. Sections are arranged in rows from anterior to posterior. All sections are coronal and nuclei are counterstained with TO-PRO-3 (blue). White arrows point to the midline. Anterior sections through a (A) wild type and (B) *Foxg1*$^{-/-}$ chiasm showing the absence of SSEA-1 and CD44 protein at the midline. Axons (a) are visible as TO-PRO-3-negative regions approaching the midline laterally in both the wild type and mutant. (C – E) Wild type and (F – H) *Foxg1*$^{-/-}$ anterior chiasm just posterior to (A) & (B). Note that in the *Foxg1*$^{-/-}$ embryo, the right side is slightly posterior to the left. (C, F) SSEA-1 and CD44 (small white arrows in D, G) are visible in the lateral regions of the hypothalamus where CD44 is found dorso-laterally in relation to SSEA-1. In a section just posterior to the point where axons decussate, wild types (I – K) and *Foxg1* nulls (L – N) both display CD44 and SSEA-1 on neuronal processes lateral to and at the midline dorsal to axons. CD44 expression is more restricted to the midline, whereas SSEA-1 extends further laterally. (K, N) There is some co-localisation (yellow) between SSEA-1 and CD44 where their expression domains overlap near the midline but they do not co-localise extensively. (O – Q) Wild type and (R – T) *Foxg1*$^{-/-}$ sections just posterior to (I – N) showing a reduction in SSEA-1 and CD44 directly at the midline. (U – W) and (X – Z) High power magnifications of (O – Q) and (R – T) showing stronger lateral expression of SSEA-1 and CD44 but weak midline expression. Abbreviations: D, dorsal; V, ventral; a, axons. Scale bars: A, B, I – N: 100μm; C – H, O – T: 200μm; U – Z: 50μm.

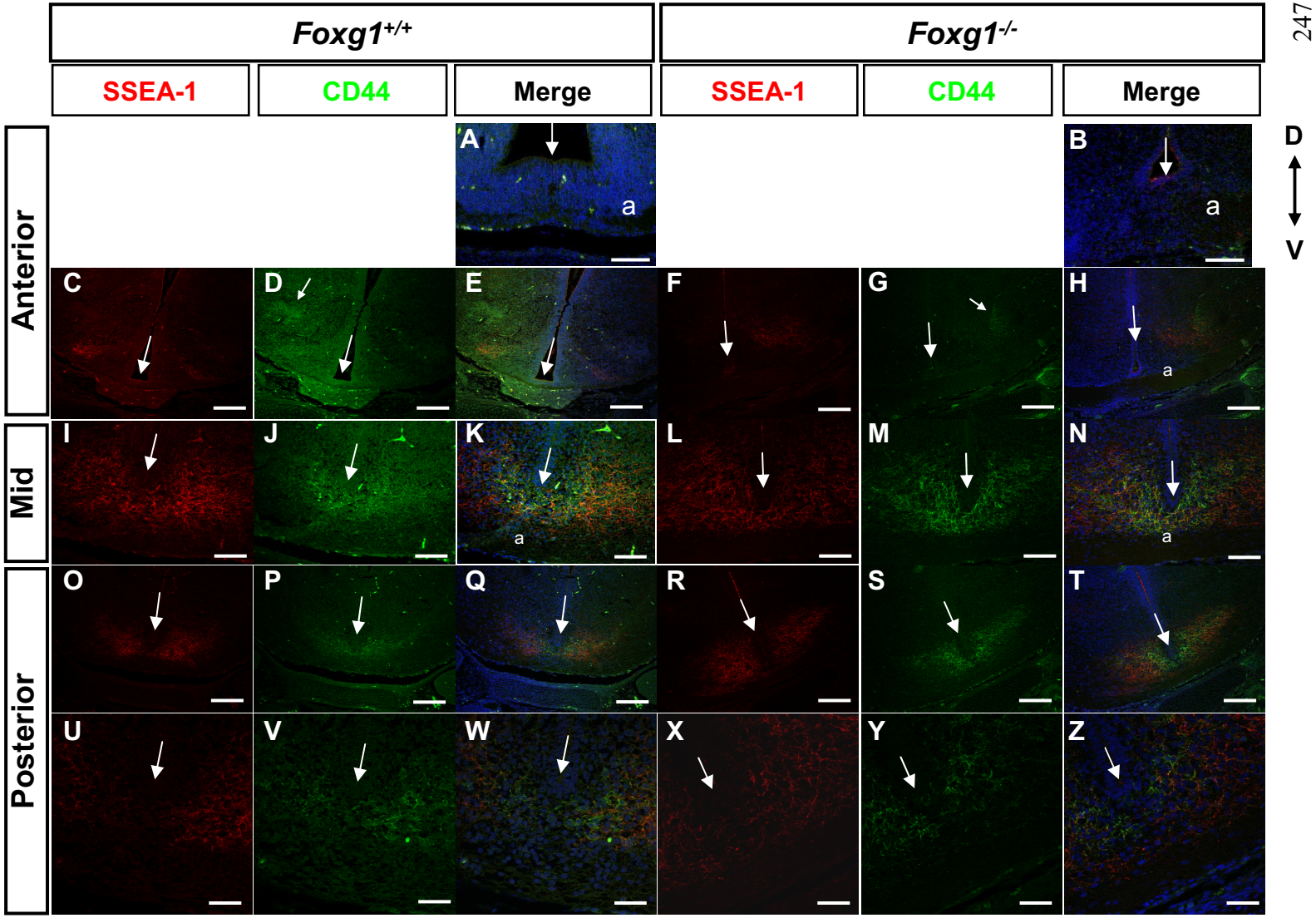
Foxg1+/+
Foxg1-/-
SSEA-1
CD44
Merge
SSEA-1
CD44
Merge
Anterior
Mid
Posterior
A
B
a
a
D
V
C
D
E
F
G
H
a
I
J
K
L
M
N
a
a
O
P
Q
R
S
T
U
V
W
X
Y
Z

Figure 6. Nkx2.2 expression at the E13.5 optic chiasm

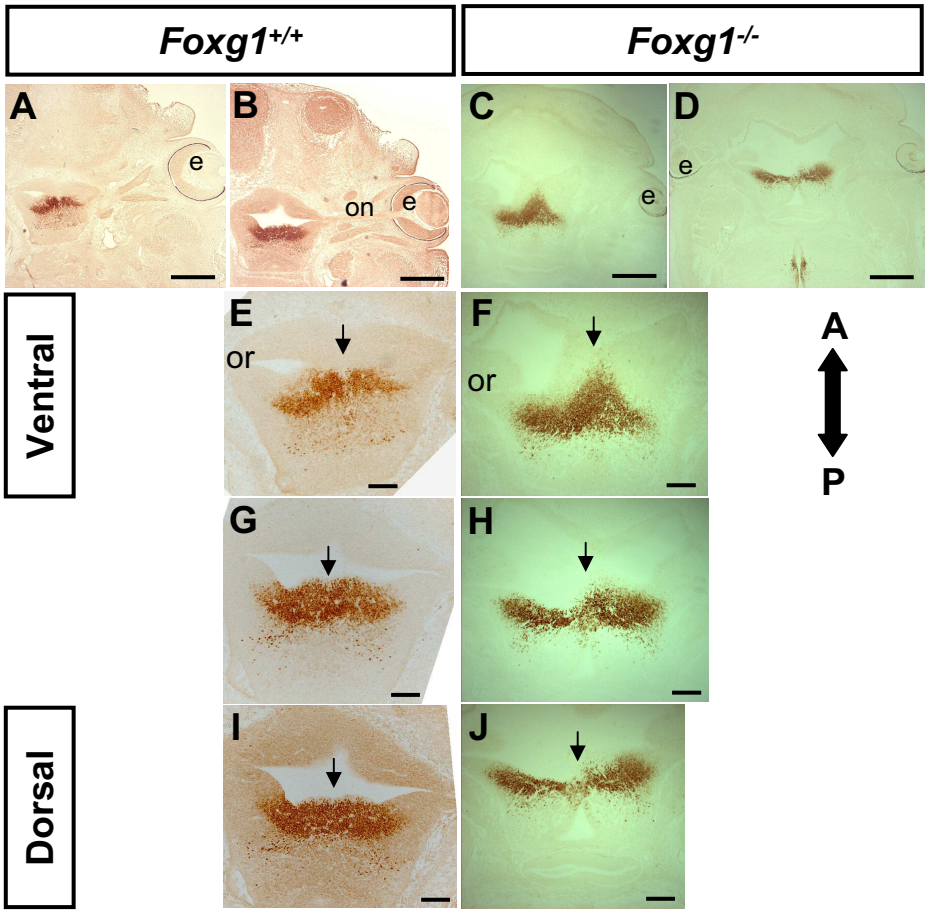

Figure 6. Nkx2.2 expression at the optic chiasm.
Nkx2.2 protein expression revealed by DAB at the (A, B, E, G, I) wild type and (C, D, F, H, J) *Foxg1*$^{-/-}$ optic chiasm at E13.5. All sections are horizontal with anterior pointing upwards. (A – D) Low power magnifications of equivalent ventral (A, C) and dorsal (B, D) sections in a wild type (A, B) and (C, D) *Foxg1*$^{-/-}$ embryo. (E – J) Series of high power magnifications of the chiasm region from ventral (E, F) to dorsal (I, J) show Nkx2.2 expression in cells directly at and lateral to the wild type and *Foxg1*$^{-/-}$ midline. Abbreviations: A, anterior; P, posterior; or, optic recess. Scale bars: A – D: 400μm, E – J: 100μm.

normal in *Foxg1*$^{-/-}$ embryos at the time when RGC axons are starting to project and interact with cells and guidance molecules at the optic chiasm.

6.4.5. Ephrin-B2 expression is maintained at the *Foxg1*$^{-/-}$ chiasm.

Ephrin-B2 is expressed by a palisade of midline radial glial cells at the chiasm, which control RGC axon divergence (Marcus & Mason, 1995; Marcus et al., 1995; Nakagawa et al., 2000; Williams et al., 2003). Although the shape of the diencephalon was slightly abnormal in *Foxg1* null embryos, expression of ephrin-B2 was maintained at both E13.5 (Figures 7A - D) and E16.5 (Figures 7E – H) at the chiasm midline. Strong ephrin-B2 expression was observed in the ventricular epithelium of the third ventricle at E13.5 (Figs. 7B, D) and E16.5 (Figs. 7E - H) and in horizontal sections the expression domain of ephrin-B2 spread laterally in more anterior regions (Figures 7E, H). Weak ephrin-B2 expression was seen in wild type and *Foxg1*$^{-/-}$ retinal axons at E16.5 (Figs. 7F, G) and in the wild type optic nerve (Fig. 7I).

Figure 7. Ephrin-B2 expression at the optic chiasm

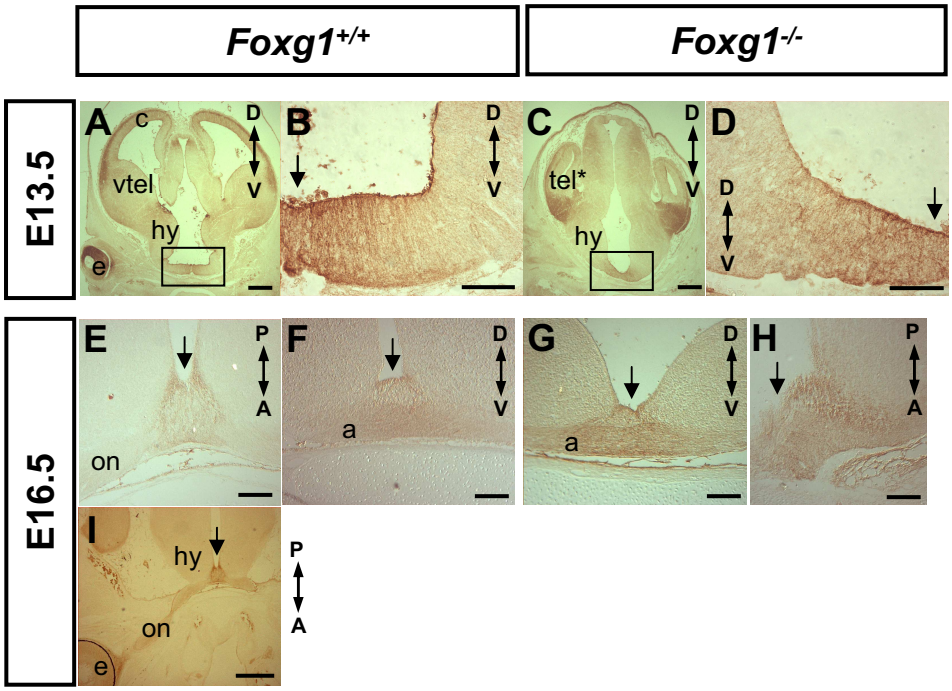

Figure 7. Ephrin-B2 expression at the optic chiasm.
Ephrin-B2 protein expression at the E13.5 and E16.5 (A, B, E, F) wild type and (C, D, G, H) *Foxg1*$^{-/-}$ chiasm. (A – D, F, G) are cut coronally, (E, H) are horizontal. (A, B) In the wild type at E13.5, ephrin-B2 is expressed in dorsal regions of the developing forebrain and eye and ventrally at the hypothalamus midline. (C) In the E13.5 *Foxg1*$^{-/-}$ embryos, ephrin-B2 is expressed in the hypoplastic telencephalon (tel*) and ventral hypothalamus. (B) Wild type and (D) *Foxg1*$^{-/-}$ high power magnifications of the ventral hypothalamus shown as boxed areas in (A) and (B) showing ephrin-B2 expression at the midline. (E, I) E16.5 wild type section showing ephrin-B2-expressing midline cells abutting the optic nerve. (E) High power magnification of chiasm region in (I). (H) E16.5 *Foxg1*$^{-/-}$ section equivalent to (E). As in (E), strong ephrin-B2 expression is present in the ventricular epithelium of the 3rd ventricle and spreads laterally in more anterior regions. Coronal sections of the E16.5 wild type (F) and *Foxg1*$^{-/-}$ (G) chiasm showing midline ephrin-B2 expression dorsal to axons that express ephrin-B2 weakly. Abbreviations: e, eye; cc, cerebral cortex; vtel, ventral telencephalon; tel*, mutant telencephalon; hy, hypothalamus. Scale bars: A, C, I: 200μm, B, D, E – H: 50μm. [Note: Immunohistochemical staining at E16.5 shown in Figures (E - I) was performed by Dr Thomas Pratt.]

6.5. DISCUSSION

During retinofugal development in *Foxg1*$^{-/-}$ embryos, the presence of a chiasm that resembles the wild type in morphology and the presence of RGC axons in their expected location relative to the ventral hypothalamus indicate that *Foxg1* expression is not essential for chiasm formation. This contrasts with achiasmatic animals that completely lack a physical chiasm structure (Williams et al., 1994) and also differs from the agenesis of the chiasm region in *Pax2* mutants (Torres et al., 1996). The lack of major anatomical abnormalities at the *Foxg1*$^{-/-}$ chiasm is surprising given the morphological defects of the eyes, hypoplastic telencephalon, unusually wide third ventricle and associated changes in the angle of the ventricular zone of the diencephalon away from the vertical relative to wild types. The latter may be due to the reduced size of the *Foxg1*$^{-/-}$ telencephalon, which lacks ventral tissue that may normally constrain the wild type diencephalon. The wider area and reduced fasciculation of *Foxg1*$^{-/-}$ retinal axons (this Chapter and Pratt et al., 2004) compared to wild type axons suggest either a fasciculation defect or simply the lack of a narrow channel to funnel axons to the midline, a role that is usually served by the optic stalk. The wide area occupied by retinal axons at the *Foxg1*$^{-/-}$ chiasm shares similarities with the dispersal of RGC axons over a larger region of the ventral surface of the diencephalon in *GAP-43* mutants (Sretavan and Kruger, 1998). However, *GAP-43* RGC axons are unable to form optic tracts after they leave the chiasm, unlike those of *Foxg1* null embryos.

6.5.1. *Foxg1* activation in the *Foxg1* null hypothalamus occurs in anterior chiasm cells as in the wild type.

Foxg1$^{LacZ/LacZ}$ and *Foxg1*$^{LacZ/+}$ embryos displayed *Foxg1* activation in cells of the anterior chiasm, including at the midline. Detailed examination of serial sections in the horizontal and coronal planes failed to reveal major differences in *lacZ* reporter expression between

Foxg1$^{LacZ/LacZ}$ and *Foxg1*$^{LacZ/+}$ embryos. These findings support those of the histological analysis showing that mutant chiasms are similar morphologically to *Foxg1*-expressing chiasms and that cells that would normally express *Foxg1* have not been deleted in *Foxg1* null embryos.

6.5.2. The expression patterns of SSEA-1, CD44 and Nkx2.2 are broadly maintained in *Foxg1*$^{-/-}$ embryos.

The expression patterns of SSEA-1, CD44 on *Foxg1*$^{-/-}$ chiasm neurons and of Nkx2.2 in *Foxg1*$^{-/-}$ chiasm cells displayed a similar pattern to those of wild type embryos, although their expression domains appeared slightly wider. In order to determine whether the wider spatial expression of these posterior chiasm markers is a consequence of abnormal molecular patterning of the chiasm or distortion of the *Foxg1*$^{-/-}$ diencephalon, *Foxg1* could be conditionally knocked out specifically in cells of the ventral hypothalamus once it has formed. Any changes in SSEA-1, CD44 and Nkx2.2 expression could then be attributed to molecular changes rather than distorted chiasm morphology.

There were indications that CD44 expression was slightly stronger in the *Foxg1*$^{-/-}$ chiasm neurons. Since immunohistochemistry is not an accurate method of quantifying protein expression and the fact that other embryonic ages were not examined due to a lack of *Foxg1*$^{-/-}$ tissue, it would be interesting to investigate the possibility of greater CD44 protein expression at the E13.5 to E16.5 *Foxg1*$^{-/-}$ chiasm quantitatively by Western blotting. Investigation of more brains at these ages would also eliminate the possibility of variation in the intensity of antibody staining between wild type and *Foxg1*$^{-/-}$ embryos. This is considered unlikely given that wild type and *Foxg1*$^{-/-}$ embryos were processed in parallel under identical conditions. It is tempting to speculate that the stronger expression of CD44 in the *Foxg1*$^{-/-}$ diencephalon at E15.5, demonstrated by brighter antibody staining, might be responsible for the increased ipsilateral routing of retinal axons.

Evidence for this comes from previous findings of a reduced ipsilateral projection in brain slices of the E15.5 mouse visual pathway when CD44 was disrupted (Lin et al., 2003). Interestingly, the ipsilateral projection is unaffected at earlier ages prior to the formation of the permanent ipsilateral projection, yet CD44 is critical for the decussation of contralateral axons. This implies that CD44 specifically promotes the uncrossed routing of axons and that the response of retinal axons to chiasmatic CD44 varies with developmental age.

Although the spatiotemporal expression patterns of SSEA-1, CD44 and Nkx2.2 did not show major differences between *Foxg1*$^{-/-}$ and wild type embryos, it remains possible that *Foxg1*$^{-/-}$ retinal axons interact with chiasm cells and neurons in a different way to wild types, for example, by following a different path along the borders of their expression domains. An interesting follow-up experiment would be to fluorescently label a few RGC axons using focal DiI or rhodamine-dextran injections in the *Foxg1*$^{-/-}$ and wild type retina. Combined with immunohistochemistry for the chiasm molecules mentioned in this chapter it would be possible to observe how ipsilateral and contralateral axons interact with these chiasm markers in a similar way to that used by Erskine et al. (2000).

Another way in which *Foxg1*$^{-/-}$ retinal axons could behave differently at the chiasm despite apparently normal expression of chiasm molecules is through exposure to a different environment. A recent study showed that selective inhibition of retinal axons from the VT retina to chondroitin sulphate only occurred when axons were grown in the presence of laminin and polylysine that supports growth but not in their absence (Cheung et al., 2005). Laminin-1 can convert netrin-mediated attraction of *Xenopus* retinal growth cones to repulsion by changes in cAMP levels (Hopker et al., 1999; Shewan et al., 2002). *Foxg1*$^{-/-}$ embryos never develop an optic stalk, where axons normally contact laminin deposits from astroglial cells (Liesi and Silver, 1988) and other molecules, including CSPGs, HSPGs and SSEA-1. These interactions may normally prime retinal axons from different regions in the retina to interact in characteristic ways with guidance cues and

cells at the chiasm, rather like road signs providing directional information to motorists prior to junctions. In the absence of pathway-derived experience from the optic stalk, *Foxg1*$^{-/-}$ retinal axons may diverge abnormally despite experiencing a relatively normal molecular environment at and surrounding the chiasm midline itself. However, this hypothesis is thought to be unlikely because in Chapter 3, *Foxg1*$^{-/-}$ retinal explants co-cultured with *Foxg1*$^{-/-}$ chiasm cells still displayed reduced axon outgrowth relative to control co-cultures, even though the *Foxg1*-expressing retinal axons do not grow through an optic stalk and the only factors influencing axon growth were those present in the retina or chiasm.

Investigation of Shh expression at the chiasm is an area for future work because Shh has been shown to be involved in the guidance of retinal axons at the optic chiasm (Trousse et al., 2001) and recently it has been shown to act as an axon guidance molecule itself (Charron et al., 2003). Shh is also important for proper morphogenesis of the retina and optic stalk (Dakubo et al., 2003), structures that develop abnormally in *Foxg1*$^{-/-}$ embryos, raising the possibility that the expression of Shh is altered in the forebrain of the *Foxg1* null mouse. Previous findings revealed that *Shh* mRNA was maintained in the *Foxg1*$^{-/-}$ ventral diencephalon despite loss of *Shh* expression from the *Foxg1*$^{-/-}$ telencephalon at E10.5 (Huh et al., 1999). However, the expression pattern of Shh in the chiasm region at later embryonic ages during the period of retinal axon navigation through the chiasm is unknown, as is the expression pattern of Shh expression in the *Foxg1* null eye. Increased Shh expression around the chiasm region has previously been associated with a 100% ipsilateral projection in *Pax2* null embryos (Torres et al., 1996). In order to test the hypothesis of altered Shh expression at the *Foxg1*$^{-/-}$ chiasm, *Shh* qRT PCR on chiasm tissue and immunohistochemistry for Shh protein would be required. A read-out of Shh signalling could also be assessed by measuring transcript levels of the Shh receptors *patched* (*Ptch*) and *Gli* by qRT PCR.

6.5.3. Ephrin-B2.

Immunohistochemistry revealed that the expression pattern of ephrin-B2 at the *Foxg1*$^{-/-}$ optic chiasm is not altered or dramatically expanded compared to wild types at E13.5 or E16.5, although the shape of the *Foxg1*$^{-/-}$ chiasm is slightly different (published in Pratt et al., 2004). Ephrin-B2 is expressed by midline radial glia and at high power magnifications, the ephrin-B2-expressing glial cell processes were observed running dorso-ventrally in wild types. The presence of ephrin-B2 expression in *Foxg1*$^{-/-}$ chiasm cells indirectly suggests that the midline glial specialization is present as in the wild type. Nevertheless, given more time and access to *Foxg1* null embryos, it would be prudent to confirm the presence of these glial cells using standard radial glial markers, such as RC2 and GLAST (Marcus et al., 1995). Immunohistochemistry is at best only semi-quantitative (staining intensity can only be compared on the same section), the possibility remains that the quantitative expression of ephrin-B2 increases. This can be resolved using quantitative real-time PCR and Western blots to quantify mRNA and protein levels respectively.

Chiasm neurons are a heterogeneous population in terms of surface antigen expression. In addition to SSEA-1 and CD44, they also express chondroitin sulphate (Chung et al., 2000b) and the growth-promoting molecules L1 and NCAM (Sretavan et al., 1994; Lustig et al., 2001). These molecules are all prime candidates for influencing the route taken by retinal axons and may regulate the availability of growth-inhibitory and growth-promoting cues to axons. Enzymatic removal of chondroitin moieties in the E13.5 mouse results in the stalling or misrouting of the majority of axons (Chung et al., 2000a, 2000b). However, when chondroitin is eliminated at later ages, the ipsilateral projection is reduced but contralateral axons remain unaffected. It follows that an increased ipsilateral projection could result if the expression of chondroitin sulphate proteoglycans (CS-PGs) increases at the chiasm. However, it is unlikely that the situation is so straightforward since CS-PGs are also expressed in the retina (Chung et al., 2000b), have been shown to

maintain fiber order in the optic nerve (Leung et al., 2003) and the addition of exogenous CS-PGs can disrupt axons in similar ways to CS-PG removal (Anderson et al., 1998; Walz et al., 2002). Chiasm neurons also express heparan sulphate, which are glycosaminoglycan polysaccharides that are found on a structurally diverse group of extracellular matrix proteins called heparan sulphate proteoglycans (HSPGs). Modifications to the sulphation status of heparan sulphate have been shown to affect the response of navigating growth cones to Slit2, a guidance molecule expressed around the chiasm (Pratt et al., 2006). In fact, heparan sulphate is one of the sugar moieties present on CD44 and has been shown to sequester axon growth-promoting factors (Bennett et al., 1995; Chung et al., 2001; Jones et al., 2000; Lin et al., 2002; Walz et al., 1997). The lack of antibodies for HSPGs and their huge structural diversity rendered it unfeasible to conduct a comprehensive investigation of HSPG expression at the *Foxg1*$^{-/-}$ chiasm. Nevertheless, all these chiasm molecules are suitable candidates for future study and given the diversity of molecules expressed in the vicinity of the chiasm, it is probable that a variety of different cues, rather than a single 'master cue', is required for axon divergence at the midline.

6.5.4. Slits.

Slit proteins are expressed in the ventral diencephalon (Erskine et al., 2000; Pratt et al., 2006) but are absent from the ventral midline and have not been associated with ipsilateral-contralateral axon pathfinding at the chiasm. However, they are involved in channeling retinal axons and preventing them from wandering inappropriately from their correct tracts into neighbouring tissue (Plump, 2002; Pratt et al., 2006; Thompson et al., 2006a, 2006b). Moreover, expanded Slit2 expression has been shown to affect the routing of retinal axons in *Foxd1* null embryos, which display an increased ipsilateral projection among other projection abnormalities (Herrera et al., 2004). Examination of

Slit2 spatial and temporal expression at the chiasm as well as quantification using qRT PCR is a project for the near future.

In conclusion, no obvious defects in the cellular and molecular architecture of the *Foxg1*$^{-/-}$ chiasm were observed during the period when retinal axons project to the chiasm. This does not exclude a chiasm abnormality but rules out changes in a couple of major players in retinal axon guidance.

CHAPTER 7: The expression profile of Foxg1 protein.

7.1. ABSTRACT

Foxg1 protein expression was more widespread but found in the same locations as the pattern of *Foxg1* mRNA expression observed previously by *in situ* hybridization and in $Foxg1^{LacZ}$ reporter mice. In the retina, Foxg1 protein was expressed more widely than the mRNA with expression throughout all retinal layers, although some sections revealed slightly stronger expression in the nasal retina, resembling $Foxg1^{LacZ}$ reporter expression. Foxg1 protein appeared to be more strongly expressed in the retina at E13.5 compared to the later age of E14.5. Foxg1 protein was expressed in both cells and axons at the optic chiasm, the latter of which suggests a more direct role in the guidance of axons from within the growth cone. It is not known whether Foxg1 is expressed in both contralateral and ipsilateral axons or if its expression is restricted to nasal RGC axons in which Foxg1 is most prominent. Future investigation into the exact role(s) of Foxg1 in retinal axons and its interacting partners will help to further understanding of the functions of this transcription factor in axon guidance.

7.2. INTRODUCTION

Axons navigate over large distances with the consequence that the distance between growth cones and their cell bodies becomes larger as axons grow further from their origins towards their targets. The growth cone often has to make rapid steering decisions upon encountering a new molecular or cellular environment and it is unlikely that such a swift response could occur if navigation relied on protein synthesis from the cell body alone (Campbell and Holt, 2001). Growth cones that are cut off from their axons and cell bodies are still capable of growing in culture, showing that they can steer

independently in the absence of a connection with the cell body (Shaw and Bray, 1977). Growth cones from retinal axons can also steer correctly *in vivo* following separation from their cell bodies (Harris et al., 1987). These early studies prompted investigations into the contents of growth cones leading to findings that they contain mRNAs (Crino and Eberwine, 1996) as well as machinery for translation (Crino and Eberwine, 1996; Davis et al., 1992) and protein degradation (Campbell & Holt, 2001). The hypothesis that growth cones synthesize proteins locally in order to steer directionally in response to axon guidance cues was supported by *in vitro* findings in which growth cone steering was abolished by inhibiting protein synthesis (Campbell & Holt, 2001).

Recent findings have shown that Foxg1 protein is present in *Xenopus* olfactory axons and also in the mouse E15.5 cortex where it can be regulated post-translationally (Regad et al., 2007). This raises the possibility that Foxg1 protein is also present in retinal axons where it could influence guidance decisions by the navigating growth cone. The availability of a Foxg1 antibody made it possible to compare the expression patterns of *Foxg1* mRNA and protein in the developing mouse forebrain. These observations are the first known descriptions of the localization of Foxg1 protein in the mouse retina and ventral diencephalon.

7.3. METHODS

7.3.1. Mice.

Wild type (CBA) embryos were taken at E13.5 and E14.5.

7.3.2. Foxg1 immunohistochemistry.

Immunohistochemistry on 10μm thick wax sections was conducted as for Nkx2.2. Slides were blocked in 5% goat serum, 0.2% BSA and 0.1% Triton-X-100 in PBS. Primary antibody incubation: sections were reacted with the rabbit polyclonal Foxg1 antibody (Abcam ab18259, 1:30 dilution) overnight at 4°C followed by final detection using the Envision+ (Rabbit) Kit (Dako K4010) following the manufacturers instructions.

7.4. RESULTS

The expression of Foxg1 protein was investigated by immunohistochemistry at E13.5 and E14.5. Foxg1 expression was observed in the wild type retina, anterior ventral hypothalamus and optic chiasm region, optic stalks, lens, nasal epithelium (Figure 1), telencephalon and ganglionic eminences (Figure 2). As expected, Foxg1 protein was absent from all *Foxg1*$^{-/-}$ forebrain structures at E14.5 (Fig. 3). Most importantly for this thesis, close examination of serial sections showed that Foxg1 expression was absent from the eyes, anterior thalamus and hypoplastic telencephalon (Fig. 3A). Although some weak DAB staining was observed in the hindbrain, at higher magnifications this appeared to be non-specific (Fig. 3B). The low background for this antibody also improved confidence in the validity of Foxg1-expressing regions observed in the wild type embryos.

7.4.1. Foxg1 expression in the retina.

In the E13.5 wild type retina, Foxg1 protein was found in all layers of the retina. However, in some dorsal and ventral regions, a shallow high nasal to low temporal

Figure 1. Foxg1 expression in the eyes, optic chiasm cells and retinal axons.

Foxg1 immunohistochemistry revealed by DAB staining. (A - N, Q - S) E13.5 and (O, P) E14.5 wild type embryos. All sections are horizontal. Vertical arrows in (Q, R, S) indicate the position of the midline. (A - G) Ventral to dorsal series showing Foxg1 expression in the retina, anterior ventral hypothalamus, optic stalks, lens and nasal epithelium. (D - G) Foxg1 expression is limited to the anterior diencephalon. (H, I) Ventral retina showing Foxg1 expression in all retinal layers. Strong expression is seen nasally in the outermost retinal layer adjacent to the RPE. (J) Weak staining visible in the optic nerve. (K) Medial retinal section just dorsal to the optic stalks showing expression in all retinal layers and the lens. (L, M) Dorsal retina showing a low to high temporal to nasal shallow gradient. (N) Section dorsal to (M) showing strong expression medially with weaker expression in outer layers and laterally. (O, P) E14.5 retinas. Section (P) is dorsal to (O). (O) Ventral retina showing Foxg1 expression limited to the outermost nasal retinal layer. (P) Foxg1 expression in all retinal layers but slightly stronger expression nasolaterally. (Q) Foxg1 expression in axons in the ventral optic chiasm and in a few cells at the midline posterior to axons. (R) Dorsal to (Q) showing axons entering the optic tract in the lateral hypothalamus. (S) Nuclear Foxg1 expression in anterior chiasm cells. Abbreviations: r, retina; l, lens; hy, hypothalamus; on, optic nerve; d, diencephalon; ne, nasal epithelium; RP, Rathke's pouch; V3, 3rd ventricle; N, nasal; T, temporal. Scale bars: A - G, S: 200μm, H - N, O, P, Q, R: 100μm.

Figure 1. Foxg1 protein expression in the retina & chiasm

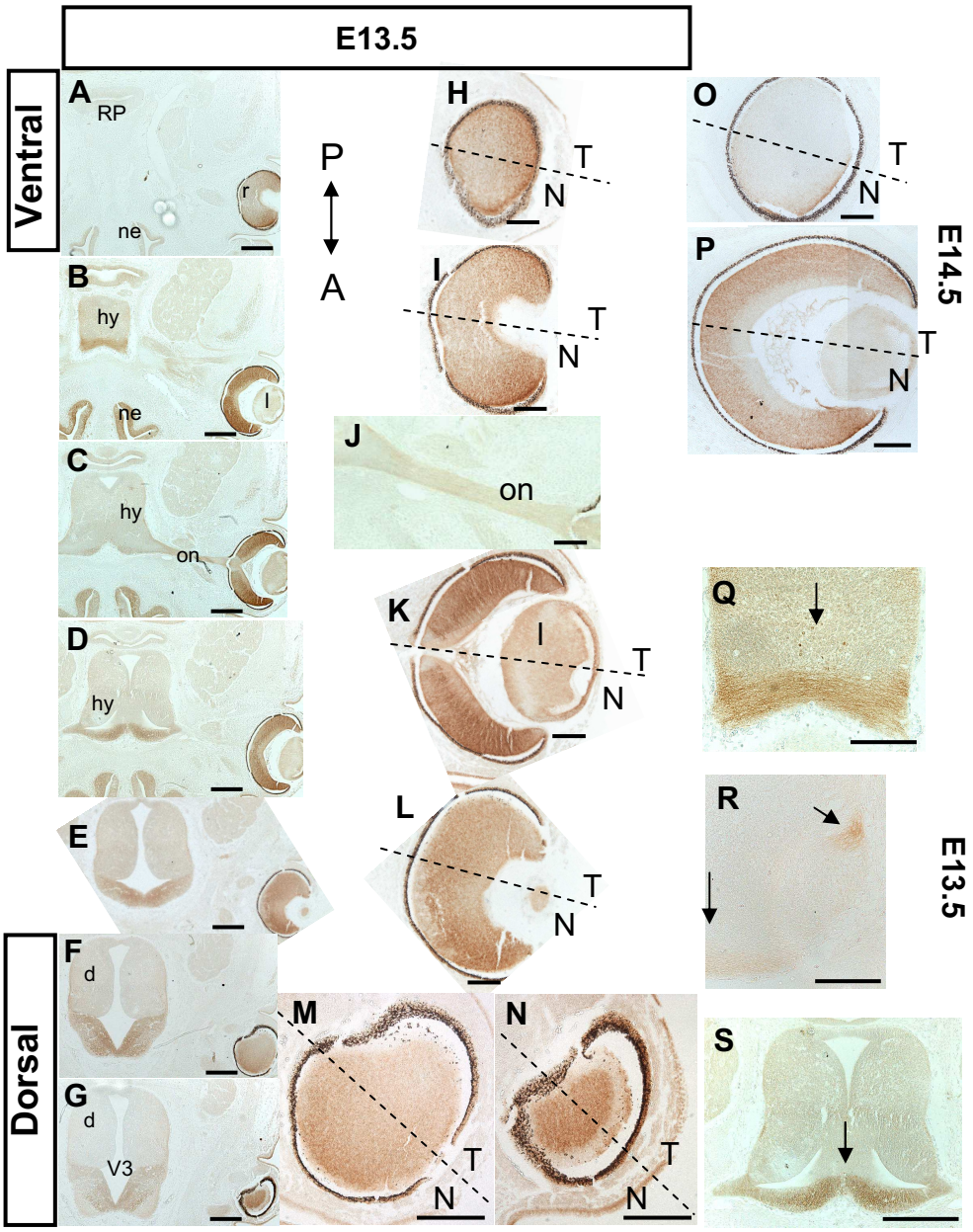

Figure 2. Foxg1 expression in the telencephalon.
Foxg1 immunohistochemistry in wild type embryos. (A, B) Coronal E13.5 sections. (C) Horizontal E14.5 section. (A, B) E13.5 embryos show strong Foxg1 expression in the telencephalon and weaker expression in the ganglionic eminences. (B) section posterior to (A) showing telencephalic expression. (C) Horizontal E14.5 section through the dorsal brain showing telencephalic expression. Abbreviations: tel, telencephalon; GE, ganglionic eminence; r, retina; on, optic nerve; d, diencephalon; dt, dorsal thalamus. D, dorsal; V, ventral; A, anterior; P, posterior. Scale bars: A, B: 200μm, C: 100μm, D: 500μm.

Figure 3. Foxg1 protein expression is absent from *Foxg1*$^{-/-}$ embryos.
Foxg1 immunohistochemistry performed on an E14.5 *Foxg1*$^{-/-}$ embryo. Sections are horizontal and are not counterstained. (A) Anterior brain structures, including the eyes, anterior thalamus and hypoplastic telencephalon lack Foxg1 protein. The borders of the thalamus and left telencephalon are marked with a dotted line. (B) Posterior to (A) but sectioned at the same dorsoventral level, showing weak non-specific staining in the hindbrain but not in the thalamus. The thalamus-hindbrain border is shown with a dotted line. Abbreviations: RPE, retinal pigment epithelium; tel; telencephalon; t, thalamus; V3, third ventricle; h, hindbrain. Scale bars: 500μm.

Figure 2. Foxg1 expression in the telencephalon

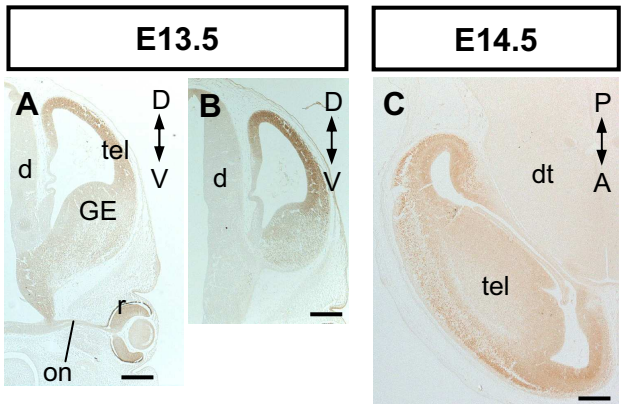

Figure 3. Foxg1 protein expression is absent from *Foxg1*$^{-/-}$ embryos

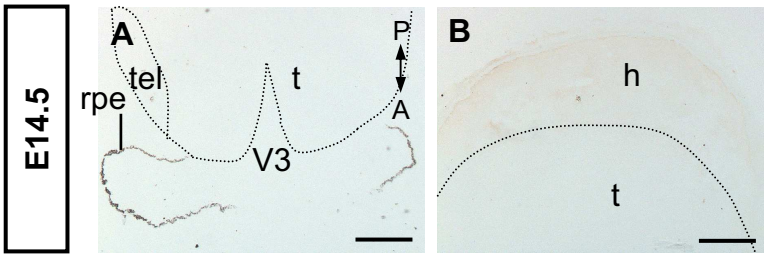

gradient was observed (Figs. 1L, M). Ventrally, strong expression was found concentrated in the outermost layer of the nasal retina adjacent to the RPE (Figs. 1H, I). In medial sections at the level of the optic stalks, Foxg1 was expressed in the entire retina, although the outer retinal layers tended to show stronger expression. In the E14.5 wild type retina, strong expression in the outermost nasal retinal cells was observed ventrally, whereas weaker expression was seen in the ventrotemporal region (Fig. 1O). Foxg1 expression was not as strong in the E14.5 retina compared to the E13.5 retina, particularly in the VT retina (compare Figs. 1H & 1O). In more medial sections, Foxg1 was located in all retinal layers, although the outer layers expressed protein more strongly as at E13.5 (Fig. 1P). The strongest expression was found laterally in the region of the CMZ in nasal retina.

7.4.2. Foxg1 expression in optic chiasm cells.

Foxg1 protein was also expressed by cells of the anterior hypothalamus, including the optic chiasm region (Figs. 1D - G, S). There was an obvious boundary between the Foxg1-expressing anterior hypothalamus and Foxg1-negative posterior regions of the diencephalon (Figs. 1D - G). Foxg1 was localized within the nuclei of chiasm cells (Fig. 1S).

7.4.3. Foxg1 expression in retinal axons.

Foxg1 was also expressed in retinal axons in the optic nerve (Fig. 1C, J), at the ventral optic chiasm (Fig. 1Q) and in the optic tracts (Fig. 1R) at E13.5 and E14.5.

7.5. DISCUSSION

7.5.1. Foxg1 protein is widespread in the retina.

Restriction of Foxg1 protein to anterior regions of the hypothalamus, including the future optic chiasm, mirrors the results observed in *Foxg1*^{LacZ} reporter mice (Chapter 6 this thesis) and by *in situ* hybridization (Hatini et al., 1994; Huh et al., 1999). However, in the eyes, expression of Foxg1 protein was more widespread in the retina than predicted from expression of the *Foxg1*^{LacZ} reporter allele and previous *in situ* hybridization findings (Chapter 5, Hatini et al., 1994; Huh et al., 1999). A nasal bias was observed in some dorsal and ventral sections, but in sections midway between the dorsal and ventral surfaces, Foxg1 appeared to be expressed evenly across nasal and temporal retina. Foxg1 protein did not appear to be located in the nucleus in the retina and neither was it concentrated in the RGC layer. In fact, at E14.5, protein levels in the inner retinal layer were noticeably weaker compared to outer layers, which is the inverse of the pattern of mRNA expression, which showed strongest staining in the RGC layer (Chapter 5). These observations imply that Foxg1 protein diffuses away from sites of Foxg1 mRNA transcription and translation, influencing cells that never express *Foxg1* non-autonomously. At E13.5, Foxg1 protein was expressed more strongly in the retina, particularly in VT regions, compared to E14.5 retinas. In Chapter 4 it was hypothesized that Foxg1 might repress Zic2 in the nasal retina based on the finding of an increased proportion of Zic2-expressing RGCs in the *Foxg1* null nasal retina only. The reduction in levels of Foxg1 protein in the VT retina from E13.5 to E14.5 coincides with the onset of Zic2 expression in the VT periphery (Herrera et al., 2003). Further detailed Foxg1 immunohistochemical and quantitative analyses (using Western blotting) are required at these embryonic ages to study this phenomenon in greater depth and to ensure that the observation of reduced Foxg1 protein at E14.5 is reproducible. Performing double immunohistochemistry to visualize the location of both Foxg1 and Zic2 proteins and Western blotting to quantify levels of Foxg1 and

Zic2 proteins in the retina would be ideal to investigate whether there are actual changes in the levels and/or spatial expression domains of these two proteins during development and if so, whether they are spatiotemporally correlated.

7.5.2. Foxg1 protein is present in retinal axons.

Foxg1 was found in retinal axons in the optic nerves, at the chiasm and in the optic tracts. At present, the role of Foxg1 in axons remains speculative. It is plausible that Foxg1 protein is transported along axons from the cell body of RGCs where Foxg1 mRNA is located (Chapter 5; Hatini et al., 1994; Pratt et al., 2004), perhaps influencing the navigating growth cone. It is unlikely that Foxg1 protein is synthesized locally within the growth cone because no evidence (in the literature or this thesis) exists of Foxg1 mRNA in retinal axons. The results presented here cannot tell whether Foxg1 protein is located within the growth cone of axons. This could be examined by fluorescence immunohistochemistry for Foxg1 and confocal imaging at high magnifications to visualize whether Foxg1 is actually present in the growth cone. If Foxg1 is present within the axon and growth cone, the question of whether Foxg1 is synthesized locally within growth cones could be addressed by applying inhibitors of protein synthesis, such as cycloheximide, to growth cones separated from their retinal axons. If Foxg1 protein is still detected following cycloheximide treatment, it is more likely that Foxg1 protein is synthesized in the RGC and transported along axons rather than locally within the growth cone.

Foxg1 has been shown to have both DNA-dependent and DNA-independent mechanisms of action in controlling progenitor cell proliferation and differentiation in the neocortex (Hanashima et al., 2002) and also in nasal-temporal patterning in the chick retina (Takahashi et al., 2003; Yamagata et al., 1999; Yuasa et al., 1996). It is not known whether both DNA-binding and DNA-binding-independent mechanisms apply in the mouse retina and/or optic chiasm, since no studies to date have investigated this.

If so, Foxg1 may play a dual role both as a transcription factor and as a protein that has DNA-independent effects in the guidance of retinal axons, as discovered for En-2 (Brunet et al., 2005; Collinson et al., 2004; Collinson et al., 2000; Joliot and Prochiantz, 2004; Lesaffre et al., 2007; Prochiantz, 2000; Prochiantz and Joliot, 2003). The expression of Foxg1 protein across the whole retina suggests that Foxg1 diffuses from its site of production to retinal cells that do not express *Foxg1*, where Foxg1 protein could potentially have DNA-binding-independent effects.

Within retinal axons, Foxg1 may regulate the translation of local mRNAs, leading to the synthesis of a particular complement of proteins that participate in the signaling cascades resulting from guidance cue and receptor binding, or the production of receptors inserted into the leading edge of the growth cone. A transcription factor that has been reported to play a role in retinotectal mapping via internalization into retinal growth cones and the subsequent local synthesis of new proteins is the homeoprotein Engrailed-2 (En-2) (Brunet et al., 2005; Itasaki et al., 1991; Itasaki and Nakamura, 1996; Joyner and Martin, 1987; Retaux and Harris, 1996). In *Xenopus*, the presence of Engrailed-2 protein in retinal axon growth cones was associated with a growth cone turning reponse that occurred even when axons were separated from their cell bodies but was abolished when protein synthesis was inhibited, demonstrating that local protein synthesis rather than transcriptional activity was responsible (Brunet et al., 2005). This study could provide clues as to Foxg1's mode of action in retinal axons.

It is also possible that Foxg1 protein is required in retinal axons for proper retinotectal mapping along the anterior-posterior axis of the tectum/superior colliculus. Previous experiments in chick in which *CBF1*, the chick homologue of *Foxg1*, was misexpressed in the temporal retina, led to retinotectal projection defects, demonstrating that Foxg1 influences tectal mapping from the retina (Yuasa et al., 1996; Takahashi et al., 2003). It is possible that the presence of Foxg1 in axons produces a differential response in nasal and temporal retinal axons to cells in the superior colliculus, influencing their final

termination zones. This mechanism of retinotectal guidance is also thought to be used by the En-2 protein within growth cones, which might produce an attractive or repulsive response in nasal and temporal retinal axons respectively to an En-2 expression gradient along the anterior-posterior tectum (Brunet et al., 2005). In order to invoke hypotheses that concern differential effects of Foxg1 protein in nasal and temporal axons, it is crucial to investigate whether Foxg1 protein is present in all retinal axons or just contralateral axons that originate from *Foxg1*-expressing RGCs. This question could be studied using rhodamine dextran to backlabel axons from one optic tract followed by Foxg1 fluorescence immunohistochemistry. If axons in the ipsilateral optic nerve never co-label with Foxg1-immunoreactive axons and if axons in the contralateral optic nerve always co-label with Foxg1-immunoreactive axons, this would show that Foxg1 is present exclusively in contralateral RGCs. If Foxg1 is present in all axons, both ipsilateral and contralateral, then perhaps it controls their guidance in different ways, as for En-2.

7.5.3. Summary.

In summary, the presence of Foxg1 in axons as well as in cells along the retinotectal pathway supports previous reports that this transcription factor is involved in the guidance of retinal axons (Pratt et al., 2002, 2004) and in the morphogenesis and patterning of anterior forebrain regions, most notably the eyes and telencephalon (Hatini et al., 1994; Xuan et al., 1995; Huh et al., 1999). The presence of Foxg1 protein in axons suggests that, like En-2, this transcription factor could control retinal axon guidance directly from within the growth cone. Other molecules also multi-task in this way, including the transcription factor Pax6 (Ericson et al., 1997); Mastick et al., 1997; Pratt et al., 2000; Pratt et al., 2002) and the diffusible proteins from the Wnt (Hall et al., 2000; Yoshikawa et al., 2003), bone morphogenetic protein (BMP) (Augsburger et al., 1999) and hedgehog (Charron et al., 2003) families. The close association between transcription factor expression domains and the paths of early axons (Marcus et al.,

1999; Macdonald et al., 1994) raises the possibility that more examples of transcription factors with axon guidance roles will arise in the future.

CHAPTER 8: FINAL DISCUSSION

8.1. SUMMARY

The retina-chiasm co-cultures revealed that in the absence of *Foxg1* in the *Foxg1*$^{-/-}$ retina or chiasm, the behaviour of DN retinal axons becomes more ipsilateral in character. It was speculated that this could be caused by increased expression of an ipsilateral determinant, confirmed in Chapter 4 by Zic2 expression analysis, or the reduction of a contralateral determinant in DN retina. Increased expression of the ipsilateral determinant Zic2 suggested that the *Foxg1*$^{-/-}$ retina had become more ventral or temporal in character, leading to increased specification of ipsilateral RGCs. This hypothesis of altered retinal patterning was addressed in Chapter 5, which revealed normal dorso-ventral patterning of the retina but could not confirm whether naso-temporal patterning was altered. At the optic chiasm, candidates for expression studies were chosen based on the hypotheses that a repulsive guidance cue is increased or that important cells and neurons in the chiasm region show morphological defects when *Foxg1* is absent *in vivo*. However, Chapter 6 revealed that the optic chiasm of *Foxg1*$^{-/-}$ embryos shares many morphological, cellular and molecular features with that of wild types and failed to show expanded domains of expression for a couple of key repulsive guidance cues. Chapter 7 examined the distribution of Foxg1 protein in the developing eye and chiasm regions and discovered that it is present more widely in the eye than suggested by its pattern of mRNA expression. Additionally Foxg1 protein was observed in axons where it could influence axon navigation in multiple ways.

The following paragraphs discuss these findings in greater detail and provide a model hypothesizing how Foxg1 directs retinal axon divergence at the optic chiasm based on the new findings presented in this thesis.

8.2. *Foxg1* influences the guidance of dorsonasal axons from within the retina and at the chiasm.

The *in vitro* co-cultures of wild type retina and wild type chiasm (described in Chapter 3) reproduced previous findings that VT axons grow significantly less well than DN axons in the presence of chiasm cells (Herrera et al., 2004; Herrera et al., 2003; Marcus et al., 1995; Marcus and Mason, 1995; Marcus et al., 1996b; Wang et al., 1995). Low axon outgrowth reflected the selective repulsion of axons from the VT retina in the presence of chiasm cells reflecting their ipsilateral routing *in vivo*. These reproducible findings bolstered confidence in the validity of the co-culture method as an *in vitro* representation of the *in vivo* crossing behaviour of retinal axons. In $Foxg1^{-/-} \leftrightarrow Foxg1^{-/-}$ co-cultures, DN retinal axons grew less well on $Foxg1^{-/-}$ chiasm cells compared to control co-cultures consisting entirely of wild type DN retina and chiasm. These *in vitro* findings mirrored the increased ipsilateral projection observed from the nasal retina of *Foxg1* null embryos (Pratt et al., 2004). The possibility that $Foxg1^{-/-}$ retinal axons grow inherently less well than their *Foxg1*-expressing counterparts is thought unlikely given that the absence of *Foxg1* had no effect on the degree of axon outgrowth from DN or VT retinal explants grown in the absence of chiasm cells.

In contrast to DN axons, VT retinal axons in $Foxg1^{-/-} \leftrightarrow Foxg1^{-/-}$ co-cultures failed to show a significant difference in outgrowth compared to the wild type-only controls. Given that *Foxg1* is absent from the VT retina (Hatini et al., 1994; Huh et al., 1999; Chapter 5 of this thesis), any influence of Foxg1 on the guidance of VT axons would suggest a non-autonomous influence. However, this possibility cannot be eliminated and the slight, although statistically insignificant, decrease in VT axon outgrowth from $Foxg1^{-/-} \leftrightarrow Foxg1^{-/-}$ co-cultures relative to control co-cultures of VT retina may suggest a small non-autonomous influence. As discussed in Chapter 3, it is possible that the co-culture experiment might not reveal an influence of Foxg1 in the guidance of VT retinal axons due to its inability to discriminate between low outgrowth and very low outgrowth from VT retina in co-culture. However, if the co-culture findings are taken at face-value,

indicating that Foxg1 is not involved (even non-autonomously) in the navigation of VT RGC axons, it is conceivable that the increased projection from the *Foxg1*$^{-/-}$ temporal retina previously described is caused by loss of *Foxg1* at the chiasm, which could potentially alter the guidance of retinal axons from the entire retina. This possibility was investigated in Chapter 6.

The *Foxg1*$^{-/-}$ ↔ *Foxg1*$^{-/-}$ co-cultures prepared from DN retina did not show whether the loss of Foxg1 from the retina or the chiasm region produced the reduction in axon outgrowth. This was investigated by mixing and matching control (*Foxg1*-expressing) and *Foxg1*$^{-/-}$ retinal explants and chiasm cells and vice-versa. The control ↔ *Foxg1*$^{-/-}$ co-cultures prepared from DN retina supported a requirement for *Foxg1* in DN retina and also showed a requirement for *Foxg1* in optic chiasm cells for the guidance of DN retinal axons. Identical co-cultures of control and *Foxg1*$^{-/-}$ tissue, using explants from VT retina instead of DN retina, failed to show any significant differences relative to the VT control co-cultures, again suggesting that Foxg1 is not involved in VT axon guidance.

It is important to remember the limitations of this *in vitro* co-culture experiment as for any other *in vitro* system. The *in vivo* situation can only be reconstructed up to a point and so *in vitro* systems will not recreate the exact *in vivo* environment encountered by growing axons. *In vitro*, dissociation of the chiasm abolished the 3-dimensional chiasm structure, which produced a more homogeneous environment for retinal axons, possibly influencing their divergence by altering the cellular and molecular environment (Baker, 1990; Baker and Jeffery, 1989; Marcus and Mason, 1995; Reese and Baker, 1990; 1992). Therefore, it would be ideal to repeat these cultures using whole chiasm explants, maintaining their 3D structure.

In summary, the co-cultures suggest that Foxg1 normally promotes the midline crossing of DN retinal axons and that Foxg1 exerts its influence autonomously from within the DN retina and also non-autonomously at the chiasm.

8.3. The *Foxg1*$^{-/-}$ nasal retina contains an increased number of RGCs expressing the ipsilateral determinant Zic2.

Chapter 4 showed a significant increase in the proportion of RGCs expressing the ipsilateral determinant Zic2 in the *Foxg1*$^{-/-}$ nasal retina, providing a molecular explanation for the increased ipsilateral routing of *Foxg1*$^{-/-}$ nasal retinal axons and *in vitro* co-culture results presented in this thesis. *Foxg1*$^{-/-}$ retinas contained similar numbers of RGCs compared to those of wild types, excluding the possibility that a larger number of RGCs produced a corresponding increase in the number of Zic2-positive cells in the nasal retina, whilst maintaining a wild type proportion of Zic2-expressing cells. It is crucial to confirm whether the *Foxg1*$^{-/-}$ RGCs that ectopically express Zic2 in the nasal retina are the same RGCs that project ipsilaterally in abnormally large numbers at the *Foxg1*$^{-/-}$ chiasm. This can be achieved by using rhodamine dextran to backlabel contralateral and ipsilateral axons from one optic tract followed by Zic2 immunohistochemistry on the ipsilateral and contralateral retina (Herrera et al., 2003). Herrera et al. showed that in the wild type VT retina, colocalisation with Zic2 only occurred in a small percentage of backlabeled RGCs in the ipsilateral eye due to downregulation of Zic2 in retinal axons upon crossing the chiasm midline. However, the technique was sufficiently powerful to reach the conclusion that only ipsilateral RGCs, but never contralateral RGCs, express Zic2. If there is a direct association between Zic2 expression and the increased uncrossed axon trajectory in *Foxg1* null mice, backlabeled ipsilateral RGCs should colocalise with Zic2-expressing RGCs in the nasal retina.

Numbers of Zic2-positive RGCs did not increase in the *Foxg1*$^{-/-}$ temporal retina. The temporal retina normally expresses *Foxg1* only in dorsal regions in the wild type (Chapter 5). Nevertheless, the *Foxg1*$^{-/-}$ VT quadrant showed a decrease in the proportion of Zic2-positive RGCs at E14.5, which was significant using DAB immunohistochemistry. The DT quadrant showed a small but significant increase in Zic2-positive RGCs at E14.5 and E16.5 (Figure 12, Chapter 4). Although these findings hint at possible changes in the temporal retina, the most obvious and consistent finding of

Chapter 4 was the increase in Zic2-expressing RGCs in the nasal retina, which was reproducible using both chromogenic and fluorescent detection methods for Zic2 protein. The fact that altered Zic2 expression is primarily a feature of the *Foxg1*$^{-/-}$ nasal retina, where the majority of cells normally express Foxg1, suggests that *Foxg1* primarily acts autonomously in *Foxg1*-expressing cells to specify a contralateral path in nasal RGC axons by regulating the proportion of RGCs expressing Zic2 protein.

8.3.1. Hypotheses to explain the altered proportion of Zic2-expressing RGCs in the *Foxg1* null retina.

Hypothesis 1: Foxg1 normally represses Zic2 in *Foxg1*-expressing RGCs, thereby preventing an ipsilateral program. In *Foxg1* null embryos, repression of Zic2 is relieved in the nasal retina.

Based on the results shown in Chapter 4 it was hypothesized that Foxg1 might normally repress Zic2 in the *Foxg1*-expressing nasal retina, thus repressing an ipsilateral program in nasal axons. The hypothesis that Foxg1 represses Zic2 may explain why Zic2 is mostly confined to the VT retina, where *Foxg1* mRNA is not found (as shown in Chapter 5), but only weakly expressed in RGCs and other retinal layers in DN, DT and VN retina where *Foxg1* mRNA is normally present (Chapters 4 & 5).

A transcription factor that has been shown to repress Zic2 specifically in VT RGCs and prevent the ipsilateral routing of their axons is Islet-2 (Pak et al., 2004). Thus Foxg1 and Islet-2 may repress Zic2 in the nasal and VT retina respectively (see Chapter 4, Figure 18). Foxg1 is known to act as a transcriptional repressor *in vitro* (Dou et al., 2000; Yao et al., 2001; Hardcastle & Papalopulu, 2000; Castella et al., 2000). Transcriptional repression of Zic2 may occur directly, via binding of Foxg1 to *Zic2* or indirectly via Foxg1-mediated transcriptional regulation of genes whose products have a repressive effect on Zic2.

Regardless of whether Foxg1 represses Zic2 directly or indirectly, in *Foxg1* null embryos, the repressive effect of Foxg1 on *Zic2* in the nasal retina would be relieved, activating its expression in nasal RGCs. There is convincing *in vitro* and *in vivo* evidence that links *EphB1* expression in the VTC to the ipsilateral projection (Williams et al., 2003). Zic2 is thought to be required for *EphB1* expression based on reports that Zic2 and EphB1 normally co-localise in the VT retina (Pak et al., 2004) and increased or reduced expression of Zic2 produces a corresponding increase or reduction in *EphB1* expression (Williams et al., 2003; Pak et al., 2004; Williams et al., 2006). Therefore, nasal RGCs that ectopically express Zic2 might activate *EphB1* leading to the repulsion of EphB1-bearing retinal axons upon contact with ephrin-B2-expressing midline radial glia at the chiasm (Williams et al., 2003). If this hypothesis is true, the proportion of EphB1-expressing RGCs in the *Foxg1*$^{-/-}$ nasal retina should increase reflecting the greater proportion of Zic2-expressing RGCs in *Foxg1* null embryos. Moreover, nasal RGCs that ectopically express EphB1 should co-localise with Zic2 (Pak et al., 2004). This theory could be tested by *in situ* hybridization for EphB1 followed by Zic2 immunohistochemistry or by two-colour *in situ* hybridization for EphB1 and Zic2 in the *Foxg1* null retina.

In order to understand the mechanism by which Foxg1 exerts its repressive effects, coimmunoprecipitation (Ransone, 1995) could be used to identify the proteins that Foxg1 binds to. To test the validity of a direct interaction between the Zic2 promoter and Foxg1, chromatin immunoprecipitation could be utilized (Solomon and Varshavsky, 1985). Chromatin immunoprecipitation enables analysis of the interaction of proteins with specific chromatin regions. *In vivo* footprinting could also be used to map the precise DNA sequences to which Foxg1 binds *in vivo* (Becker et al., 1993; Grange et al., 1997).

Hypothesis 2: Foxd1 is ectopically expressed in the nasal retina of *Foxg1* null embryos producing an increase in Zic2-expressing RGCs.

An explanation for the VT-restricted expression of *Zic2* in wild type embryos is that activation of *Zic2* expression requires the transcription factor Foxd1, which is expressed in the VT retina and affects the ipsilateral-contralateral ratio (Herrera et al., 2004). Any influence by Foxd1 is thought to be indirect because the VT domain of Foxd1 expression in the retina has been shown to extend beyond the region occupied by Zic2-expressing cells in the VTC in the peripheral retina (Herrera et al., 2004). In wild type mouse embryos, Foxg1 may normally repress Foxd1 in the nasal retina, as demonstrated in the developing chick embryo (Takahashi et al., 2003). This would limit Foxd1 to temporal regions where it might activate *Zic2* expression and is an example of Foxg1 repressing Zic2 indirectly via repression of Foxd1 (Hypothesis 1). In the *Foxg1* null retina, ectopic activation of *Foxd1* is expected to occur in nasal regions that normally express *Foxg1* through the absence of repression by Foxg1, resulting in the ectopic expression of Zic2 in these areas. There is evidence for aberrant expression of Foxd1 in the *Foxg1* null retina in the mouse at E10.5 (Huh et al., 1999). In order to test the validity of this hypothesis, the spatial distribution of Foxd1 mRNA in relation to Foxg1 and Zic2 could be examined by two-colour *in situ* hybridization for Foxd1 and Foxg1 followed by Zic2 immunohistochemistry at E14.5, when Zic2 appears in the VT retina. The relative orientations of the expression domains of Foxg1 and Foxd1 have not been investigated to date within the same retina in an E14.5 wild type embryo. Therefore, a wild type control is crucial. In the *Foxg1*$^{-/-}$ retina, two-colour *in situ* hybridization for Foxd1 and Zic2 or *in situ* hybridization for Foxd1 followed by Zic2 immunohistochemistry would be expected to show ectopic expression of Foxd1 and Zic2 in the nasal retina and overlapping expression domains.

Ectopic Foxd1 expression in the *Foxg1*$^{-/-}$ nasal retina may also come about via disrupted nasal-temporal patterning. Parts of the retina that would normally express *Foxg1* might be respecified as 'temporal' regions. Since Foxd1 is expressed in the temporal retina at

early embryonic ages, the misspecification of nasal RGCs as temporal RGCs might result in the ectopic expression of *Foxd1* in the nasal retina, which might in turn activate *Zic2* expression.

In order to distinguish between hypothesis (1): whether Foxg1 represses Zic2 and hypothesis (2): whether Foxd1 activates Zic2, *Foxg1* or *Foxd1* could be ectopically expressed in regions of the wild type retina from which they are normally absent or alternatively *Foxg1* or *Foxd1* could be blocked in the wild type retina by RNAi (Fire et al., 1998). In order to see whether Zic2 expression is eliminated, reduced or elevated, Zic2 protein could be visualized using immunohistochemistry and protein levels quantified by Western blot or Zic2 mRNA quantified by qRT PCR. *Foxd1* expression levels would have to be monitored following manipulation of *Foxg1* and vice-versa to see if they are altered in response to overexpression or elimination of *Foxg1* or *Foxd1* as suggested by previous reports (Herrera et al., 2004; Takahashi et al., 2003; Huh et al., 1999; Yamagata et al., 1999). In order to eliminate possible changes in *Foxg1* protein levels when testing for a regulatory effect of Foxd1 on Zic2, Foxd1 could be overexpressed or eliminated in the *Foxg1*$^{-/-}$ eye and the effect on Zic2 expression studied.

Hypothesis 3: Aberrant migration of Zic2-expressing RGCs from ventrotemporal to nasal regions of the *Foxg1* null retina produces an increased proportion of nasal Zic2-expressing RGCs.

Cells in the *Foxg1*$^{-/-}$ temporal retina may migrate abnormally into the nasal retina. This hypothesis was suggested by the finding of a reduction in the number of RGCs activating *Foxg1* in DN regions (Chapter 5), which might suggest the presence of cells with 'temporal' characteristics. The aberrant migration of RGCs from temporal to nasal regions might lead to the redistribution of Zic2-expressing cells in nasal regions. The proportion of Zic2-expressing cells was reduced in the VT quadrant at E14.5 and this was significant using DAB immunohistochemistry (Figure 12B, Chapter 4). This VT

reduction in Zic2 may be linked to increased activation of *Foxg1* in this quadrant (Chapter 5), resulting in the VT region containing more cells with 'nasal' characteristics. Thus the VT reduction in Zic2-expressing RGCs may be caused by VT cells leaving this region and migrating to the nasal retina and/or through nasal cells abnormally entering the VT quadrant, thus reducing the proportion of Zic2-expressing cells.

This hypothesis is probably the least likely out of all the three possibilities explaining changes in the proportion of Zic2-positive RGCs. The main drawback is that a migratory defect cannot account for the overall increase in the number of Zic2-expressing cells in the *Foxg1*$^{-/-}$ retina. Defective intraretinal migration might be expected to produce a random mixing of nasal and temporal cells and a corresponding random distribution in Zic2-positive cells. However, Zic2 did not appear to be randomly distributed over the *Foxg1* null retina. Instead Zic2 was mainly confined to peripheral DN and VN retinal quadrants. Also, some degree of nasal-temporal polarity is maintained in the *Foxg1*$^{-/-}$ retina because the majority of ipsilateral projections still arise from the temporal retina (Pratt et al., 2004). The hypothesis of abnormal migration could be tested by fluorescently tagging single cells in the intact *Foxg1*$^{-/-}$ nasal or temporal retina *in vitro* and following their progress through development.

8.4. Dorsoventral retinal patterning appears to be maintained in the *Foxg1*$^{-/-}$ eye.

Despite the abnormal squashed, medially-elongated appearance of the *Foxg1*$^{-/-}$ retina, the main retinal layers were maintained. This corroborates findings in Chapter 4 that retinal ganglion cells are present in an equivalent location to wild types in the inner retinal layer. The RGC layer covered a larger area in anterior-most regions but abnormal folding of the *Foxg1*$^{-/-}$ retina in this region could have resulted in the RGC layer being sectioned at an angle (Chapter 5). A 3-dimensional image of the *Foxg1* null eye would help distinguish true morphological defects from sectioning artifacts.

There was no evidence for disrupted dorsoventral patterning, analysed by ephrin-B2 and EphB2 protein gradients along the DV axis (this thesis, published in Pratt et al., 2004). It is possible, but considered unlikely, that ephrin-B2 and EphB2 gradients are maintained in the *Foxg1*$^{-/-}$ retina despite abnormal DV patterning. Given more time, this hypothesis could be tested by conducting a thorough expression analysis of EphA, ephrin-As and the other EphB and ephrin-Bs in the eye and perhaps some of the earlier markers of DV polarity, such as Vax and Tbx5. If the expression gradients of these molecules are maintained as normal in the *Foxg1*$^{-/-}$ eye, this would strengthen the findings of normal DV patterning presented here and weaken the argument for an expanded ventral retina contributing to the increased ipsilateral projections.

8.5. *Foxg1* expression is hypothesized to show spatiotemporal changes during development.

From E13.5 in *Foxg1*$^{LacZ/+}$ eyes, the *Foxg1*^{LacZ} reporter revealed that *Foxg1* is most widely expressed nasally and temporally in the dorsal retina with expression becoming increasingly restricted to nasal regions in ventral retina, such that the ventrotemporal quadrant does not express *Foxg1* (Chapter 5). This result differs from previous reports claiming that *Foxg1* was restricted to the nasal half of the retina (Hatini et al., 1994; Huh et al., 1999). These studies examined Foxg1 mRNA expression using the same *Foxg1*^{LacZ} reporter mice and also *in situ* hybridization. The mRNA expression pattern also differed from the spatial pattern of Foxg1 protein in the retina (Chapter 7), which was more widespread and covered much of the temporal retina. Similarly, Huh et al. (1999) reported that nasal-temporal patterning was maintained in the retina of *Foxg1*$^{LacZ/LacZ}$ embryos. However, in observations presented in this thesis *Foxg1*$^{LacZ/LacZ}$ eyes consistently lacked a clear boundary between nasal *Foxg1*-expressing and temporal *Foxg1*-negative regions. Moreover, an increase in the number of RGCs activating *Foxg1*

was observed in temporal regions of the *Foxg1* null retina, whereas a reduction in RGCs activating *Foxg1* was seen in dorsonasal regions.

There are a number of possibilities that could explain the discrepancies between these previous studies and the findings presented in Chapter 5 of this thesis. Firstly, previous studies used $Foxg1^{LacZ/+}$ or $Foxg1^{LacZ/LacZ}$ embryos prior to or at E12.5 rather than embryos between E13.5 and E15.5. Therefore, it is plausible that the spatial pattern of *Foxg1* activation changes between E12 and E14. In $Foxg1^{LacZ/+}$ embryos, *Foxg1* might be restricted to nasal regions at earlier ages until E12.5 followed by a change in expression pattern later on in development to the one described here (see Figure 11, Chapter 5).

In the $Foxg1^{LacZ/LacZ}$ eye, the presence of cells that activate *Foxg1* in temporal regions where *Foxg1* is not usually expressed in the wild type, suggests that either temporal cells are misspecified as 'nasal', suggesting a nasal-temporal patterning defect, or that nasal cells are able to migrate abnormally to the temporal retina. In the latter instance, nasotemporal patterning might be set up as normal in the *Foxg1* null embryo but then migratory defects affect the position of nasal cells at the ages examined in this thesis. These two hypotheses cannot be distinguished at present. Considered in isolation, the $Foxg1^{LacZ/LacZ}$ results suggest a breakdown of nasal-temporal polarity. However, it would be wise to corroborate the $Foxg1^{LacZ/LacZ}$ findings to exclude the possibility of ectopic activation of the $Foxg1^{LacZ}$ reporter. Moreover, the $Foxg1^{LacZ}$ reporter only marks cells that are predominantly found in the nasal retina. Therefore, the hypothesis of disrupted NT patterning could be examined further by investigating the expression of more nasal and temporal patterning genes and their proteins in the retina, such as EphA3, SOHo1, GH6, ephrin A2 and ephrin A5 nasally (Takahashi et al., 2003) and Foxd1 and EphA5/EphA6 temporally (Flanagan, 2006). The hypothesis of abnormal migration could be examined by fluorescently labeling and tracing the migration of single cells in the nasal or temporal retina.

Another possible reason for discrepancies between this thesis and previous studies lies in the use of slightly different planes of section, which might alter the regions that are defined as nasal and temporal retina. In other words, *Foxg1* expression might not change between E12.5 and E14.5 but only appears to do so due to sectioning differences. An additional explanation that primarily concerns $Foxg1^{LacZ/+}$ embryos is the possibility that the developing wild type retina tilts such that the NT axis changes orientation during development. Finally, there may be differences in the placement of the nasal-temporal axis between this thesis and previous studies, such that there is no discrepancy between the findings. One solution to address these problems would be to perform whole-mount lacZ staining on $Foxg1^{LacZ/+}$ or $Foxg1^{LacZ/LacZ}$ eyes or *Foxg1* fluorescent *in situ* hybridization on the eyes of $Foxg1^{LacZ/+}$ embryos. This would provide a 3-dimensional view of the eye and areas in which *Foxg1* is expressed or transcriptionally activated, which would also have the advantage of eliminating problems of tissue distortion that can be associated with processing. More importantly, a double *in situ* hybridization for *Foxg1* and *Foxd1* mRNA would enable their expression patterns to be visualized in relation to one another within the same wild type retina. This would facilitate mapping of the eye with reference to both their expression domains, rather than using the expression pattern of *Foxg1* or *Foxd1* alone to position the nasal-temporal axis. The choroid fissure in the wild type ventral retina could also be used as a reference point to see whether the retina changes orientation during development. In addition, a 3-dimensional *Foxg1* null eye would provide a clearer picture of retinal folding and the degree of morphological variation between eyes than is possible in 2-dimensions alone.

8.5.1. Foxg1 may specify a 'contralateral' domain within the nasal retina.

If whole-mount studies of *Foxg1* expression reveal a spatiotemporal change between early and later stages of eye development, then this appears to coincide with the spatiotemporal change in *Foxd1* expression from the temporal half of the retina at early

stages of eye development (Hatini et al., 1994; Huh et al., 1999) to restricted expression in the VT retinal quadrant at around E14.5 (Herrera et al., 2004) (See Figure 1). These changes in *Foxg1* and *Foxd1* might be coincidental. Alternatively, the shift in *Foxg1* expression at E13.5/E14.5, such that *Foxg1* occupies the DT retina, might cause the restriction of *Foxd1* to the VT retina, given that *Foxg1* represses *Foxd1* (Yamagata et al., 1999; Takahashi et al., 2003).

Interestingly, *Foxd1*, and now *Foxg1* (this thesis), alter their spatiotemporal expression patterns at E13.5 - E14.5, which coincides with the projection of many contralateral and the first permanent ipsilateral axons out of the retina. One hypothesis for this spatiotemporal change is that at early developmental stages these two forkhead transcription factors are involved in nasal-temporal patterning (Figure 1A), whereas at later stages from E13.5 - E14.5, *Foxg1* activation in the nasal retina demarcates a 'contralateral domain' that produces contralateral RGC axons and *Foxd1* activation in VT retina demarcates an 'ipsilateral domain' that produces ipsilateral RGC axons (Figure 1B). This hypothesis could still apply if *Foxg1* is not shown to change its spatial expression pattern (ie. if no discrepancies exist between previous studies and this thesis).

Foxg1 can hypothetically affect the contralateral or ipsilateral routing of RGC axons in a number of different ways. These possibilities can be viewed in a hierarchical manner from the requirement for Foxg1 in a whole region, such as the entire anterior forebrain or the retina or optic chiasm, right down to the details of which molecules interact with Foxg1 in a given cell or axon and whether this interaction is direct or indirect. Numerous studies have shown that Foxg1 acts as a classical transcription factor, which binds DNA and influences the transcription of certain genes (Hanashima et al., 2002; Yao et al., 2001; Hardcastle & Papalopulu, 2000; Castella et al., 2000) but Foxg1 can also influence molecules in the retina in a DNA-binding-independent fashion (Yamagata et al., 1999; Takahashi et al., 2003). These DNA-dependent and DNA-independent mechanisms of action add complexity to the potential myriad effects that Foxg1 could have upon the guidance of retinal axons at the optic chiasm.

Figure 1. Hypothesised changes in the roles of *Foxg1* and *Foxd1* during eye development

(A) NT patterning: optic cup stage until ~ E12.5

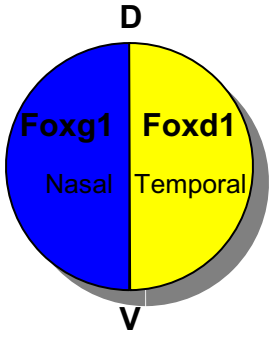

Early in eye development, *Foxg1* (blue) and *Foxd1* (yellow) define the nasal and temporal retina by means of their spatially distinct expression patterns (Hatini et al., 1994; Huh et al., 1999).

(B) *Foxg1* specifies a 'contralateral domain' within the nasal retina from ~E13.5 – E14.5

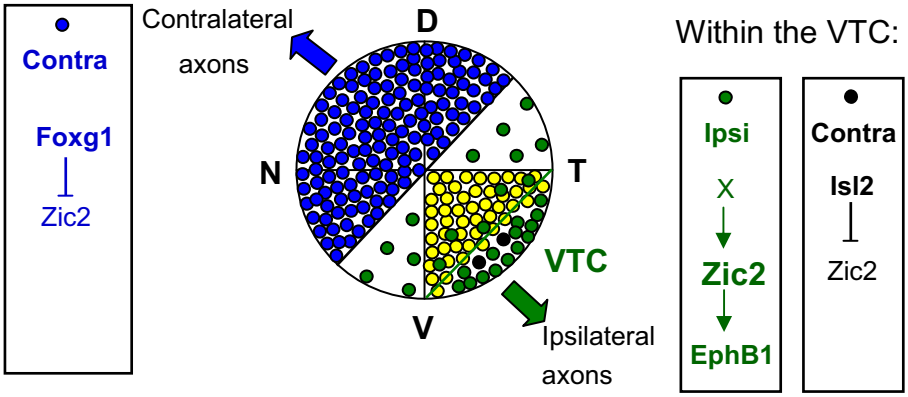

From ~ E14.5, *Foxg1* (blue circles) is expressed in half of the retina, most widely in DN retina but declining towards VT retina where it is absent. Its expression defines a 'contralateral domain' and RGCs (depicted as circles) within it project contralaterally. This might occur via Foxg1 repression of Zic2. *Foxd1* (yellow circles) is expressed in VT retina and defines an 'ipsilateral domain'. Zic2-expressing RGCs (green circles) are highly concentrated in the VTC in peripheral VT retina (Herrera et al., 2003) but are also found in other regions of the temporal and nasal retina (Chapter 4, this thesis). An unknown regulator (denoted as 'X') activates Zic2 expression and it is thought that Foxd1 may be required upstream of 'X' for Zic2 activation (Herrera et al., 2004). Black circles indicate contralateral RGCs that express Isl2, which represses Zic2 within the VTC (Pak et al., 2004). Abbreviations: Ipsi = ipsilateral RGCs, Contra = contralateral RGCs, VTC = ventrotemporal crescent.

The following paragraphs describe the possible ways in which Foxg1 may control contralateral-ipsilateral axon navigation from (1) the retina, (2) within axons and (3) at the optic chiasm. These three possibilities are not mutually exclusive, as the co-culture experiments in this thesis suggest (Chapter 3) and it is likely that they act in combination.

8.5.2. Control from the retina.

Foxg1 may influence the contralateral-ipsilateral routing from the first time it is expressed in the optic cup by setting up nasal-temporal polarity in the retina. The specification of a 'contralateral domain' within much of the nasal retina at E13.5/E14.5 might then result in Foxg1 promoting the contralateral routing, or preventing the ipsilateral routing, of axons that project from RGCs that express *Foxg1* themselves. This can be described as a cell-autonomous mode of action within RGCs because Foxg1 affects the same cells in which it is expressed. Foxg1 might also influence the routing of axons that project from RGCs that do not express *Foxg1*, for example those in the VT retina. This can be described as a non-autonomous mode of action within RGCs because Foxg1 affects cells in which it is not expressed.

The findings presented in Chapter 4 suggest that Foxg1 prevents an uncrossed path in axons that originate from *Foxg1*-expressing nasal RGCs, via repression of Zic2. Within Foxg1-expressing RGCs, the repression of Zic2 by Foxg1 is thought to be cell-autonomous because Zic2-expressing cells increase in RGCs of the *Foxg1*$^{-/-}$ nasal and dorsotemporal retina that would normally express *Foxg1*. However, there are hints at non-autonomous effects by Foxg1 on Zic2 in the VT quadrant, which showed a slight decrease in Zic2-expressing cells at E14.5. Earlier in this discussion it was hypothesized that the abnormal proportion of Zic2-expressing RGCs in these quadrants may be fully or partly explained by defective nasal-temporal patterning of the retina or by defective migration when *Foxg1* is absent.

Another layer of complexity is added by considering the multiple ways through which Foxg1 might repress Zic2 and other downstream target genes that influence axon

navigation. Repression by Foxg1 could occur via DNA-binding-dependent or DNA-binding-independent means. In terms of DNA-binding, Foxg1 might repress Zic2 either (1) directly via binding to the *Zic2* promoter or (2) indirectly via transcriptional repression of another gene that represses Zic2. The DNA-independent mechanism could take the form of a direct protein-protein interaction between Foxg1 and Zic2 or an interaction between Foxg1 and a molecule that is required for regulating *Zic2*, such that Foxg1 represses Zic2 indirectly. Although Zic2 was used as an example here, Foxg1 potentially affects other target genes or molecules in this way.

It remains plausible that Foxg1 promotes the crossing of retinal axons projecting from *Foxg1*-expressing RGCs by regulating expression of 'contralateral determinants' that result in axons growing across the chiasm midline. However, no such contralateral determinant has been discovered in the literature. The only known molecules expressed by contralateral RGCs, Nr-CAM and Islet-2, affect the crossing of axons produced later than the onset of the *Foxg1*$^{-/-}$ axon projection defect in the case of Nr-CAM (Williams et al., 2006) or the crossing of axons within the VT retina only in the case of Islet-2 (Pak et al., 2004). Therefore, it is unlikely that altered expression of Nr-CAM or Islet-2 is responsible for the increased ipsilateral projection in *Foxg1* null embryos. In order to completely rule out this hypothesis, protein and mRNA expression patterns of Nr-CAM and Islet-2 could be investigated in the developing *Foxg1*$^{-/-}$ retina by immunohistochemistry or *in situ* hybridization respectively.

8.5.3. Control from within retinal axons.

Chapter 7 showed that Foxg1 protein was found in retinal axons. An interesting area for future investigation would be to determine whether Foxg1 protein is confined to contralateral axons only that arise from *Foxg1*-expressing RGCs or whether it is also found in ipsilateral (VT) axons. If Foxg1 is found in all axons, does it influence their navigation differentially and if so what is/are the mechanism(s) involved? It is unknown whether Foxg1 protein is locally synthesized within the growing axon or whether protein

is made in the cell bodies of RGCs and then transported along axons to their tips. Within the cell bodies of RGCs, Foxg1 protein may act as a transcription factor to mediate receptor-ligand signaling at the growth cone via the transcriptional regulation of downstream effectors. For example, transcriptional regulation by Foxg1 may ultimately lead to the production of a particular complement of receptors that cause the growth cone to steer in a particular manner. Foxg1 protein in navigating axons may have numerous actions, particularly since Foxg1 is known to have DNA-independent effects (Yuasa et al., 1996; Yamagata et al., 1999; Hanashima et al., 2002; Takahashi et al., 2003). Within the growth cone, Foxg1 might affect the cytoskeleton and influence the extension or retraction of filopodia or perhaps Foxg1 protein is transported retrogradely from the growth cone to the RGC cell body where it can act as a transcription factor. All these possibilities are speculative at present and demand further experiments, some of which are discussed in Chapter 7 of this thesis. The answers to these questions will help to unravel the mechanism through which Foxg1 affects axon navigation.

8.5.4. The *Foxg1*$^{-/-}$ chiasm retains many wild type characteristics.

The presence of an optic chiasm in *Foxg1*$^{-/-}$ embryos that retains many wild type anatomical and molecular features showed that Foxg1 is not required for chiasm formation (Chapter 6). Expression of the *Foxg1*^{LacZ} reporter in *Foxg1* null embryos revealed *Foxg1* activation in anterior hypothalamic cells corresponding to the location of *Foxg1*-expressing cells in wild types. This demonstrated that cells that would normally express *Foxg1* are present in *Foxg1*$^{-/-}$ embryos and can still respond to cues that activate *Foxg1* expression. Also previous DiI tracing studies revealed that *Foxg1*$^{-/-}$ axons decussate in an 'X'-shape at the chiasm midline, which is reminiscent of the shape formed by wild type axons at the optic chiasm, although *Foxg1*$^{-/-}$ axons appear less fasciculated (Pratt et al., 2004).

The midline cytoarchitecture of the *Foxg1*$^{-/-}$ chiasm appeared grossly normal. A palisade of cells that expressed ephrin-B2, a molecule known to be expressed by midline radial glia, was maintained at the *Foxg1*$^{-/-}$ midline. However, the presence of these midline radial glial cells needs to be confirmed using a specific radial glial marker, such as RC2 (Godement et al., 1994).

The cell-surface glycoproteins SSEA-1 and CD44 and the transcription factor Nkx2.2 were all present in their expected locations in the ventral diencephalon. This suggests that the population of early-differentiating neurons that are required for establishing the chiasm architecture and inhibiting the growth of retinal axons into inappropriate regions of the diencephalon are present as normal in *Foxg1* null embryos. However, it is conceivable that *Foxg1*$^{-/-}$ contralateral and ipsilateral axons interact or position themselves abnormally in relation to these chiasm molecules, producing misrouting at the midline; a possibility that should be investigated in the near future. Observations of slightly stronger expression of CD44 at the chiasm midline warrant more detailed investigation in the future, encompassing a greater range of embryonic ages and quantitation by Western-blotting. Since the presence of CD44 in the ventral diencephalon has been reported to promote the ipsilateral routing of axons (Lin et al., 2003, 2005), it is plausible that increased CD44 expression plays a role in repelling more nasal and temporal RGC axons into the uncrossed tract, explaining the increased ipsilateral projection from the entire *Foxg1*$^{-/-}$ retina.

A change in *Foxd1* expression at the chiasm may also affect axon guidance by affecting the cellular and/or molecular environment encountered by growing axons. No studies to date have explored *Foxd1* expression patterns around the chiasm in *Foxg1* null mice. *Foxd1*$^{-/-}$ embryos display an increased ipsilateral projection from the entire retina, which was attributed to expanded Slit2 expression in the diencephalon (Herrera et al., 2004). Perhaps an expansion in *Foxd1* expression at the *Foxg1*$^{-/-}$ chiasm results in abnormalities in the expression of chiasm or diencephalic guidance cues, such as Slit2, thereby increasing the proportion of uncrossed axons. This hypothesis could be tested by

comparing *Foxd1* and Slit2 expression in *Foxg1* null versus wild type embryos from E13.5 – E16.5 by *in situ* hybridization, quantitative RT PCR and Western-blotting.

Many more extracellular matrix molecules affect axon guidance but time limitations did not permit exhaustive expression analyses of these. Therefore, it remains a possibility that the expression of some of these molecules is altered in the *Foxg1*$^{-/-}$ ventral diencephalon or midline, altering the uncrossed projection. A microarray comparison of wild type and *Foxg1*$^{-/-}$ cDNA taken from the retina and chiasm would enable a comprehensive survey of differences in expression levels in these regions of the embryo. This would identify whether the expression of certain genes is altered relative to the wild type retina or chiasm and provide candidates for functional analyses.

8.6. Foxg1 could regulate expression of a midline chemoattractant.

One way in which Foxg1 could promote axon crossing is through the positive regulation of a midline chemoattractant, such that in Foxg1's absence, the midline is less attractive to axons resulting in a greater number of axons being diverted into the ipsilateral tract. The reason for focusing on inhibitory or chemorepulsive molecules at the chiasm is due to the paucity of diffusible chemoattractants identified to date. These constitute members of three families: Netrins, scatter factor/hepatocyte growth factors (SF/HGF), neurotrophins (Ebens et al., 1996; O'Connor and Tessier-Lavigne, 1999; Tessier-Lavigne and Goodman, 1996). Recently Shh was added to this list due to its chemoattractive properties towards commissural spinal axons (Charron et al., 2003). It is likely that more chemoattractants will be found in the future but in the meantime an interesting extension of the chiasm expression studies would be to investigate the protein or mRNA expression patterns of some of these molecules. Moreover *Foxg1*$^{-/-}$ retinal explants could be cultured in the presence of netrin, Shh and other chemoattractive candidates to test whether the growth of their axons is altered compared to those from wild type retinas.

In summary, Foxg1 appears to have roles in eye and forebrain morphogenesis, roles in the guidance of retinal axons from the retina and at the chiasm and also, hypothetically, a role in axon guidance from within navigating axons themselves.

8.7. An emerging picture of the regulatory and molecular control of contralateral-ipsilateral divergence at the optic chiasm.

Over the past decade, a picture has gradually emerged in which the source of ipsilateral projections, the VTC in the VT retina, appears to be molecularly distinct from other regions in the developing retina from E13 onwards. Zic2 is thought to program VT RGCs to project ipsilaterally via the expression of EphB1 that is repelled by ephrin-B2-expressing midline radial glia at the chiasm (Herrera et al., 2003; Williams et al., 2003). Nr-CAM is expressed by contralateral RGCs in the entire retina, apart from in the VT Zic2-expressing region (Williams et al., 2006) and appears to suppress ipsilateral projections from the VT retina only at late embryonic stages. Isl2 is expressed by only a subset of contralateral RGCs that includes a few in the VT retina (Pak et al., 2004). In the VTC, Isl2-expressing RGCs are thought to suppress Zic2 and EphB1 expression, allowing them to project contralaterally. The results presented in this thesis add to this knowledge by showing that Foxg1 is required autonomously within the nasal retina but also at the chiasm for the contralateral guidance of nasal retinal axons. These findings led to the hypothesis that Foxg1 might influence the contralateral-ipsilateral ratio by setting up a contralateral domain within the nasal retina in which Zic2 and the ipsilateral program is repressed and that this part of the retina is distinct from the VT region where *Foxd1* and *Zic2* are expressed. Foxg1 may also direct guidance more directly from within nasal RGCs or non-autonomously within RGCs that never express Foxg1 or within the growth cones of axons that contain Foxg1 protein. Finally, a slight change in CD44

expression was seen at the *Foxg1*$^{-/-}$ chiasm. Further molecular changes may be revealed in the future as plenty of candidate molecules remain to be explored.

Despite this knowledge, many questions remain as to how these molecules control the guidance of ipsilateral and contralateral axons at the chiasm midline. For example, is the contralateral path a default route that needs to be suppressed in the VTC by Zic2 for ipsilateral projections to form? If so, how do the earliest transient ipsilateral projections form prior to Zic2-expressing RGCs appearing in the retina? Also, how and why do these early projections turn away directly into the uncrossed optic tract without contacting neuroepithelial and glial cells at the chiasm midline? Even though Zic2 and EphB1 provide an explanation for the majority of ipsilateral projections, other molecules or interactions are required because *Zic2*$^{kd/kd}$ and *EphB1*$^{-/-}$ mice still display a few residual uncrossed axons (Herrera et al., 2003; Williams et al., 2003). Also, genes such as Zic2, Foxd1, Foxg1 and Nr-CAM are expressed both in the retina and at the chiasm and Nr-CAM and Foxg1 are also present in axons. The presence of these molecules in multiple locations makes it harder to separate their relative contributions to contralateral-ipsilateral divergence at each of these locations. Also, the recent findings that growth cones can alter their response to guidance cues depending on the presence of particular molecules in the extracellular environment, such as heparan sulphate proteoglycans, opens up the possibility for a whole host of interactions using only a limited number of guidance cues (reviewed in Bulow and Hobert, 2004; Charron et al., 2003; Hussain et al., 2006; Ichijo, 2004; Stein and Tessier-Lavigne, 2001).

By investigating the influence that *Foxg1* has on the contralateral-ipsilateral routing of retinal axons at the chiasm, the findings presented here significantly add to increasing knowledge about the roles transcription factors play in regulating axon guidance and provide a basis for future investigation.

BIBLIOGRAPHY

Adesina, A. M., Nguyen, Y., Mehta, V., Takei, H., Stangeby, P., Crabtree, S., Chintagumpala, M., and Gumerlock, M. K. (2007). FOXG1 dysregulation is a frequent event in medulloblastoma. *J Neurooncol*. **85(2),** 111-122.

Anderson, R. B., and Holt, C. E. (2002). Expression of UNC-5 in the developing Xenopus visual system. *Mech Dev* **118,** 157-60.

Anderson, R. B., Walz, A., Holt, C. E., and Key, B. (1998). Chondroitin sulfates modulate axon guidance in embryonic Xenopus brain. *Dev Biol* **202,** 235-43.

Artavanis-Tsakonas, S., Rand, M. D., and Lake, R. J. (1999). Notch signaling: cell fate control and signal integration in development. *Science* **284,** 770-6.

Aruga, J. (2004). The role of Zic genes in neural development. *Mol Cell Neurosci* **26,** 205-21.

Aruga, J., Mizugishi, K., Koseki, H., Imai, K., Balling, R., Noda, T., and Mikoshiba, K. (1999). Zic1 regulates the patterning of vertebral arches in cooperation with Gli3. *Mech Dev* **89,** 141-50.

Aruga, J., Nagai, T., Tokuyama, T., Hayashizaki, Y., Okazaki, Y., Chapman, V. M., and Mikoshiba, K. (1996). The mouse zic gene family. Homologues of the Drosophila pair-rule gene odd-paired. *J Biol Chem* **271,** 1043-7.

Aruga, J., Tohmonda, T., Homma, S., and Mikoshiba, K. (2002). Zic1 promotes the expansion of dorsal neural progenitors in spinal cord by inhibiting neuronal differentiation. *Dev Biol* **244,** 329-41.

Aruga, J., Yokota, N., Hashimoto, M., Furuichi, T., Fukuda, M., and Mikoshiba, K. (1994). A novel zinc finger protein, zic, is involved in neurogenesis, especially in the cell lineage of cerebellar granule cells. *J Neurochem* **63,** 1880-90.

Augsburger, A., Schuchardt, A., Hoskins, S., Dodd, J., and Butler, S. (1999). BMPs as mediators of roof plate repulsion of commissural neurons. *Neuron* **24,** 127-41.

Baker, G. E. (1990). Prechiasmatic Reordering of Fibre Diameter Classes in the Retinofugal Pathway of Ferrets. *Eur J Neurosci* **2,** 24-33.

Baker, G. E., and Jeffery, G. (1989). Distribution of uncrossed axons along the course of the optic nerve and chiasm of rodents. *J Comp Neurol* **289,** 455-61.

Barbieri, A. M., Broccoli, V., Bovolenta, P., Alfano, G., Marchitiello, A., Mocchetti, C., Crippa, L., Bulfone, A., Marigo, V., Ballabio, A., and Banfi, S. (2002). Vax2 inactivation in mouse determines alteration of the eye dorsal-ventral axis, misrouting of the optic fibres and eye coloboma. *Development* **129,** 805-13.

Barresi, M. J., Hutson, L. D., Chien, C. B., and Karlstrom, R. O. (2005). Hedgehog regulated Slit expression determines commissure and glial cell position in the zebrafish forebrain. *Development* **132,** 3643-56.

Bashaw, G. J., and Goodman, C. S. (1999). Chimeric axon guidance receptors: the cytoplasmic domains of slit and netrin receptors specify attraction versus repulsion. *Cell* **97,** 917-26.

Baumer, N., Marquardt, T., Stoykova, A., Ashery-Padan, R., Chowdhury, K., and Gruss, P. (2002). Pax6 is required for establishing naso-temporal and dorsal characteristics of the optic vesicle. *Development* **129,** 4535-45.

Becker, P. B., Weih, F., and Schutz, G. (1993). Footprinting of DNA-binding proteins in intact cells. *Methods Enzymol* **218,** 568-87.

Belloni, E., Muenke, M., Roessler, E., Traverso, G., Siegel-Bartelt, J., Frumkin, A., Mitchell, H. F., Donis-Keller, H., Helms, C., Hing, A. V., Heng, H. H., Koop, B., Martindale, D., Rommens, J. M., Tsui, L. C., and Scherer, S. W. (1996). Identification of Sonic hedgehog as a candidate gene responsible for holoprosencephaly. *Nat Genet* **14,** 353-6.

Bennett, K. L., Jackson, D. G., Simon, J. C., Tanczos, E., Peach, R., Modrell, B., Stamenkovic, I., Plowman, G., and Aruffo, A. (1995). CD44 isoforms containing exon V3 are responsible for the presentation of heparin-binding growth factor. *J Cell Biol* **128,** 687-98.

Bernfield, M., Gotte, M., Park, P. W., Reizes, O., Fitzgerald, M. L., Lincecum, J., and Zako, M. (1999). Functions of cell surface heparan sulfate proteoglycans. *Annu Rev Biochem* **68,** 729-77.

Bertuzzi, S., Hindges, R., Mui, S. H., O'Leary, D. D., and Lemke, G. (1999). The homeodomain protein vax1 is required for axon guidance and major tract formation in the developing forebrain. *Genes Dev* **13,** 3092-105.

Bhat, K. M. (2005). Slit-roundabout signaling neutralizes netrin-Frazzled-mediated attractant cue to specify the lateral positioning of longitudinal axon pathways. *Genetics* **170,** 149-59.

Birgbauer, E., Cowan, C. A., Sretavan, D. W., and Henkemeyer, M. (2000). Kinase independent function of EphB receptors in retinal axon pathfinding to the optic disc from dorsal but not ventral retina. *Development* **127,** 1231-41.

Bourguignon, C., Li, J., and Papalopulu, N. (1998). XBF-1, a winged helix transcription factor with dual activity, has a role in positioning neurogenesis in Xenopus competent ectoderm. *Development* **125,** 4889-900.

Braisted, J. E., McLaughlin, T., Wang, H. U., Friedman, G. C., Anderson, D. J., and O'Leary D, D. (1997). Graded and lamina-specific distributions of ligands of EphB receptor tyrosine kinases in the developing retinotectal system. *Dev Biol* **191,** 14-28.

Brennan, C., Monschau, B., Lindberg, R., Guthrie, B., Drescher, U., Bonhoeffer, F., and Holder, N. (1997). Two Eph receptor tyrosine kinase ligands control axon growth and may be involved in the creation of the retinotectal map in the zebrafish. *Development* **124,** 655-64.

Brewster, R., Lee, J., and Ruiz i Altaba, A. (1998). Gli/Zic factors pattern the neural plate by defining domains of cell differentiation. *Nature* **393,** 579-83.

Brose, K., Bland, K. S., Wang, K. H., Arnott, D., Henzel, W., Goodman, C. S., Tessier-Lavigne, M., and Kidd, T. (1999). Slit proteins bind Robo receptors and have an evolutionarily conserved role in repulsive axon guidance. *Cell* **96,** 795-806.

Brown, L. Y., Kottmann, A. H., and Brown, S. (2003). Immunolocalization of Zic2 expression in the developing mouse forebrain. *Gene Expr Patterns* **3,** 361-7.

Brown, L. Y., Odent, S., David, V., Blayau, M., Dubourg, C., Apacik, C., Delgado, M. A., Hall, B. D., Reynolds, J. F., Sommer, A., Wieczorek, D., Brown, S. A., and Muenke, M. (2001). Holoprosencephaly due to mutations in ZIC2: alanine tract expansion mutations may be caused by parental somatic recombination. *Hum Mol Genet* **10,** 791-6.

Brown, S. A., Warburton, D., Brown, L. Y., Yu, C. Y., Roeder, E. R., Stengel-Rutkowski, S., Hennekam, R. C., and Muenke, M. (1998). Holoprosencephaly due to mutations in ZIC2, a homologue of Drosophila odd-paired. *Nat Genet* **20,** 180-3.

Brunet, I., Weinl, C., Piper, M., Trembleau, A., Volovitch, M., Harris, W., Prochiantz, A., and Holt, C. (2005). The transcription factor Engrailed-2 guides retinal axons. *Nature* **438,** 94-8.

Bulow, H. E., and Hobert, O. (2004). Differential sulfations and epimerization define heparan sulfate specificity in nervous system development. *Neuron* **41,** 723-36.

Butler, S. J., and Dodd, J. (2003). A role for BMP heterodimers in roof plate-mediated repulsion of commissural axons. *Neuron* **38,** 389-401.

Butowt, R., Jeffrey, P. L., and von Bartheld, C. S. (2000). Purification of chick retinal ganglion cells for molecular analysis: combining retrograde labeling and immunopanning yields 100% purity. *J Neurosci Methods* **95,** 29-38.

Campbell, D. S., and Holt, C. E. (2001). Chemotropic responses of retinal growth cones mediated by rapid local protein synthesis and degradation. *Neuron* **32,** 1013-26.

Carlsson, P., and Mahlapuu, M. (2002). Forkhead transcription factors: key players in development and metabolism. *Dev Biol* **250,** 1-23.

Castella, P., Sawai, S., Nakao, K., Wagner, J. A., and Caudy, M. (2000). HES-1 repression of differentiation and proliferation in PC12 cells: role for the helix 3-helix 4 domain in transcription repression. *Mol Cell Biol* **20,** 6170-83.

Chan, S. O., and Chung, K. Y. (1999). Changes in axon arrangement in the retinofugal [correction of retinofungal] pathway of mouse embryos: confocal microscopy study using single- and double-dye label. *J Comp Neurol* **406,** 251-62.

Chan, S. O., Cheung, W. S., and Lin, L. (2002). Differential responses of temporal and nasal retinal neurites to regional-specific cues in the mouse retinofugal pathway. *Cell Tissue Res* **309,** 201-8.

Charron, F., Stein, E., Jeong, J., McMahon, A. P., and Tessier-Lavigne, M. (2003). The morphogen sonic hedgehog is an axonal chemoattractant that collaborates with netrin-1 in midline axon guidance. *Cell* **113,** 11-23.

Cheung, A. W., Lam, J. S., and Chan, S. O. (2005). Selective inhibition of ventral temporal but not dorsal nasal neurites from mouse retinal explants during contact with chondroitin sulphate. *Cell Tissue Res* **321,** 9-19.

Chiang, C., Litingtung, Y., Lee, E., Young, K. E., Corden, J. L., Westphal, H., and Beachy, P. A. (1996). Cyclopia and defective axial patterning in mice lacking Sonic hedgehog gene function. *Nature* **383,** 407-13.

Chow, R. L., and Lang, R. A. (2001). Early eye development in vertebrates. *Annu Rev Cell Dev Biol* **17,** 255-96.

Chung, K. Y., Leung, K. M., Lin, L., and Chan, S. O. (2001). Heparan sulfate proteoglycan expression in the optic chiasm of mouse embryos. *J Comp Neurol* **436,** 236-47.

Chung, K. Y., Shum, D. K., and Chan, S. O. (2000a). Expression of chondroitin sulfate proteoglycans in the chiasm of mouse embryos. *J Comp Neurol* **417,** 153-63.

Chung, K. Y., Taylor, J. S., Shum, D. K., and Chan, S. O. (2000b). Axon routing at the optic chiasm after enzymatic removal of chondroitin sulfate in mouse embryos. *Development* **127,** 2673-83.

Clark, K. L., Halay, E. D., Lai, E., and Burley, S. K. (1993). Co-crystal structure of the HNF-3/fork head DNA-recognition motif resembles histone H5. *Nature* **364,** 412-20.

Colello, R. J., and Guillery, R. W. (1990). The early development of retinal ganglion cells with uncrossed axons in the mouse: retinal position and axonal course. *Development* **108,** 515-23.

Collinson, J. M., Chanas, S. A., Hill, R. E., and West, J. D. (2004). Corneal development, limbal stem cell function, and corneal epithelial cell migration in the Pax6(+/-) mouse. *Invest Ophthalmol Vis Sci* **45,** 1101-8.

Collinson, J. M., Hill, R. E., and West, J. D. (2000). Different roles for Pax6 in the optic vesicle and facial epithelium mediate early morphogenesis of the murine eye. *Development* **127,** 945-56.

Connor, R. J., Menzel, P., and Pasquale, E. B. (1998). Expression and tyrosine phosphorylation of Eph receptors suggest multiple mechanisms in patterning of the visual system. *Dev Biol* **193,** 21-35.

Crino, P. B., and Eberwine, J. (1996). Molecular characterization of the dendritic growth cone: regulated mRNA transport and local protein synthesis. *Neuron* **17,** 1173-87.

Dakubo, G. D., Wang, Y. P., Mazerolle, C., Campsall, K., McMahon, A. P., and Wallace, V. A. (2003). Retinal ganglion cell-derived sonic hedgehog signaling is required for optic disc and stalk neuroepithelial cell development. *Development* **130,** 2967-80.

Davis, L., Dou, P., DeWit, M., and Kater, S. B. (1992). Protein synthesis within neuronal growth cones. *J Neurosci* **12,** 4867-77.

Deiner, M. S., Kennedy, T. E., Fazeli, A., Serafini, T., Tessier-Lavigne, M., and Sretavan, D. W. (1997). Netrin-1 and DCC mediate axon guidance locally at the optic disc: loss of function leads to optic nerve hypoplasia. *Neuron* **19,** 575-89.

Deiner, M. S., and Sretavan, D. W. (1999). Altered midline axon pathways and ectopic neurons in the developing hypothalamus of netrin-1- and DCC-deficient mice. *J Neurosci* **19,** 9900-12.

Dou, C., Lee, J., Liu, B., Liu, F., Massague, J., Xuan, S., and Lai, E. (2000). BF-1 interferes with transforming growth factor beta signaling by associating with Smad partners. *Mol Cell Biol* **20,** 6201-11.

Dou, C. L., Li, S., and Lai, E. (1999). Dual role of brain factor-1 in regulating growth and patterning of the cerebral hemispheres. *Cereb Cortex* **9,** 543-50.

Drager, U. C. (1985). Birth dates of retinal ganglion cells giving rise to the crossed and uncrossed optic projections in the mouse. *Proc R Soc Lond B Biol Sci* **224,** 57-77.

Drager, U. C., and Olsen, J. F. (1980). Origins of crossed and uncrossed retinal projections in pigmented and albino mice. *J Comp Neurol* **191,** 383-412.

Drescher, U., Bonhoeffer, F., and Muller, B. K. (1997). The Eph family in retinal axon guidance. *Curr Opin Neurobiol* **7,** 75-80.

Dutting, D., and Meyer, S. U. (1995). Transplantations of the chick eye anlage reveal an early determination of nasotemporal polarity. *Int J Dev Biol* **39,** 921-31.

Dutting, D., and Thanos, S. (1995). Early determination of nasal-temporal retinotopic specificity in the eye anlage of the chick embryo. *Dev Biol* **167,** 263-81.

Ebens, A., Brose, K., Leonardo, E. D., Hanson, M. G., Jr., Bladt, F., Birchmeier, C., Barres, B. A., and Tessier-Lavigne, M. (1996). Hepatocyte growth factor/scatter factor is an axonal chemoattractant and a neurotrophic factor for spinal motor neurons. *Neuron* **17,** 1157-72.

Echelard, Y., Epstein, D. J., St-Jacques, B., Shen, L., Mohler, J., McMahon, J. A., and McMahon, A. P. (1993). Sonic hedgehog, a member of a family of putative signaling molecules, is implicated in the regulation of CNS polarity. *Cell* **75,** 1417-30.

Ekker, S. C., Ungar, A. R., Greenstein, P., von Kessler, D. P., Porter, J. A., Moon, R. T., and Beachy, P. A. (1995). Patterning activities of vertebrate hedgehog proteins in the developing eye and brain. *Curr Biol* **5,** 944-55.

Elms, P., Scurry, A., Davies, J., Willoughby, C., Hacker, T., Bogani, D., and Arkell, R. (2004). Overlapping and distinct expression domains of Zic2 and Zic3 during mouse gastrulation. *Gene Expr Patterns* **4,** 505-11.

Ericson, J., Rashbass, P., Schedl, A., Brenner-Morton, S., Kawakami, A., van Heyningen, V., Jessell, T. M., and Briscoe, J. (1997). Pax6 controls progenitor cell identity and neuronal fate in response to graded Shh signaling. *Cell* **90,** 169-80.

Erskine, L., Williams, S. E., Brose, K., Kidd, T., Rachel, R. A., Goodman, C. S., Tessier-Lavigne, M., and Mason, C. A. (2000). Retinal ganglion cell axon guidance in the mouse optic chiasm: expression and function of robos and slits. *J Neurosci* **20,** 4975-82.

Falk, J., Bechara, A., Fiore, R., Nawabi, H., Zhou, H., Hoyo-Becerra, C., Bozon, M., Rougon, G., Grumet, M., Puschel, A. W., Sanes, J. R., and Castellani, V. (2005). Dual functional activity of semaphorin 3B is required for positioning the anterior commissure. *Neuron* **48,** 63-75.

Flanagan, J. G. (2006). Neural map specification by gradients. *Curr Opin Neurobiol* **16,** 59-66.

Flanagan, J. G., and Vanderhaeghen, P. (1998). The ephrins and Eph receptors in neural development. *Annu Rev Neurosci* **21,** 309-45.

Fukuda, Y., Sawai, H., Watanabe, M., Wakakuwa, K., and Morigiwa, K. (1989). Nasotemporal overlap of crossed and uncrossed retinal ganglion cell projections in the Japanese monkey (Macaca fuscata). *J Neurosci* **9,** 2353-73.

Garbe, D. S., and Bashaw, G. J. (2007). Independent functions of Slit-Robo repulsion and Netrin-Frazzled attraction regulate axon crossing at the midline in Drosophila. *J Neurosci* **27,** 3584-92.

Godement, P., Wang, L. C., and Mason, C. A. (1994). Retinal axon divergence in the optic chiasm: dynamics of growth cone behavior at the midline. *J Neurosci* **14,** 7024-39.

Grange, T., Rigaud, G., Bertrand, E., Fromont-Racine, M., Espinals, M. L., Roux, J., and Pictet, R. (1997). In Vivo Footprinting of the Genetic Interaction of Proteins with DNA and RNA. *In* "Advances in Molecular and Cell Biology" (I. L. Cartwright, Ed.), Vol. 21. Elsevier.

Grant, S., and Binns, K. E. (2003). Reduced influence of the ipsilateral ear on spatial tuning of auditory neurons in the albino superior colliculus: a knock-on effect of anomalies of the acoustic chiasm? *Exp Brain Res* **151,** 478-88.

Gripp, K. W., Wotton, D., Edwards, M. C., Roessler, E., Ades, L., Meinecke, P., Richieri-Costa, A., Zackai, E. H., Massague, J., Muenke, M., and Elledge, S. J. (2000).

Mutations in TGIF cause holoprosencephaly and link NODAL signalling to human neural axis determination. *Nat Genet* **25,** 205-8.

Gu, C., Rodriguez, E. R., Reimert, D. V., Shu, T., Fritzsch, B., Richards, L. J., Kolodkin, A. L., and Ginty, D. D. (2003). Neuropilin-1 conveys semaphorin and VEGF signaling during neural and cardiovascular development. *Dev Cell* **5,** 45-57.

Guillery, R. W., Mason, C. A., and Taylor, J. S. (1995). Developmental determinants at the mammalian optic chiasm. *J Neurosci* **15,** 4727-37.

Guimond, S. E., and Turnbull, J. E. (1999). Fibroblast growth factor receptor signalling is dictated by specific heparan sulphate saccharides. *Curr Biol* **9,** 1343-6.

Hall, A. C., Lucas, F. R., and Salinas, P. C. (2000). Axonal remodeling and synaptic differentiation in the cerebellum is regulated by WNT-7a signaling. *Cell* **100,** 525-35.

Han, D. C., Shen, T. L., Miao, H., Wang, B., and Guan, J. L. (2002). EphB1 associates with Grb7 and regulates cell migration. *J Biol Chem* **277,** 45655-61.

Hanashima, C., Li, S. C., Shen, L., Lai, E., and Fishell, G. (2004). Foxg1 suppresses early cortical cell fate. *Science* **303,** 56-9.

Hanashima, C., Shen, L., Li, S. C., and Lai, E. (2002). Brain factor-1 controls the proliferation and differentiation of neocortical progenitor cells through independent mechanisms. *J Neurosci* **22,** 6526-36.

Hao, Y. L., Chan, S. O., and Dong, W. R. (2006). Changes of retinofugal pathway development in mouse embryos after Sonic hedgehog antibody perturbation. *Nan Fang Yi Ke Da Xue Xue Bao* **26,** 1679-84.

Hardcastle, Z., and Papalopulu, N. (2000). Distinct effects of XBF-1 in regulating the cell cycle inhibitor p27(XIC1) and imparting a neural fate. *Development* **127,** 1303-14.

Harris, W. A., Holt, C. E., and Bonhoeffer, F. (1987). Retinal axons with and without their somata, growing to and arborizing in the tectum of Xenopus embryos: a time-lapse video study of single fibres in vivo. *Development* **101,** 123-33.

Hatini, V., Tao, W., and Lai, E. (1994). Expression of winged helix genes, BF-1 and BF-2, define adjacent domains within the developing forebrain and retina. *J Neurobiol* **25,** 1293-309.

Hebert, J. M., and McConnell, S. K. (2000). Targeting of cre to the Foxg1 (BF-1) locus mediates loxP recombination in the telencephalon and other developing head structures. *Dev Biol* **222,** 296-306.

Henkemeyer, M., Orioli, D., Henderson, J. T., Saxton, T. M., Roder, J., Pawson, T., and Klein, R. (1996). Nuk controls pathfinding of commissural axons in the mammalian central nervous system. *Cell* **86,** 35-46.

Herrera, E., Brown, L., Aruga, J., Rachel, R. A., Dolen, G., Mikoshiba, K., Brown, S., and Mason, C. A. (2003). Zic2 patterns binocular vision by specifying the uncrossed retinal projection. *Cell* **114,** 545-57.

Herrera, E., Marcus, R., Li, S., Williams, S. E., Erskine, L., Lai, E., and Mason, C. (2004). Foxd1 is required for proper formation of the optic chiasm. *Development* **131,** 5727-39.

Hill, R. E., Favor, J., Hogan, B. L., Ton, C. C., Saunders, G. F., Hanson, I. M., Prosser, J., Jordan, T., Hastie, N. D., and van Heyningen, V. (1991). Mouse small eye results from mutations in a paired-like homeobox-containing gene. *Nature* **354,** 522-5.

Hindges, R., McLaughlin, T., Genoud, N., Henkemeyer, M., and O'Leary, D. D. (2002). EphB forward signaling controls directional branch extension and arborization required for dorsal-ventral retinotopic mapping. *Neuron* **35,** 475-87.

Hiramoto, M., and Hiromi, Y. (2006). ROBO directs axon crossing of segmental boundaries by suppressing responsiveness to relocalized Netrin. *Nat Neurosci* **9,** 58-66.

Holash, J. A., and Pasquale, E. B. (1995). Polarized expression of the receptor protein tyrosine kinase Cek5 in the developing avian visual system. *Dev Biol* **172,** 683-93.

Holash, J. A., Soans, C., Chong, L. D., Shao, H., Dixit, V. M., and Pasquale, E. B. (1997). Reciprocal expression of the Eph receptor Cek5 and its ligand(s) in the early retina. *Dev Biol* **182,** 256-69.

Holt, C. E., Bertsch, T. W., Ellis, H. M., and Harris, W. A. (1988). Cellular determination in the Xenopus retina is independent of lineage and birth date. *Neuron* **1,** 15-26.

Hopker, V. H., Shewan, D., Tessier-Lavigne, M., Poo, M., and Holt, C. (1999). Growth-cone attraction to netrin-1 is converted to repulsion by laminin-1. *Nature* **401,** 69-73.

Huh, S., Hatini, V., Marcus, R. C., Li, S. C., and Lai, E. (1999). Dorsal-ventral patterning defects in the eye of BF-1-deficient mice associated with a restricted loss of shh expression. *Dev Biol* **211,** 53-63.

Hussain, S. A., Piper, M., Fukuhara, N., Strochlic, L., Cho, G., Howitt, J. A., Ahmed, Y., Powell, A. K., Turnbull, J. E., Holt, C. E., and Hohenester, E. (2006). A molecular mechanism for the heparan sulfate dependence of slit-robo signaling. *J Biol Chem* **281,** 39693-8.

Ichijo, H. (2004). Proteoglycans as cues for axonal guidance in formation of retinotectal or retinocollicular projections. *Mol Neurobiol* **30,** 23-33.

Inoue, T., Hatayama, M., Tohmonda, T., Itohara, S., Aruga, J., and Mikoshiba, K. (2004). Mouse Zic5 deficiency results in neural tube defects and hypoplasia of cephalic neural crest derivatives. *Dev Biol* **270,** 146-62.

Insausti, R., Blakemore, C., and Cowan, W. M. (1984). Ganglion cell death during development of ipsilateral retino-collicular projection in golden hamster. *Nature* **308,** 362-5.

Itasaki, N., Ichijo, H., Hama, C., Matsuno, T., and Nakamura, H. (1991). Establishment of rostrocaudal polarity in tectal primordium: engrailed expression and subsequent tectal polarity. *Development* **113,** 1133-44.

Itasaki, N., and Nakamura, H. (1996). A role for gradient en expression in positional specification on the optic tectum. *Neuron* **16,** 55-62.

Jeffery, G. (2001). Architecture of the optic chiasm and the mechanisms that sculpt its development. *Physiol Rev* **81,** 1393-414.

Jeffery, G., Cowey, A., and Kuypers, H. G. (1981). Bifurcating retinal ganglion cell axons in the rat, demonstrated by retrograde double labelling. *Exp Brain Res* **44,** 34-40.

Joliot, A., and Prochiantz, A. (2004). Transduction peptides: from technology to physiology. *Nat Cell Biol* **6,** 189-96.

Jones, M., Tussey, L., Athanasou, N., and Jackson, D. G. (2000). Heparan sulfate proteoglycan isoforms of the CD44 hyaluronan receptor induced in human inflammatory macrophages can function as paracrine regulators of fibroblast growth factor action. *J Biol Chem* **275,** 7964-74.

Joyner, A. L., and Martin, G. R. (1987). En-1 and En-2, two mouse genes with sequence homology to the Drosophila engrailed gene: expression during embryogenesis. *Genes Dev* **1,** 29-38.

Kaprielian, Z., Runko, E., and Imondi, R. (2001). Axon guidance at the midline choice point. *Dev Dyn* **221,** 154-81.

Kennedy, T. E., Serafini, T., de la Torre, J. R., and Tessier-Lavigne, M. (1994). Netrins are diffusible chemotropic factors for commissural axons in the embryonic spinal cord. *Cell* **78,** 425-35.

Kidd, T., Bland, K. S., and Goodman, C. S. (1999). Slit is the midline repellent for the robo receptor in Drosophila. *Cell* **96,** 785-94.

Kidd, T., Brose, K., Mitchell, K. J., Fetter, R. D., Tessier-Lavigne, M., Goodman, C. S., and Tear, G. (1998). Roundabout controls axon crossing of the CNS midline and defines a novel subfamily of evolutionarily conserved guidance receptors. *Cell* **92,** 205-15.

Kintner, C. (2002). Neurogenesis in embryos and in adult neural stem cells. *J Neurosci* **22,** 639-43.

Klein, R. (2004). Eph/ephrin signaling in morphogenesis, neural development and plasticity. *Curr Opin Cell Biol* **16,** 580-9.

Koshiba-Takeuchi, K., Takeuchi, J. K., Matsumoto, K., Momose, T., Uno, K., Hoepker, V., Ogura, K., Takahashi, N., Nakamura, H., Yasuda, K., and Ogura, T. (2000). Tbx5 and the retinotectum projection. *Science* **287,** 134-7.

Koyabu, Y., Nakata, K., Mizugishi, K., Aruga, J., and Mikoshiba, K. (2001). Physical and functional interactions between Zic and Gli proteins. *J Biol Chem* **276,** 6889-92.

Kruger, K., Tam, A. S., Lu, C., and Sretavan, D. W. (1998). Retinal ganglion cell axon progression from the optic chiasm to initiate optic tract development requires cell autonomous function of GAP-43. *J Neurosci* **18,** 5692-705.

Kullander, K., and Klein, R. (2002). Mechanisms and functions of Eph and ephrin signalling. *Nat Rev Mol Cell Biol* **3,** 475-86.

Lambot, M. A., Depasse, F., Noel, J. C., and Vanderhaeghen, P. (2005). Mapping labels in the human developing visual system and the evolution of binocular vision. *J Neurosci* **25,** 7232-7.

Lander, A. D. (1987). Molecules that make axons grow. *Mol Neurobiol* **1,** 213-45.

Lehmann, O. J., Ebenezer, N. D., Jordan, T., Fox, M., Ocaka, L., Payne, A., Leroy, B. P., Clark, B. J., Hitchings, R. A., Povey, S., Khaw, P. T., and Bhattacharya, S. S. (2000). Chromosomal duplication involving the forkhead transcription factor gene FOXC1 causes iris hypoplasia and glaucoma. *Am J Hum Genet* **67,** 1129-35.

Lehmann, O. J., Sowden, J. C., Carlsson, P., Jordan, T., and Bhattacharya, S. S. (2003). Fox's in development and disease. *Trends Genet* **19,** 339-44.

Lesaffre, B., Joliot, A., Prochiantz, A., and Volovitch, M. (2007). Direct non-cell autonomous Pax6 activity regulates eye development in the zebrafish. *Neural Develop* **2,** 2.

Li, J., Thurm, H., Chang, H. W., Iacovoni, J. S., and Vogt, P. K. (1997). Oncogenic transformation induced by the Qin protein is correlated with transcriptional repression. *Proc Natl Acad Sci U S A* **94,** 10885-8.

Liesi, P., and Silver, J. (1988). Is astrocyte laminin involved in axon guidance in the mammalian CNS? *Dev Biol* **130,** 774-85.

Lin, D. M., and Goodman, C. S. (1994). Ectopic and increased expression of Fasciclin II alters motoneuron growth cone guidance. *Neuron* **13,** 507-23.

Lin, L., and Chan, S. O. (2003). Perturbation of CD44 function affects chiasmatic routing of retinal axons in brain slice preparations of the mouse retinofugal pathway. *European Journal of Neuroscience* **17,** 2299-312.

Lin, L., Cheung, A. W., and Chan, S. O. (2005). Chiasmatic neurons in the ventral diencephalon of mouse embryos--changes in arrangement and heterogeneity in surface antigen expression. *Brain Res Dev Brain Res* **158,** 1-12.

Lin, L., Taylor, J. S., and Chan, S. O. (2002). Changes in expression of fibroblast growth factor receptors during development of the mouse retinofugal pathway. *J Comp Neurol* **451,** 22-32.

Lindwall, C., Fothergill, T., and Richards, L. J. (2007). Commissure formation in the mammalian forebrain. *Curr Opin Neurobiol* **17,** 3-14.

Long, H., Sabatier, C., Ma, L., Plump, A., Yuan, W., Ornitz, D. M., Tamada, A., Murakami, F., Goodman, C. S., and Tessier-Lavigne, M. (2004). Conserved roles for Slit and Robo proteins in midline commissural axon guidance. *Neuron* **42,** 213-23.

Lupo, G., Liu, Y., Qiu, R., Chandraratna, R. A., Barsacchi, G., He, R. Q., and Harris, W. A. (2005). Dorsoventral patterning of the Xenopus eye: a collaboration of Retinoid, Hedgehog and FGF receptor signaling. *Development* **132,** 1737-48.

Lustig, M., Erskine, L., Mason, C. A., Grumet, M., and Sakurai, T. (2001). Nr-CAM expression in the developing mouse nervous system: ventral midline structures, specific fiber tracts, and neuropilar regions. *J Comp Neurol* **434,** 13-28.

Lyuksyutova, A. I., Lu, C. C., Milanesio, N., King, L. A., Guo, N., Wang, Y., Nathans, J., Tessier-Lavigne, M., and Zou, Y. (2003). Anterior-posterior guidance of commissural axons by Wnt-frizzled signaling. *Science* **302,** 1984-8.

Macdonald, R., Barth, K. A., Xu, Q., Holder, N., Mikkola, I., and Wilson, S. W. (1995). Midline signalling is required for Pax gene regulation and patterning of the eyes. *Development* **121,** 3267-78.

Macdonald, R., Scholes, J., Strahle, U., Brennan, C., Holder, N., Brand, M., and Wilson, S. W. (1997). The Pax protein Noi is required for commissural axon pathway formation in the rostral forebrain. *Development* **124,** 2397-408.

Macdonald, R., Xu, Q., Barth, K. A., Mikkola, I., Holder, N., Fjose, A., Krauss, S., and Wilson, S. W. (1994). Regulatory gene expression boundaries demarcate sites of neuronal differentiation in the embryonic zebrafish forebrain. *Neuron* **13,** 1039-53.

Mann, F., Peuckert, C., Dehner, F., Zhou, R., and Bolz, J. (2002). Ephrins regulate the formation of terminal axonal arbors during the development of thalamocortical projections. *Development* **129,** 3945-55.

Mao, X., Fujiwara, Y., and Orkin, S. H. (1999). Improved reporter strain for monitoring Cre recombinase-mediated DNA excisions in mice. *Proc Natl Acad Sci U S A* **96,** 5037-42.

Marcus, R. C., Blazeski, R., Godement, P., and Mason, C. A. (1995). Retinal axon divergence in the optic chiasm: uncrossed axons diverge from crossed axons within a midline glial specialization. *J Neurosci* **15,** 3716-29.

Marcus, R. C., and Mason, C. A. (1995). The first retinal axon growth in the mouse optic chiasm: axon patterning and the cellular environment. *J Neurosci* **15,** 6389-402.

Marcus, R. C., Matthews, G. A., Gale, N. W., Yancopoulos, G. D., and Mason, C. A. (2000). Axon guidance in the mouse optic chiasm: retinal neurite inhibition by ephrin "A"-expressing hypothalamic cells in vitro. *Dev Biol* **221,** 132-47.

Marcus, R. C., Shimamura, K., Sretavan, D., Lai, E., Rubenstein, J. L., and Mason, C. A. (1999). Domains of regulatory gene expression and the developing optic chiasm: correspondence with retinal axon paths and candidate signaling cells. *J Comp Neurol* **403,** 346-58.

Marcus, R. C., Gale, N. W., Morrison, M. E., Mason, C. A., and Yancopoulos, G. D. (1996a). Eph family receptors and their ligands distribute in opposing gradients in the developing mouse retina. *Dev Biol* **180,** 786-9.

Marcus, R. C., Wang, L. C., and Mason, C. A. (1996b). Retinal axon divergence in the optic chiasm: midline cells are unaffected by the albino mutation. *Development* **122,** 859-68.

Martynoga, B., Morrison, H., Price, D. J., and Mason, J. O. (2005). Foxg1 is required for specification of ventral telencephalon and region-specific regulation of dorsal telencephalic precursor proliferation and apoptosis. *Dev Biol* **283,** 113-27.

Mason, C. A., and Wang, L. C. (1997). Growth cone form is behavior-specific and, consequently, position-specific along the retinal axon pathway. *J Neurosci* **17,** 1086-100.

Mason, C. A., and Sretavan, D. W. (1997). Glia, neurons, and axon pathfinding during optic chiasm development. *Curr Opin Neurobiol* **7,** 647-53.

Mastick, G. S., Davis, N. M., Andrew, G. L., and Easter, S. S., Jr. (1997). Pax-6 functions in boundary formation and axon guidance in the embryonic mouse forebrain. *Development* **124,** 1985-97.

McAdams, B. D., and McLoon, S. C. (1995). Expression of chondroitin sulfate and keratan sulfate proteoglycans in the path of growing retinal axons in the developing chick. *J Comp Neurol* **352,** 594-606.

McLaughlin, T., Hindges, R., and O'Leary, D. D. (2003). Regulation of axial patterning of the retina and its topographic mapping in the brain. *Curr Opin Neurobiol* **13,** 57-69.

Mitchell, K. J., Doyle, J. L., Serafini, T., Kennedy, T. E., Tessier-Lavigne, M., Goodman, C. S., and Dickson, B. J. (1996). Genetic analysis of Netrin genes in Drosophila: Netrins guide CNS commissural axons and peripheral motor axons. *Neuron* **17,** 203-15.

Mizugishi, K., Aruga, J., Nakata, K., and Mikoshiba, K. (2001). Molecular properties of Zic proteins as transcriptional regulators and their relationship to GLI proteins. *J Biol Chem* **276,** 2180-8.

Mui, S. H., Hindges, R., O'Leary, D. D., Lemke, G., and Bertuzzi, S. (2002). The homeodomain protein Vax2 patterns the dorsoventral and nasotemporal axes of the eye. *Development* **129,** 797-804.

Murphy, D. B., Wiese, S., Burfeind, P., Schmundt, D., Mattei, M. G., Schulz-Schaeffer, W., and Thies, U. (1994). Human brain factor 1, a new member of the fork head gene family. *Genomics* **21,** 551-7.

Nagai, T., Aruga, J., Minowa, O., Sugimoto, T., Ohno, Y., Noda, T., and Mikoshiba, K. (2000). Zic2 regulates the kinetics of neurulation. *Proc Natl Acad Sci U S A* **97,** 1618-23.

Nagai, T., Aruga, J., Takada, S., Gunther, T., Sporle, R., Schughart, K., and Mikoshiba, K. (1997). The expression of the mouse Zic1, Zic2, and Zic3 gene suggests an essential role for Zic genes in body pattern formation. *Dev Biol* **182,** 299-313.

Nakagawa, S., Brennan, C., Johnson, K. G., Shewan, D., Harris, W. A., and Holt, C. E. (2000). Ephrin-B regulates the Ipsilateral routing of retinal axons at the optic chiasm. *Neuron* **25,** 599-610.

Niclou, S. P., Jia, L., and Raper, J. A. (2000). Slit2 is a repellent for retinal ganglion cell axons. *J Neurosci* **20,** 4962-74.

O'Connor, R., and Tessier-Lavigne, M. (1999). Identification of maxillary factor, a maxillary process-derived chemoattractant for developing trigeminal sensory axons. *Neuron* **24,** 165-78.

O'Leary, D. D., and McLaughlin, T. (2005). Mechanisms of retinotopic map development: Ephs, ephrins, and spontaneous correlated retinal activity. *Prog Brain Res* **147,** 43-65.

Oppenheim, R. W. (1991). Cell death during development of the nervous system. *Annu Rev Neurosci* **14,** 453-501.

Pak, W., Hindges, R., Lim, Y. S., Pfaff, S. L., and O'Leary, D. D. (2004). Magnitude of binocular vision controlled by islet-2 repression of a genetic program that specifies laterality of retinal axon pathfinding. *Cell* **119,** 567-78.

Pan, L., Yang, Z., Feng, L., and Gan, L. (2005). Functional equivalence of Brn3 POU-domain transcription factors in mouse retinal neurogenesis. *Development* **132,** 703-12.

Pasterkamp, R. J., and Kolodkin, A. L. (2003). Semaphorin junction: making tracks toward neural connectivity. *Curr Opin Neurobiol* **13,** 79-89.

Perrimon, N., and Bernfield, M. (2000). Specificities of heparan sulphate proteoglycans in developmental processes. *Nature* **404,** 725-8.

Peters, M. A. (2002). Patterning the neural retina. *Curr Opin Neurobiol* **12,** 43-8.

Placzek, M., Tessier-Lavigne, M., Yamada, T., Dodd, J., and Jessell, T. M. (1990). Guidance of developing axons by diffusible chemoattractants. *Cold Spring Harb Symp Quant Biol* **55,** 279-89.

Plump, A. S., Erskine, L., Sabatier, C., Brose, K., Epstein, C. J., Goodman, C. S., Mason, C. A., and Tessier-Lavigne, M. (2002). Slit1 and Slit2 cooperate to prevent premature midline crossing of retinal axons in the mouse visual system. *Neuron* **33,** 219-32.

Polyak, S. (1957). "The Vertebrate Visual System." University of Chicago Press,
Prada, C., Puga, J., Perez-Mendez, L., Lopez, R., and Ramirez, G. (1991). Spatial and Temporal Patterns of Neurogenesis in the Chick Retina. *Eur J Neurosci* **3,** 559-569.

Pratt, T., Conway, C. D., Tian, N. M., Price, D. J., and Mason, J. O. (2006). Heparan sulphation patterns generated by specific heparan sulfotransferase enzymes direct distinct aspects of retinal axon guidance at the optic chiasm. *J Neurosci* **26,** 6911-23.

Pratt, T., Quinn, J. C., Simpson, T. I., West, J. D., Mason, J. O., and Price, D. J. (2002). Disruption of early events in thalamocortical tract formation in mice lacking the transcription factors Pax6 or Foxg1. *J Neurosci* **22,** 8523-31.

Pratt, T., Tian, N. M., Simpson, T. I., Mason, J. O., and Price, D. J. (2004). The winged helix transcription factor Foxg1 facilitates retinal ganglion cell axon crossing of the ventral midline in the mouse. *Development* **131,** 3773-84.

Pratt, T., Vitalis, T., Warren, N., Edgar, J. M., Mason, J. O., and Price, D. J. (2000). A role for Pax6 in the normal development of dorsal thalamus and its cortical connections. *Development* **127,** 5167-78.

Prochiantz, A. (2000). Messenger proteins: homeoproteins, TAT and others. *Curr Opin Cell Biol* **12,** 400-6.

Prochiantz, A., and Joliot, A. (2003). Can transcription factors function as cell-cell signalling molecules? *Nat Rev Mol Cell Biol* **4,** 814-9.

Provis, J. M., and Penfold, P. L. (1988). Cell death and the elimination of retinal axons during development. *Prog Neurobiol* **31,** 331-47.

Quina, L. A., Pak, W., Lanier, J., Banwait, P., Gratwick, K., Liu, Y., Velasquez, T., O'Leary, D. D., Goulding, M., and Turner, E. E. (2005). Brn3a-expressing retinal ganglion cells project specifically to thalamocortical and collicular visual pathways. *J Neurosci* **25,** 11595-604.

Rachel, R. A., Dolen, G., Hayes, N. L., Lu, A., Erskine, L., Nowakowski, R. S., and Mason, C. A. (2002). Spatiotemporal features of early neuronogenesis differ in wild-type and albino mouse retina. *J Neurosci* **22,** 4249-63.

Ransone, L. J. (1995). Detection of protein-protein interactions by coimmunoprecipitation and dimerization. *Methods Enzymol* **254,** 491-7.

Reese, B. E., and Baker, G. E. (1990). The Course of Fibre Diameter Classes Through the Chiasmatic Region in the Ferret. *Eur J Neurosci* **2,** 34-49.

Reese, B. E., and Baker, G. E. (1992). Changes in fiber organization within the chiasmatic region of mammals. *Vis Neurosci* **9,** 527-33.

Reese, B. E., and Colello, R. J. (1992). Neurogenesis in the retinal ganglion cell layer of the rat. *Neuroscience* **46,** 419-29.

Regad, T., Roth, M., Bredenkamp, N., Illing, N., and Papalopulu, N. (2007). The neural progenitor-specifying activity of FoxG1 is antagonistically regulated by CKI and FGF. *Nat Cell Biol* **9,** 531-40.

Retaux, S., and Harris, W. A. (1996). Engrailed and retinotectal topography. *Trends Neurosci* **19,** 542-6.

Reza, H. M., Takahashi, Y., and Yasuda, K. (2007). Stage-dependent expression of Pax6 in optic vesicle/cup regulates patterning genes through signaling molecules. *Differentiation*.

Ringstedt, T., Braisted, J. E., Brose, K., Kidd, T., Goodman, C., Tessier-Lavigne, M., and O'Leary, D. D. (2000). Slit inhibition of retinal axon growth and its role in retinal axon pathfinding and innervation patterns in the diencephalon. *J Neurosci* **20,** 4983-91.

Roessler, E., Belloni, E., Gaudenz, K., Jay, P., Berta, P., Scherer, S. W., Tsui, L. C., and Muenke, M. (1996). Mutations in the human Sonic Hedgehog gene cause holoprosencephaly. *Nat Genet* **14,** 357-60.

Rohr, K. B., Schulte-Merker, S., and Tautz, D. (1999). Zebrafish zic1 expression in brain and somites is affected by BMP and hedgehog signalling. *Mech Dev* **85,** 147-59.

Runko, E., and Kaprielian, Z. (2002). Expression of Vema in the developing mouse spinal cord and optic chiasm. *J Comp Neurol* **451,** 289-99.

Sakuta, H., Suzuki, R., Takahashi, H., Kato, A., Shintani, T., Iemura, S., Yamamoto, T. S., Ueno, N., and Noda, M. (2001). Ventroptin: a BMP-4 antagonist expressed in a double-gradient pattern in the retina. *Science* **293,** 111-5.

Salie, R., Niederkofler, V., and Arber, S. (2005). Patterning molecules; multitasking in the nervous system. *Neuron* **45,** 189-92.

Schulte, D., and Cepko, C. L. (2000). Two homeobox genes define the domain of EphA3 expression in the developing chick retina. *Development* **127,** 5033-45.

Schulte, D., Furukawa, T., Peters, M. A., Kozak, C. A., and Cepko, C. L. (1999). Misexpression of the Emx-related homeobox genes cVax and mVax2 ventralizes the retina and perturbs the retinotectal map. *Neuron* **24,** 541-53.

Seoane, J. (2004). p21(WAF1/CIP1) at the switch between the anti-oncogenic and oncogenic faces of TGFbeta. *Cancer Biol Ther* **3,** 226-7.

Serafini, T., Colamarino, S. A., Leonardo, E. D., Wang, H., Beddington, R., Skarnes, W. C., and Tessier-Lavigne, M. (1996). Netrin-1 is required for commissural axon guidance in the developing vertebrate nervous system. *Cell* **87,** 1001-14.

Serafini, T., Kennedy, T. E., Galko, M. J., Mirzayan, C., Jessell, T. M., and Tessier-Lavigne, M. (1994). The netrins define a family of axon outgrowth-promoting proteins homologous to C. elegans UNC-6. *Cell* **78,** 409-24.

Shaw, G., and Bray, D. (1977). Movement and extension of isolated growth cones. *Exp Cell Res* **104,** 55-62.

Shewan, D., Dwivedy, A., Anderson, R., and Holt, C. E. (2002). Age-related changes underlie switch in netrin-1 responsiveness as growth cones advance along visual pathway. *Nat Neurosci* **5,** 955-62.

Shimamura, K., Hartigan, D. J., Martinez, S., Puelles, L., and Rubenstein, J. L. (1995). Longitudinal organization of the anterior neural plate and neural tube. *Development* **121,** 3923-33.

Shirasaki, R., Mirzayan, C., Tessier-Lavigne, M., and Murakami, F. (1996). Guidance of circumferentially growing axons by netrin-dependent and -independent floor plate chemotropism in the vertebrate brain. *Neuron* **17,** 1079-88.

Silver, J. (1993). Glia-neuron interactions at the midline of the developing mammalian brain and spinal cord. *Perspect Dev Neurobiol* **1,** 227-36.

Solomon, M. J., and Varshavsky, A. (1985). Formaldehyde-mediated DNA-protein crosslinking: a probe for in vivo chromatin structures. *Proc Natl Acad Sci U S A* **82,** 6470-4.

Song, H., Ming, G., He, Z., Lehmann, M., McKerracher, L., Tessier-Lavigne, M., and Poo, M. (1998). Conversion of neuronal growth cone responses from repulsion to attraction by cyclic nucleotides. *Science* **281,** 1515-8.

Song, H. J., and Poo, M. M. (1999). Signal transduction underlying growth cone guidance by diffusible factors. *Curr Opin Neurobiol* **9,** 355-63.

Soriano, P. (1999). Generalized lacZ expression with the ROSA26 Cre reporter strain. *Nat Genet* **21,** 70-1.

Sperry, R. W. (1963). Chemoaffinity in the Orderly Growth of Nerve Fiber Patterns and Connections. *Proc Natl Acad Sci U S A* **50,** 703-10.

Sretavan, D. W. (1990). Specific routing of retinal ganglion cell axons at the mammalian optic chiasm during embryonic development. *J Neurosci* **10,** 1995-2007.

Sretavan, D. W., Feng, L., Pure, E., and Reichardt, L. F. (1994). Embryonic neurons of the developing optic chiasm express L1 and CD44, cell surface molecules with opposing effects on retinal axon growth. *Neuron* **12,** 957-75.

Sretavan, D. W., and Kruger, K. (1998). Randomized retinal ganglion cell axon routing at the optic chiasm of GAP-43-deficient mice: association with midline recrossing and lack of normal ipsilateral axon turning. *J Neurosci* **18,** 10502-13.

Sretavan, D. W., Pure, E., Siegel, M. W., and Reichardt, L. F. (1995). Disruption of retinal axon ingrowth by ablation of embryonic mouse optic chiasm neurons. *Science* **269,** 98-101.

Sretavan, D. W., and Reichardt, L. F. (1993). Time-lapse video analysis of retinal ganglion cell axon pathfinding at the mammalian optic chiasm: growth cone guidance using intrinsic chiasm cues. *Neuron* **10,** 761-77.

Stein, E., and Tessier-Lavigne, M. (2001). Hierarchical organization of guidance receptors: silencing of netrin attraction by slit through a Robo/DCC receptor complex. *Science* **291,** 1928-38.

Steindler, D. A. (1993). Glial boundaries in the developing nervous system. *Annu Rev Neurosci* **16,** 445-70.

Suter, D. M., and Forscher, P. (1998). An emerging link between cytoskeletal dynamics and cell adhesion molecules in growth cone guidance. *Curr Opin Neurobiol* **8,** 106-16.

Takahashi, H., Shintani, T., Sakuta, H., and Noda, M. (2003). CBF1 controls the retinotectal topographical map along the anteroposterior axis through multiple mechanisms. *Development* **130,** 5203-15.

Takahashi, T., Nowakowski, R. S., and Caviness, V. S., Jr. (1993). Cell cycle parameters and patterns of nuclear movement in the neocortical proliferative zone of the fetal mouse. *J Neurosci* **13,** 820-33.

Tao, W., and Lai, E. (1992). Telencephalon-restricted expression of BF-1, a new member of the HNF-3/fork head gene family, in the developing rat brain. *Neuron* **8,** 957-66.

Tessier-Lavigne, M., and Goodman, C. S. (1996). The molecular biology of axon guidance. *Science* **274,** 1123-33.

Tessier-Lavigne, M., Placzek, M., Lumsden, A. G., Dodd, J., and Jessell, T. M. (1988). Chemotropic guidance of developing axons in the mammalian central nervous system. *Nature* **336,** 775-8.

Thanos, S., and Mey, J. (2001). Development of the visual system of the chick. II. Mechanisms of axonal guidance. *Brain Res Brain Res Rev* **35,** 205-45.

Thanos, S., Puttmann, S., Naskar, R., Rose, K., Langkamp-Flock, M., and Paulus, W. (2004). Potential role of Pax-2 in retinal axon navigation through the chick optic nerve stalk and optic chiasm. *J Neurobiol* **59,** 8-23.

Thompson, H., Barker, D., Camand, O., and Erskine, L. (2006b). Slits contribute to the guidance of retinal ganglion cell axons in the mammalian optic tract. *Dev Biol* **296,** 476-84.

Thompson, H., Camand, O., Barker, D., and Erskine, L. (2006a). Slit proteins regulate distinct aspects of retinal ganglion cell axon guidance within dorsal and ventral retina. *J Neurosci* **26,** 8082-91.

Tole, S., and Patterson, P. H. (1995). Regionalization of the developing forebrain: a comparison of FORSE-1, Dlx-2, and BF-1. *J Neurosci* **15,** 970-80.

Torres, M., Gomez-Pardo, E., and Gruss, P. (1996). Pax2 contributes to inner ear patterning and optic nerve trajectory. *Development* **122,** 3381-91.

Trousse, F., Marti, E., Gruss, P., Torres, M., and Bovolenta, P. (2001). Control of retinal ganglion cell axon growth: a new role for Sonic hedgehog. *Development* **128,** 3927-36.

Turner, D. L., and Cepko, C. L. (1987). A common progenitor for neurons and glia persists in rat retina late in development. *Nature* **328,** 131-6.

Tuttle, R., Braisted, J. E., Richards, L. J., and O'Leary, D. D. (1998). Retinal axon guidance by region-specific cues in diencephalon. *Development* **125,** 791-801.

Vidovic, M., and Marotte, L. R. (2003). Analysis of EphB receptors and their ligands in the developing retinocollicular system of the wallaby reveals dynamic patterns of expression in the retina. *Eur J Neurosci* **18,** 1549-58.

Vidovic, M., Marotte, L. R., and Mark, R. F. (1999). Marsupial retinocollicular system shows differential expression of messenger RNA encoding EphA receptors and their ligands during development. *J Neurosci Res* **57,** 244-54.

Wallis, D. E., Roessler, E., Hehr, U., Nanni, L., Wiltshire, T., Richieri-Costa, A., Gillessen-Kaesbach, G., Zackai, E. H., Rommens, J., and Muenke, M. (1999). Mutations in the homeodomain of the human SIX3 gene cause holoprosencephaly. *Nat Genet* **22,** 196-8.

Walter, J., Kern-Veits, B., Huf, J., Stolze, B., and Bonhoeffer, F. (1987). Recognition of position-specific properties of tectal cell membranes by retinal axons in vitro. *Development* **101,** 685-96.

Walther, C., and Gruss, P. (1991). Pax-6, a murine paired box gene, is expressed in the developing CNS. *Development* **113,** 1435-49.

Walz, A., Anderson, R. B., Irie, A., Chien, C. B., and Holt, C. E. (2002). Chondroitin sulfate disrupts axon pathfinding in the optic tract and alters growth cone dynamics. *J Neurobiol* **53,** 330-42.

Walz, A., McFarlane, S., Brickman, Y. G., Nurcombe, V., Bartlett, P. F., and Holt, C. E. (1997). Essential role of heparan sulfates in axon navigation and targeting in the developing visual system. *Development* **124,** 2421-30.

Wang, L. C., Dani, J., Godement, P., Marcus, R. C., and Mason, C. A. (1995). Crossed and uncrossed retinal axons respond differently to cells of the optic chiasm midline in vitro. *Neuron* **15,** 1349-64.

Wang, L. C., Rachel, R. A., Marcus, R. C., and Mason, C. A. (1996). Chemosuppression of retinal axon growth by the mouse optic chiasm. *Neuron* **17,** 849-62.

Weigel, D., and Jackle, H. (1990). The fork head domain: a novel DNA binding motif of eukaryotic transcription factors? *Cell* **63,** 455-6.

Weigel, D., Jurgens, G., Kuttner, F., Seifert, E., and Jackle, H. (1989). The homeotic gene fork head encodes a nuclear protein and is expressed in the terminal regions of the Drosophila embryo. *Cell* **57,** 645-58.

Wetts, R., and Fraser, S. E. (1988). Multipotent precursors can give rise to all major cell types of the frog retina. *Science* **239,** 1142-5.

Williams, R. W., Hogan, D., and Garraghty, P. E. (1994). Target recognition and visual maps in the thalamus of achiasmatic dogs. *Nature* **367,** 637-9.

Williams, S. E., Grumet, M., Colman, D. R., Henkemeyer, M., Mason, C. A., and Sakurai, T. (2006). A role for Nr-CAM in the patterning of binocular visual pathways. *Neuron* **50,** 535-47.

Williams, S. E., Mann, F., Erskine, L., Sakurai, T., Wei, S., Rossi, D. J., Gale, N. W., Holt, C. E., Mason, C. A., and Henkemeyer, M. (2003). Ephrin-B2 and EphB1 mediate retinal axon divergence at the optic chiasm. *Neuron* **39,** 919-35.

Wilson, S. W., Brennan, C., Macdonald, R., Brand, M., and Holder, N. (1997). Analysis of axon tract formation in the zebrafish brain: the role of territories of gene expression and their boundaries. *Cell Tissue Res* **290,** 189-96.

Winberg, M. L., Mitchell, K. J., and Goodman, C. S. (1998). Genetic analysis of the mechanisms controlling target selection: complementary and combinatorial functions of netrins, semaphorins, and IgCAMs. *Cell* **93,** 581-91.

Wizenmann, A., Thanos, S., von Boxberg, Y., and Bonhoeffer, F. (1993). Differential reaction of crossing and non-crossing rat retinal axons on cell membrane preparations from the chiasm midline: an in vitro study. *Development* **117,** 725-35.

Xiang, M., Zhou, L., Macke, J. P., Yoshioka, T., Hendry, S. H., Eddy, R. L., Shows, T. B., and Nathans, J. (1995). The Brn-3 family of POU-domain factors: primary structure, binding specificity, and expression in subsets of retinal ganglion cells and somatosensory neurons. *J Neurosci* **15,** 4762-85.

Xuan, S., Baptista, C. A., Balas, G., Tao, W., Soares, V. C., and Lai, E. (1995). Winged helix transcription factor BF-1 is essential for the development of the cerebral hemispheres. *Neuron* **14,** 1141-52.

Yamagata, M., Mai, A., Pollerberg, G. E., and Noda, M. (1999). Regulatory interrelations among topographic molecules CBF1, CBF2 and EphA3 in the developing chick retina. *Dev Growth Differ* **41,** 575-87.

Yao, J., Lai, E., and Stifani, S. (2001). The winged-helix protein brain factor 1 interacts with groucho and hes proteins to repress transcription. *Mol Cell Biol* **21,** 1962-72.

Yoshikawa, S., McKinnon, R. D., Kokel, M., and Thomas, J. B. (2003). Wnt-mediated axon guidance via the Drosophila Derailed receptor. *Nature* **422,** 583-8.

Yoshikawa, S., and Thomas, J. B. (2004). Secreted cell signaling molecules in axon guidance. *Curr Opin Neurobiol* **14,** 45-50.

Young, R. W. (1985). Cell differentiation in the retina of the mouse. *Anat Rec* **212,** 199-205.

Yu, T. W., and Bargmann, C. I. (2001). Dynamic regulation of axon guidance. *Nat Neurosci* **4 Suppl,** 1169-76.

Yuasa, J., Hirano, S., Yamagata, M., and Noda, M. (1996). Visual projection map specified by topographic expression of transcription factors in the retina. *Nature* **382,** 632-5.

Zhang, F., Lu, C., Severin, C., and Sretavan, D. W. (2000). GAP-43 mediates retinal axon interaction with lateral diencephalon cells during optic tract formation. *Development* **127,** 969-80.

Zhang, J. H., Cerretti, D. P., Yu, T., Flanagan, J. G., and Zhou, R. (1996). Detection of ligands in regions anatomically connected to neurons expressing the Eph receptor Bsk: potential roles in neuron-target interaction. *J Neurosci* **16,** 7182-92.

Zheng, J. Q., Wan, J. J., and Poo, M. M. (1996). Essential role of filopodia in chemotropic turning of nerve growth cone induced by a glutamate gradient. *J Neurosci* **16,** 1140-9.

The winged helix transcription factor Foxg1 facilitates retinal ganglion cell axon crossing of the ventral midline in the mouse

Thomas Pratt*, Natasha M. M.-L. Tian, T. Ian Simpson, John O. Mason and David J. Price

Genes and Development Group, Biomedical Sciences, George Square, The University of Edinburgh, Edinburgh EH8 9XD, UK
*Author for correspondence (e-mail: t.pratt@ed.ac.uk)

Accepted 27 April 2004

Development 131, 3773-3784
Published by The Company of Biologists 2004
doi:10.1242/dev.01246

Summary

During normal development, retinal ganglion cells (RGCs) project axons along the optic nerve to the optic chiasm on the ventral surface of the hypothalamus. In rodents, most RGC growth cones then cross the ventral midline to join the contralateral optic tract; those that do not cross join the ipsilateral optic tract. Contralaterally projecting RGCs are distributed across the retina whereas ipsilaterally projecting RGCs are concentrated in temporal retina. The transcription factor Foxg1 (also known as BF1) is expressed at several key locations along this pathway. Analysis of *Foxg1* expression using *lacZ* reporter transgenes shows that *Foxg1* is normally expressed in most, if not all, nasal RGCs but not in most temporal RGCs, neither at the time they project nor earlier in their lineage. Foxg1 is also expressed at the optic chiasm. Mice that lack Foxg1 die at birth and, although the shape of their eyes is abnormal, their retinas still project axons to the brain via the optic chiasm. Using anterograde and retrograde tract tracing, we show that there is an eightfold increase in the ipsilateral projection in *Foxg1*$^{-/-}$ embryos. The distributions of cells expressing the transcription factors Foxg1 and Nkx2.2, and cell-surface molecules Ephb2, ephrin B2 and SSEA-1 (Fut4) have been correlated to the normally developing retinothalamic projection and we show they are not much altered in the developing *Foxg1*$^{-/-}$ retina and optic chiasm. As much of the increased ipsilateral projection in *Foxg1*$^{-/-}$ embryos arises from temporal RGCs that are unlikely to have an autonomous requirement for Foxg1, we propose that the phenotype reflects at least in part a requirement for Foxg1 outwith the RGCs themselves, most likely at the optic chiasm.

Key words: Eye, BF1, Optic chiasm, Retinal ganglion cell axons, Ipsilateral, Contralateral, Ephb, Ephrin B, Tract tracing, Mouse

Introduction

During brain development, neurons project axons tipped with navigating growth cones. Ultimately, these axons reach and form synaptic connections with their target cells. Axon tracts connecting brain regions can be divided into two classes depending on whether they cross the midline. Ipsilateral (or longitudinal) tracts, such as the thalamocortical tract, connect regions on the same side of the brain. Contralateral (or commissural) tracts, such as the corpus callosum, cross the midline of the brain and connect regions in different halves. The visual system exhibits both types of tract. Each optic nerve carries RGC axons from the retina towards the optic chiasm on the ventral surface of the hypothalamus. At the optic chiasm some RGC axons progress contralaterally and others progress ipsilaterally to join the optic tract and grow towards their targets in the forebrain and midbrain. This way of organising retinal output results in parts of the brain receiving binocular input, which is useful for judging positions of objects in space.

The behaviour of a growth cone at a specific point along its route is defined by its interaction with the cells and molecules it encounters. In the mouse, RGC axons exit the retina and start to navigate along the optic stalk (forming the optic nerve) at embryonic day 11 (E11) (Colello and Guillery, 1990). By E15.5, the chiasm has acquired its mature configuration although progressively more axons navigate this route during subsequent development (Marcus et al., 1995). At the optic chiasm RGC growth cones respond to cues generated by a specialised population of midline cells (Wizenmann et al., 1993; Sretavan and Reichardt, 1993; Marcus et al., 1995). Their importance is shown by the failure of optic tract formation in mice with an immunoablated chiasm (Sretavan et al., 1995) and the development of only ipsilateral projections in *Pax2*$^{-/-}$ or *Vax1*$^{-/-}$ mice with agenesis of the chiasm (Torres et al., 1996; Hallonet et al., 1999). Contralaterally projecting RGCs (the majority in mice) are distributed all over the retinal surface. Ipsilaterally projecting RGCs are concentrated in ventrotemporal retina and their axons are repelled at the optic chiasm (Sretavan and Reichardt, 1993; Herrera et al., 2003; Williams et al., 2003).

Several transcription factors are regionally expressed in the developing visual system and are poised to regulate the development of its structures and axonal connections (Torres et al., 1996; Halonet et al., 1999; Barbieri et al., 2002; Mui et al., 2002; Wang et al., 2002; de Melo et al., 2003; Herrera et al., 2003). The winged helix transcription factor Foxg1 is strongly expressed in the developing nasal retina and optic stalk, optic chiasm, telencephalon and superior colliculus (Xuan et al., 1995; Huh et al., 1999; Marcus et al., 1999). The most obvious anatomical defects in embryos homozygous for a targeted deletion of *Foxg1* are abnormally shaped eyes and a hypoplastic telencephalon (Xuan et al., 1995; Huh et al., 1999).

We have shown by injecting tract-tracers into the eyes of these mutants that the retina projects axons to an optic tract growing over the surface of the thalamus (Pratt et al., 2002).

To test the potential for Foxg1 to influence axon navigation, we used carbocyanine dyes to trace retinal axons in mice carrying a targeted deletion of *Foxg1* (Xuan et al., 1995; Hebert and McConnell, 2000). We found that mice lacking Foxg1 have an increased ipsilateral projection arising from both nasal and temporal retina. To characterise this defect, we (1) used *lacZ* reporter transgenes to identify potential sites at which Foxg1 expression might influence the navigation of retinofugal axons; and (2) examined several molecular markers expressed in the normal retina and optic chiasm, namely the transcription factors Foxg1 and Nkx2.2, the receptor tyrosine kinase Ephb2 and its ligand ephrin B2, and the stage-specific embryonic antigen 1 (SSEA-1; Fut4 – Mouse Genome Informatics) (Marcus et al., 1999; Barbieri et al., 2002; Williams et al., 2003) in $Foxg1^{-/-}$ embryos.

Materials and methods

Foxg1 alleles and genetic background

To identify cells in which the *Foxg1* locus is transcriptionally active, we exploited the $Foxg1^{tm1M}$ (or $Foxg1^{lacZ}$) allele in which coding sequences are replaced by a *lacZ* cassette (Xuan et al., 1995). For tract tracing, we used the $Foxg1^{tm1(cre)Skm}$ (or $Foxg1^{Cre}$) allele in which coding sequences are replaced by a Cre recombinase cassette (Hebert and McConnell, 2000). $Foxg1^{Cre}$ and $Foxg1^{lacZ}$ are predicted null alleles (designated $Foxg1^{-}$) (Xuan et al., 1995; Hebert and McConnell, 2000). For lineage tracing, we used $Gtrosa26^{tm1Sho}$ (*R26RS*) reporter mice (Mao et al., 1999). Cre-mediated recombination in $Foxg1^{Cre}$;*R26RS* embryos irreversibly activates *lacZ* expression from the *ROSA26* locus (Mao et al., 1999; Hebert and McConnell, 2000). Tract tracing and lineage tracing experiments used the $Foxg1^{Cre}$ allele on an albino Swiss Webster background (as described by Hebert and McConnell, 2000). Other experiments used $Foxg1^{lacZ}$ and/or $Foxg1^{Cre}$ alleles on a mixed pigmented CBA/C57Bl6/Swiss Webster background. *Foxg1* homozygous mutants ($Foxg1^{Cre/Cre}$) and compound heterozygotes ($Foxg1^{Cre/lacZ}$) were identified by their hypoplastic telencephalon and distorted eyes. Heterozygous embryos (i.e. $Foxg1^{+/-}$) were identified by PCR genotyping: they were indistinguishable morphologically from wild type (Xuan et al., 1995; Huh et al., 1999) and we detected no RGC axon projection defects at the optic chiasm (data not shown).

PCR genotyping *Foxg1* alleles

$Foxg1^{+}$ was detected with primers Foxg1ORFFor 5′-CTG ACG CTC AAT GGC ATC TA-3′ and Foxg1ORFRev 5′-TTT GAG TCA ACA CGG AGC TG-3′ which give a product of 438 bp; $Foxg1^{lacZ}$ allele was detected with primers Foxg1_5′UTRF 5′-GCT GGA CAT GGG AGA TAG GA-3′ and Foxg1*lacZ*_ORFR 5′-GAC AGT ATC GGC CTC AGG AA-3′ which give a 550 bp product; $Foxg1^{Cre}$ allele was detected with primers NLSCreF 5′-CAT TTG GGC CAG CTA AAC AT-3′; NLSCreR 5′-ATT CTC CCA CCG TCA GTAC G-3′, which give a 307 bp product. For all primers, cycling conditions were 96°C for 2 minutes followed by [96°C for 30 seconds, 58.5°C for 30 seconds and 72°C for 30 seconds] for 35 cycles.

lacZ staining

E14.5 $Foxg1^{lacZ/+}$ and $Foxg1^{lacZ/Cre}$ embryonic heads were dissected and fixed for 1 hour at 4°C in 4% paraformaldehyde, 0.02% NP40, 0.01% sodium deoxycholate, 5 mM EGTA, 2mM $MgCl_2$ in phosphate-buffered saline (PBS). In some cases, heads were equilibrated in 30% sucrose/PBS and sectioned (10 μm) on a cryostat. Tissues were rinsed several times in wash buffer (2 mM $MgCl_2$, 0.02% NP40, 0.01% sodium deoxycholate in PBS), transferred to staining solution (wash buffer supplemented with 5 mM potassium ferricyanide, 5 mM potassium ferrocyanide and 1 mg/ml X-gal), and stained overnight (cryostat sections on slides) or for 2 days with agitation (wholemounts) at 37°C in darkness. Staining was stopped with 20 mM EDTA in PBS. Some wholemounts were sectioned with a vibratome (200 μm) or processed to wax, sectioned (10 μm) and mounted. Cryostat sections were counterstained with Nuclear Fast Red.

Tract tracing

Embryos (E13.5) or heads (E15.5) were fixed at 4°C in 4% paraformaldehyde in PBS overnight. For retrograde labelling, the back of the head and tissues overlying the thalamus were removed, and small DiI or DiA crystals (Molecular Probes) were placed in a line over the dorsal thalamus on one side to ensure unilateral labelling of the optic tract. For anterograde labelling, the lens was removed and the optic cup packed with larger clumps of crystals. Embryos were returned to 4% paraformaldehyde in PBS in the dark at room temperature for about one month to allow tracers to diffuse along axons. Vibratome sections (200 μm) were cleared by sinking in 1:1 glycerol: PBS containing the nuclear counterstain TOPRO3 (0.2 μM, Molecular Probes) and then 9:1 glycerol:PBS. Sections were stored at 4°C. Images were acquired using an epifluorescence microscope and digital camera (Leica Microsystems, Germany) or a TCS NT confocal microscope (Leica Microsystems, Germany). For quantification DiI-labelled RGCs were assigned to either nasal or temporal retina (Fig. 1B,C,J,K) in serial horizontal sections (for examples of sections used, see Fig. 4). In epifluorescence (TRITC filter) images (Fig. 3A-J; Fig. 4D-F,K,L) DiI appears orange and TOPRO3 appears red and in confocal images (Fig. 3K,L; Fig. 4A-C,G-J,M-O) DiI appears red, DiA is green and TOPRO3 appears blue.

Immunohistochemistry

Ephb2 and ephrin B2 immunohistochemistry was performed as described (Batlle et al., 2002). Embryos (E13.5) or heads (E16.5) were fixed overnight in 4% paraformaldehyde in phosphate buffer high salt (PBHS) [0.04 M phosphate, 0.03 M NaCl (pH7.0)] at 4°C, processed to wax and sectioned (10 μm). After rehydration, endogenous peroxidase activity was blocked with 90% methanol:3% hydrogen peroxide. Antigens were unmasked by microwaving in 10 mM sodium citrate buffer (pH 6.0) before reacting overnight with primary antibody followed by a bridge rabbit anti-goat antibody and detection using the Envision^{+} (Rabbit) Kit (Dako K4010). Antibody incubation and pre-incubation blocking were carried out in 1% bovine serum albumin in PBS at room temperature. SSEA-1 and Nkx2.2 immunohistochemistry was performed as described [SSEA-1 (Marcus and Mason, 1995), Nkx2.2 (Pratt et al., 2000)] except that detection of the primary antibody was carried out using the Envision^{+} (Mouse) Kit (Dako K4006). Primary antibodies were goat anti-mouse ephrin B2 (R&D Systems AF496) used at 1:500; goat anti-mouse Ephb2 (R&D Systems AF467) used at 1:1000; rabbit anti-goat (Dako Z0228) used at 1:400; mouse monoclonal anti-Nkx2.2 antibody (DSHB, USA 74.5A5) used at 1:30; and mouse monoclonal anti-SSEA1 antibody (DSHB, USA MC-480) was used at 1:50. Following a diaminobenzidine colour reaction, sections were dehydrated and mounted.

Results

Foxg1 expression in the developing eye and chiasm at E14.5 in $Foxg1^{lacZ/+}$ and $Foxg1^{lacZ/Cre}$ embryos

To identify cells that express *Foxg1*, we took advantage of a ‘knock-in’ to the *Foxg1* locus in which a *lacZ* cassette replaces *Foxg1*-coding sequences and is expressed in cells transcriptionally activating the *Foxg1* locus. These cells are stained blue after incubation with X-gal solution (Fig. 1). If

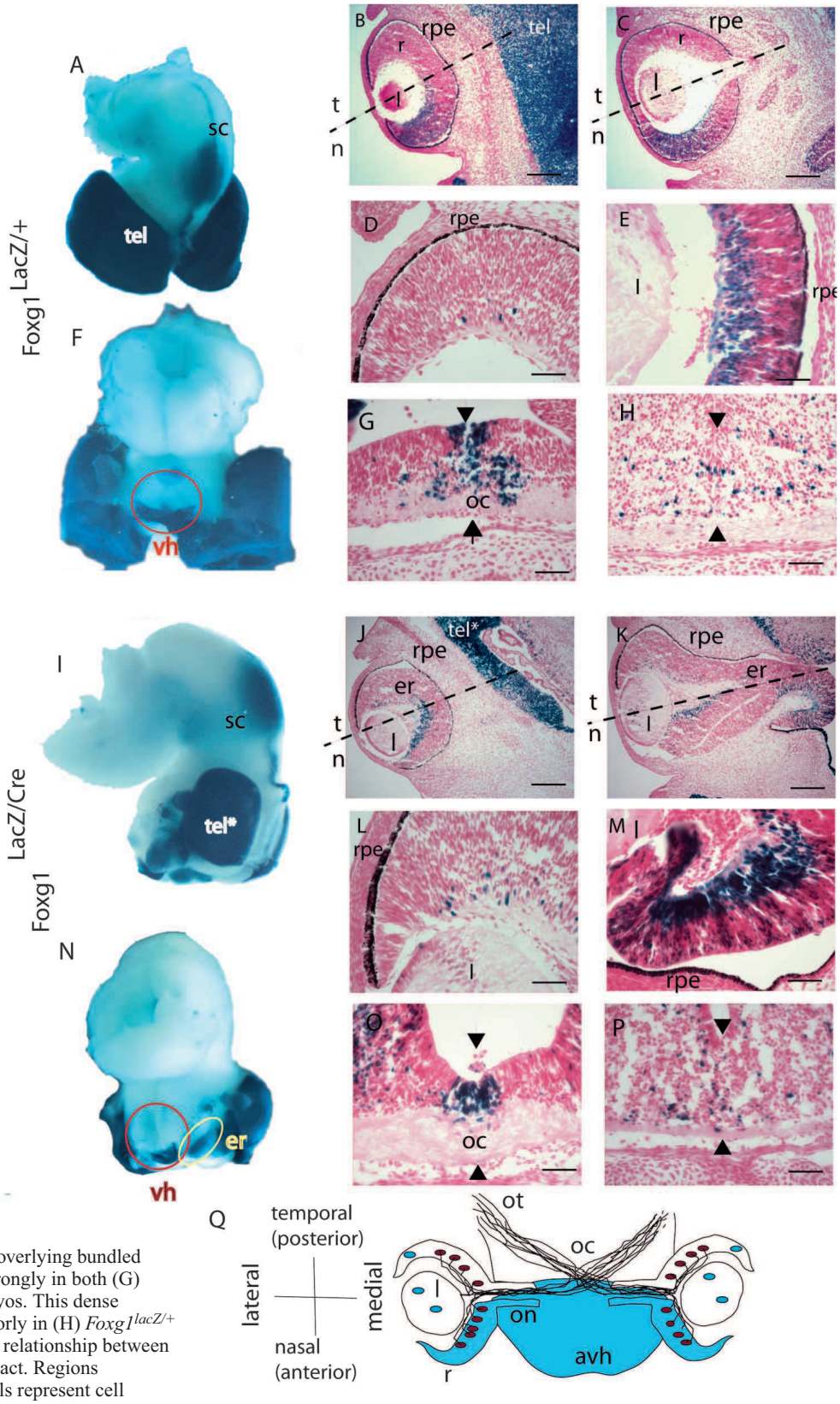

Fig. 1. Transcriptional activation of the *Foxg1* gene in tissues involved in RGC axon guidance in E14.5 embryos with and without Foxg1. *Foxg1*$^{lacZ/+}$ embryos have one functional copy of *Foxg1* and are phenotypically normal. *Foxg1*$^{lacZ/Cre}$ embryos are unable to produce Foxg1 protein. The *Foxg1*^{lacZ} allele reports transcriptional activation of the *Foxg1* gene by expression of *lacZ* protein. (A,F,I,N) X-gal stained brains. (A,F) *Foxg1*$^{lacZ/+}$ brain viewed (A) dorsolaterally to show staining of the superior colliculus (sc), dorsal midline and telencephalon (tel). (F) Ventral view shows staining in the anterior part of the ventral hypothalamus (vh; circled in red). (I,N) *Foxg1*$^{lacZ/Cre}$ brain showing (I) staining in the superior colliculus, along the dorsal midline and in the hypoplastic telencephalon (tel*). (N) A ventral view shows that, as in *Foxg1*$^{lacZ/+}$ embryos, staining is restricted to anterior ventral hypothalamus. The yellow oval encloses the mutant elongated retina (er), which has remained attached to the brain. The retinal pigment epithelium (rpe) has been removed to show that *lacZ* staining is far stronger in the anterior (nasal) retina. (B-E,G,H,J-M,O,P) X-gal stained cryostat sections with nuclei stained red. (B-E,J-M) Sections through the eye. Both (B-E) *Foxg1*$^{lacZ/+}$ and (J-M) *Foxg1*$^{lacZ/Cre}$ retinas exhibit predominantly nasal (n) *lacZ* staining, although in both cases a few stained cells are also detected in temporal (t) retina. J is dorsal to K. (K) Nasal staining in the medial elongation of the mutant retina. B and J are dorsal to D and K, respectively. (D,E,L,M) Higher magnifications of *Foxg1*$^{lacZ/+}$ and *Foxg1*$^{lacZ/Cre}$ (D,L) temporal and (E,M) nasal retina, showing pronounced staining of the nasal RGC layer. (G,H,O,P) Sections through the ventral hypothalamus with paired arrows demarcating its midline. A population of midline cells overlying bundled axons at the optic chiasm (oc) stains strongly in both (G) *Foxg1*$^{lacZ/+}$ and (O) *Foxg1*$^{lacZ/Cre}$ embryos. This dense midline staining is absent more posteriorly in (H) *Foxg1*$^{lacZ/+}$ and (P) *Foxg1*$^{lacZ/Cre}$ embryos. (Q) The relationship between Foxg1 expression and the retinofugal tract. Regions expressing Foxg1 are shaded blue. Ovals represent cell bodies. The retinofugal tract comprises RGCs (red) projecting axons (black lines) towards the optic chasm and into the brain. l, lens; ot, optic tract; r, retina; avh, anterior ventral hypothalamus; on, optic nerve. Wholemounts (A,F,I,N) are shown with anterior facing downwards. Cryostat sections (B-D,J-L) are horizontal with anterior (nasal) at the bottom; (E,G,H,M,O,P) coronal sections. Scale bars: 200 μm in B,C,J,K; 50 μm in D,EG,H,L,M,O,P.

these cells possess a functional *Foxg1* allele (i.e. in *Foxg1*$^{lacZ/+}$ embryos) they can make Foxg1 protein.

We examined *Foxg1* expression in *Foxg1*$^{lacZ/+}$ embryos at E14.5, because this is the time at which RGC axons are navigating the midline. *Foxg1* expression was strongest in the nasal retina (Fig. 1B,C); 51% of nasal cells were *lacZ*$^{+}$ in counts across several sections. By contrast, only a few temporal cells were lacZ^{+} (2%) (visible at higher magnifications in Fig. 1D). These findings are consistent with previous results of in situ hybridisation (Hatini et al., 1994). In the centronasal retina, staining was particularly prominent in the inner layer occupied by the RGCs (Fig. 1E). Foxg1 was expressed in the anterior hypothalamus (Fig. 1F) with a population of expressing cells at the ventral midline overlying bundled axons at the optic chiasm (Fig. 1G,H). Foxg1 was also expressed by other structures encountered (or avoided) by RGC axons, including the telencephalon, dorsal midline and superior colliculus (Fig. 1A).

We examined *lacZ* expression in *Foxg1*$^{lacZ/Cre}$ compound heterozygotes, which can produce no functional Foxg1 protein, so as to identify cells in which the mutant gene was transcriptionally activated at E14.5. As *Foxg1*$^{lacZ/Cre}$ cells had the same *lacZ* gene dose as *Foxg1*$^{lacZ/+}$ cells (one copy), *lacZ* staining intensity could be directly compared between the two genotypes. The *Foxg1*$^{-/-}$ eye is distorted (Fig. 1J,K) with an abnormally small lens and a medially elongated retina that extends towards the optic chiasm. The nasal bias of *Foxg1* expression in *Foxg1*$^{lacZ/+}$ embryos described above was also apparent in *Foxg1*$^{lacZ/Cre}$ embryos (see whole mount in Fig. 1N and sectioned material in Fig. 1J-M). We counted 21% *lacZ*$^{+}$ cells in nasal retina compared with only 3% *lacZ*$^{+}$ cells in temporal retina. The reduced count nasally reflects the absence of *lacZ*$^{+}$ cells in outer layers of the Foxg1$^{lacZ/Cre}$ lateral retina (compare Fig. 1B,C with J,K). Previous work at a younger age, E12.5, also showed *lacZ* expression in the eyes of *Foxg1*$^{lacZ/lacZ}$ embryos confined mainly to the nasal region of the mutant retina (Huh et al., 1999). As in *Foxg1*$^{lacZ/+}$ embryos, *lacZ* staining was prominent in the inner layer of the nasal retina (compare Fig. 1J-M with B-E). These data show that the nasotemporal polarity of the retina is maintained in *Foxg1*$^{-/-}$ mutants until at least E14.5; this conclusion is further supported by data presented later.

In E14.5 *Foxg1*$^{lacZ/Cre}$ compound heterozygotes, the anterior hypothalamus continued to express *Foxg1* around the ventral midline at the point contacted by the expanded mutant retina (Fig. 1N). As in *Foxg1*$^{lacZ/+}$ embryos, stained cells were detected at the ventral midline (Fig. 1O,P) indicating that Foxg1 is not required for the maintenance of this population of cells at the optic chiasm. *lacZ* staining was also retained in the telencephalon, along the dorsal midline and in the superior colliculus (Fig. 1I).

Lineage tracing of retinal cells that have expressed *Foxg1*

The experiments described above show that *Foxg1* is expressed by many nasal RGCs at the time their growth cones are navigating the chiasm. The few expressing cells we detected in the temporal retina were near to the lateral lip (or ciliary margin) of the temporal retina where progenitor cells proliferate (Perron et al., 1998; Zuber et al., 2003). It was therefore possible that Foxg1-expressing progenitors might populate the temporal retina with RGCs, the navigational responses of which were influenced by transient expression of Foxg1 earlier in their lineage. Crossing *Foxg1*$^{Cre/+}$ mice with *R26RS* reporter mice generates embryos in which a Cre recombinase-mediated recombination event irreversibly enables *lacZ* expression from the *Rosa26* locus in cells that express *Foxg1* (Mao et al., 1999; Hebert and McConnell, 2000). These cells and their descendants express *lacZ* protein, regardless of whether the *Foxg1* locus remains active. The *lacZ* expression pattern provides a convenient means of visualising cells whose fate may have been influenced by autonomous exposure to Foxg1.

As expected, the nasal retina of *Foxg1*$^{Cre/+}$*; R26RS* embryos exhibited uniform *lacZ* staining (Fig. 2A-D). Strong staining was also seen in lens, optic nerve and at the optic chiasm. In

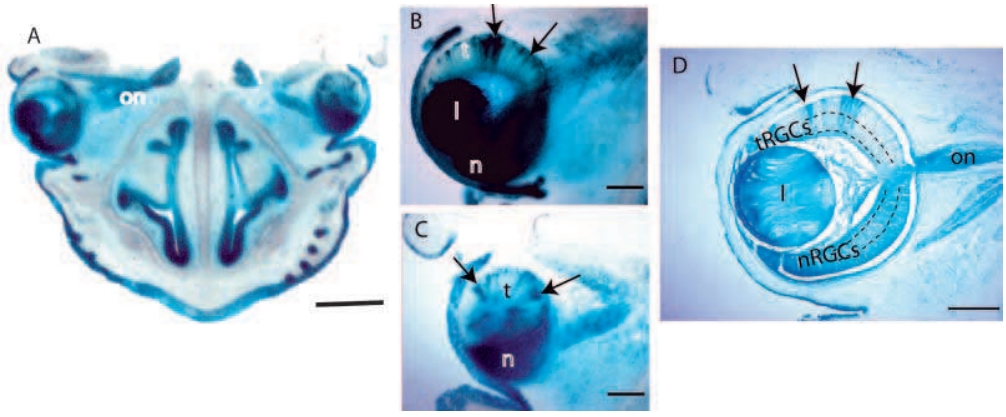

Fig. 2. Lineage tracing of *Foxg1*-expressing cells in E14.5 *Foxg1*$^{Cre/+}$*; R26RS* embryos. (A) Thick horizontal section of X-gal-stained facial whole mount (the eye on the right is sectioned more ventrally). *lacZ* staining is uniformly intense throughout the lens (l) and nasal (n) retina but appears patchy in the temporal (t) retina. (B,C) Thick horizontal sections of the eye. (B) Medial section; (C) ventral retina. (D) Thin horizontal section through the eye showing the distribution of *lacZ*-stained cells. Broken lines demarcate the position occupied by nasal RGCs (nRGCs) and temporal RGCs (tRGCs). In the nasal retina, *lacZ* staining is uniformly strong. In the temporal retina radial columns of *lacZ*-expressing cells are embedded in larger areas of non-expressing cells. In B and D, these columns are viewed side-on and in C they are viewed from above. Arrows in B-D indicate examples of *lacZ*-stained radial stripes. on, optic nerve. Scale bars: 500 μm in A; 200 μm in B-D.

the temporal retina of *Foxg1*$^{Cre/+}$*; R26RS* embryos, *lacZ* stained cells were found in radial stripes most of which were one or two cells wide while others were wider (Fig. 2B-D; arrows indicate radial stripes in temporal retina). A similar stripy distribution has been described before in chimeras and arises because the retina is constructed from radially oriented clones of cells (Reese et al., 1999). Examination of serial sections though the eyes of six embryos did not reveal any clear pattern in the size or density of these radial stripes, implying that the exposure of their ancestors to Foxg1 did not predispose them to occupy any particular part of the temporal retina. It was also apparent that most temporal RGCs were located outside the *lacZ*-expressing clones. These *lacZ*-expressing clones included cells outside the RGC layer showing that ancestral *Foxg1* expression was not restricted to RGCs. We also detected mosaic activation of *lacZ* expression in the temporal retinal pigment epithelium (a derivative of the optic cup, as is the retina) suggesting that a subpopulation of these cells are derived from Foxg1-expressing cells.

In conclusion, nasal RGCs express Foxg1 at the time their axons are negotiating the optic chiasm. By contrast, although some temporal RGCs are descended from Foxg1-expressing precursors, the vast majority do not express Foxg1 at this time and have never expressed Foxg1 at any time in their lineage.

Disruption to RGC axon navigation in embryos lacking Foxg1

The polarisation of *Foxg1* expression in the retina suggests that it could play an autonomous role in the navigation of nasal RGC growth cones but is unlikely to play an autonomous role in the navigation of most temporal RGC growth cones. Foxg1 may, however, influence the navigation of both nasal and temporal RGC growth cones by regulating the properties of the optic chiasm. To test these possibilities, we used DiI and DiA to trace the RGC projections in embryos lacking Foxg1.

We examined RGC projections in wild type at E13.5 (Fig. 3A-C) and E15.5 (Fig. 3F-H), over which period the optic chiasm develops its mature configuration. Progressing through the brain from rostral to caudal, sections show the injection in the eye (Fig. 3A,F), the optic nerve approaching the optic chiasm along the ventral surface of the brain (Fig. 3B,G) and the optic tract growing dorsally over the thalamus (Fig. 3C,H). At both ages, the contralateral optic tract is more strongly labelled, indicating that the majority of RGC axons cross the midline at the optic chiasm (Fig. 3C,H). Double labelling with DiI injected into one eye and DiA into the other illustrates the X-shape formed by RGC axons at the chiasm (Fig. 3K). Labelling of the optic tract is predominantly from the

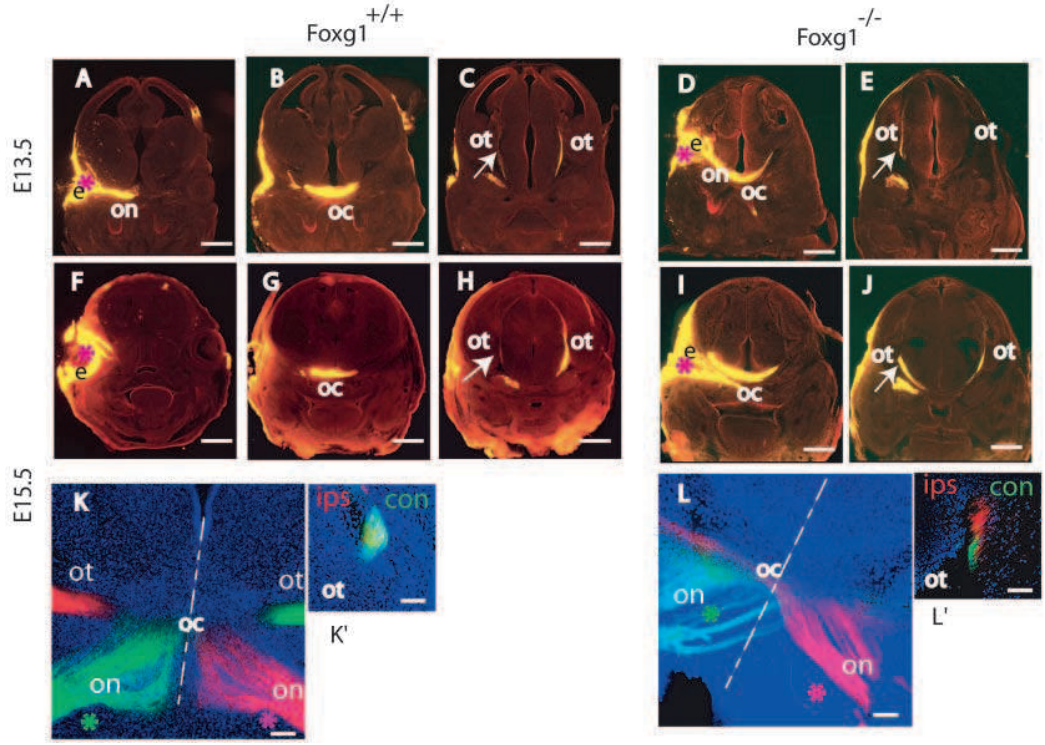

Fig. 3. RGC axon navigation in wild-type and *Foxg1*$^{-/-}$ embryos visualised by anterograde tract tracing at (A-E) E13.5 and (F-L) E15.5. For each age, progressively more caudal coronal sections of an individual embryo show injections of DiI (red asterisks) (A,F) in wild-type eye (e) and (D,I) in mutant eye; (B,G,D,I) labelling of optic nerve (on) and optic chiasm (oc); and (C,H,E,J) labelling of optic tracts (ot). (C,H) In the wild-type optic tracts, contralateral labelling is stronger than the ipsilateral labelling (white arrows). (E,J) In the mutant optic tracts, ipsilateral labelling appears stronger (white arrows). (K,L) Horizontal sections of embryos in which DiI was injected into one eye and DiA into the other eye of (K) an E15.5 wild-type and (L) an E15.5 *Foxg1*$^{-/-}$ embryo (ventral midline is marked by broken white line). (K′) Horizontal sections of the wild-type optic tract, growing over the diencephalon, from the same embryo as in K showing that each optic tract is predominantly labelled with dye from the contralateral (con) eye, although some ipsilateral (ips) label is also detectable (appears yellow where dyes overlap). (L′) Horizontal sections of the mutant optic tract from the same embryo as in L, showing abnormally high levels of red label from the ipsilateral eye. Scale bars: 500 μm in A-E; 650 μm in F-J; 100 μm in K,K′,L,L′.

contralateral eye, as shown by cross-sections of the optic tract as it grows dorsally over the thalamus (Fig. 3K′).

In E13.5 and E15.5 *Foxg1*$^{-/-}$ embryos many of the general features of RGC axon navigation were similar to those in wild type. RGC axons from both eyes converged on the ventral surface of the hypothalamus where they were sorted into ipsilateral and contralateral optic tracts growing dorsally over the thalamus (Fig. 3D,E,I,J). In contrast to the wild-type, the ipsilateral tract in mutants appeared greatly increased [compare panels for wild type (Fig. 3C,H) with mutants (Fig. 3E,J); arrows indicate the ipsilateral tract]. Double labelling with DiI injected into one eye and DiA into the other indicated that, although RGC axons converged at the hypothalamic midline, the balance of midline crossing was shifted in the mutants. Although many RGC axons still crossed the midline (Fig. 3L), a large proportion of axons in the optic tracts was labelled from the ipsilateral eye (Fig. 3L′).

To quantify the shift in the proportion of RGC axons projecting ipsilaterally and to identify the sites of origin in the retina of the aberrant ipsilateral projections, we retrogradely labelled RGCs with DiI or DiA from the thalamus. The numbers of nasal and temporal RGCs projecting ipsilaterally and contralaterally were counted in wild-type and mutant embryos at E15.5. As gene expression studies (Huh et al., 1999) (present study) indicate that, despite its medial elongation, the mutant retina does not exhibit greatly disturbed polarity, mutant eyes were divided into nasal and temporal halves using the same anatomical criteria as for wild-type eyes.

Wild-type embryos showed the expected patterns of projection. Retrograde label filled the optic tracts, optic chiasm and optic nerves, and showed most axons originating contralaterally (Fig. 4A-H). Contralaterally projecting RGCs were distributed across nasal and temporal retina (Fig. 4F,G). The much smaller number of ipsilaterally projecting RGCs were more frequently found temporally (Fig. 4G; Table 1). The density of labelled RGCs was highest medially, towards the optic nerve head, and decreased sharply in more lateral retina (Fig. 4F,G). RGC cell bodies were orientated radially with their axons projecting towards the optic nerve head along the inner surface of the retina (Fig. 4H).

In the mutant embryos, retrograde label filled the optic tracts, optic chiasm and optic nerves as in wild type (Fig. 4I-O) but many more axons originated ipsilaterally than in wild type [compare mutant (Fig. 4J) with wild type (Fig. 4C)]. This increased ipsilateral projection arose from both nasal and temporal retina (Fig. 4K,K′,M). Counts of ipsilateral RGCs in serial sections from four mutant and four wild-type E15.5 embryos (Table 1) showed an approximately eightfold increase in ipsilaterally projecting RGCs from both nasal and temporal retina in the mutants. There were no significant changes in the mutants in the numbers of RGCs projecting contralaterally from the nasal or temporal retina (Table 1). Total numbers of RGCs counted in the retina were not significantly altered in mutants. Ipsilaterally and contralaterally projecting RGCs were intermingled in the nasal and temporal retina (Fig. 4M, with higher magnification of RGCs in N) showing that all parts of the mutant retina contain RGCs capable of projecting to either side of the brain. We did not detect double-labelled cells, indicating that the increased ipsilateral projection did not result from large numbers of individual RGCs projecting to both sides of the brain.

As in the wild type, the majority of mutant RGCs are located in the inner layer of the retina and are radially orientated with their axons projecting along the inner surface of the retina (compare Fig. 4O with Fig. 4H), although the mutant RGCs do exhibit a broader radial spread. Again, reminiscent of the wild-type situation, mutant RGC axons fasciculate to form the mutant correlate of the optic nerve, which exits the elongated retina at its point of attachment to the ventral brain (seen in Fig. 4K) and approaches the optic chiasm (seen in a ventral adjacent section in Fig. 4L). As in the wild type, mutant retinal axons form an X-shaped chiasm (compare wild types in Fig. 3K, Fig. 4B,C,E with mutants in Fig. 3L, Fig. 4I,J,L), although their shapes are not identical. Given the distortions to the mutant eye it is remarkable that its retinal projection retains so many features in common with the wild type.

Our results in *Foxg1*$^{-/-}$ mutants indicate an increase in the proportion of RGCs whose axons are repelled by the midline and join the ipsilateral optic tract. As in wild type, significantly more ipsilateral projections originated in temporal retina (χ^2 test; Table 1). This finding provides further evidence for the retention of nasotemporal polarity, as was suggested by the expression pattern of *Foxg1* in mutants (see above).

Expression of Ephb2 and ephrin B2 in the developing retina

As well as being expressed in the developing retina itself, Foxg1 is expressed in cells that surround and may influence the patterns of expression of other genes in the retina as it develops (Dou et al., 1999). It was possible that in embryos lacking Foxg1 the patterning of the retina might have been altered fundamentally and this might have had consequences for RGC axon navigation. Results above suggested that the nasotemporal polarity of the *Foxg1*$^{-/-}$ retina is similar to wild type. Here, we addressed the nature of the other major axis of the mutant retina, i.e. dorsoventral. This was important as most ipsilateral RGC projections normally originate ventrally in the temporal retina (Drager, 1985) and so a repatterning of *Foxg1*$^{-/-}$ retina, such that it adopts a predominantly ventral character might have explained an increased ipsilateral projection.

The receptor tyrosine kinase Ephb2 and its ligand ephrin B2 are expressed in complementary dorsoventral gradients in the developing retina and their distributions in the retina and chiasm have been related to RGC axon midline crossing behaviour (Barbieri et al., 2002; Williams et al., 2003). In wild-type embryos at E13.5 and E16.5, ephrin B2 exhibits a dorsal$^{[high]}$ to ventral$^{[low]}$ gradient of expression in the retina with the strongest expression dorsolaterally (Fig. 5A,B). At E13.5, Ephb2 is expressed throughout the retina in a ventral$^{[high]}$ to dorsal$^{[low]}$ gradient (Fig. 5E). By E16.5 Ephb2 is more evenly distributed across the retina (Fig. 5F), although levels still appear to be slightly higher ventrolaterally. Ephb2 is also strongly expressed in the optic nerve, consistent with expression of Ephb2 protein on the RGC axons (Fig. 5E-F,I-J). RGC axons continue to express Ephb2 protein as they approach the optic chiasm and exit into the optic tract (Fig. 5I,J). By contrast, the optic nerve stains weakly for ephrin B2 protein (Fig. 5A,B).

The dorsoventral gradients of Ephb2 and ephrin B2 proteins are retained in the mutant. In E13.5 *Foxg1*$^{-/-}$ embryos, the retina expresses ephrin B2 protein in a dorsal$^{[high]}$ to

ventral[low] gradient (Fig. 5C) and Ephb2 protein in a complementary ventral[high] to dorsal[low] gradient (Fig. 5G). At E16.5, ephrin B2 expression is strongest in the dorsolateral retina (Fig. 5D) and Ephb2 protein is more evenly distributed across the retina with slightly higher levels ventrolaterally (Fig. 5H). As in wild types Ephb2 protein is expressed by mutant RGC axons as they cross the optic chiasm and enter the optic tracts (Fig. 5K,L).

In the wild type the eye is roughly spherical and is attached to the ventral surface of the diencephalon by the optic stalk, whereas the mutant eye lacks an optic stalk and is attached directly to brain. Perhaps as a mechanical consequence of this the mutant eye is elongated medially and squashed dorsoventrally relative to the wild-type eye. To distinguish whether this is only a change in shape or also involves a change in retinal volume, we measured retinal area (mm^2) in every 20th 10 µm horizontal serial section through the eyes of wild-type and mutant embryos. As each section was 0.01 mm thick, retinal volumes approximated to Σ(retinal area × 0.2) mm^3. Average volumes obtained for wild-type (0.86 mm^3) and mutant (0.88 mm^3) eyes were very similar. The proportion of the *Foxg1*$^{-/-}$ retina that is elongated medially (marked 'er' in Fig. 1K) probably corresponds to the central third of the wild-type retina. Consistent with this idea, the medial expansion of

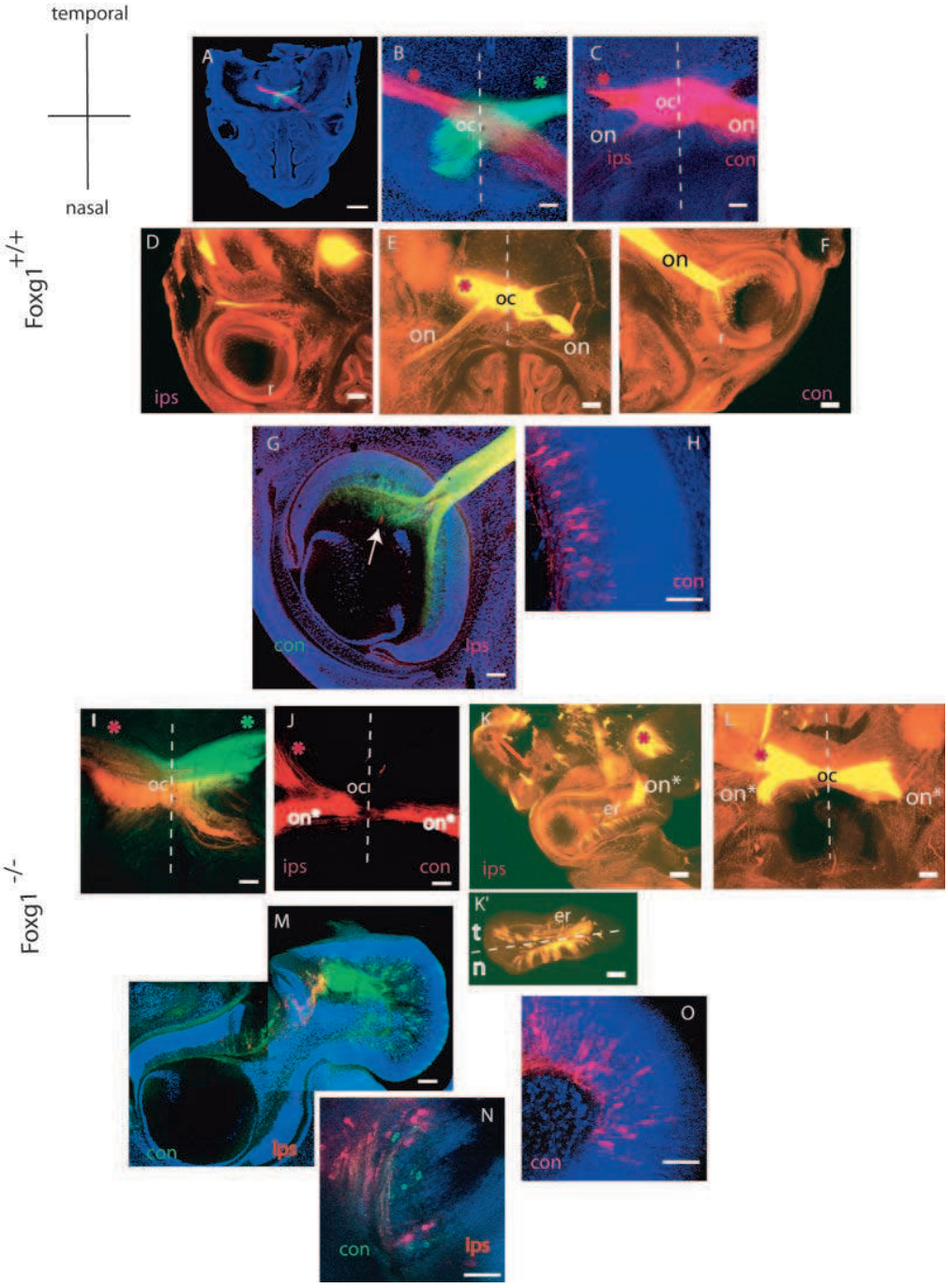

Fig. 4. Mapping ipsilateral and contralateral projecting RGCs in *Foxg1*$^{+/+}$ and *Foxg1*$^{Cre/Cre}$ embryos by retrograde tract tracing from the optic tract growing over the thalamus at E15.5. (A-H) Wild type. (A,B,G) DiI and DiA double-label experiment showing predominance of contralateral (con) projections (A,B) at the optic chiasm (oc) and (G) in the retina; an ipsilaterally (ips) labelled cell (red) is marked with arrow in G. (C-F,H) Single DiI-labelling experiments. (C,E) At the optic chiasm, the majority of labelling is in the contralateral optic nerve (on). (D,F) In the contralateral retina (F) a large number of labelled cells are distributed both nasally and temporally. (D) In the ipsilateral retina, far fewer cells are labelled. (I-O) Mutants. (I,M,N) Double-label experiment showing (I) the optic chiasm and (M,N) ipsilaterally (red) and contralaterally (green) projecting RGCs in the retina (note the absence of double labelled, yellow, RGCs). (J-L,O) Single label experiment showing increased ipsilateral labelling (compared with wild type) in (K,K′) both nasal (n) and temporal (t) parts of the elongated retina (er) and (J-L) their axons in the mutant correlate of the optic nerve (on*). (H,O) Higher magnification showing the disposition of RGCs in (H) wild-type and (O) mutant retina. All sections are horizontal with anterior (nasal) at the bottom. Each asterisk indicates which optic tract was injected with DiI (red) and DiA (green). Broken lines indicate the ventral midline. Scale bars: 500 µm in A; 100 µm in B,C,G,I,J,M; 200 µm in D-F,K,L; 50 µm in H,N,O.

Table 1. RGCs retrogradely labelled by dye placement in the optic tract

Midline crossing behaviour	Ipsilateral			Contralateral		
Hemiretina of origin	Temporal retina	Nasal retina	Temporal+ nasal retina	Temporal retina	Nasal retina	Temporal+ nasal retina
Foxg1$^{+/+}$ (*n*=4)	47	24	71	281	371	652
Foxg1$^{-/-}$ (*n*=4)	341	199	540	257	249	506
P values (*t*-test, *Foxg1*$^{+/+}$ versus *Foxg1*$^{-/-}$)	0.003*	0.021*	0.006*	0.84	0.48	0.6

Quantification of ipsilaterally and contralaterally projecting RGCs in nasal and temporal retina of *Foxg1*$^{+/+}$ and *Foxg1*$^{-/-}$ E15.5 embryos. DiI was injected into the optic tract on one side of the brain. After diffusion of DiI to the retina, serial horizontal sections were examined to determine: (1) the number of RGCs projecting to the injection site on the same side (ipsilateral) or opposite side (contralateral) of the brain; and (2) the number of RGCs of each class projecting from the nasal hemiretina or temporal hemiretina. Total RGC counts in serial sections from *Foxg1*$^{+/+}$ (*n*=4) and *Foxg1*$^{-/-}$ (*n*=4) embryos are tabulated. A χ^2 test was used to test the null hypothesis that nasal and temporal retina projected equal numbers of ipsilateral axons. The null hypothesis was rejected both for wild type (χ^2=3.73, P<0.05) and mutants (χ^2=18.6, P<0.05), indicating that both exhibited a significant temporal bias in the origin of ipsilateral projections. *P* values (Student's *t*-test) for *Foxg1*$^{+/+}$ versus *Foxg1*$^{-/-}$ comparison for each type of RGC counted are shown in the bottom row (*a significant difference).

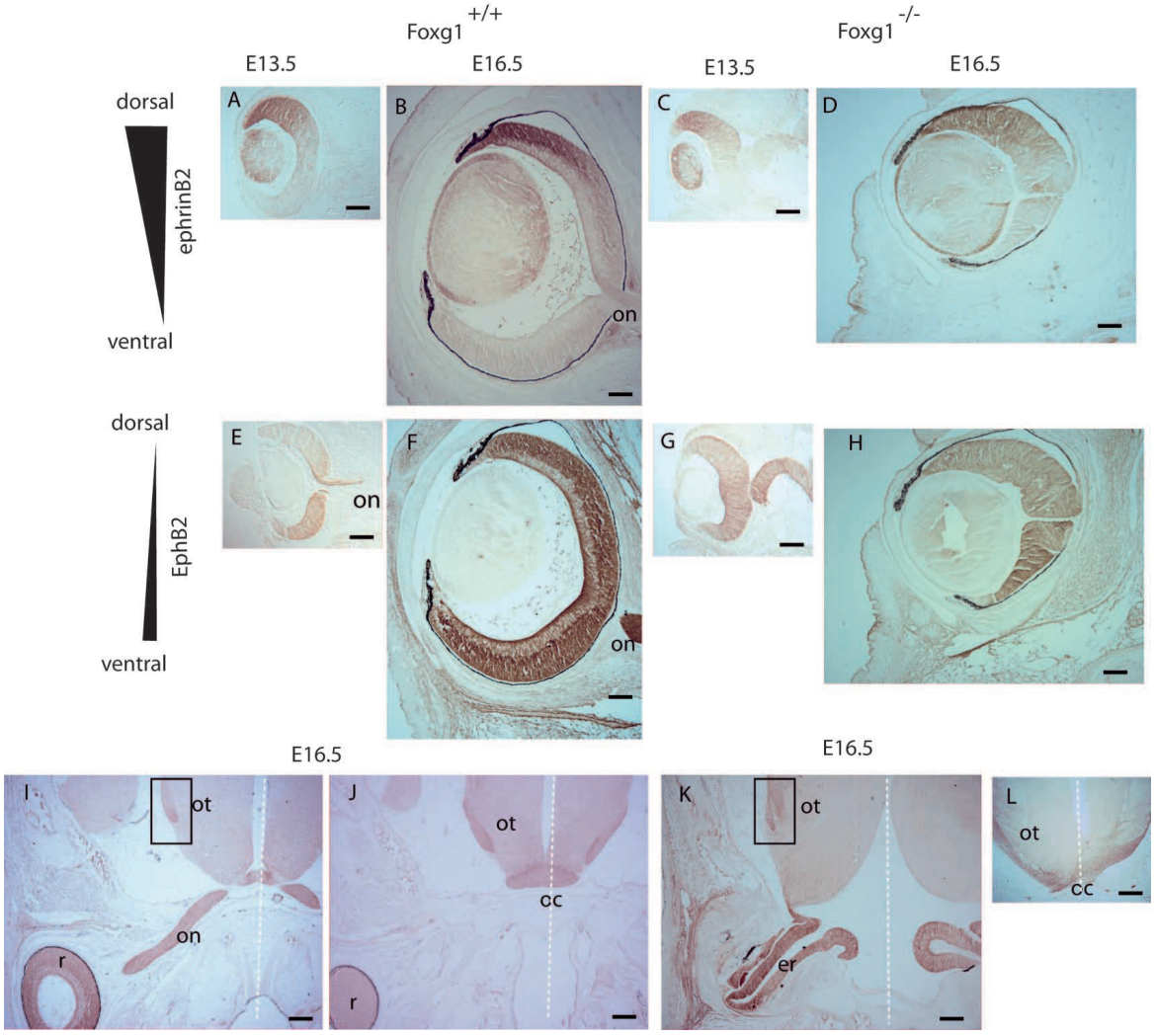

Fig. 5. The distributions of Ephb2 and ephrin B2 proteins in the developing retina and its axons are not dramatically altered in the *Foxg1*$^{-/-}$ mutant. Ephrin B2 protein forms a dorsolateral$^{[High]}$ to ventrolateral$^{[Low]}$ gradient in the developing retina at E13.5 in (A) the wild-type and (C) the mutant. This gradient remains at E16.5 in both (B) wild-type and (D) mutant. Ephb2 protein forms a complementary ventrolateral$^{[High]}$ to dorsolateral$^{[Low]}$ gradient in the developing retina at E13.5 in both (E) wild-type and (G) mutant retina. At E16.5, these gradients are shallower than at E13.5 in both (F) wild type and (H) mutant. The optic nerve (on) stains strongly for Ephb2 protein consistent with Ephb2 expression by navigating RGC axons. (I,J) In the wild type, Ephb2 is present in the optic nerve as it leaves the retina (r) and approaches the optic chiasm (oc) to emerge into the optic tract (ot) (boxed area in I). (K,L) In the mutant, Ephb2 is expressed in the elongated retina (er), at the optic chiasm and in the mutant optic tract as it emerges from the chiasm (boxed area in K). (A-H) Coronal sections (dorsal is towards the top); (I-L) horizontal sections (posterior is towards the top). Scale bars: 100 μm in A-H; 200 μm I-L.

the mutant retina expressed levels of ephrin B2 and Ephb2 intermediate between the extremes of the expression gradients shown in Fig. 5D,H (data not shown), as did the wild-type central retina.

These data indicate that, as in the nasotemporal axis, patterning of the retina along the dorsoventral axis is similar in *Foxg1*$^{-/-}$ and in wild-type embryos.

Expression of Nkx2.2, SSEA-1 and ephrin B2 at the developing chiasm

The presence of cells at the chiasm that turn on *Foxg1* in both *Foxg1*$^{+/+}$ and *Foxg1*$^{-/-}$ embryos (Fig. 1) prompted us to examine the mutant chiasm in more detail. The expression patterns of the transcription factor Nkx2.2 and the cell-surface molecule stage-specific embryonic antigen 1 (SSEA-1) define stages of normal chiasm development (Marcus and Mason, 1995; Marcus et al., 1999). SSEA-1 is expressed by a population of early differentiating neurons that provides an anatomical template to guide RGC axons at the developing chiasm (Sretavan et al., 1994; Marcus and Mason, 1995; Sretavan et al., 1995). We speculated that changes in the distribution of neurons expressing SSEA-1 in the mutant might perturb RGC axon midline crossing behaviour. However, we were unable to detect any clear shift in the expression domains of SSEA-1 between the wild-type (Fig. 7A,C,E) and mutant (Fig. 7B,D,F) chiasm at E13.5. The transcription factor Nkx2.2 defines a domain through which RGC axons grow at the midline (Marcus et al., 1999), but we did not find evidence of differences between Nkx2.2 expression in the wild-type and mutant (compare Fig. 7G with 7H). Ephrin B2 is expressed by radial glial cells that form a palisade at the chiasm and control RGC axon divergence (Marcus and Mason, 1995; Marcus et al., 1995; Nakagawa et al., 2000; Williams et al., 2003). Although the shape of the tissues surrounding the optic chiasm was slightly abnormal in *Foxg1* mutants, expression of ephrin B2 was observed along the ventral midline of the diencephalon in both wild-type and mutant embryos at E13.5 and E16.5 (Fig. 6). These data show that the mutant chiasm does not show major defects in the expression of at least three molecules known to be important for its interaction with RGC axons.

Discussion

Dual role for Foxg1 in eye morphogenesis and RGC axon guidance

During normal development, the eye field in the anterior neural plate splits into a right and a left half separated by the developing floor plate (reviewed by Rubenstein and Beachy, 1998; Rubenstein et al., 1998). On each side, the optic cup (from which retina and retinal pigment epithelium are derived) forms laterally, the optic stalk forms medially and the retina projects axons along the optic stalk to the chiasm. *Foxg1* is first expressed in the surface ectoderm immediately anterior to the neural plate at around E8 in mice. Over the following day, its expression appears in the anterior neural plate and, as this region becomes the anterior neural tube, demarcates the telencephalic neuroepithelium, optic chiasm and nasal retina (Hatini et al., 1994; Xuan et al., 1995; Dou et al., 1999; Huh et al., 1999). The domain of *Foxg1* expression in nasal retina includes the locations of projecting RGCs. Only a few cells in the temporal retina, which are located towards the ciliary margin, express *Foxg1*. Our data show that most RGCs in the temporal retina are descended from lineages in which *Foxg1* has never been expressed. These expression patterns indicate that Foxg1 is unlikely to have a significant cell autonomous effect on the development of cells in temporal retina, but may have such an effect on cells in nasal retina.

Our results show that Foxg1 is required to ensure a normal ipsilateral projection from RGCs. The *Foxg1*$^{-/-}$ retina produces an increased ipsilateral projection, arising from RGCs located

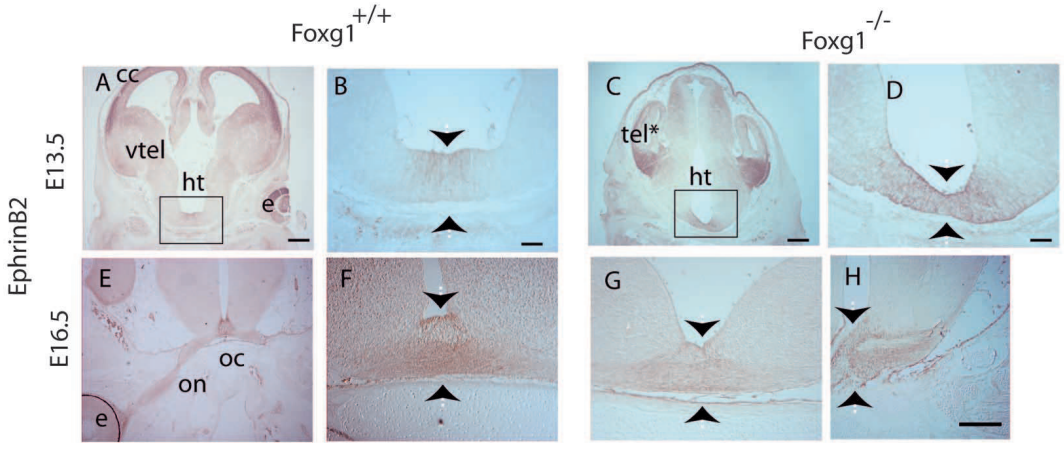

Fig. 6. Ephrin B2 protein is expressed at the ventral hypothalamic midline in both the *Foxg1*$^{-/-}$ mutant and the wild type. (A,B,E,F) Wild type. (A,B) At E13.5, ephrin B2 expression is most widespread in the more dorsal structures in the developing forebrain and eye (e). Ventrally ephrin B2 is detected at the ventral hypothalamic (ht) midline (B shows area boxed in A at higher power). (E,F) At E16.5, ephrin B2 protein is detected at the optic chiasm (oc) where expressing cells contact the optic nerve (on). (F) Higher magnification of the optic chiasm. (C,D,G,H) Mutant. (C,D) At E13.5, ephrin B2 is expressed in the hypoplastic telencephalon (tel*) and in the developing eye (see Fig. 5). Ephrin B2 is also detected at the hypothalamic midline (D shows area boxed in C at higher power). (G,H) At E16.5 ephrin B2 expression persists at the mutant optic chiasm where it contacts Ephb2-expressing axons (section in H is adjacent to the Ephb2 stained section shown in Fig. 5L). Paired arrows indicate the ventral hypothalamic midline. (A-D,F,G) Coronal sections with dorsal towards the top. (E,H) Horizontal sections with posterior towards the top. cc, cerebral cortex; vtel, ventral telencephalon. Scale bars: 200 μm in A,C,E; 50 μm in B,D,F-H.

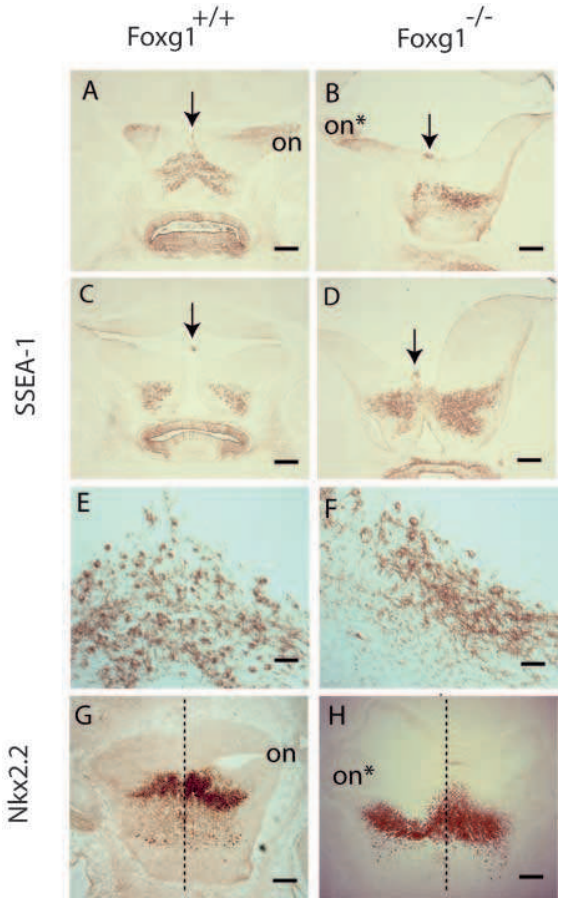

Fig. 7. Patterning of the chiasm at E13.5. Sections are horizontal, anterior is upwards. Immunohistochemistry was performed using antibodies for SSEA-1 (A-F) and Nkx2.2 (G,H). (A) Wild-type section through the optic chiasm showing SSEA-1-positive neurons arrayed in an inverted 'V'-shape. Arrow indicates the tip of the 'V'. SSEA-1 expression is also evident in the optic nerves (on). (B) A *Foxg1*$^{-/-}$ section equivalent to (A) showing SSEA-1 expression in the mutant correlate of the optic nerve (on*). Note that the plane of section is slightly tilted such that the left side is ventral to the right. The SSEA-1-positive 'arm' of the 'V' is visible on the right side, but is less clear on the left, which is further ventral. (C,D) Immediately dorsal to the optic chiasm, wild-type and *Foxg1*$^{-/-}$ embryos show bilaterally symmetrical SSEA-1 expression posterior to the third ventricle. SSEA-1 expression extends posteriorly and laterally in both C and D. (E,F) High magnification showing the morphology of SSEA-1 neurons in the wild type and *Foxg1*$^{-/-}$ mutant. (G,H) In the wild type and *Foxg1*$^{-/-}$ mutant, Nkx2.2 is expressed at the posterior optic chiasm, where it overlaps partly with SSEA-1 expression. Broken lines indicate the position of the midline. Scale bar: 200 μm in A,B; 100 μm in C,D,G,H; 50 μm in E,F.

both nasally and temporally. Given the expression patterns discussed above, abnormal development of RGC axons from both nasal and temporal territories argues against a completely cell-autonomous role for Foxg1 in the control of RGC projections. Foxg1 may autonomously regulate the behaviour of nasal RGC growth cones at the optic chiasm, e.g. by influencing their expression of cell surface molecules, but this can not be the case for most temporal RGCs.

The eyes of mice lacking Foxg1 have an abnormal shape (Xuan et al., 1995; Huh et al., 1999) (present study). A striking feature of the *Foxg1*$^{-/-}$ phenotype is the lack of an optic stalk connecting the retina to the brain. This could result in the retina becoming stretched medially as the head grows. Consistent with this, the overall volume and patterning of gene expression along its nasotemporal and dorsoventral axes are similar to wild-type retina. This argues against a fundamental repatterning of the retina in the absence of Foxg1. Changes in *Foxg1*$^{-/-}$ retinal morphology might also be secondary to defective development of the lens, which expresses Foxg1 early in its formation and is smaller than normal in mutants (Figs 2, 5) (Hatini et al., 1994; Xuan et al., 1995; Dou et al., 1999; Huh et al., 1999). Previous studies have shown that, although lens is not necessary to instruct the differentiation of neuroretina, it does influence the morphology of the retina either mechanically or molecularly (Ashery-Padan et al., 2000).

Foxg1 can be added to the growing list of proteins with a dual role in tissue morphogenesis and axon growth and morphology. Others on this list include transcription factors such as Pax6 (Ericson et al., 1997; Mastick et al., 1997; Pratt et al., 2000; Pratt et al., 2002) and secreted proteins of the Wnt (Hall et al., 2000; Yoshikawa et al., 2003), bone morphogenetic protein (BMP) (Augsburger et al., 1999) and hedgehog (Charron et al., 2003) families. Enzymes involved in regulating the sulphation status of extracellular heparan sulphate proteoglycans are implicated in Shh, Wnt and BMP signalling, tissue morphogenesis (Merry and Wilson, 2002; McLaughlin et al., 2003a) and RGC axon guidance (Walz et al., 1997; Irie et al., 2002).

Foxg1 may act at the optic chiasm to control RGC growth cone navigation

The simplest explanation of our finding an increased ipsilateral projection in embryos lacking Foxg1 is that Foxg1 normally regulates the proportions of crossed and uncrossed projections by a direct action on both temporal and nasal axons at the chiasm itself. In the chick, Foxg1 has been shown to autonomously regulate the retinotectal mapping of RGC axons (Yuasa et al., 1996) and it is possible that in the mouse Foxg1 expression by RGCs is involved in retinotectal mapping rather than in regulating midline crossing at the optic chiasm.

In the wild-type the diencephalon is surrounded on each side by a large telencephalic vesicle. This physical support is missing in the mutant, which has a hypoplastic telencephalon and, as a consequence, the diencephalon adopts a more 'open' conformation. Nevertheless, we found that many morphological and molecular features of the wild-type chiasm were retained in the mutant. The normal developing chiasm has been characterised in terms of the expression of transcription factors and regulatory molecules whose expression domains coincide with navigating RGC axons (Marcus et al., 1999; Nakagawa et al., 2000; Williams et al., 2003). We did not detect any gross abnormalities in the distribution of cells expressing the transcription factors Foxg1 or Nkx2.2 or of cells expressing cell surface molecules SSEA-1 or ephrin B2 at the developing chiasm. Despite its elongated shape, the mutant eye projects a correlate of the optic nerve, which converges to form the optic chiasm. It is extremely unlikely that anatomical alterations of the mutant eye or brain are solely responsible for the alterations

in the balance of ipsilateral and contralateral projections. Taken together, these findings point to a more specific defect causing the change in RGC axon midline crossing in mutants.

The mechanisms that regulate RGC growth cone navigation at the normal optic chiasm are not well understood, although it is known that Ephb and ephrin B family members are likely to participate in regulating midline crossing of RGC growth cones (Nakagawa et al., 2000; Barbieri et al., 2002; Williams et al., 2003). We did not detect obvious alterations in the distributions of Ephb2 and ephrin B2 protein in the mutant retina and optic chiasm but this does not necessarily preclude a role for Foxg1 in the control of Ephb/ephrin B signalling. There are several precedents for a particular receptor/ligand interaction leading to either attraction or repulsion depending on other factors. The presence of the extracellular matrix molecule laminin has been shown to convert the attraction of RGC growth cones towards a source of netrin to a repulsion of RGC growth cones away from a source of netrin (Hopker et al., 1999). Levels of an intracellular guanylate cyclase control the response of neocortical growth cones to a Sema3a gradient (Polleux et al., 2000). Although an analagous mechanism has not been demonstrated for Ephb/ephrin B signalling it appears that Ephb-expressing axons can be either attracted or repelled by ephrin B in different situations (McLaughlin et al., 2003b; Hindges et al., 2002).

Foxg1 may, therefore, regulate expression at the optic chiasm of one or more of a potentially very large number of modulators of signalling pathways activated by, for example, Ephb/ephrin B. The identification of transcriptional targets of Foxg1 will allow a systematic survey of these possibilities. The final choice made by each RGC growth cone whether to go ipsilateral or contralateral at the optic chiasm probably depends on the balance between attractive and repulsive signals at the chiasm and the nature of the response of each growth cone to those signals. Most probably loss of Foxg1 promotes ipsilateral projections at the optic chiasm by perturbing these balances.

We thank Katy Gillies, Ben Martynoga, James O'Connor, Duncan Mcneil and Linda Wilson (Biomedical Sciences Confocal Facility) for their contribution to this work. We thank Lijian Shen and Eseng Lai for providing the *Foxg1^{lacZ}* mice, and Jean Hebert and Susan McConnell for providing the *Foxg1^{Cre}* mice. The Nkx2.2 (74.5A5) and Ssea1 (MC-480) antibodies developed by Thomas Jessell and Davor Solter, respectively, were obtained from the Developmental Studies Hybridoma Bank developed under the auspices of the NICHD and maintained by The University of Iowa, Department of Biological Sciences, Iowa City, IA 52242. This work was supported by the Wellcome Trust, MRC and BBSRC.

References

Ashery-Padan, R., Marquardt, T., Zhou, X. and Gruss, P. (2000). Pax6 activity in the lens primordium is required for lens formation and for correct placement of a single retina in the eye. *Genes Dev.* **14**, 2701-2711.

Augsburger, A., Schuchardt, A., Hoskins, S., Dodd, J. and Butler, S. (1999). BMPs as mediators of roof plate repulsion of commissural neurons. *Neuron* **24**, 127-141.

Barbieri, A. M., Broccoli, V., Bovolenta, P., Alfano, G., Marchitiello, A., Mocchetti, C., Crippa, L., Bulfone, A., Marigo, V., Ballabio, A. et al. (2002). Vax2 inactivation in mouse determines alteration of the eye dorsal-ventral axis, misrouting of the optic fibres and eye coloboma. *Development* **129**, 805-813.

Batlle, E., Henderson, J. T., Beghtel, H., van den Born, M. M., Sancho, E., Huls, G., Meeldijk, J., Robertson, J., van de Wetering, M., Pawson, T. et al. (2002). Beta-catenin and TCF mediate cell positioning in the intestinal epithelium by controlling the expression of EphB/ephrinB. *Cell* **111**, 251-263.

Charron, F., Stein, E., Jeong, J., McMahon, A. P. and Tessier-Lavigne, M. (2003). The morphogen sonic hedgehog is an axonal chemoattractant that collaborates with netrin-1 in midline axon guidance. *Cell* **113**, 11-23.

Colello, R. J. and Guillery, R. W. (1990). The early development of retinal ganglion cells with uncrossed axons in the mouse: retinal position and axonal course. *Development* **108**, 515-523.

de Melo, J., Qiu, X., Du, G., Cristante, L. and Eisenstat, D. D. (2003). Dlx1, Dlx2, Pax6, Brn3b, and Chx10 homeobox gene expression defines the retinal ganglion and inner nuclear layers of the developing and adult mouse retina. *J. Comp. Neurol.* **461**, 187-204.

Dou, C. L., Li, S. and Lai, E. (1999). Dual role of brain factor-1 in regulating growth and patterning of the cerebral hemispheres. *Cereb. Cortex* **9**, 543-550.

Drager, U. C. (1985). Birth dates of retinal ganglion cells giving rise to the crossed and uncrossed optic projections in the mouse. *Proc. R. Soc. London B. Biol. Sci.* **224**, 57-77.

Ericson, J., Rashbass, P., Schedl, A., Brenner-Morton, S., Kawakami, A., van Heyningen, V., Jessell, T. M. and Briscoe, J. (1997). Pax6 controls progenitor cell identity and neuronal fate in response to graded Shh signaling. *Cell* **90**, 169-180.

Hall, A. C., Lucas, F. R. and Salinas, P. C. (2000). Axonal remodeling and synaptic differentiation in the cerebellum is regulated by WNT-7a signaling. *Cell* **100**, 525-535.

Hallonet, M., Hollemann, T., Pieler, T. and Gruss, P. (1999). Vax1, a novel homeobox-containing gene, directs development of the basal forebrain and visual system. *Genes Dev.* **13**, 3106-3114.

Hatini, V., Tao, W. and Lai, E. (1994). Expression of winged helix genes, BF-1 and BF-2, defines adjacent domains within the developing forebrain and retina. *Neurobiology* **25**, 1293-1309.

Hébert, J. M. and McConnell, S. K. (2000). Targeted introduction of *Cre* into the *Foxg1* (*BF-1*) locus mediates *loxP* recombination in the telencephalon and other developing head structures. *Dev. Biol.* **222**, 296-306.

Herrera, E., Brown, L., Aruga, J., Rachel, R. A., Dolen, G., Mikoshiba, K., Brown, S. and Mason, C. A. (2003). Zic2 patterns binocular vision by specifying the uncrossed retinal projection. *Cell* **114**, 545-557.

Hindges, R., McLaughlin, T., Genoud, N., Henkemeyer, M. and O'Leary, D. D. (2002). EphB forward signaling controls directional branch extension and arborization required for dorsal-ventral retinotopic mapping. *Neuron* **35**, 475-487.

Hopker, V. H., Shewan, D., Tessier-Lavigne, M., Poo, M. and Holt, C. (1999). Growth-cone attraction to netrin-1 is converted to repulsion by laminin-1. *Nature* **401**, 69-73.

Huh, S., Hatini, V., Marcus, R. C., Li, S. C. and Lai, E. (1999). Dorsal-ventral patterning defects in the eye of BF-1-deficient mice associated with a restricted loss of shh expression. *Dev. Biol.* **211**, 53-63.

Irie, A., Yates, E. A., Turnbull, J. E. and Holt, C. E. (2002). Specific heparan sulfate structures involved in retinal axon targeting. *Development* **129**, 61-70.

Mao, X., Fujiwara, Y. and Orkin, S. H. (1999). Improved reporter strain for monitoring Cre recombinase-mediated DNA excisions in mice. *Proc. Natl. Acad. Sci. USA* **96**, 5037-5042.

Marcus, R. C. and Mason, C. A. (1995). The first retinal axon growth in the mouse optic chiasm: axon patterning and the cellular environment. *J. Neurosci.* **15**, 6389-6402.

Marcus, R. C., Blazeski, R., Godement, P. and Mason, C. A. (1995). Retinal axon divergence in the optic chiasm: uncrossed axons diverge from crossed axons within a midline glial specialisation. *J. Neurosci.* **15**, 3716-3729.

Marcus, R. C., Shimamura, K., Sretavan, D., Lai, E., Rubenstein, J. L. R. and Mason, C. A. (1999). Domains of regulatory gene expression and the developing optic chiasm: correspondence with retinal axon paths and candidate signaling cells. *J. Comp. Neurol.* **403**, 346-358.

Mastick, G. S., Davis, N. M., Andrew, G. L. and Easter, S. S., Jr (1997). Pax-6 functions in boundary formation and axon guidance in the embryonic mouse forebrain. *Development* **124**, 1985-1997.

McLaughlin, D., Karlsson, F., Tian, N., Pratt, T., Bullock, S. L., Wilson, V. A., Price, D. J. and Mason, J. O. (2003a). Specific modification of heparan sulphate is required for normal cerebral cortical development. *Mech. Dev.* **120**, 1481-1488.

McLaughlin, T., Hindges, R., Yates, P. A. and O'Leary, D. D. (2003b). Bifunctional action of ephrin-B1 as a repellent and attractant to control

bidirectional branch extension in dorsal-ventral retinotopic mapping. *Development* **130**, 2407-2418.

Merry, C. L. and Wilson, V. A. (2002). Role of heparan sulfate-2-O-sulfotransferase in the mouse. *Biochim. Biophys. Acta* **157**, 319-327.

Mui, S. H., Hindges, R., O'Leary, D. D., Lemke, G. and Bertuzzi, S. (2002). The homeodomain protein Vax2 patterns the dorsoventral and nasotemporal axes of the eye. *Development* **129**, 797-804.

Nakagawa, S., Brennan, C., Johnson, K. G., Shewan, D., Harris, W. A. and Holt, C. E. (2000). Ephrin-B regulates the Ipsilateral routing of retinal axons at the optic chiasm. *Neuron* **25**, 599-610.

Perron, M., Kanekar, S., Vetter, M. L. and Harris, W. A. (1998). The genetic sequence of retinal development in the ciliary margin of the *Xenopus* eye. *Dev. Biol.* **199**, 185-200.

Polleux, F., Morrow, T. and Ghosh, A. (2000). Semaphorin 3A is a chemoattractant for cortical apical dendrites. *Nature* **404**, 567-573.

Pratt, T., Vitalis, T., Warren, N., Edgar, J. M., Mason, J. O. and Price, D. J. (2000). A role for Pax6 in the normal development of dorsal thalamus and its cortical connections. *Development* **127**, 5167-5178.

Pratt, T., Quinn, J. C., Simpson, T. I., West, J. D., Mason, J. O. and Price, D. J. (2002). Disruption of early events in thalamocortical tract formation in mice lacking the transcription factors Pax6 or Foxg1. *J. Neurosci.* **22**, 8523-8531.

Reese, B. E., Necessary, B. D., Tam, P. P. L., Faulkner-Jones, B. and Tan, S.-S. (1999). Clonal expansion and cell dispersion in the developing mouse retina. *Eur. J. Neurosci.* **11**, 2965-2978.

Rubenstein, J. L. and Beachy, P. A. (1998). Patterning of the embryonic forebrain. *Curr. Opin. Neurobiol.* **8**, 18-26.

Rubenstein, J. L., Shimamura, K., Martinez, S. and Puelles, L. (1998). Regionalization of the prosencephalic neural plate. *Annu. Rev. Neurosci*. **21**, 445-477.

Sretavan, D. W. and Reichardt, L. F. (1993). Time-lapse video analysis of retinal ganglion cell axon pathfinding at the mammalian optic chiasm: growth cone guidance using intrinsic chiasm cues. *Neuron* **10**, 761-777.

Sretavan, D. W., Feng, L., Pure, E. and Reichardt, L. F. (1994). Embryonic neurons of the developing optic chiasm express L1 and CD44, cell surface molecules with opposing effects on retinal axon growth. *Neuron* **12**, 957-975.

Sretavan, D. W., Pure, E., Siegel, M. W. and Reichardt, L. F. (1995). Disruption of retinal axon ingrowth by ablation of embryonic mouse optic chiasm neurons. *Science* **269**, 98-101.

Torres, M., Gomez-Pardo, E. and Gruss, P. (1996). Pax2 contributes to inner ear patterning and optic nerve trajectory. *Development* **122**, 3381-3391.

Walz, A., McFarlane, S., Brickman, Y. G., Nurcombe, V., Bartlett, P. F. and Holt, C. E. (1997). Essential role of heparan sulfates in axon navigation and targeting in the developing visual system. *Development* **124**, 2421-2430.

Wang, S. W., Mu, X., Bowers, W. J., Kim, D. S., Plas, D. J., Crair, M. C., Federoff, H. J., Gan, L. and Klein, W. H. (2002). Brn3b/Brn3c double knockout mice reveal an unsuspected role for Brn3c in retinal ganglion cell axon outgrowth. *Development* **129**, 467-477.

Williams, S. E., Mann, F., Erskine, L., Sakurai, T., Wei, S., Rossi, D. J., Gale, N. W., Holt, C. E., Mason, C. A. and Henkemeyer, M. (2003). Ephrin-B2 and EphB1 mediate retinal axon divergence at the optic chiasm. *Neuron* **39**, 919-935.

Wizenmann, A., Thanos, S., von Boxberg, Y. and Bonhoeffer, F. (1993). Differential reaction of crossing and non-crossing rat retinal axons on cell membrane preparations from the chiasm midline: an in vitro study. *Development* **117**, 725-735.

Xuan, S., Baptista, C. A., Balas, G., Tao, W., Soares, V. C. and Lai, E. (1995). Winged helix transcription factor BF-1 is essential for the development of the cerebral hemispheres. *Neuron* **14**, 1141-1152.

Yoshikawa, S., McKinnon, R. D., Kokel, M. and Thomas, J. B. (2003). Wnt-mediated axon guidance via the *Drosophila* derailed receptor. *Nature* **422**, 583-588.

Yuasa, J., Hirano, S., Yamagata, M. and Noda, M. (1996). Visual projection map specified by topographic expression of transcription factors in the retina. *Nature* **382**, 632-635.

Zuber, M. E., Gestri, G., Viczian, A. S., Barsacchi, G. and Harris, W. A. (2003). Specification of the vertebrate eye by a network of eye field transcription factors. *Development* **130**, 5155-5167.